Multiphoton Absorbing Materials: Molecular Designs, Characterizations, and Applications

Guang S. He, Loon-Seng Tan, Qingdong Zheng, and Paras N. Prasad

Chem. Rev., **2008**, 108 (4), 1245-1330 • DOI: 10.1021/cr050054x

Multiphoton Absorbing Materials: Molecular Designs, Characterizations, and Applications

Guang S. He,*,† Loon-Seng Tan,‡ Qingdong Zheng,† and Paras N. Prasad†

Institute for Lasers, Photonics and Biophotonics, State University of New York at Buffalo, New York 14260-3000, and Polymer Branch, Materials & Manufacturing Directorate, Air Force Research Laboratory, Wright-Patterson AFB, Ohio 45433-7750

Received January 4, 2007

Contents

* To whom correspondence should be addressed. E-mail: gshe@acsu.buffalo.edu.
† State University of New York at Buffalo.
‡ Air Force Research Laboratory.

10.1021/cr050054x CCC: $71.00
Published on Web 03/25/2008

Guang S. He is a Senior Research Scientist jointed the Photonics Research Laboratory at the State University of New York at Buffalo in 1987 and the Institute for Lasers, Photonics and Biophotonics since 1999. His major research activities cover the areas of laser physics, nonlinear optics, multiphoton processes and technology. His current research efforts are focused on multiphoton-excitation-based novel devices and applications. He has published more than 130 scientific articles and coauthored five monographs including the later book "*Physics of Nonlinear Optics*" (World Scientific, 2000).

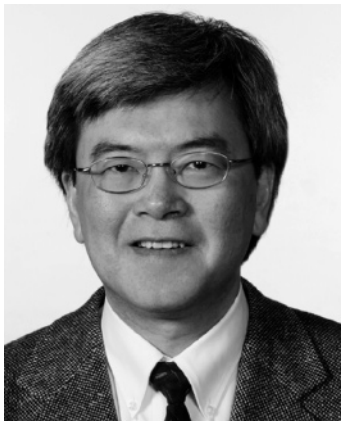

Loon-Seng Tan received his B.S. in chemistry (advisor: Prof. Mitsuru Kubota) from Harvey Mudd College, Claremont, California in 1976 and Ph.D. in Inorganic/Organometallic Chemistry (advisors: Profs. Barry Haymore and Malcolm Chisholm) from Indiana University, Bloomington, Indiana in 1981. In 1981–83, he was an NIH Postdoctoral fellow (advisor: Prof. Sue Cummings) and a visiting assistant professor of chemistry at Wright State University, Dayton, Ohio. He is currently a principal chemist and a research group leader at the Air Force Research Laboratory's Polymer Branch, Materials and Manufacturing Directorate, which he has been associated with since 1983. His research activities have been dealing primarily with the synthetic aspects of high-temperature linear, cross-linked, and dendritic polymers, molecular composites, nanoscale carbon materials, and nonlinear optical materials. The results of his research efforts have been documented in over 200 publications, US patents, and technical presentations.

1. Introduction

1.1. Basic Historical Facts

In the first quarter of the twentieth century, one of the most significant events in physics and chemistry was the establishment of the quantum theories of radiation, matter, and their interactions. According to these revolutionary theories, a radiation (light) field consists of one type of unit, namely photons, while matter consists of another type of unit, namely molecules or atoms. Through the interaction between these two types of elementary particles, there is an energy exchange between the radiation and the matter, which in general can be described as the absorption or emission of photons by the matter. In the early developmental stage of the quantum theories, scientists mostly considered only the processes of either one-photon absorption or one-photon emission; both processes were easily observed under common experimental conditions and in our daily life. The substance of a one-photon process is that a molecule (or atom) may absorb a photon from the incident light field and simultaneously make a transition from a lower energy level to a higher level, or conversely, the molecule may emit a photon through a transition from a higher energy level to a lower level. Owing to the conservation of energy, in these cases, the absorbed (or emitted) photon's energy must equal the spacing between the two energy levels involved in a molecular transition.

In 1931, the concept of the two-photon absorption (2PA) process was first proposed by M. Göppert-Mayer (1906−1972) in her doctoral dissertation[1] at Göttingen University, which was supervised by Max Born, a Nobel laureate and one of the most distinguished physicists in the twentieth century. In this pioneering paper, she theoretically predicted that a simultaneous 2PA process should also lead to a transition between a lower and a higher energy level of an atom or a molecule. This prediction was based on the principles of the newly established quantum theory of radiation,[2] and the key issue to support her argument was to introduce the concept of an intermediate state. Based on this concept, the author derived an expression for the 2PA probability which involved the summation over all eigenstates of the atomic or molecular system. This probability was too small to be measured with any conventional (incoherent) light for excitation. Due to this reason, no real 2PA had been observed until the advent of the laser in the beginning of 1960s.

In 1961, 1 year after the invention of the first laser device,[3] Kaiser and Garrett reported the first observation of a 2PA-induced frequency-upconversion fluorescence in a $CaF_2:Eu^{2+}$

Qingdong Zheng received the B.S. degree in fine chemicals and the M.S. degree in applied chemistry from East China University of Science and Technology, China, in 1998 and 2001, respectively. In 2005, he obtained his Ph.D. degree in chemistry from the State University of New York (SUNY) at Buffalo with Professor Paras N. Prasad in the design, synthesis and applications of multiphoton absorbing materials. Currently, he is a postdoctoral research associate in the Institute for Lasers, Photonics and Biophotonics, SUNY at Buffalo. His research interests are in area of photon-active materials and their applications including multiphoton-induced biosensing, lasing, photodynamic therapy, and optical power limiting. He is the author/coauthor of more than 25 publications in scientific journals.

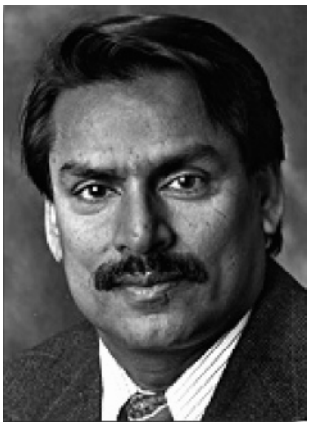

Paras N. Prasad, Executive Director of the Institute for Lasers, Photonics and Biophotonics, is a Distinguished Professor of Chemistry, Physics, Medicine and Electrical Engineering at the State University of New York at Buffalo. He also holds the Samuel P. Capen Chair. He has published more than 500 scientific papers and co-edited 5 books. He coauthored a monograph, "Introduction to Nonlinear Optical Effects in Molecules and Polymers" (Wiley) and authored two recent monographs, "*Introduction to Biophotonics*" (Wiley Publication) and "*Nanophotonics*" (Wiley Publication). Dr. Prasad is a Fellow of the American Physical Society and a Fellow of the Optical Society of America. He is also a recipient of the prestigious Sloan and Guggenheim fellowships.

crystal sample, excited by the intense coherent radiation of 694.3 nm wavelength from a pulsed ruby-crystal laser.[4] This was the first experimental confirmation of the prediction given by Göppert-Mayer 30 years before. Since then, a new major research area of two-photon and multiphoton processes has been opened to scientists and engineers. Relying on the advantages of high directionality, high monochromaticity, high brightness, and tunability of coherent radiation from various types of laser devices, it is now possible to oberve not only 2PA related processes but also three-photon absorption (3PA), four-photon absorption (4PA), and even higher-order multiphoton excitation related processes.

It is interesting to note that, as the idea originator of two-photon process, Göppert-Mayer won the Nobel Prize in physics in 1963, not for her two-photon work but for her major contribution to nuclear physics, i.e., the nuclear shell model. However, her seminal contribution to the multiphoton studies will also be remembered.

1.2. Significance of Multiphoton Related Studies

Multiphoton related studies include both fundamental research and applications of multiphoton absorption, multiphoton excitation, and multiphoton active materials. Here, multiphoton absorption means simultaneous absorption of a number (≥ 2) of photons, accompanied by the transition of an absorbing molecule from a lower energy level to a higher level. However, multiphoton excitation has a much broader meaning that includes other physical, chemical, and biological effects upon simultaneous interaction of a number (≥ 2) of photons with matter. For instance, multiphoton excitation not only may lead to nonlinear attenuation of an incident coherent light beam but also may create various other effects, such as enhanced refractive-index changes of the medium, molecular dissociation or ionization, electron emission from the material's surface, induced conductivity in semiconductors, and induced polymerization. All materials that can manifest such photophysical or photochemical responses upon multiphoton excitation are multiphoton active. In order to realize such higher-order multiphoton excitation, a high local intensity (in units of MW/cm^2 or GW/cm^2) of the incident light beam is needed.

From the viewpoint of fundamental research, multiphoton related studies may greatly enrich and deepen our knowledge and understanding about interactions of intense coherent radiation with matter.[5−10] The following are several specific examples that have shown how much our prior knowledge has to be renewed and how valuable new information is obtained from these studies.

(i) *Multiphoton-induced surface photoelectric effect*: According to the previous theory of one-photon-induced electron emission from the surface of a given photocathode material, once the wavelength of light signals is longer than the so-called "red-limit", no electron emission from the surface can be observed. This is one of the key experimental facts on which Einstein based his postulate of light radiation consisting of photons. Now people know that, by utilizing an intense IR coherent radiation with a wavelength longer (or much longer) than the red-limit, a two-photon- or multiphoton-induced electron emission from the same photoelectric device can be observed. A similar situation also exists for the volume photoelectric effect in a semiconductor device.

(ii) *Multiphoton-induced photochemical reactions*: It was previously known that some photochemical reactions, including the most familiar photographic effect, depend not only on the illumination intensity but also on the wavelength of the light signal. For a given photographic emulsion material, if the light wavelength is notably longer than a certain limit, no photographic response can be expected. This was true for the light signals from incoherent light sources, and it was another experimental fact based on which Einstein made his postulate about photons. Similar rules also held for some other photochemical reactions (such as photopolymerization) that need UV or short-wavelength visible radiation. In the wake following the invention of lasers, however, it has been found that the aforementioned photochemical reactions could also be produced using intense coherent IR radiation, based on two-photon or multiphoton excitation processes.

(iii) *New knowledge brought by two-photon-process studies*: In general, the selection rules and pathways of molecular transitions upon multiphoton excitation may be different from those of one-photon excitation. For this reason, valuable new spectral information about molecular energy-level structure and transition properties of multiphoton active media can be obtained through multiphoton related studies.[11] During the 1970s and 1980s, the main research theme in this new area was focused on two-photon spectroscopy of simple atomic and molecular gaseous systems, organic solvents and compounds, as well as inorganic crystals and semiconductors. All these studies have brought a great deal of new information and knowledge on electronic, vibrational, and even rotational states of the investigated atomic and molecular systems. Over this time period, many research groups contributed their excellent work to this new field. It is worth mentioning some of them, including Hochstrasser et al.,[12] McClain et al.,[13] Birge et al.,[14] Haas et al.,[15] Hohlneicher et al.,[16] Schlag et al.,[17] Froehlich et al.,[18] Hänsch et al.,[19] Grynberg et al.,[20] and Levenson et al.[21]

(iv) *High-order multiphoton studies*: After the advent of lasers, many researchers still thought that a two-photon excitation process was easy to observe by utilizing a pulsed and focused laser beam, but a high-order multiphoton excitation would be more difficult to produce. Further development of relevant studies has shown that, by excitation with nanosecond laser pulses, three-photon absorption (3PA) can be readily realized in semiconductors and organic dye solutions, and four-photon absorption (4PA) can also be easily produced by using femtosecond laser pulses in organic materials. In addition, the early investigations of multiphoton-induced molecular dissociation even showed that a process involving a ten-photon excitation was observable at quite low-intensity levels of an IR laser beam with long wavelengths.[5] In other words, experimental results have shown that, in many cases, multi(>2)-photon excitation processes can be produced much easier than what had been thought before. A fundamental interpretation of these experimental facts has been an interesting subject for further studies.

From the 1990s on, researchers put more effort on developing various multiphoton active materials and seeking for their applications. Multiphoton studies have provided great potentials and opportunities for developing various new techniques that exhibit some specific advantages, compared to other conventional techniques based on one-photon processes. All these advantages are based on the following two features, which are inherently possessed by all types of multiphoton processes: (i) a longer or much longer wavelength of coherent light can be used, and (ii) there is a nonlinear dependence of the multiphoton excitation probability on the local intensity of the applied coherent light field. The major areas of multiphoton-excitation-based applications include (but are not limited to) the following: *(1) multiphoton pumped (MPP) frequency-upconversion lasing, (2) multiphoton-absorption (MPA)-based optical limiting, stabilization, and reshaping, (3) MPA-based stimulated scattering, (4) multiphoton-excitation (MPE)-based frequency-upconversion imaging and scanning microscopy, and (5) MPE-based three-dimensional data storage and microfabrication.* The technical details and specific advantages of these applications will be discussed in section 6.

1.3. Scope and Organization of This Review

As we mentioned above, since the early 1990s, the interests in the multiphoton areas have shifted from pure spectroscopy of individual molecules to developing new materials and exploring their technical applications. Particularly, in the past 10−15 years, the studies of various multiphoton active materials have progressed much faster than before, mainly promoted by the tremendous potentials and prospects of their applications. For this reason, this review is mainly to summarize and evaluate the achievements in multiphoton related studies within the recent 10−15 years and to focus on the following three major issues: (*i) design and synthesis of novel organic multiphoton active materials (from small organic chromophores to dendrimers, polymers as well as metal-containing compounds and other advanced materials), (ii) nonlinear optical characterization of these novel materials, and (iii) multiphoton-technique-based applications of these materials*.

To show the increasing research momentum of multiphoton related studies in the past decade, we may consider the numbers of research papers with the multiphoton theme published in this period of time. One may easily use the software *SciFinder* as a tool for searching the pertinent papers. For instance, if one simply specifies "*two-photon absorption*" as the keyword to search only the articles published in scientific journals written in English, the number of papers published from 1985 to 1995 was ∼700, whereas ∼2900 papers were published from 1995 to 2006.

Since there is a large amount of published references, we have to restrict the number of citations in this review. For this reason, only a limited number of papers published in journals peer-reviewed and written in English are cited in this review, based on their novelty, significance, innovation, technical merit, or the sequence of their publication dates. For the same reason, other types of references, such as patents, preprints, abstracts, and summaries of conference presentations, are not cited. Also, short review papers and articles in the proceedings of meetings are generally not cited in this review, with a few exceptions. As the paper search is based on the *SciFinder* system by using appropriate keywords, some publications of importance may still be inadvertently missed; if that is the case, we apologize to the authors of those papers.

2. Basic Concepts and Descriptions of Multiphoton Absorption

2.1. Basic Descriptions of Multiphoton Absorption (MPA)

In principle, there are two regimes of theories which can be utilized to describe the nonlinear optical effects, including MPA processes. The first is the semiclassical theory, and the second is the quantum electrodynamical theory.[5−7]

The most essential feature of the semiclassical theory is that the media composed of atoms or molecules are described by the theory of quantum mechanics, while the light fields are described by the classical Maxwell theory. The key feature of the semiclassical theory in nonlinear optics is an explicit expression for the nonlinear electric polarization of an optical medium. It is generally known that the electric polarization vector $\vec{\mathbf{P}}$ of a medium is defined by the summation of the light field-induced electric-dipole-moment vectors of all molecules within a unit volume. In the case of applying a weak light field from an incoherent light source, $\vec{\mathbf{P}}$ is linearly proportional to the applied electric field $\vec{\mathbf{E}}$. If this field is a monochromatic wave with an angular frequency ω, we have

$$\vec{\mathbf{P}}(\omega) = \vec{\mathbf{P}}^{(1)}(\omega) = \epsilon_0 \chi^{(1)}(\omega)\vec{\mathbf{E}}(\omega) \quad (1)$$

Here $\chi^{(1)}(\omega)$ is the first-order (linear) susceptibility (in SI units) of a given medium, and ϵ_0 is the free-space permittivity. In general, $\chi^{(1)}(\omega)$ is a complex parameter in the form of a second-rank tensor; its real part determines the refractive index of the medium, while its imaginary part can be used to determine the linear (one-photon) absorption.[7] To further consider the nonlinear absorption of a strong monochromatic coherent light of frequency ω, which penetrates through an isotropic or centrosymmetric medium, eq 1 has to be generalized as

$$\begin{aligned}\vec{\mathbf{P}}(\omega) &= \vec{\mathbf{P}}^{(1)}(\omega) + \vec{\mathbf{P}}^{(3)}(\omega) + \vec{\mathbf{P}}^{(5)}(\omega) + ... \\ &= \epsilon_0[\chi^{(1)}(\omega)\vec{\mathbf{E}}(\omega) + \chi^{(3)}(\omega,\omega,-\omega)\vec{\mathbf{E}}(\omega)\vec{\mathbf{E}}(\omega)\vec{\mathbf{E}}^*(\omega) + \\ &\chi^{(5)}(\omega,\omega,-\omega,\omega,-\omega)\vec{\mathbf{E}}(\omega)\vec{\mathbf{E}}(\omega)\vec{\mathbf{E}}^*(\omega)\vec{\mathbf{E}}(\omega)\vec{\mathbf{E}}^*(\omega) + ...] \end{aligned} \quad (2)$$

Here $\vec{\mathbf{E}}^*(\omega)$ is the complex conjugate of the electric-field function $\mathbf{E}(\omega)$ of the applied light wave. $\chi^{(3)}(\omega,\omega,-\omega)$ is the third-order nonlinear susceptibility of the nonlinear absorbing medium; in general, it is a complex fourth-rank tensor: its real part describes the induced refractive index change depending on the light intensity $I(\omega) \propto |\vec{\mathbf{E}}^*(\omega)\cdot\vec{\mathbf{E}}(\omega)|$, while the imaginary part can be utilized to phenomenologically describe the 2PA.[7,8] Similarly, $\chi^{(5)}(\omega,\omega,-\omega,\omega,-\omega)$ is the fifth-order nonlinear susceptibility; in general, it is a complex sixth-rank tensor: its real part describes the induced refractive index change which depends on the square of the light intensity, $I^2(\omega)$, while the imaginary part can be utilized to phenomenologically describe the three-photon absorption (3PA). In more general cases, when the applied optical field consists of more than one frequency component, various nonlinear multiwave frequency-mixing processes may take place and can be described by corresponding nonlinear susceptibilities. In these cases, the nonlinear susceptibility of the medium will depend on the applied frequency components as well as the outcomes of their various possible combinations. However, it should be noted that this type of semiclassical theory treats light waves as classical electromagnetic fields, no quantized concept of "photon" is involved; therefore, it does not provide a rigorous description of the elementary processes of MPA.

In contrast, the quantum theory of radiation in the regime of quantum electrodynamics treats the medium and the optical field as a combined quantized system.[22−24] In other words, both the medium and the optical field should be described quantum-mechanically. As a result, the wave function of the combined system is expressed by the product of the eigenfunction of a molecular system and the eigenfunction of a quantized photon field. In this case, the key issue is to determine the probability of state changes of the combined system due to interaction between the photon field and the medium. Usually, state changes of the combined system are related to the transition of the molecular system from an initial eigenstate to a final state, accompanied by simultaneous changes of the photon numbers among different photon modes (or photon states).

The quantum theory of radiation is a more rigorous approach that, in principle, can be perfectly used to explain MPA processes in both qualitative and quantitative ways. To do so, it is necessary to introduce the concept of intermediate states occupied by the combined system of the photon field and a molecular system. Based on the concept of intermediate states, the principles and mechanisms of nonlinear optical effects (including MPA) can be consistently interpreted.[7]

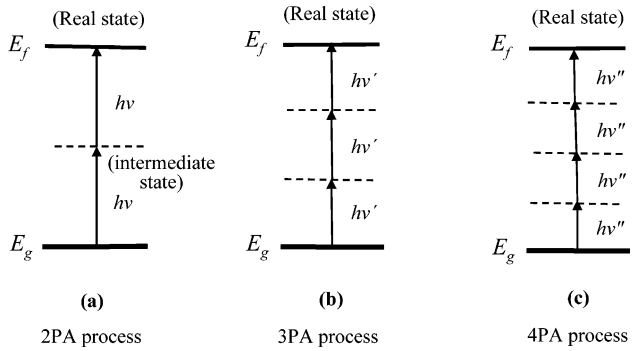

Figure 1. Schematic description of an elementary multiphoton-induced molecular transition process. Solid lines represent real eigen states; dashed lines represent intermediate states.

For simplicity, let us first consider the elementary process of 2PA induced by a single laser beam of frequency ν passing through a nonlinear absorbing medium. The schematic diagram for this process in the regime of quantum theory is shown in Figure 1a with the help of introducing the concept of an intermediate state that can be schematically represented by a dashed line level between two real eigenstates of the molecule. In this case, the occurrence of 2PA inducing molecular transition between its two real states can be visualized as a "two-step" event. (i) In the first step, one photon is absorbed while the molecule leaves its initial state E_g to be excited to an intermediate state. (ii) In the second step, another photon will be absorbed while the same molecule completes its transition from the intermediate state to the final real state E_f. The key connection between these two steps is the intermediate state in which the molecular status is not certain in the sense that the molecule may stay in all its possible eigenstates (except E_g and E_f) with a certain probability of distribution on them. Because this uncertainty of the distribution range is so large, according to the uncertainty principle, the residence time of the molecule in the intermediate state should be infinitely short. Thus, it means that these imagined "two steps" of 2PA actually occur simultaneously. In other words, the real 2PA is a single elementary process that is essentially different from the so-called *cascaded* two-step one-photon processes. In the first step of the latter case, the molecule absorbs one photon to reach a real excited state with a certain lifetime, followed by the second step when this excited molecule absorbs another photon to reach a higher real level. Obviously, in this situation the two transition steps can take place in different time sequences.

Similarly, as shown in Figure 1b, we can describe the elementary process of 3PA, in which three photons can be simultaneously absorbed by a single molecule through two intermediate states schematically represented by two dashed lines. For easy understanding, this 3PA process may be imagined by the following three "steps": (i) in the first step, one photon is absorbed while the molecule leaves its initial state E_g to be excited to an intermediate state represented by the lower dashed line; (ii) in the second step, another photon is absorbed while the same molecule makes a transition to another intermediate state (the middle dashed line); (iii) in the third step, one more photon is absorbed when the excited molecule reaches its final real state E_f.

Based on the same consideration of the uncertainty principle, these imagined "three steps" take place simultaneously. In this sense, the real 3PA of a molecule is also a single elementary process, resulting from the quantized interaction between radiation and matter. A similar description can be applied to multi(>3)-photon absorption by involving more intermediate states. As one more example, Figure 1c shows the elementary process of 4PA. In all these cases, to meet the requirement of conservation of energy, the following resonance conditions should be fulfilled:

$$E_f - E_g = 2h\nu \text{ (2PA)}; \quad E_f - E_g = 3h\nu' \text{ (3PA)}; \quad E_f - E_g = 4h\nu'' \text{ (4PA)} \quad (3)$$

So far we have only considered the absorption of multiple photons having the same frequency, which is termed *degenerate* multiphoton absorption. In more general cases, the applied light field may contain two or more frequency components, and the simultaneous absorption of several photons having different frequencies is also possible. This is termed *nondegenerate* multiphoton absorption. The theoretical descriptions are essentially the same for both degenerate and nondegenerate MPA processes.

From the viewpoint of the semiclassical theory of nonlinear optics, 2PA is a third-order nonlinear optical process which requires a high light intensity; 3PA is a fifth-order nonlinear optical process which requires even a much higher light intensity. The quantum theory of radiation gives the same conclusions.

2.2. Brief Formulations of MPA-Induced Light Attenuation

The attenuation of a light beam passing through an optical medium can be generally expressed by the following phenomenological expression:

$$\frac{dI(z)}{dz} = -\alpha I(z) - \beta I^2(z) - \gamma I^3(z) - \eta I^4(z) \ldots \quad (4)$$

Here $I(z)$ is the intensity of the incident light beam propagating along the z-axis and α, β, γ, and η are the one-, two-, three-, and four-photon absorption coefficients of the transmitting medium, respectively. For simplicity, here we have assumed that the incident light has a uniform transverse intensity distribution and the initial intensity is not dependent on time. Under the conditions that there is no linear absorption ($\alpha = 0$) at the wavelength λ of the incident light, and only 2PA satisfying eq 3 takes place, we have

$$\frac{dI(z)}{dz} = -\beta I^2(z) \quad (5)$$

The physical meaning of this expression is that the 2PA probability of molecules in a given position is proportional to the square of the local light intensity. The solution of eq 5 is

$$I(z,\lambda) = \frac{I_0(\lambda)}{1 + \beta(\lambda)\, I_0(\lambda) z} \text{ (2PA)} \quad (6)$$

Here, $I_0(\lambda)$ is the incident light intensity with a top-hat pulse shape, z is the propagation length in the medium, and $\beta(\lambda)$ is the 2PA coefficient that is a material parameter which depends on the wavelength of the incident light. As a macroscopic parameter that depends on the concentration of the two-photon absorbing molecules, $\beta(\lambda)$ (in units of cm/GW) can be further expressed as

$$\beta(\lambda) = \sigma'_2(\lambda) N_0 = \sigma'_2(\lambda) N_A d_0 \times 10^{-3} \quad (7)$$

Here σ'_2 is the molecular 2PA cross section (in units of cm^4/GW), N_0 is the molecular density (in units of 1/cm^3), N_A is Avogadro's number, and d_0 is the molar concentration of the absorbing molecules (in units of M). Equation 7 is precisely valid only when it can be assumed that the 2PA process is not too strong and most molecules are staying in their ground states. Otherwise, N_0 should be replaced by $\Delta N = N_1 - N_2$, where N_1 is the population density of the ground state and N_2 is the population density of the two-photon excited state. If N_2 is negligible, we have $\Delta N \approx N_0$. When two-photon excitation is strong enough and the depletion of the ground-state population is no longer negligible, the 2PA coefficient β will not be a material constant even for a given wavelength and concentration; instead it will depend on the input excitation intensity. This is the so-called 2PA saturation effect that will be further discussed in subsection 5.3.3.

Though the parameter $\sigma'_2(\lambda)$ is a directly measurable quantity (in units of cm^4/GW) that characterizes the average two-photon absorbability per molecule, one can also use another parallel expression for the 2PA cross section, defined by

$$\sigma_2(\lambda) = \sigma'_2(\lambda) \cdot h\nu \quad (8)$$

Here $h\nu$ is the photon energy of the input light beam. According to this definition, $\sigma_2(\lambda)$ is in units of cm^4/(photon/s) or simply cm^4 s. In practice, most of the measured values of $\sigma_2(\lambda)$ are in the range from 10^{-51} to 10^{-46} cm^4 s. For this reason, some researchers prefer to use another informal unit (GM, the name abbreviation of Göppert-Mayer), defined by

$$1 \text{ GM} = 10^{-50} \text{ cm}^4 \text{ s} \quad (9)$$

Based on eq 6, the nonlinear transmission for a two-photon absorbing medium with optical path length l_0 can be written as

$$T(I_0,\lambda) = \frac{I(l_0,\lambda)}{I_0(\lambda)} = \frac{1}{1 + \beta(\lambda)\, I_0(\lambda) l_0} \text{ (2PA)} \quad (10)$$

Similarly, for a pure 3PA process, eq 4 becomes

$$\frac{dI(z)}{dz} = -\gamma I^3(z) \quad (11)$$

The physical meaning of this expression is that the 3PA probability of molecules in a given position is proportional to the third power of the local light intensity. The solution of eq 11 is

$$I(z,\lambda) = \frac{I_0(\lambda)}{\sqrt{1 + 2\gamma(\lambda)\, I_0^2(\lambda) z}} \text{ (3PA)} \quad (12)$$

Here $\gamma(\lambda)$ is the 3PA coefficient (in units of cm^3/GW^2) of a given material, which is a macroscopic parameter depending on the concentration of the three-photon absorbing molecules. It can be further expressed as

$$\gamma(\lambda) = \sigma'_3(\lambda)N_0 = \sigma'_3(\lambda)N_A d_0 \times 10^{-3} \quad (13)$$

Here $\sigma'_3(\lambda)$ is the molecular 3PA cross section (in units of cm^6/GW^2). There is also a parallel definition of the 3PA cross section, i.e., $\sigma_3(\lambda) = \sigma'_3(\lambda)\cdot(h\nu)^2$ (in units of $cm^6\ s^2$). In obtaining eq 13, it is assumed that the 3PA process is not too strong and most of the molecules are staying in their ground state. Otherwise, N_0 should be replaced by $\Delta N = N_1 - N_2$, as described previously in connection with the 2PA process. Based on eq 12, the nonlinear transmission for a three-photon absorbing medium with a thickness of l_0 can be written as

$$T(I_0,\lambda) = \frac{1}{\sqrt{1 + 2\gamma(\lambda)\, I_0{}^2(\lambda) l_0}}\ (3PA) \quad (14)$$

For a pure 4PA process, we have

$$\frac{dI(z)}{dz} = -\xi I^4(z) \quad (15)$$

The physical meaning of this expression is that the 4PA probability of molecules in a given position is proportional to the fourth power of the local light intensity. The solution of eq 15 is

$$I(z,\lambda) = \frac{I_0(z)}{[1 + 3\xi(\lambda)\, I_0{}^3(\lambda) z]^{1/3}}\ (4PA) \quad (16)$$

Here $\xi(\lambda)$ is the 4PA coefficient (in units of cm^5/GW^3), which can be further expressed as

$$\xi(\lambda) = \sigma'_4(\lambda)N_0 = \sigma'_4(\lambda)N_A d_0 \times 10^{-3} \quad (17)$$

$\sigma'_4(\lambda)$ is the molecular 4PA cross section (in units of cm^8/GW^3). The parallel definition of the 4PA cross section is $\sigma_4(\lambda) = \sigma'_4(\lambda)\cdot(h\nu)^3$ (in units of $cm^8\ s^3$). Based on eq 16, the nonlinear transmission for a four-photon absorbing medium with a thickness l_0 is given by

$$T(I_0,\lambda) = \frac{1}{[1 + 3\xi(\lambda)\, I_0{}^3(\lambda) l_0]^{1/3}}\ (4PA) \quad (18)$$

In principle, the cross section values of σ_2, σ_3, and σ_4 for a given nonlinear absorbing medium can be theoretically calculated, provided that the complete information of the molecular eigenstate structure and transition parameters (including matrix elements of the dipole-moment operator for all possible transition combinations) are known. Unfortunately, for most commonly studied organic materials, the exact molecular eigenstate structure and transition properties are too complicated to calculate; thus, in many cases, theoreticians have to rely on some greatly simplified models to pursue the theoretical calculations. Nevertheless, it is much easier to experimentally determine MPA coefficient values by simply measuring the nonlinear transmission of the tested samples as a function of incident intensity levels at a given wavelength. If the input laser wavelength can be tuned over a broader spectral range, the complete MPA spectra can be eventually obtained.

It should be pointed out that all formulations presented in this subsection are based on the assumption that the incident light intensity is not dependent on time and has a uniform intensity distribution perpendicular to the beam direction. In the practice of multiphoton excitation, the applied light usually is a focused and pulsed laser beam, of which the intensity is a function of both space and time. In this case, to obtain more accurate results for the nonlinear absorption cross section, the above-mentioned formulations can be further modified, depending on the specific experimental conditions.[8]

2.3. Theoretical Descriptions of the 2PA Cross Section

A convenient way to derive a theoretical expression for the TPA cross section is the one used by M. Göppert-Mayer in her original work. Here the intermediate state shown in Figure 1 is expanded onto the eigenstates of the system under consideration, which form a complete set. For two coherent monochromatic beams linearly polarized, which are of different frequencies ω_1 and ω_2 and in resonance with an absorbing isotropic medium at the two-photon transition frequency, the 2PA cross section (in units of cm^4 s) for a molecule taking a direct transition from its ground state (o) to a final excited state (t) can be expressed (in SI units) as[7]

$$\sigma_2(\omega_1,\omega_2) = \left(\frac{2\pi}{c}\right)^2 \frac{\omega_1\omega_2}{6\epsilon_0{}^2 h^2} \left| \sum_b \left[\frac{(p_1)_{ob}(p_2)_{bt}}{\omega_{bo} - \omega_1} + \frac{(p_2)_{ob}(p_1)_{bt}}{\omega_{bo} - \omega_2} \right] \right|^2 g(\omega_1 + \omega_2)$$

$$= \left(\frac{2\pi}{c}\right)^2 \frac{\omega_1\omega_2}{6\epsilon_0{}^2 h^2} |\Lambda|^2 g(\omega_1 + \omega_2) \quad (19)$$

Here h is Planck's constant and ϵ_0 is the permittivity of free space; p_1 and p_2 are the components of the molecular dipole-moment vector operator along the polarization directions of the two light beams; the summation is over all one-photon transition-allowed eigenstates (b) of the molecule; $g(\omega_1 + \omega_2)$ is a normalized line shape function (with a dimension of second), and Λ represents all of the summation terms.

In more general cases, one (or two) of the incident light beams may possess more complicated polarization properties (such as being circularly or elliptically polarized). In these cases, according to ref 13a, one may introduce a generalized polarization unit vector ($\vec{\mathbf{S}}$) to describe the polarization state of an input light beam. For example, if the light is linearly polarized, we have $\vec{\mathbf{S}} = \{\cos\theta_x, \cos\theta_y, \cos\theta_z\}$; here θ_x, θ_y, and θ_z are the angles between the light polarization direction and the x-, y-, and z-axes of the laboratory coordinate system; for right circularly polarized light, we have $\vec{\mathbf{S}} = (1/2)^{1/2}\{1, -i, 0\}$; and for left circularly polarized light, we have $\vec{\mathbf{S}} = (1/2)^{1/2}\{1, i, 0\}$. Assuming that the two incident light beams have different polarization properties ($\vec{\mathbf{S}}_1$ and $\vec{\mathbf{S}}_2$), the summation terms in eq 19 can be rewritten as[13a]

$$|\Lambda|^2 = \left| \sum_b \left[\frac{(\vec{\mathbf{S}}_1\cdot\vec{\mathbf{p}}_{ob})(\vec{\mathbf{S}}_2\cdot\vec{\mathbf{p}}_{bt})}{\omega_{bo} - \omega_1} + \frac{(\vec{\mathbf{S}}_2\cdot\vec{\mathbf{p}}_{ob})(\vec{\mathbf{S}}_1\cdot\vec{\mathbf{p}}_{bt})}{\omega_{bo} - \omega_2} \right] \right|^2 \quad (20)$$

Here, $\vec{\mathbf{p}}_{ob}$ and $\vec{\mathbf{p}}_{bt}$ are the corresponding matrix elements of the molecular dipole moment operator. From this expression, one can clearly see that the magnitude of the 2PA cross section and the related selection rules are dependent on the combination of the two input light fields. On the other hand, the direction of the molecular dipole-moment vector is

generally dependent on the molecular orientation; therefore, for a system consisting of a great number of randomly orientated molecules, it is necessary to take an orientation average over the molecular assembly. Based on the above expression, researchers may investigate the details of molecular energy structures, selection rules, and other 2PA related properties by changing the polarization states of the input light fields.[13]

In the simplest case for a degenerate 2PA process, the input is a single linearly polarized light beam. In this case, eq 19 simplifies to

$$\sigma_2(\omega) = \left(\frac{2\pi}{c}\right)^2 \frac{\omega^2}{6\epsilon_0{}^2 h^2} \left| \sum_b \left[2\frac{(p_s)_{ob}(p_s)_{bt}}{\omega_{bo} - \omega} \right] \right|^2 g(2\omega) \quad (21)$$

Here $(p_s)_{ob}$ is the transition matrix element of the electric dipole-moment component along the polarization direction of the input light field. Once again, an orientational average is needed if the light-induced dipole-moment vector is dependent on the molecular orientation.

At the end of this section, it is worth indicating the following several remarks.

(1) Equations 19−21 are called sum-over-states expressions, as they include the summation over all eigenstates of the molecular system. In practice, it is extremely difficult to acquire a complete solution of all the eigenstates even for a simple chromophore system. To overcome these difficulties, researchers have to develop different approaches to simplify the theoretical modeling and simulation. Some of these approaches will be discussed in subsection 3.7.

(2) For an isotropic sample, the light polarization can change the cross section by not more than a factor of 2, which is negligible compared to the uncertainties of absolute cross section measurements that are described in section 5. However, the situation may be different for ordered samples such as a single-crystal system. In an extreme case, such a sample may be two-photon absorbing along one axis and two-photon transparent along another.

(3) The selection rules for one- and two-photon transitions are mutually exclusive, in the case of a centrosymmetric molecule. Since the dipole operator is ungerade, only an ungerade state can be reached from the usually gerade ground state. For the products of matrix elements that appear in eqs 19−21, the intermediate state b must be ungerade; otherwise, $(p)_{ob}$ vanishes. To make the second matrix element $(p)_{bt}$ nonzero, the final state t must be gerade. Transitions from the ground state to such a state are one-photon forbidden. The mutual exclusion between one- and two-photon transitions in centrosymmetric molecules is similar to the one known for IR and Raman transitions.

(4) In practice, there are several methods that can be used to measure the MPA coefficient and cross section values for a given medium. Since it is assumed that most readers who are interested in strongly multiphoton absorbing materials know how these materials are characterized, we present in the next section some strategies for the design of molecules with strong two-photon activity and then in section 4 a survey of novel two-photon active materials. The technical details of the methods that are used to characterize these materials are discussed in section 5. Readers that are not familiar with these methods are recommended to read section 5 first and then continue with section 3.

3. Strategies for Molecular Design: Some Important Considerations

As the recent flurries of activities in materials and applications development for multiphoton absorption (MPA) processes in research laboratories over the world continue unabated, the successful proofs-of-concept demonstrations in diverse areas, such as microfabrication, bioimaging, photodynamic therapy, frequency upconverted lasing, etc., indicate that the utility potential is tremendous. Much of the impetus for this technological exploration was provided by the syntheses of new dyes in the mid-1990s, which are much more efficient in direct 2PA than those commercially available. However, in the ensuing years, it became evident that, for the two-photon technology to realize its full potential, the design and synthesis of more active chromophores, together with the no-less-important secondary properties such as processability, photostability, and durability that depend on specific applications, will play a pivotal role. To facilitate the design and synthesis of new and more responsive dye molecules, a continuing need is to establish and fine-tune the structure/property relationships for a large number of organic and organic/inorganic structures with systematically varied molecular-structure factors and precisely reproducible characterization of multiphoton properties.

3.1. Molecular Structural Factors

The quantitative sensitivity of a two-photon molecular entity is determined by its 2PA cross section, commonly denoted by the symbols σ_2 or σ'_2, as described in a preceding section. For consistency, σ_2 will mainly be used in this review paper. The 2PA cross section σ_2 is, by definition, a molecular property in the sense that it is controlled by the molecular structure. This is different from the 2PA coefficient β, which is a macroscopic or bulk parameter proportional to the product of the 2PA cross section and the concentration of absorbing molecules or absorbing centers. Thus, an understanding of the structure−property relation requires a microscopic (quantum mechanical) theory describing electronic eigenstates as well as the transition behavior of a molecule. However, as we will see in section 5, in practice there are at least three extrinsic factors that have to be considered during the experimental determination of the 2PA cross section for a given molecular system: (a) the time scale involved in various absorption mechanisms, and the response speed limited by a specific measurement technique; (b) the perturbation of the state structure by the surroundings; and (c) the intensity limit at which other nonlinear absorptions and/or photochemical events may cause permanent changes in the molecular structure. In other words, for a meaningful comparison of σ_2 values of structurally similar or related molecular systems, the experimental conditions should be kept the same.

With electronic band gaps generally in the visible region, most organic π-conjugated molecules are naturally promising materials for 2PA applications in the near-IR, where they are usually transparent. From the viewpoint of electronic structures and photophysical processes, there is a strong correlation between intramolecular charge-transfer processes and two-photon absorptivity. Thus, it follows that the permanent ground-state dipole moment as well as the transition dipole connected to either the ground state or the excited state are theoretically considered to be key factors

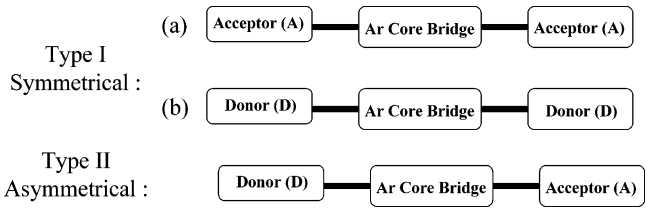

Figure 2. Molecular-structure motifs for one-dimensional two-photon absorbing chromophores. Ar = aromatic building block.

in 2PA process.[25] From the standpoint of designing an ideal molecular structure for a highly active 2PA chromophore,[26] a number of key molecular features have been identified. With an intramolecular charge-transfer process as the driving force,[27] the necessary, but not sufficient, presence of an electron-rich (π-donor) component, an electron-demanding (π-acceptor) component, or both components is rather obvious. In addition, the extent (i.e., path length) of conjugation has been identified as particularly important to the 2PA cross section, as it leads to states with extended charge separation.[28−30] Coplanarity is also critical in enhancing the efficiency of an intramolecular charge transfer. The detrimental presence of meta-linkages on the two-photon cross section has been nicely illustrated by the phenylethynyl-linked dipolar chromophores.[31] Additionally, the ground-state dipole strength in nonsymmetric molecules or the multipolar transition-dipole strength in centrosymmetric molecules has also been shown to greatly influence the 2PA in organic systems.[28,32,33] Increasing the number of conjugation paths, or connecting several linear paths to form a two-dimentional (2D) or a three-dimentional (3D) configuration has also been shown theoretically[34] and experimentally[33,35] to be able to greatly increase 2PA responses. It is also noteworthy that while solvent polarity (as ranked by the dielectric constants) can adversely influence the 2PA cross section values, hydrogen-bonding and the capability of the solvent to promote aggregation of the 2PA solutes are also important factors to consider.[36] While the performance of certain 2PA fluorophores was considerably reduced in aqueous environment compared to toluene, the micellar encapsulation of these 2PA fluorophores can greatly enhance their 2PA sensitivity to the extent that the cross section values are quite similar.[37] By and large, it appears that the effective cross section is more sensitive to the polarity of the local environment than the intrinsic 2PA properties.[38] More recently, the molecular structures that encourage the resonance conditions between two-photon states, one-photon states, and pulse wavelength have also been shown to have a drastic effect on the 2PA spectral outcomes.[39,40]

3.2. Evolution of Molecular Structure Motifs: Dipolar, Quadrupolar, and Octupolar Structures

Two parallel collaborative efforts should be credited with rekindling the R&D interest in two-photon materials with their fundamental work in structure−property relationships for this class of nonlinear optical materials, which continues to grow at an accelerating pace.[41,42] In an early publication of molecular structures with enhanced 2PA reported by Reinhardt, Prasad, et al.,[43] two general organic structural types were considered: (a) Type I chromophores (Figure 2) are symmetrical in nature and as, an example, consist of a π electron rich thiophene aromatic bridge flanked on either side with an electron poor heterocyclic benzothiazole group; (b) Type II chromophores (Figure 2) are asymmetrical molecules

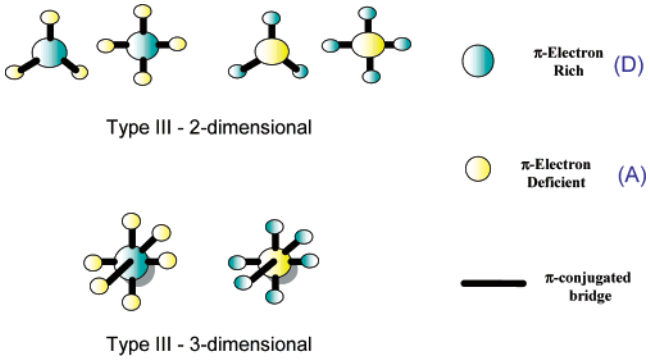

Figure 3. Basic structural motifs for 2D and 3D two-photon absorbing octupoles.

consisting of a highly fluorescent π electron rich aromatic/olefinic bridge flanked on one side by a thiophene or diarylamine π electron donor and on the other side by a pyridine or benzothiazole as a π electron acceptor. Pendant alkyl chains (R) are added to the aromatic bridge for solubility, and π electron donor functional groups (X) can be added to the aryl groups on the amine to increase electron density or provide reactive functional groups for the formation of high molecular weight polymers. Based on the results from a systematic variation of molecular structures, the type II asymmetrical, namely the dipolar molecules appeared to be more effective 2PA chromophores.

In about the same time period, Brédas, Marder, Perry, and co-workers also identified and articulated the design criteria for symmetrical structures [both types I(a) and I(b)] based on the direct correlation between large changes in quadrupole moment during photoexcitation and the 2PA cross section.[28] Accordingly, such quadrupolar molecules with alternating vinyl and 1,4-arylene groups as the π-connectors between two identical electron-pulling or electron-pushing (π-accepting) terminal groups are favored as more two-photon responsive chromophores. They are also described as either "push−push" [type I(a)] or "pull−pull [type I(b)]" chromophores, depending on whether the direction of intramolecular charge transfer is from the ends to the center of the molecule or vice versa. For designing the one-dimensional 2PA molecules, this model has gained increasing popularity in the ensuing years.

The important benefit of multidimensional conjugation was quickly recognized, and the use of molecular branching to further enhance the cross section values of 2PA molecules was first demonstrated in the three-branched structures such as AF-380,[44] AF-350,[45,46] and PRL-701.[47] This refined design concept (Type III, Figure 3) has since led to a rapidly growing collection of multibranched (or multiarmed) 2PA organics and is, in fact, a formal unification of type I and type II structures of Figure 2 with the added dimensionality. Thus, two or more dipolar molecules are joined together with extended conjugation. The flow of intramolecular charge transfer can be either from the ends to the center of the molecule or vice versa ("outside in" or "inside out"). These types of 2PA chromophores are octupolar when their overall molecular geometry belongs to the following symmetry classification: (octahedral) O_h, (tetrahedral) T_d, trigonal planar D_{nh} (n = 3, 4, ...), and trigonal bipyramid (C_{3h}).[48] Ideally, this design concept has two key elements that can result in a "cooperative effect" to enhance two-photon absorptivity: (a) an increase in the number density of active 2PA units per molecule and (b) the synergistic interactions

between the 2PA units via conjugation (through bonds) or perhaps "through-space but close-proximity" electronic interactions. Naturally, a variation of this concept using dendritic structures has also been investigated and validated with novel dendrimers[49,50] and hyperbranched polymers. In addition, this multidimensionality concept has also been applied successfully to coordination and organometallic compounds as well as nanoscale materials such as fullerenes. Extensive theoretical studies by several research groups have shown quantitatively the direct effects of various aspects of the molecular structure[33,51−54] as well as local surrounding effects on the 2PA cross section.

During the first phase of research activities on 2PA materials synthesis, a common objective appeared to be improving the nonlinear absorption efficiency for practical applications using near IR excitation. In addition, because of the popularity and easy availability of 800 nm laser sources, designing and synthesizing 2PA chromophores with the optimal performance at this wavelength was the main goal. However, the structural elements which can increase the effective conjugation length, degree of coplanarity, and extent of polarizability of the molecule not only increase the 2PA cross section but most likely shift the 2PA maxima toward the longer wavelength region. Hence, a major molecular design challenge at that time was to increase the molecular two-photon cross section without shifting the 2PA peak away from 800 nm. As the field evolves in parallel with the rapid advances made in laser equipment, and more potential applications are being identified to take the advantages (i.e., incident light with half the energy; greater depth penetration; localized excitation with spatial control; intensity-based switching) offered by the multiphoton processes, it became apparent that, in addition to 800 nm, other wavelengths such as 1.3 and 1.5 μm which are important in telecommunication as well as wavelengths in the visible are also of interest to specific groups of photonic device designers.

3.3. Molecular Components: Donors, Acceptors, and π-Bridges

There are three essential components that are required for highly two-photon active chromophores, namely a strong π-electron donor (D), a polarizable π-bridge, and a strong π-electron acceptor (A). The D and A groups can serve as either terminal groups or π-cores. Appropriate combinations and numbers of these components result in dipolar (asymmetric), quadrupolar (symmetric), or octupolar structures. Classical electron-withdrawing groups which have been used are nitro,[55−60] cyano/malononitrile,[28] sulfonyl,[57,59,61−67] triflyl (CF_3SO_2-),[62,63] arylcarbonyl (ArCO-), aldehyde (CHO),[59,68,69] and phosphonate.[55] Other structure units used as the terminal A groups include π-deficient heterocyclics,[70] such as 4-pyridyl, 2-benzoxazole, 2-benzimidazole, 2-benzothiazole,[68,69,71] quinoxazole, quinoline, oxadiazole,[72] thiazolothiazole,[73] 1,3,5-triazine, 4-pyridine-*N*-oxide,[74] triazole,[75] as well as the related ionic analogues, such as *N*-methylpyridium,[76,77] *N*-methylbenzothiazolium,[78] 1,3,3-trimethylindolium,[78] and organoboron groups.[79] However, it should be noted that an ionic character or a complete charge separation (i.e., zwitterionic) in a two-photon chromophore is expected not only to red-shift the one-photon absorption and emission but also to affect the two-photon spectrum, generally in the same direction. An interesting case where one-photon and 2PA bands were shifted in opposite directions has been reported for a quadrupolar pair with pyridine and ethylpyridium as terminal groups.[77] For the terminal D components, the disubstituted amino groups (dialkyl or diphenyl) are most common, mainly because of the ready availability as well as the balance in the oxidative stability and electron-donating capability of the amine. N-Substituted carbazoles and pyrroles are also acceptable terminal D components. For an intramolecular charge-transfer process to occur, an efficient π-conjugated bridge is required to facilitate the electronic flow. Phenylene-vinylene and its homologues, 2,7-fluorenyl and ethynyl/phenylethynyl, are popular hydrocarbon-based bridges for two-photon chromophore designs. Dihydrophenanthrene,[80] phenanthroline,[81] and anthracene[82] have also been shown to be quite effective; so are benzofuran and indole,[83] which is a promising approach for circumventing the problem of photoisomerization of a stilbene-like C═C bond. The combinations of aromatic carbocycles and heterocycles (thiophene, pyrrole, 2,1,3-benzothiadiazole, etc.) have also been used.[84,85] An interesting utilization of a paracyclophane structure to increase the molecular dimensionality and number density has been reported.[86]

3.4. Importance of Excited State Absorption in Cross Section Determination

The role of excited-state absorption (ESA) in magnifying the apparent two-photon cross section has to be pointed out because inherent in the nonlinear absorption (transmission) or fluorescence measurement using nanosecond or even picosecond laser pulses as excitation sources is the assumption that the direct (simultaneous) 2PA is the predominant process causing the observed intensity-dependent nonlinear absorption (excitation). However, as many researchers have indicated, a strong 2PA process may considerably increase molecular populations in excited states; thus, a secondary process, i.e., the cascaded one-photon absorption from an excited state may create an additional contribution to the observed nonlinear attenuation of the input laser beam (a 2PA-assisted excited-state absorption, ESA, i.e., a two-step, three-photon process).[87] In fact, 2PA followed by ESA has been described in the literature as early as 1974, with an estimated value for the product of the ESA cross section and the excited-state lifetime of the chromophore based on a rate equation analysis.[88] Several research groups have firmly demonstrated the effects of excited states on nonlinear absorption and refraction from the degenerate four-wave mixing and Z-scan experiments.[89−92] Evidence of ESA has also been reported from the nonlinear transmission (NLT) and Z-scan measurements of organic dyes,[93,94] and the ESA cross section values have been estimated from the intensity dependent 2PA coefficients.[92,95,96]

Since it is difficult to separate these two contributions through the NLT measurement in the nanosecond−picosecond range, the term "effective 2PA cross section" has been recommended to describe the σ_2 values under these excitation conditions for a two-photon chromophore. The effective cross section of a 2PA chromophore, often the value measured in the nanosecond regime by the NLT method, can be more than 2 orders of magnitude larger than the intrinsic cross section value obtained via a femtosecond measurement. A quantitative model has been proposed to determine the contribution of ESA to the 2PA coefficients obtained using nanosecond laser pulses for selected AFX chromophores.[97,98] A recent paper independently identified and characterized excited-state absorption dynamics and used this information

to theoretically predict or model nanosecond NLT measurements.[99] More details of this issue will be discussed in subsection 5.3.1.

3.5. Branching Effect and Cooperative Enhancement

By definition, cooperative enhancement or effect in multiphoton absorption (MPA) results in the measured cross section value being greater than the sum of the discrete MPA units that constitute the entire molecular system. The first experimental cooperative effect in an organic two-photon absorbing system was observed in multibranched 2PA molecules by Prasad et al.[47] Subsequently, the concept of higher dimensionality has been extended to conjugated systems such as phenylene-vinylene-based dendrimers[100,101] and organometallic dendrimers.[50] Similar 2PA enhancements in the multibranched and dendrimeric systems based on various types of cores such as 4,4′,4″-triphenylamine,[47,62,64,102−108] s-triazine,[109,110] 2,4,6-alkylpyridinium,[111] 1,3,5-tricyanobenzene,[112] 1,3,5-benzene,[85] truxene,[113] 3,5-dicyano-2,4,6-tristyrylpyridine,[114] and formally trivalent nitrogen (AF-380)[44] have been reported. It is rather surprising to observe a 2PA enhancement also in 1,3,5-benzene system, which has a much weaker electron-donating and -accepting ability in comparison to other cores. Hitherto, the largest cooperative 2PA enhancement (13−23 times the cross section value of the respective 2PA subunit, i.e., 4.5−7.5 fold enhancement) was reported for the 2,4,6-alkylpyridinium-based systems.[111]

Drobizhev et al. have developed a new quantitative method to determine the extent of conjugation described by the number and size of coherent domains (extent of conjugation) by comparing one- and three-photon measurements for two series of stilbene- and 1,4-distyrylbenzene-based dendrimers containing amine and diphenylamino moieties as branching points and end groups, respectively.[115] It is found that, in terms of the largest coherence domain size, the 4SG0 dendrimer, which contains an effective maximum number of conjugated π-electrons, $N_\pi \sim 150$, is the optimal dendrimer generation. This method of determining coherence domain size may be applicable also to other complex molecular nanosystems, such as *J*-aggregates, π-conjugated polymers, etc.[115] Based on a collection of stilbene- and 1,4-distyrylbenzene-linked quadrupolar molecules and related dendrimers, Kuzyk conducted a theoretical investigation using a sum-over-states model to compute the change in the 2PA cross section with the change in the number of effective π-electrons and developed an expression for the maximum limit of resonant two-photon cross section values.[116] The results for the related dendrimers indicated that while there was an increase in 2PA cross section with increasing number of effective π-electrons of the highly branched system and the magnitude of the 2PA effect would increase for larger structures, the intrinsic nonlinear response when normalized with the maximum-limit values would actually be quite similar to the magnitude obtained from the linear (monomer) or dimer system.[116]

3.6. Quantum Chemical Modeling of Multiphoton Absorption

Theoretical modeling, that is, numerical simulations of materials in order to describe their properties and interactions with applied fields, has become an increasingly viable and popular approach in contemporary research, covering a wide range of phenomena of technical as well as fundamental importance. Reliable theoretical predictions of structure-to-property relations are of importance as a potential alternative to costly and time-consuming synthesis and nonlinear optical measurements. Moreover, remarkable progress of efficient quantum chemistry methods, as well as of low-cost computer hardware, has sparked a broad interest in computations of nonlinear optical properties of molecules based on first principles. Substantial efforts have been made to improve the predictive capability of the first principle computations. In particular, density functional theory (DFT)[117] has gained acceptance in what concerns quantum chemical calculations of nonlinear properties of large organic structures, especially in connection with linear scaling algorithms and parallel performance. Combined with DFT, the response theory[118] has shown promise in the calculation of general linear and nonlinear properties, including multiphoton absorption. However, the newly developed theories and methods require a thorough benchmarking and calibration. It is fortunate that an increasing number of experimental data on complete spectra of 2PA cross section has now become available. This rectifies the previously common situation where only single-wavelength data were at hand. In this subsection, we will try to give a brief review of progress in theoretical modeling and simulations of nonlinear optical properties for molecules and solutions.

The 2PA probability rate of a molecular system is defined by the 2PA cross section σ_2, which is expressed by eq 19 (for nondegeneral 2PA) or eq 21 (for degenerate 2PA). In the lowest order of perturbation theory, it is determined by the resonant two-photon transition amplitudes, sometimes also called two-photon transition moments or two-photon matrix elements (see ref 119, for example). Equation 19 is a sum-over-states (SOS) expression where the summation is taken over all intermediate states, *b*, of the molecule. The 2PA cross section is proportional to the summation term $|\Lambda|^2$, which is determined by both the dipolar transition matrix elements and the input light polarization states.[13a]

Historically, two-photon transition matrix elements were first evaluated for anthracene and naphthalene molecules, making use of a three-state model,[120] where the corresponding electric dipole oscillator strengths were mostly obtained from experiments. These early, relatively straightforward evaluations were followed by fully *ab initio* calculations of two-photon transition matrix elements, for example for a water molecule,[121] using the random phase approximation (RPA), which is equivalent to the time-dependent Hartree−Fock (TDHF) method. The authors exploited the results of the RPA to compute the one-electron transition density matrices of both the initial−intermediate and the intermediate−final transitions.

In general, the interaction between the molecular system and the electromagnetic field can be described in terms of the time-dependent perturbation theory and the results can be expressed in terms of the so-called response functions. The main advantage of the response theory (RT) is that one can avoid the tedious and time-consuming explicit summation over molecular eigenstates to get frequency dependent polarizabilities and hyperpolarizabilities. In this case, the residues of the response functions determine first, second, and higher order transition matrix elements. The RT is gaining popularity as a tool that allows for speedy screening of newly synthesized organic compounds. For example, the RT applied to the single-determinant Hartree−Fock reference

state was employed[122] to calculate the single residue of the quadratic response function that determines the 2PA transition moments, for a series of organic molecules. The effects of π-centers and symmetry were studied in this work. The same method was used to screen a series of platinum organic compounds.[123] Here, the effect of charge-transfer substitutions was discussed along with tailoring the linear absorption to a desired wavelength. Those are just two examples of a large number of works devoted, using different methods—from semiempirical to *ab initio*, to establishing structure−property relationships. It is worthwhile to note that the TDHF method is the lowest one in the hierarchy of first principles quantum chemical calculations of molecular optical properties. The multiconfigurational self-consistent field (MCSCF) method gives much better accuracy than TDHF due to a better description of the reference state by means of a linear combination of different (excited) electronic configurations (determinants). In this case, not only molecular orbital coefficients are optimized in the framework of the MO-LCAO (molecular orbital−linear combination of atomic orbitals) theory but also the weight coefficients of different configurations are. The RT applied to the MCSCF reference state was used to calculate the two-photon transition probability rate constant for H_2O,[124] argon, and CO.[125] The next level in the *ab initio* hierarchy—the coupled cluster (CC) singles (CCS) and doubles (CC2) response theory that accounts for the effect of electron correlation—was used to determine the two-photon transition probability rate constants of helium, neon, and argon, with good agreement with experimental results.[119] A benchmarking study and comparison of the coupled cluster CCS, CC2, CCSD, and CC3 results with those obtained from Hartree−Fock and density functional response theories were undertaken for formaldehyde, diacetylene, and water molecules.[126]

Unlike self-consistent field methods, the density functional theory focuses on the electron density rather than wave functions and molecular orbitals. The DFT has been employed in a vast number of applications because of its computationally less demanding way of tackling the electron correlation. The 2PA cross section described in terms of the single residues of the quadratic response function was derived from the density functional theory using the time-dependent variation principle.[127] The cross section dependence on different functionals, including generalized gradient approximation (GGA) functionals and hybrid functionals, was investigated for a set of small molecules, and the results were compared with those obtained from coupled cluster calculations. The time-dependent density functional theory (TDDFT) was applied to calculate 1- and 2PA spectra for a series of large donor−acceptor-substituted conjugated molecules.[128] In this benchmark study, the linear response in adiabatic TDDFT was used to calculate the properties of interest and the results were compared with the experiment. The effects of molecular geometry were studied, and the basis set dependence of the 2PA cross section was investigated. Coulomb-attenuated functionals proved indispensable in terms of better agreement with experiment.[129,130]

To summarize, benchmarking 2PA of novel compound designs from response theoretical methods has become more interesting as multiphoton-based techniques evolve. However, there are still significant challenges in assigning contributions to measured 2PA cross sections that result from various intrinsic, such as vibronic coupling[131] and external fields, and extrinsic, such as laser pulse duration, factors. For example, the solvent effect on 2PA cross section can be described by means of the so-called polarized continuum model (PCM) and analyzed at different levels of theory, including the RPA quadratic response,[132] the DFT few-states model,[133] and full response DFT.[134] It is worthwhile to mention here that the few-states models are of great use if one is interested in a relatively inexpensive qualitative evaluation of the nonlinear absorption cross section or if a simple interpretation of the sum-over-states approach results is needed. In fact, the few-states model descends from the SOS model that may sometimes involve hundreds of excited states. It was, for example, shown that the SOS expression for the second-order hyperpolarizability can be simplified for donor−acceptor compounds in which the first low-lying charge-transfer excited-state dominates the optical response.[135] In that case, the summations over the excited-states electric dipole coupled to the ground state can be limited to that excited state alone, and the summation over higher-lying excited states goes over those few excited states which are strongly coupled to that charge-transfer (CT) state. This simplified SOS expression was used to study the effect of donor−acceptor substitution on 2PA cross section, and the evolution of the 2PA cross section in substituted stilbenes as a function of the degree of ground-state polarization.[136] The same model was used to calculate the 2PA cross section to the second excited state, where the use of a double-resonance approach enhanced the 2PA capability of some stilbene derivatives.[51] Generalized three- and four-state models of 2PA of charge-transfer organic compounds were developed and tested, making use of TDDFT calculations of corresponding excitation energies and transition dipole moments.[137] It has also been shown that even a simple two-states model involving the ground and the charge-transfer state can describe the 2PA cross section of an acceptor−π-donor system without a substantial loss of accuracy.[28]

Pertaining to the problem of assigning absolute values to 2PA cross section values, vibronic effects were studied for a series of multibranched molecules by means of the response theory, applied to a single determinant Hartree−Fock reference state (RPA).[138] It has been shown that the electronic coupling between adjacent branches alone cannot explain the experimental finding of a strong enhancement of the 2PA cross section over the single branch structure, whereas vibronic contributions can play an important role in this respect. Also, the effect of the electron acceptor strength on the 2PA cross section of a series of donor−acceptor *trans*-stilbene derivatives was considered,[52] where the RT applied to the Kohn−Sham reference state was employed and the account of vibrational broadening of the absorption spectra proved important for getting the correct order of magnitude of calculated 2PA cross section values.

As mentioned before, the first principles computations cannot account for some effects occurring in a real laser-beam-based experiment for multiphoton related study. Very often, the values of theoretically obtained parameters differ drastically, sometimes by orders of magnitude, from those obtained from experimental data. This issue was addressed in a series of papers,[139−143] where a dynamical theory of pulse propagation through a multiphoton active medium was developed. This theory, which relies on *ab initio* calculations of the molecular parameters (energies and transition dipoles) of few-states molecular models and thus combines quantum mechanics with classical electrodynamics, was applied to the problem of propagation of laser pulses of different length

through two- and three-photon active chromophores and also to the effect of cavityless lasing induced by 3PA. The intrinsic feature of the theory is that it does not employ conventional expansion of the nonlinear polarization in the power series over the electric field strength but rather uses the coupled equations for the density matrix which allow us to treat saturation effects and sequential processes of any order. The sequential mechanism of 2PA, with two consecutive one-photon absorption steps as opposed to conventional coherent one-step 2PA, plays an important role in the nonlinear attenuation of longer than femtosecond pulses and completely dominates in the nanosecond regime, which has long been a source of confusion when comparing the results of *ab initio* computations with the measured cross section values. It has been shown[139−143] that direct comparison of theoretical *ab initio* values with the experimentally measured ones is only possible when the latter are obtained from femtosecond pulse measurements. The sequential mechanism is not to be confused with the excited-state absorption mechanism (one-step 2PA followed by the excited-state absorption), which can be readily identified due to its cubic dependence on the input intensity. The sequential mechanism was demonstrated to lead to a pronounced difference in the band shapes of one-photon and 2PA spectra,[144] and its vital role in the formation of the 2PA spectrum was assessed to the dynamical interplay between coherent two-photon and two-step 2PA channels governed by the lifetime broadenings of the excited states and the dephasing rate of molecular coherence. The same mechanism involving the triplet manifold of states was shown to be crucial for clamping to occur in optical power limiting.[130,145]

In addition to the theoretical studies mentioned above, Das et al.[97,98,146] and Ren et al.[147,148] have presented their theoretical modeling and calculations of 2PA properties for some types of organic chromophore structures. Andrews et al.[149,150] have contributed their theoretical efforts to another interesting subject, i.e., the so-called fluorescence resonance energy transfer (FRET) or resonance energy transfer (RET) under multiphoton excitation conditions. There are also some theoretical analyses of 3PA properties in solids[151−153] and in organic chromophore structures.[54,154]

4. Survey of Novel Multiphoton Active Materials

Under an intense optical field, many classes of materials have been shown to be capable of participating in direct 2PA processes. In his rather extensive compilation of two-photon property data from the literature coverage up through ∼1995, Kershaw[155] has grouped them into (i) biological materials (bacteriorhodopsin, β-carotene, chlorophyll, NADH, i.e., the reduced form of nicotinamide adenine dinucleotide, retinal and derivatives, retinol, etc.); (ii) various commercial dyes; (iii) liquid crystals; (iv) oligomers and polymers; (v) organometallic materials; and (vi) other organic molecules ranging from simple aromatic hydrocarbons (benzene, naphthalene, pyrene, etc.) to heterocyclics (pyridine, pyrimidine, 5,10-diphenylphenazine, 1,4-bis[4-phenyloxazolyl]benzene, etc.).

Since 1995, the studies of two-photon active structures and materials have dramatically expanded. This section provides a survey of multiphoton materials with emphasis on 2PA cross section data. Because of the space limitation, the main literature coverage is from 1995 to 2005, but part of 2006 is included where possible.

4.1. Multiphoton Absorbing Systems

From the standpoint of developing photonic applications for nonlinear optical (NLO) materials, it could be said that, prior to approximately the mid-1990s, the interest in MPA materials was closely tied to developing molecular and polymeric materials that possess useful third-order optical nonlinearity or $\chi^{(3)}$ properties. Specifically, new and advanced $\chi^{(3)}$ materials were sought for all-optical computing and signal processing for telecommunication applications. For this application, the MPA processes, which are related to the imaginary component of third-order susceptibility and contribute to the attenuation of optical signals over a long distance, were to be minimized. While these nonlinear absorption processes had been shown to enhance $\chi^{(3)}$ properties of certain materials,[156] most research efforts in developing the $\chi^{(3)}$ materials for telecommunication applications were to find ways to curtail the adverse effects of MPA and other optical loss processes. As a consequence, prior to 1995, the reported materials (mainly organic dyes) had molecular 2PA cross section values of the order $1-10^2$ GM (1 GM = 10^{-50} cm^4 s, see eq 9). However, much larger values ($>10^3$ GM) have been reported in the last 10 years. This is truly spectacular progress over the past decade in designing and producing materials with extraordinarily high 2PA cross section values. Given the increasingly widespread interest, this rapid advance can be attributed to (i) a better understanding of the molecular design criteria for highly efficient materials; (ii) the improved and faster NLO characterization techniques which provide interactive feedback for further development; (iii) the appeal of using lower energy photons to achieve the results that would otherwise require using photons of two or more times the amount of energy.

4.2. Organic Molecules

Based on the discussion of the molecular design for small organic 2PA systems in the preceding section, organic molecules that show two-photon activity can be grouped into three general classes: (i) dipolar, A-π-D; (ii) quadrupolar, A-π-A; D-π-D; A-π-D-π-A; D-π-A-π-D; and (iii) octupolar; 3-branched, A_3-(D-core) and D_3-(A-core). Since many research groups have synthesized and characterized 2PA-active materials more or less along these guidelines of molecular design, and there is also an inherent difficulty in comparing 2PA cross section results obtained from different measurement techniques and under different experimental conditions, it is more convenient to tabulate the 2PA cross section data from each research group in separate tables. In this way, the compilation effort becomes more manageable and provides consistency in the data of each table (Tables 1−11 and Charts 1−11).

Before going through these tables, some remarks should be pointed out. First, even for the same sample tested at the same wavelength, and by using the same (nonlinear transmission) method, the apparent values of a 2PA cross section measured in the nanosecond regime are significantly greater than that measured in the femtosecond regime (e.g., see Tables 1 and 4). Second, some experimental results have shown that by using the two-photon excited fluorescence (2PEF) method, the measured σ_2 values of the same sample are almost the same in both the nanosecond and femtosecond regimes (e.g., see Tables 2 and 7). Finally, in some cases, there are obviously overestimated values of σ_2, reported without supplemental confirmations. Therefore, it is not fully

Chart 1. Structures for Organic Molecules Listed in Table 1

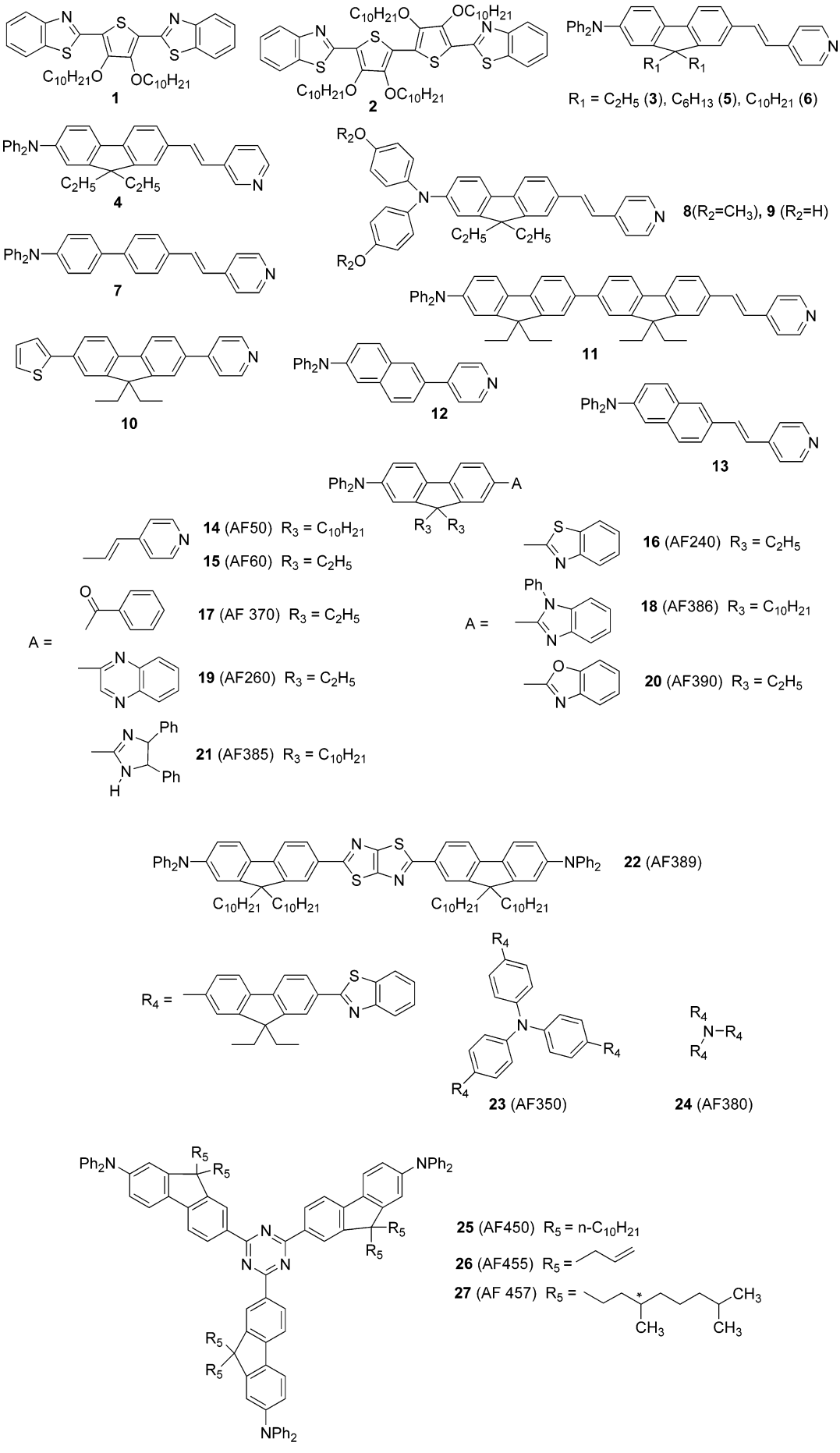

Table 1. 2PA Coefficients (β) and Cross Section Values (σ_2) for Organic Molecules[a]

material	method	β (cm/GW)	solvent	σ_2/GM	other properties
1	NLT, ns	0.2	490	$\lambda_{abs} = 390$ nm, $\lambda_{em} = 465$ nm	70
2	NLT, ns	1.4	2850	$\lambda_{abs} = 430$ nm, $\lambda_{em} = 521$ nm	70
3	NLT, ns	4.7	9700	$\lambda_{abs} = 388$ nm, $\lambda_{em} = 488$ nm	70
4	NLT, ns	4.7	7940	$\lambda_{abs} = 385$ nm, $\lambda_{em} = 478$ nm	70
5	NLT, ns	5.1	10610	$\lambda_{abs} = 389$ nm, $\lambda_{em} = 494$ nm	70
6	NLT, ns	5.6	11560	$\lambda_{abs} = 390$ nm, $\lambda_{em} = 492$ nm	70
7	NLT, ns	1.9	3900	$\lambda_{abs} = 367$ nm, $\lambda_{em} = 485$ nm	70
8	NLT, ns	5.6	11480	$\lambda_{abs} = 386$ nm, $\lambda_{em} = 488$ nm	70
9	NLT, ns	5.0	10300	$\lambda_{abs} = 392$ nm, $\lambda_{em} = 500$ nm	70
10	NLT, ns	0.06	131	$\lambda_{abs} = 345$ nm, $\lambda_{em} = 410$ nm	70
11	NLT, ns	3.8	7940	$\lambda_{abs} = 384$ nm, $\lambda_{em} = 492$ nm	70
12	NLT, ns	0.6	1290	$\lambda_{abs} = 347$ nm, $\lambda_{em} = 453$ nm	70
13	NLT, ns	3.3	6840	$\lambda_{abs} = 388$ nm, $\lambda_{em} = 488$ nm	70
14	NLT, ns	5.6	11560	$\lambda_{abs} = 390$ nm, $\lambda_{em} = 492$ nm	43
15	NLT, ns	4.7	9690	$\lambda_{abs} = 388$ nm, $\lambda_{em} = 488$ nm	43
16	NLT, ns	4.7	9770	$\lambda_{abs} = 392$ nm, $\lambda_{em} = 479$ nm	43
17	NLT, ns	4.1	8450	$\lambda_{abs} = 386$ nm, $\lambda_{em} = 490$ nm	43
18	NLT, ns	3.3	6710	$\lambda_{abs} = 370$ nm, $\lambda_{em} = 439$ nm	43
19	NLT, ns	1.9	3920	$\lambda_{abs} = 403$ nm, $\lambda_{em} = 552$ nm	43
20	NLT, ns	1.1	2270	$\lambda_{abs} = 389$ nm, $\lambda_{em} = 468$ nm	43
21	NLT, ns	0.2	390	$\lambda_{abs} = 384$ nm, $\lambda_{em} = 449$ nm	43
22	NLT, ns		58200	$\lambda_{abs} = 440$ nm, $\lambda_{em} = 508$ nm	43
22	NLT, fs		250		43
23	NLT, ns (fs)	13.5 (0.064)	23800 (132)	$\lambda_{abs} = 400$ nm, $\lambda_{em} = 485$ nm	109
24	NLT, ns (fs)	12.0 (0.047)	22800 (97)	$\lambda_{abs} = 428$ nm, $\lambda_{em} = 485$ nm	109
25	NLT, ns (fs)	19.2 (0.066)	39500 (137)	$\lambda_{abs} = 416$ nm, $\lambda_{em} = 505$ nm	109
26	NLT, ns (fs)	16.1 (0.061)	33300 (127)	$\lambda_{abs} = 410$ nm, $\lambda_{em} = 500$ nm	109
27	NLT, ns (fs)	13.5 (0.054)	27800 (112)	$\lambda_{abs} = 414$ nm, $\lambda_{em} = 518$ nm	109

[a] All the 2PA data are obtained by the nonlinear transmission (NLT) method in 0.02 M THF solutions. ~800 nm, ~8 ns dye-laser pulses and ~790 nm, ~140 fs Ti:sapphire laser pulses were used for these measurements. Nanosecond values measured at 800 nm; femtosecond values at ~790 nm are in parentheses. The nanosecond values are overestimated in comparison with femtosecond values, due to the excited-state absorption (for details, see the first paragraph of section 4.2).

meaningful to simply compare the σ_2 values reported by different research groups under different experimental conditions. The basic reason causing these discrepancies is that there are several different physical mechanisms that may lead to a huge divergence of the measurement results under different conditions. In addition, inappropriate designs of optical setups for 2PA measurements could easily lead to artificial results. All these issues will be addressed in section 5 in detail.

4.3. Organic Liquids and Liquid Crystals

Liquid crystals (LCs) are important materials for electronic display applications and because of their conjugative structure; their linear and nonlinear optical properties are actively investigated. However, there are only a few reports on molecular systems that possess thermotropic liquid crystalline properties and are capable of responding to a MPA process under appropriate temperature conditions. The MPA behaviors of organic liquid crystals reported until now have been observed mostly in their isotropic states, with a sole example (4-cyano-4′-n-pentylbipenyl or 5CB)[177,178] in a liquid crystalline phase. These examples include alkylcyanobiphenyls (5CB,[177,178] 8CB,[177−179] CB-15,[180] or a mixture of various alkylcyanobiphenyls;[181] the numeral denotes the number of methylene groups in the alkyl chain) and Schiff bases;[182] their two-photon properties were tabulated in Kershaw's review article.[155] In the case when 5CB was studied with the Z-scan (ns, 532 nm) in both the nematic and the isotropic phase, Yuan et al. reported[177,178] that it showed a large nonlinear birefringence with the ratio of refractive index parallel ($n_{2\parallel}$) and perpendicular ($n_{2\perp}$) to the beam propagation direction, $|n_{2\parallel}/n_{2\perp}|$, > 10 and strong anisotropy of the nonlinear absorption with $\beta_\parallel/\beta_\perp > 10$. As a side note, in the early work, the two-photon properties of liquid crystals *per se* were not the primary interest for this class of materials. It was during the third-order NLO experiments that substantial 2PA responses of thermotropic LCs were observed. However, rational synthesis to improve two-photon responses of liquid crystals, as illustrated by recent examples, invokes incorporating long alkyl chains to the termini of the rigid conjugated 2PA chromophores. In one case, large femtosecond 2PA cross section values in the isotropic phase (832 and 1992 GM, at 790 nm[183]) were reported, and in the other case, a large effective 2PA coefficient $\sigma_2 \sim 7 \times 10^{11}$ GM (neat sample at 100 °C, isotropic phase; $\beta = 6.25$ cm/GW, at 815 nm, 5 ns pulses) was also determined.[184]

Khoo et al. reported that 3-*n*-propyl-4′-*n*-butyldiphenylacetylene (L34), a clear liquid at room temperature, showed a two-photon coefficient of 4.1 and 25 cm/GW when the sample was irradiated with 15 ps and 7 ns laser pulse widths, respectively.[185]

4.4. Conjugated Polymers

Conjugated polymers such as polydiacetylenes,[186] poly(*p*-arylenevinylenes) (PPVs), *p*-phenylene-based ladder polymers,[187,188] as well as aromatic-heterocyclic polymers, e.g., polythiophenes,[189] polybenzobisazoles,[190] polyquinolines,[191] polyquinoxalines,[192] polyanthrazolines,[193] etc., have been the subject of intense interest for the study of third-order nonlinear optical processes.[194] Their fast responses and high third-order optical nonlinearity ($\chi^{(3)}$) could be attributed to their one-dimensional polymeric backbones with extended delocalization of the π-electrons that lends itself to the ease of polarization over large molecular distances. Therefore, for all-optical switching, and computing applications, practically all of the early research efforts in $\chi^{(3)}$ polymers were focused

Chart 2. Structures for Organic Molecules Listed in Table 2

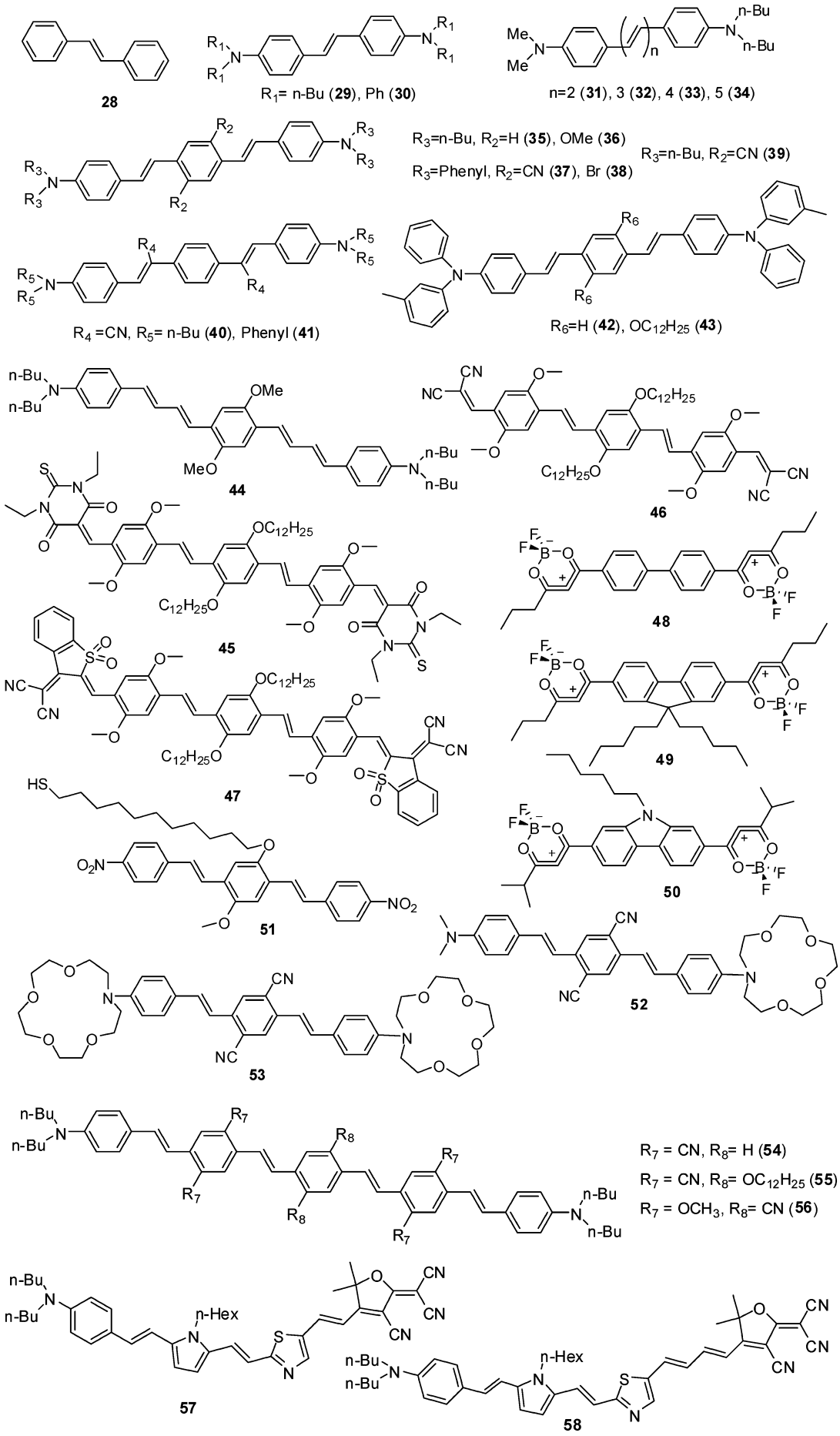

Table 2. 2PA Cross Section Values (σ_2) for Organic Molecules[a]

material	method	excitation wavelength/nm	solvent	σ_2/GM	other properties	ref
28	2PEF, ns	514	Tol	12		28
29	2PEF, ns (ps)	605 (620)	Tol	210 (110)	$\lambda_{abs} = 374$ nm, $\lambda_{em} = 410$ nm	28
30	2PEF, (ps)	(690)	Tol	(190)		96
31	2PEF, ns (ps)	640 (640)	Tol	260 (230)		96
32	2PEF, ns (ps)	710 (695)	Tol	320 (340)		96
33	2PEF, ns (ps)	730 (695)	Tol	425 (410)		96
34	2PEF, ns	730	Tol	1300		96
35	2PEF, ns (ps)	730 (725)	Tol	995 (635)	$\lambda_{abs} = 408$ nm, $\lambda_{em} = 455$ nm	28
36	2PEF, ns (ps)	730 (715)	Tol	900 (680)	$\lambda_{abs} = 428$ nm, $\lambda_{em} = 480$ nm	28
37	2PEF, ns (ps)	835 (810)	Tol	1940 (3670)	$\lambda_{abs} = 472$ nm, $\lambda_{em} = 525$ nm	28
38	2PEF, ns	800	Tol	450	$\lambda_{abs} = 424$ nm, $\lambda_{em} = 490$ nm	28
39	2PEF, ns (ps)	830 (830)	Tol	1750 (1710)	$\lambda_{abs} = 490$ nm, $\lambda_{em} = 536$ nm	28
40	2PEF, ns	790	Tol	890	$\lambda_{abs} = 438$ nm, $\lambda_{em} = 504$ nm	157
	2PEF, fs	800		860		157
41	2PEF, ns	825	Tol	730	$\lambda_{abs} = 440$ nm, $\lambda_{em} = 510$ nm	157
	2PEF, fs	825		690		157
42	2PEF, ns	745	Tol	805		157
43	2PEF, ns	745	Tol	855		96
44	2PEF, ns (ps)	775 (750)	Tol	1250 (1270)	$\lambda_{abs} = 456$ nm, $\lambda_{em} = 509$ nm	28
45	2PEF, ns	970	Tol	1750	$\lambda_{abs} = 554$ nm, $\lambda_{em} = 641$ nm	28
46	2PEF, ns	825, 940	Tol	480, 620	$\lambda_{abs} = 513$ nm, $\lambda_{em} = 580$ nm	28
	2PEF, (ps)	(815, 910)		(650, 470)		28
47	2PEF, ns (ps)	975 (945)	Tol	4400 (3700)	$\lambda_{abs} = 618$ nm, $\lambda_{em} = 745$ nm	28
48	2PEF, fs	588	CH_2Cl_2	433	$\lambda_{abs} = 373$ nm	158
49	2PEF, fs	612	CH_2Cl_2	489	$\lambda_{abs} = 414$ nm	158
50	2PEF, fs	~710	CH_2Cl_2	~530	$\lambda_{abs} = 422$ nm	158
51	2PEF, fs	770	DCB[b]	165	$\lambda_{abs} = 438$ nm, $\lambda_{em} = 599$ nm	58
52	2PEF, fs	810	CH_3CN	1800	$\lambda_{abs} = 468$ nm, $\lambda_{em} = 624$ nm	159
53	2PEF, fs	810	CH_3CN	2150	$\lambda_{abs} = 472$ nm, $\lambda_{em} = 610$ nm	159
54	2PEF, fs	970	Tol	3600	$\lambda_{abs} = 499$ nm, $\lambda_{em} = 564$ nm	160
55	2PEF, fs	960	Tol	4400	$\lambda_{abs} = 507$ nm, $\lambda_{em} = 570$ nm	160
56	2PEF, fs	970	Tol	5300	$\lambda_{abs} = 509$ nm, $\lambda_{em} = 599$ nm	160
57	2PEF, fs	840	THF	1420		161
58	2PEF, fs	1440	THF	1500	$\lambda_{abs} = 720$ nm	161

[a] All the 2PA data are obtained by the two-photon excited fluorescence method (2PEF); picosecond values are in parentheses. [b] 1,2-dichlobenzene

on minimizing the loss of optical signals over a long distance via MPA.

4.4.1. Polydiacetylenes

Polydiacetylenes are fully conjugated polymers with the generic repeat unit ═(CR−C≡C−CR)═. They are prepared by photochemical or thermal polymerization of the respective diacetylene monomers (R−C≡C−C≡C−R) in the crystalline state. The pioneering efforts of Sauteret et al. (second-harmonic generation) as well as Lequime and Hermann (2PA) in nonlinear optics in polydiacetylenes, in general, and single-crystal PTS, in particular, had stimulated the interest in these materials as nonlinear optical materials.[195] For improved solution-processability of diacetylenes, a variety of side groups are introduced. However, *n*-butoxycarbonyl-methyl-urethane as an R group, where *n* typically is 4 or 3, is commonly used, and the resulting polydiacetylenes are widely known as poly(*n*-BCMU). These conjugated polymers are organosoluble, and their wave guide samples for optical nonlinearity experiments can be fabricated via a spin coating method. The 2PA coefficient of 4,6-decadiyne-1,10-diol bis(butoxycarbonyl)methylaminocarboxylate polymer or poly(3-BCMU) has been measured at several selected wavelengths. The measurements have been performed in solution ($\beta = 0.52-0.76$ cm/GW),[196] in gel ($\beta = 0.52-0.76$ cm/GW),[197] and in a wave guide.[198] More recently, Banfi et al. reported the 2PA spectrum of a poly(3-BCMU) film, in the wavelength range $\lambda = 700-1600$ nm. The 2PA coefficient of the spin-coated film increased from ~2 cm/GW at 1450 nm to 170 cm/GW at 800 nm.[199]

Recently, Polyakov et al.[200] reported their improved femtosecond measurements of the dispersion in the nonlinear refraction and MPA in the quintessential poly(diacetylene), poly[2,4-hexadiyne-1,6-diol-bis(4-toluenesulfonate)] (commonly known as PTS), over the spectral range 1200−2200 nm. The PTS crystals (2PA coefficient ~ 60 cm/GW) used in these measurements were of much superior quality and were obtained from an improved crystal growth protocol. It was found that in addition to the major contribution of 2PA, 3- and 4-photon absorption mechanisms also contributed to the nonlinear absorption at most wavelengths and the intensity dependence at each wavelength was investigated to identify the different contributions.[200]

These nonlinear absorption results on poly(diacetylenes) and 5CB seem to indicate that the strong and positive influence of anisotropy in the bulk state (spin-coated film, crystal phase, and liquid crystalline nematic phase) can be due to MPA processes. However, on the molecular level, a recent semiempirical study has predicted that the orientation and alignment of dipoles can have a significant impact on the 2PA responses depending on whether the two covalently linked dipole molecules (labeled as M, $D_{\uparrow\uparrow}$, $D_{\downarrow\uparrow}$ for monomer and dimer in a parallel or an antiparallel geometry, in Chart 12) are in the antiparallel (negative effect) and "parallel but bent" (where $\alpha < 180°$; negative effect) or collinear (where $\alpha = 180°$, positive or enhancing effect) fashion.[201]

4.4.2. Polyphenylenevinylenes (PPVs)

Among the conjugated polymers, phenylenevinylene-based polymers are very promising for optoelectronic and photonic

Chart 3. Structures for Organic Molecules Listed in Table 3

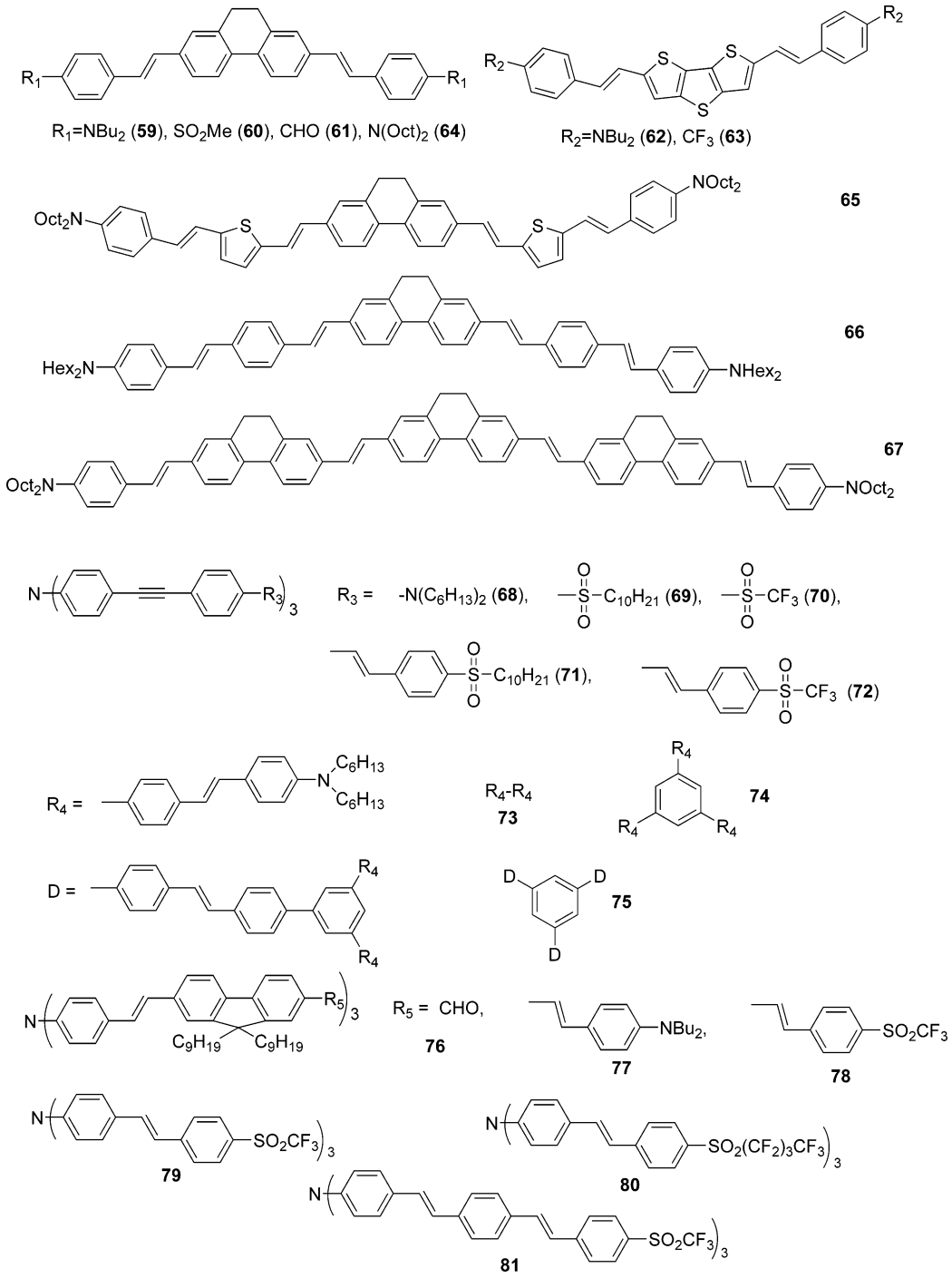

applications due to the combination of their excellent film-forming properties with their feasibility in tuning electrical and optical properties.[202] Of particular interest to the applications driven by nonlinear optical processes, PPV derivatives were shown to possess attractive multiphoton properties and the potential for their use in up-conversion lasing applications.[203]

Samoc et al.[204] reported the femtosecond 2PA coefficient for the parent PPV film samples that were prepared by the soluble polyelectrolyte precursor using tetrahydrothiophene as the leaving group rather than dimethylsulfide.[205] Their β values ($\sim$ 8 cm/GW at 800 nm) are higher than both the 5 cm/GW value determined by Lemmer et al.[206] in a pump−probe experiment with a 620 nm pump and a 700 nm probe, and the 6.8 cm/GW value determined for 50% PPV in a sol−gel matrix at 620 nm by Pang et al.[207] As the authors have pointed out, this was probably because their measurement wavelengths were very close to the two-photon resonance (836 nm; 2.95 eV), which was first measured by Baker et al.[208]

De Boni et al. studied for the first time a very wide band (460−1000 nm), nonlinear degenerate spectrum of poly[2-methoxy-5-(2′-ethylhexyloxy)-1,4-phenylenevinylene] (MEH-PPV) in chloroform using the femtosecond Z-scan technique.[209] The values obtained for the 2PA cross section values (per repeat unit) span from 14 000 GM at 600 nm to 6000 GM at 740 nm. These values are of the same order of magnitude as those reported previously using femtosecond pulses.[210] Their results revealed a peak around 600 nm stemming from both 2PA and saturable absorption, resulting

Table 3. 2PA Cross Section Values (σ_2) for Organic Molecules[a]

material	method	excitation wavelength/nm	solvent	σ_2/GM	other properties	ref
59	TPEF, fs	765	DMSO	1200	$\lambda_{abs} = 421$ nm, $\lambda_{em} = 540$ nm	59, 80a
60	TPEF, fs	740	DMSO	160	$\lambda_{abs} = 384$ nm	
61	TPEF, fs	730	DMSO	320	$\lambda_{abs} = 397$ nm, $\lambda_{em} = 513$ nm	
62	TPEF, fs	795	DMSO	530	$\lambda_{abs} = 465$ nm, $\lambda_{em} = 582$ nm	
63	TPEF, fs	730	DMSO	180	$\lambda_{abs} = 424$ nm, $\lambda_{em} = 510$ nm	
64	2PEF, fs	740	Tol	1730	$\lambda_{abs} = 410$ nm, $\lambda_{em} = 456$ nm	80b
65	2PEF, fs	740	Tol	2560	$\lambda_{abs} = 465$ nm, $\lambda_{em} = 521$ nm	
66	2PEF, fs	740	Tol	2270	$\lambda_{abs} = 428$ nm, $\lambda_{em} = 477$ nm	
	2PEF, fs	740	$CHCl_3$	3310	$\lambda_{abs} = 428$ nm, $\lambda_{em} = 522$ nm	
67	2PEF, fs	740	$CHCl_3$	3760	$\lambda_{abs} = 422$ nm, $\lambda_{em} = 514$ nm	
68	2PEF, fs	740	Tol	30	$\lambda_{abs} = 385$ nm, $\lambda_{em} = 411$ nm	62
69	2PEF, fs	740	Tol	160	$\lambda_{abs} = 388$ nm, $\lambda_{em} = 424$ nm	
70	2PEF, fs	740	Tol	495	$\lambda_{abs} = 405$ nm, $\lambda_{em} = 450$ nm	
71	2PEF, fs	740	Tol	1065	$\lambda_{abs} = 397$ nm, $\lambda_{em} = 446$ nm	
72	2PEF fs	740	Tol	1080	$\lambda_{abs} = 408$ nm, $\lambda_{em} = 473$ nm	
73	2PEF, fs	755	Tol	757	$\lambda_{abs} = 401$ nm, $\lambda_{em} = 455$ nm	162
74	2PEF, fs	755	Tol	407	$\lambda_{abs} = 384$ nm, $\lambda_{em} = 438$ nm	
75	2PEF, fs	755	Tol	798	$\lambda_{abs} = 375$ nm, $\lambda_{em} = 442$ nm	
76	TPEF, fs	770	Tol	1265	$\lambda_{abs} = 426$ nm, $\lambda_{em} = 481$ nm	104
77	TPEF, fs	740	Tol	3660	$\lambda_{abs} = 428$ nm, $\lambda_{em} = 471$ nm	
78	TPPF, fs	740	Tol	2080	$\lambda_{abs} = 440$ nm, $\lambda_{em} = 517$ nm	63
79	TPPF, fs	740	Tol	1340	$\lambda_{abs} = 435$ nm, $\lambda_{em} = 498$ nm	
80	TPPF, fs	755	Tol	1430	$\lambda_{abs} = 430$ nm, $\lambda_{em} = 494$ nm	
81	TPPF, fs	800	Tol	2070	$\lambda_{abs} = 435$ nm, $\lambda_{em} = 499$ nm	

[a] All the 2PA data are obtained by the two-photon excited fluorescence method (2PEF), and femtosecond laser excitation.

in a very large effective 2PA cross section. This implied that the pure 2PA peak should be at a wavelength longer than 600 nm.[209] More recently, the same group has used the white-light continuum (WLC) Z-scan technique to determine the degenerate 2PA spectrum (590−710 nm) of MEH-PPV. The results indicated a good agreement with those based on a single-wavelength determination. Besides being at a faster data-acquisition rate because of the wavelength multiplexing introduced by the use of a broadband source, the improved spectral resolution of the WLC Z-scan also allowed the observation of a 2PA peak around 675 nm.[211]

In the report by Meyer et al., the results that covered the spectral range from 650 to 800 nm for a PPV derivative containing 2,5-dioctyl pendants (DOO-PPV) revealed a 2PA maximum around 824 nm (∼3.0 eV).[212] More recently, Chung et al.[210] have measured the degenerate 2PA spectrum for MEH-PPV in a different spectral range (700−900 nm), using two-photon excited fluorescence measurements. They observed two peaks in the 2PA intensity around 790 and 840 nm with a decreasing trend toward the blue region.

Lee et al. reported the two-photon excitation spectrum of a PPV derivative (CzEH-PPV) with 2,5-substituents of an *N*-carbazole and an ethylhexyloxy group.[213] It showed the onset at 935 nm (1.32 eV) and the maximum at 757 nm (1.63 eV). The threshold energy (2.64 eV; 648 nm) of 2PA was larger than what (2.34 eV; 528 nm) would be expected by a linear excitation emission.[213] In a follow-up work, poly(*p*-phenylenevinylene) (PPV) derivatives carrying a 9-phenylanthracene pendant in the repeat unit, namely, poly[2-(9-phenylanthracen-10-yl)-1,4-phenylenevinylene] (**P-1**) and poly[2-(2-ethylhexyloxy)-5-(9-phenylanthracen-10-yl)-1,4-phenylenevinylene] (**P-2**) were prepared. Their one- and two-photon absorption and emission properties were studied in solution in comparison to those of poly[2-methoxy-5-(2′-ethylhexyloxy)-1,4-phenylenevinylene] [MEH-PPV (**P-3**)]. **P-1** and **P-2** differ in structure by the presence of an additional 2-ethylhexyloxy pendent group in **P-2**. Both polymers were prepared by direct polymerization of the α,α′-dibromo-*p*-xylene monomers containing the pendent group(s) in the presence of excess potassium *tert*-butoxide. From nanosecond and femtosecond nonlinear transmission measurements, their effective 2PA cross section values per repeat unit (σ_2) at ∼800 nm were found to be 2960 GM for **P-1**, 16 550 GM for **P-2**, and 10 930 GM for **P-3** in nanosecond pulses and 18 GM for **P-1**, 49 GM for **P-2**, and 42 GM for **P-3** in femtosecond pulses, respectively.[210]

When a chloroform solution of poly(2,5-dialkoxy-*p*-phenylene-ethynylene) derivative (EHO-OPPE) was excited by a ∼810 nm and ∼7 ns laser pulse, it was observed that the dynamic transmission changed from $T = 0.92$ to 0.28 when the input intensity of the laser beam was increased from $I_0 = 15$ to 600 MW/cm^2. The measured nonlinear absorption coefficient (β) and the effective 2PA cross section were 14.5 cm/GW and 19 600 GM respectively.[214]

4.4.3. Polythiophenes

Oligo-thiophenes. Hein et al.[215] used the single beam Z-scan technique with 30 ps pulses at 532 nm (close to the linear absorption region) to obtain the values of the real and imaginary parts of the third-order optical nonlinear susceptibility $\chi^{(3)}$ in (dioxane, 10^{-3} mol/L) solutions of thiophene oligomers with two to six repeat units. The values of the real part of $\chi^{(3)}$ were found to be negative; the contribution of each repeat unit to this value increased with increasing chain length. 2PA coefficients of about 0.1 cm/GW were determined.[215] In hexathiophene (T_6), Taliani and co-workers[216] observed a 2PA peak at ∼1090 nm (1.13 eV), which they attributed to the origin of the 2A state (as well as a much weaker response at ∼1140 nm (1.08 eV) assigned to the 1B state, which is made partially allowed by disorder and reduction of the molecular symmetry). Based on the fact that the cubic NLO response of T_6 approaches the values measured for the polymer,[217,218] T_6 is considered a good model for the parent poly(thiophene). As such, the 2PA response associated with the 2A state should be similar in the polymer, and this is indeed in agreement with the

Chart 4. Structures for Organic Molecules Listed in Table 4

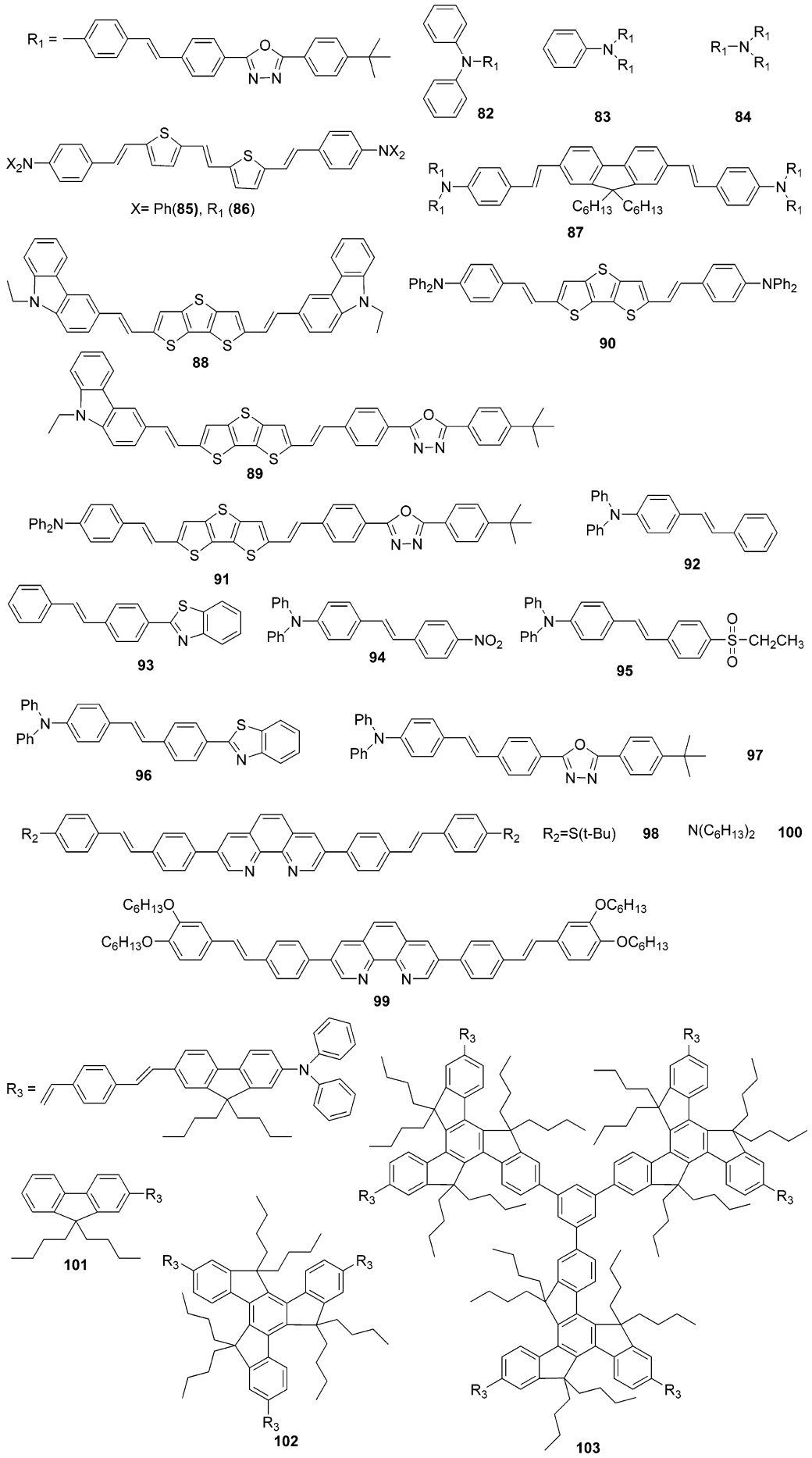

Table 4. 2PA Cross Section Values (σ_2) for Organic Molecules[a]

material	method	excitation wavelength/nm	solvent	σ_2/GM	other properties	ref
82	NLT, ns	810	TCE	14880	$\lambda_{abs} = 399$ nm, $\lambda_{em} = 503$ nm	47
	NLT, fs	796		88		47
83	NLT, ns	810	TCE	51584	$\lambda_{abs} = 417$ nm, $\lambda_{em} = 510$ nm	47
	NLT, fs	796		275		47
84	NLT, ns	810	TCE	145576	$\lambda_{abs} = 426$ nm, $\lambda_{em} = 516$ nm	47
	NLT, fs	796		600		47
85	NLT, fs	790	THF	65	$\lambda_{abs} = 460$ nm, $\lambda_{em} = 553$ nm	102
86	NLT, fs	790	THF	380	$\lambda_{abs} = 425$ nm, $\lambda_{em} = 550$ nm	102
87	NLT, fs	760	$CHCl_3$	447	$\lambda_{abs} = 418$ nm, $\lambda_{em} = 510$ nm	163
88	NLT, ns	810	TCE	105000	$\lambda_{abs} = 440$ nm, $\lambda_{em} = 480$ nm	72
89	NLT, ns	810	TCE	33500	$\lambda_{abs} = 497$ nm, $\lambda_{em} = 546$ nm	72
90	NLT, ns	810	TCE	199000	$\lambda_{abs} = 450$ nm, $\lambda_{em} = 512$ nm	72
	NLT, fs	796	TCE	270		72
91	NLT, ns	810	TCE	119000	$\lambda_{abs} = 503$ nm, $\lambda_{em} = 575$ nm	72
92	NLT, fs	750	THF	27	$\lambda_{abs} = 366$ nm	57
93	NLT, fs	747	THF	17	$\lambda_{abs} = 354$ nm	57
94	NLT, fs	840	THF	125	$\lambda_{abs} = 431$ nm $\lambda_{em} = 583$ nm	57
95	NLT, fs	748	THF	37	$\lambda_{abs} = 385$ nm $\lambda_{em} = 500$ nm	57
96	NLT, fs	761	THF	60	$\lambda_{abs} = 394$ nm $\lambda_{em} = 500$ nm	57
97	NLT, fs	779	THF	100	$\lambda_{abs} = 400$ nm $\lambda_{em} = 525$ nm	57
98	NLT, fs	696	$CHCl_3$	165	$\lambda_{abs} = 357$ nm $\lambda_{em} = 445$ nm	81
99	NLT, fs	758	$CHCl_3$	160	$\lambda_{abs} = 376$ nm $\lambda_{em} = 466$ nm	81
100	NLT, fs	788	$CHCl_3$	401	$\lambda_{abs} = 415$ nm, $\lambda_{em} = 541$ nm	81
101	NLT, fs	740	$CHCl_3$	94	$\lambda_{abs} = 402$ nm, $\lambda_{em} = 496$ nm	113
102	NLT, fs	752	$CHCl_3$	603	$\lambda_{abs} = 412$ nm, $\lambda_{em} = 497$ nm	113
103	NLT, fs	770	$CHCl_3$	1412	$\lambda_{abs} = 413$ nm, $\lambda_{em} = 497$ nm	113

[a] All 2PA data are obtained by the nonlinear transmission (NLT) method. ~800 nm, ~8 ns dye-laser pulses and ~790 nm, ~140 fs Ti:sapphire laser pulses were used for these measurements. The nanosecond values are overestimated in comparison with femtosecond values, due to the excited-state absorption (for details, see the first paragraph of section 4.2). TCE = 1,1,2,2-tetrachloroethane.

conclusion of a theoretical study.[219] In an *ab initio* response theory calculation, it was determined that the so-called "localization length", i.e. the threshold value for the molecular length, larger than which the localization of the two-photon state would occur for oligothiophene was 1.2 nm.[30b]

Pfeffer et al. investigated the 2PA spectrum of poly(3-octylthiophene) in THF solution using the picosecond Kerr ellipsometry technique.[220] They assigned the peak at 705 nm (1.75 eV) to a two-photon resonance from the ground state to the so-called *mA* state, which was in agreement with the results of a theoretical study.[219] This peak has a half-width at half-maximum value of 0.27 eV and a β value of 0.27 cm/GW measured in a 25 g/L solution. A second weaker 2PA signal at ~850 nm (1.45 eV) was also observed.

4.4.4. Other Conjugated Polymers

Structurally, ladder poly(*p*-phenylene)s or LPPPs are completely fused poly(fluorenes), and the backbone of this family of polymers is formed by the poly(*p*-phenylene) (PPP) chain, where the 1,4-phenylene rings are connected rigidly and more coplanarly by disubstituted (R and R′ group = methyl, decyl) 2,5′-methylene bridges, resulting in double-stranded, *viz*. ladder, structures. Unlike heterocyclic ladder polymers, these polymers are soluble in common organic solvents and can be spin-coated, solution-cast, or doctor-bladed into films. Thus, in their investigation of the continuous-wave 2PA in a ladder poly(*p*-phenylene), designated as m-LPPP (Chart 13), in toluene, Hohenau et al. used the 2PEF technique to locate its 2PA peak at 769 nm with a very large σ_2 value, 72 000 GM on a per repeat unit basis.[221] The 2PA coefficients of other related LPPPs in film form have been measured at 800 nm to be $\beta = 5$ cm/GW,[222] and at 718 nm (1.72 eV) to be $\beta = 11$ cm/GW.[223]

Liu et al. reported a very large 2PA coefficient (590 cm/GW) by using the Z-scan technique at 532 nm for a film sample of polyphenylquinoxaline (PPQ), which was prepared from the polycondensation of 3,3′,4,4′-biphenyltetramine and *p*-phenylenebis(phenylglyoxal).[224]

Belfield et al. synthesized two interesting heterocyclic rigid-rod polymers with alternating fluorenyl units as a π-conjugated bridge and benzo[1,2-d:4,5-d′]bisthiazole or thiazolo[5,4-d]thiazole moieties as electron acceptors.[225] They found a relatively large 2PA cross section per repeat unit (420 GM; ~1.0×10^{-4} M; $CHCl_3$) at 710 nm for the benzobisthiazole-based polymer upon femtosecond-pulsed laser excitation. The cross section, however, is smaller than that of a related symmetrical model compound (660 GM at 588 nm) with benzothiazole end groups.

4.4.5. Dendrimers

The 2PA-active dendrimer, first prepared by Humphrey et al., was actually a ruthenium(II)-based organometallic compound with an impressively large cross section value of 2100 GM.[50] This was followed by the report of Drobizhev et al., who described the 2PA spectral results for three generations of highly active, all-organic dendrimers based on 4,4′-bis(diphenylamino)stilbene (DPAS) repeat units.[35] The peak femtosecond two-photon cross section of these dendrimers increased almost linearly with the number of chromophore units, but the largest jump in the σ_2 value was observed when going from the parent DPAS molecule (325 GM) to the first (G-0) generation (2800 GM). The largest G-2 dendrimers that contained 29 repeat units showed the very large, intrinsic two-photon cross section of 11 000 GM at 690 nm and a three-photon cross section of 1×10^{-79} cm^6 s^2 at ~1260 nm. In addition to having high fluorescence quantum yields, these dendrimers as a structural series also exhibited a strong cooperative enhancement effect in 2PA and 3PA responses.[115] This concept was further followed by Wei et al., who prepared a series of dendritic two-photon

Chart 5. Structures for Organic Molecules Listed in Table 5

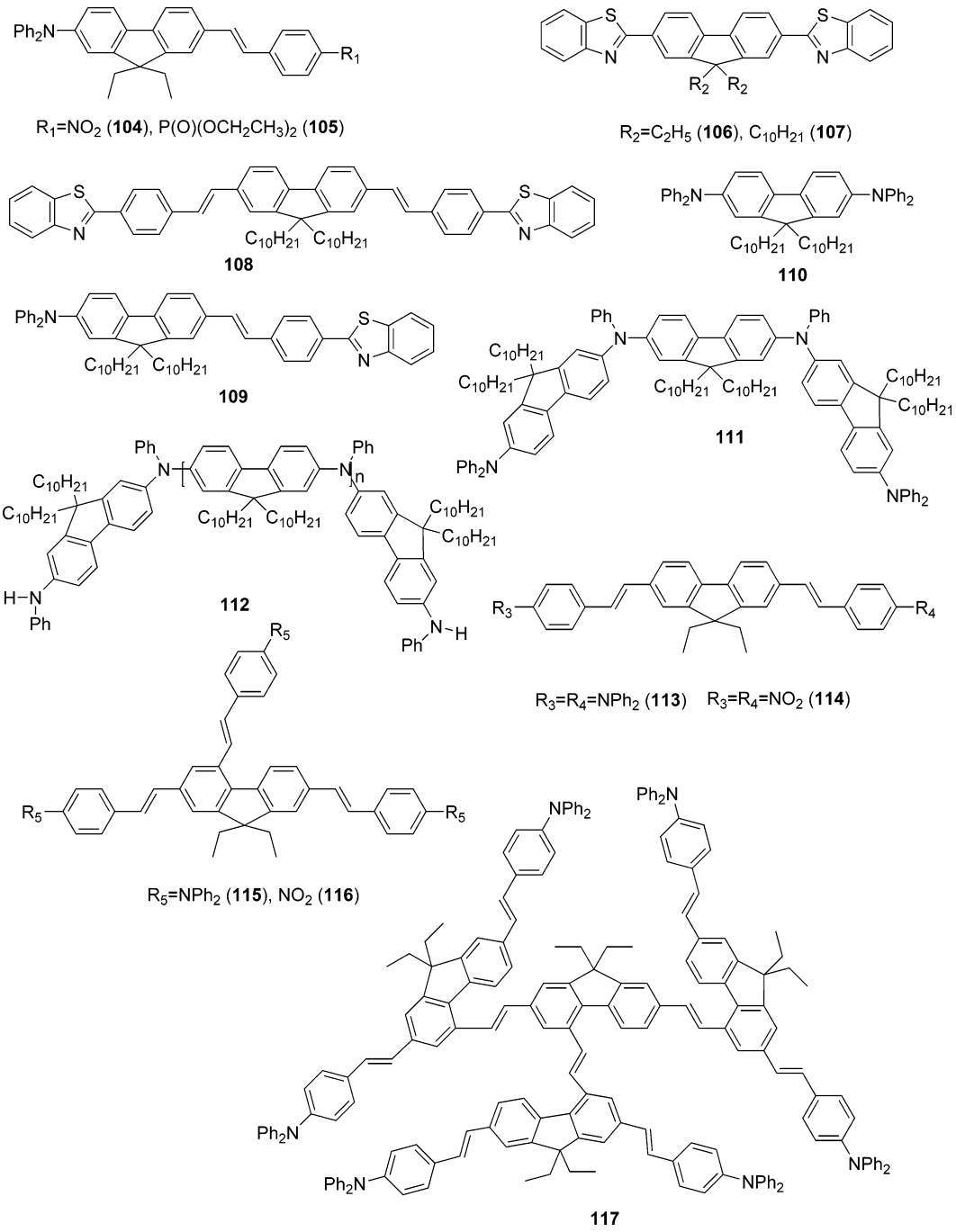

absorbing chromophores containing the triphenylamine moiety as a core or branching points through a convergent synthetic strategy. In the nanosecond time domain, these molecules exhibited large 2PA cross section values up to $(7.56-12.2) \times 10^6$ GM at 800 nm.[101]

Adronov and Fréchet et al. first synthesized novel non-π-conjugated dendrimers functionalized with 2PA chromophores at their chain ends.[226] They observed a linear correlation between the number of peripheral chromophores and the 2PA cross section of the molecule, indicating that there are neither cooperative nor deleterious effects in the dendrimers due to the high local chromophore concentration. In these π-conjugated dendrimers, Brousmiche and Fréchet et al. demonstrated efficient single-photon- and multiphoton-induced fluorescence resonance energy transfer (FRET) between two-photon absorbing chromophore moieties (donor) and a Nile-red acceptor chromophore.[227,228]

The synthesis of triphenylbenzene-cored dendrimers of first and second generation was reported by Blanchard-Desce et al. The σ_2 values for the first and the second generation were found to be 407 and 798 GM, respectively. They observed that the second generation dendritic molecule showed a 2PA cross section twice that of its first generation analogue yet being more transparent.[162]

Zheng et al. developed novel truxene containing π-conjugated dendritic chromophores with enhanced 2PA.[113] The 2PA peak value for the dendritic chromophore is 1412 GM, ~15 times larger than that for its monomer analogue (94 GM). The three-branched octupolar chromophore has a 2PA peak value of 603 GM, ~6.5 times as large as that for its monomer analogue. The enhanced 2PA found in these two

Table 5. 2PA Cross Section Values (σ_2) for Organic Molecules[a]

material	method	excitation wavelength/nm	solvent	σ_2/GM	other properties	ref
104	WLC pump probe, fs	670	CH_3CN	1300	$\lambda_{abs} = 410$ nm	55
105	WLC pump probe, fs	595	CH_3CN	650	$\lambda_{abs} = 390$ nm	55
106	2PEF, fs	600 (700)	CH_2Cl_2	370 (53)	$\lambda_{abs} = 371$ nm, $\lambda_{em} = 400$ nm	164
107	2PEF, fs	600 (700)	CH_2Cl_2	420 (45)	$\lambda_{abs} = 371$ nm, $\lambda_{em} = 400$ nm	164
108	2PEF, fs	600 (800)	CH_2Cl_2	6000 (1185)	$\lambda_{abs} = 410$ nm, $\lambda_{em} = 486$ nm	164
109	2PEF, fs	610 (790)	CH_2Cl_2	1530 (525)	$\lambda_{abs} = 388$ nm, $\lambda_{em} = 472$ nm	164
110	WLC pump probe, fs	610	hexane	1000	$\lambda_{abs} = 372$ nm, $\lambda_{em} = 390$ nm	165
	2PEF, fs	600	hexane	240		165
111	WLC pump probe, fs	600	hexane	4100	$\lambda_{abs} = 400$ nm, $\lambda_{em} = 410$ nm	165
	2PEF, fs	600	hexane	710		165
112	WLC pump probe, fs	600	hexane	17200	$\lambda_{abs} = 408$ nm, $\lambda_{em} = 414$ nm	165
	2PEF, fs	600	hexane	6800	/	165
113	Z-scan, ps	520	cyclohexane	2250	/	166
	WLC pump probe, fs	770 (570)	cyclohexane	626 (2100)	/	166
114	Z-scan, ps	520	cyclohexane	5215	/	166
115	Z-scan, ps	520	cyclohexane	3115	/	166
115	WLC pump probe, fs	570	cyclohexane	2750	/	166
116	Z-scan, ps	520	cyclohexane	5765	/	166
117	Z-scan, ps	520	cyclohexane	4250	/	166
	WLC pump probe, fs	770 (570)	cyclohexane	1603 (4194)	/	166

[a] 2PA data are obtained by the white-light continuum (WLC) pump probe method, the Z-scan method, or the two-photon excited fluorescence method (2PEF).

multibranched chromophores is attributed to the fact that the dendritic or the three-branched chromophore has both an extended π-conjugated system and an increased intramolecular charge redistribution compared to that of the monomeric dipolar chromophore.

4.4.6. Hyperbranched Polymers

Several 2PA-active, phenylenevinylene-based hyperbranched polymers have been prepared via an $A_3 + B_2$ copolymerization route using an A_3 monomer, such as 4,4′,4″-triformyltriphenylamine (TFTA) and benzene-1,3,5-tricarbaldehyde (BTA), and a B_2 monomer, such as (i) 1,4-bis(methyltriphenylphosphonium)-2,5-dihexyloxybenzene dichloride;[229] (ii) 1,4-bis(methyltriphenylphosphonium)-2,5-dimethoxybenzene dichloride;[229,230] or (iii) 1,4-phenylenediacetonitrile.[231] Thus, these hyperbranched polymers were prepared either via a modified Wittig reaction [TFTA + B_2 monomer (i) or BTA + B_2 monomer (ii)] or via a Claisen−Schmitt reaction [TFTA + B_2 monomer (iii)]. The 2PA cross section values per repeat unit determined with the Z-scan technique (120 fs pulses) were quite large. It is interesting to note that the presence of cyano groups attached directly to the vinyl groups raised the values at 800 nm considerably (1760 GM)[232] as compared to the counterpart with plain vinyl groups (159 and 355 GM).[229] Also, the chloroform solution of the hyperbranched polymer, DMA-HPV [derived from BTA and B_2 monomer (iii)] showed a high nonlinear transmission loss in the visible range of 490−610 nm, which was attributed to the combined effect of 2PA and reverse saturable absorption.[230c]

4.5. Fullerenes

In 1992, Tutt and Kost first reported the optical limiting performance of C_{60} and C_{70} solutions.[233,234] While nonlinear optical processes such as 2PA and nonlinear refraction could play some roles, the mechanism that is primarily responsible for the optical limiting properties of the fullerenes has been attributed to the so-called reverse saturable absorption (RSA), which is a linear absorption process where the excited-state absorption is much greater than the ground-state absorption. However, C_{60} and some higher fullerenes, e.g., C_{70}, have been shown experimentally[235−238] and theoretically[239,240] to possess two-photon properties. Although many organic derivatives of C_{60} were reported in the literature, multiphoton absorptivity was reported only for a few of their derivatives.

The 2PA coefficient of C_{60} has been measured in solution, amorphous thin film (vacuum-deposited), inorganic glass (sol gel), and polymer matrix using nanosecond, picosecond, and femtosecond pulses. It appears that the reverse saturable absorption dominates in the shorter-wavelength region (440−560 nm) whereas 2PA dominates in the longer-wavelength region (580−1000 nm).[235,241] Using a continuous tunable 100 fs pulse laser to measure the time-resolved degenerate four-wave-mixing (DFWM) spectra of both amorphous film C_{60} and C_{70}, Dalton et al. reported that the 2PA coefficients at the resonance maxima were about the same, with a value of $\sim 20 \pm 8$ cm/GW.[241,243,244] A recent theoretical study on the 2PA property of C_{60}, which was based on the equilibrium geometry optimized at the B3LYP/6-31G level and the ZINDO method combined with a SOS formula (see eqs 19−21) to calculate the second hyperpolarizability and the 2PA cross section of C_{60}, suggested that, in the 400−1000 nm range, there is only one 2PA peak at 518 nm with a large cross section of about 1000 GM.[239] A similar theoretical treatment of C_{70} suggested that its maximum 2PA cross section is more than twice that of C_{60}, which is consistent with the experimental measurement.[240]

There are many C_{60} derivatives that have been synthesized via various types of addition reactions to the "6−6 C═C bond", and the reverse saturable absorption and optical limiting processes associated with a number of them were extensively studied. However, there are only a few two-photon characterization efforts reported to date.[245] In their synthetic effort to obtain a covalently bonded charge-transfer complex from C_{60} and tetrathiafulvalene (TTF) in 1:2 ratio, Boulle et al. prepared an interesting C_{60}-cycloadduct intermediate. The 2-thioxo-1,3-dithiole C_{60}-cycloadduct was synthesized from the Diels−Alder reaction between C_{60} and the reactive diene, 2-thioxo-4,5-bis(methylene)-1,3-dithiole, which was generated in situ from 2-thioxo-4,5-bis(bromom-

Chart 6. Structures for Organic Molecules Listed in Table 6

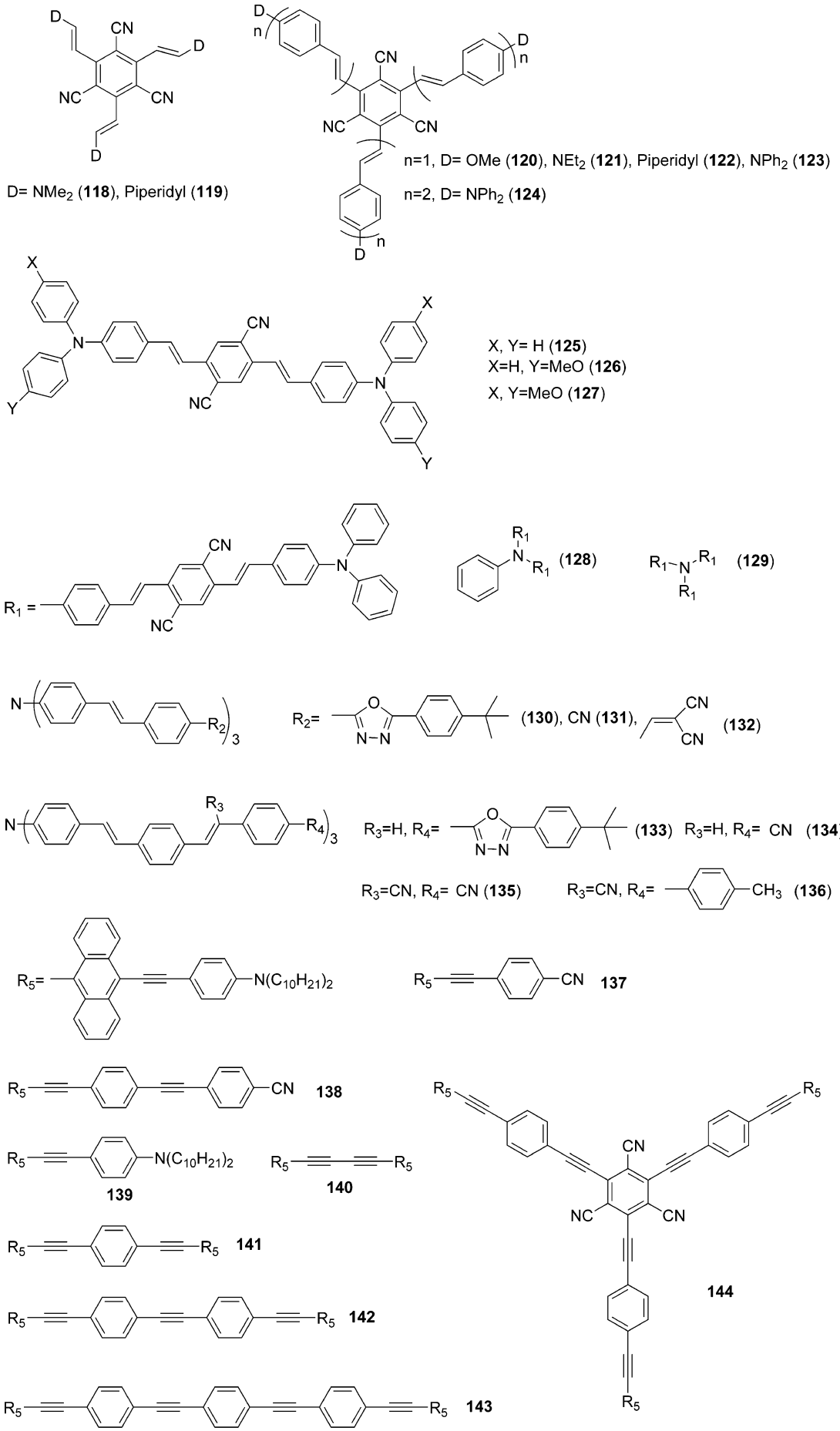

Chart 6 (Continued)

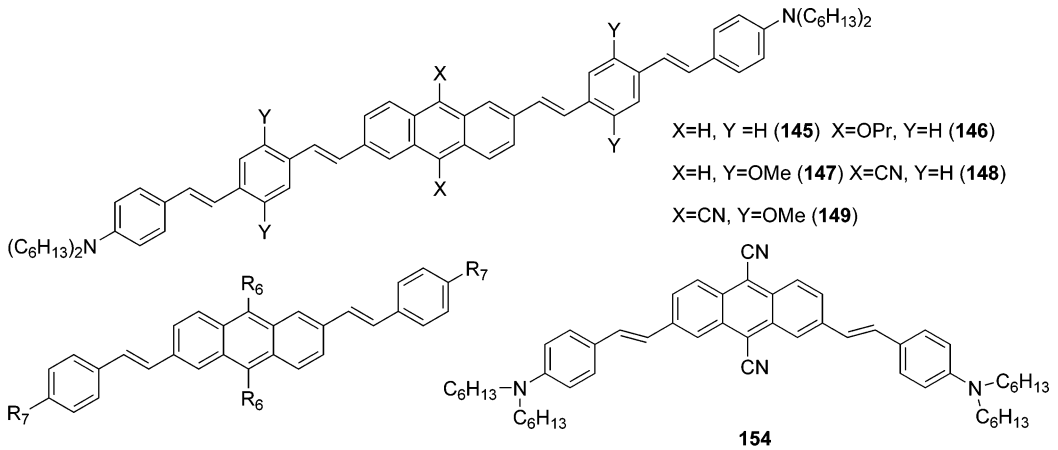

R_6=H (**150**), Ph (**151**), *p*-CNC_6H_4 (**153**), CN (**153**)

R_7=$N(C_6H_{13})_2$ (**a**), NH_2 (**a'**), N(i-amyl)tol (**b**), $N(C_6H_4$-*p*-*t*-$Bu)_2$ (**c**), $N(Ph)_2$ (**c'**)

Table 6. 2PA Cross Section Values (σ_2) for Organic Molecules[a]

material	method	excitation wavelength/nm	solvent	σ_2/GM	other properties	ref
118	2PEF, ns	800	$CHCl_3$	197	λ_{abs} = 389 nm, λ_{em} = 486 nm	112a
119	2PEF, ns	820	$CHCl_3$	295	λ_{abs} = 396 nm, λ_{em} = 485 nm	112a
120	2PEF, ns	780	$CHCl_3$	143	λ_{abs} = 388 nm, λ_{em} = 496 nm	112a
121	2PEF, ns	980	$CHCl_3$	1390	λ_{abs} = 493 nm, λ_{em} = 602 nm	112a
122	2PEF, ns	980	$CHCl_3$	1430	λ_{abs} = 468 nm, λ_{em} = 614 nm	112a
123	2PEF, ns	980	$CHCl_3$	2480	λ_{abs} = 488 nm, λ_{em} = 614 nm	112a
124	2PEF, ns	800	$CHCl_3$	2620	λ_{abs} = 468 nm, λ_{em} = 675 nm	112a
125	2PEF, ns	840	Tol	1370	λ_{abs} = 473 nm, λ_{em} = 527 nm	103
126	2PEF, ns	880	Tol	1350	λ_{abs} = 485 nm, λ_{em} = 543 nm	103
127	2PEF, ns	890	Tol	2250	λ_{abs} = 488 nm, λ_{em} = 560 nm	103
128	2PEF, ns	840	Tol	3130	λ_{abs} = 492 nm, λ_{em} = 534 nm	103
129	2PEF, ns	840	Tol	5030	λ_{abs} = 495 nm, λ_{em} = 536 nm	103
130	2PEF, ns	760	Tol	430	λ_{abs} = 410 nm, λ_{em} = 471 nm	106
131	2PEF, ns	760	Tol	220	λ_{abs} = 415 nm, λ_{em} = 467 nm	106
132	2PEF, ns	890	Tol	1200	λ_{abs} = 487 nm, λ_{em} = 570 nm	106
133	2PEF, ns	780	Tol	950	λ_{abs} = 429 nm, λ_{em} = 487 nm	106
134	2PEF, ns	780	Tol	870	λ_{abs} = 429 nm, λ_{em} = 488 nm	106
135	2PEF, ns	890	Tol	740	λ_{abs} = 464 nm, λ_{em} = 550 nm	106
136	2PEF, ns	800	Tol	1360	λ_{abs} = 450 nm, λ_{em} = 519 nm	106
137	2PEF, ns	780 (990)	Tol	210 (250)	λ_{abs} = 497 nm, λ_{em} = 556 nm	112c
138	2PEF, ns	780 (990)	Tol	370 (350)	λ_{abs} = 492 nm, λ_{em} = 553 nm	112c
139	2PEF, ns	780	Tol	540	λ_{abs} = 510 nm, λ_{em} = 543 nm	112c
140	2PEF, ns	800	Tol	990	λ_{abs} = 530 nm, λ_{em} = 600 nm	112c
141	2PEF, ns	800	Tol	720	λ_{abs} = 508 nm, λ_{em} = 558 nm	112c
142	2PEF, ns	800	Tol	760	λ_{abs} = 510 nm, λ_{em} = 550 nm	112c
143	2PEF, ns	780	Tol	820	λ_{abs} = 507 nm, λ_{em} = 547 nm	112c
144	2PEF, ns	780 (990)	Tol	840 (820)	λ_{abs} = 499 nm, λ_{em} = 555 nm	112c
145	2PEF, fs	800	Tol	1140	λ_{abs} = 427 nm, λ_{em} = 503 nm	167
146	2PEF, fs	770	Tol	1810	λ_{abs} = 448 nm, 476 nm	167
		800		1900	λ_{em} = 497 nm, 526 nm	167
147	2PEF, fs	770	Tol	2580	λ_{abs} = 465 nm, 478 nm	167
		800		2490	λ_{em} = 527 nm, 551 nm	167
148	2PEF, fs	980	Tol	5530	λ_{abs} = 531 nm, λ_{em} = 650 nm	167
149	2PEF, fs	980	Tol	3650	λ_{abs} = 575 nm, λ_{em} = 678 nm	167
150a	2PEF, ns	800	Tol	1100	λ_{abs} = 455 nm, λ_{em} = 487 nm	168
150b	2PEF, ns	780	Tol	1080	λ_{abs} = 454 nm, λ_{em} = 483 nm	168
150c	2PEF, ns	780	Tol	1340	λ_{abs} = 454 nm, λ_{em} = 479 nm	168
151a	2PEF, ns	780	Tol	770	λ_{abs} = 466 nm, λ_{em} = 501 nm	168
151b	2PEF, ns	780	Tol	700	λ_{abs} = 463 nm, λ_{em} = 495 nm	168
151c′	2PEF, ns	780	Tol	720	λ_{abs} = 458 nm, λ_{em} = 481 nm	168
152a	2PEF, ns	840	Tol	1570	λ_{abs} = 488 nm, λ_{em} = 535 nm	168
152b	2PEF, ns	840	Tol	1180	λ_{abs} = 482 nm, λ_{em} = 530 nm	168
152c′	2PEF, ns	820	Tol	1760	λ_{abs} = 474 nm, λ_{em} = 509 nm	168
153a	2PEF, ns	990	Tol	2290	λ_{abs} = 587 nm, λ_{em} = 656 nm	168
153b	2PEF, ns	990	Tol	2210	λ_{abs} = 575 nm, λ_{em} = 643 nm	168
153c	2PEF, ns	990	Tol	2490	λ_{abs} = 566 nm, λ_{em} = 635 nm	168
154	2PEF, ns	1030	Tol	720	λ_{abs} = 562 nm, λ_{em} = 650 nm	168

[a] All the 2PA data are obtained by the two-photon excited fluorescence method (2PEF) and femtosecond or nanosecond laser excitation.

Chart 7. Structures for Organic Molecules Listed in Table 7

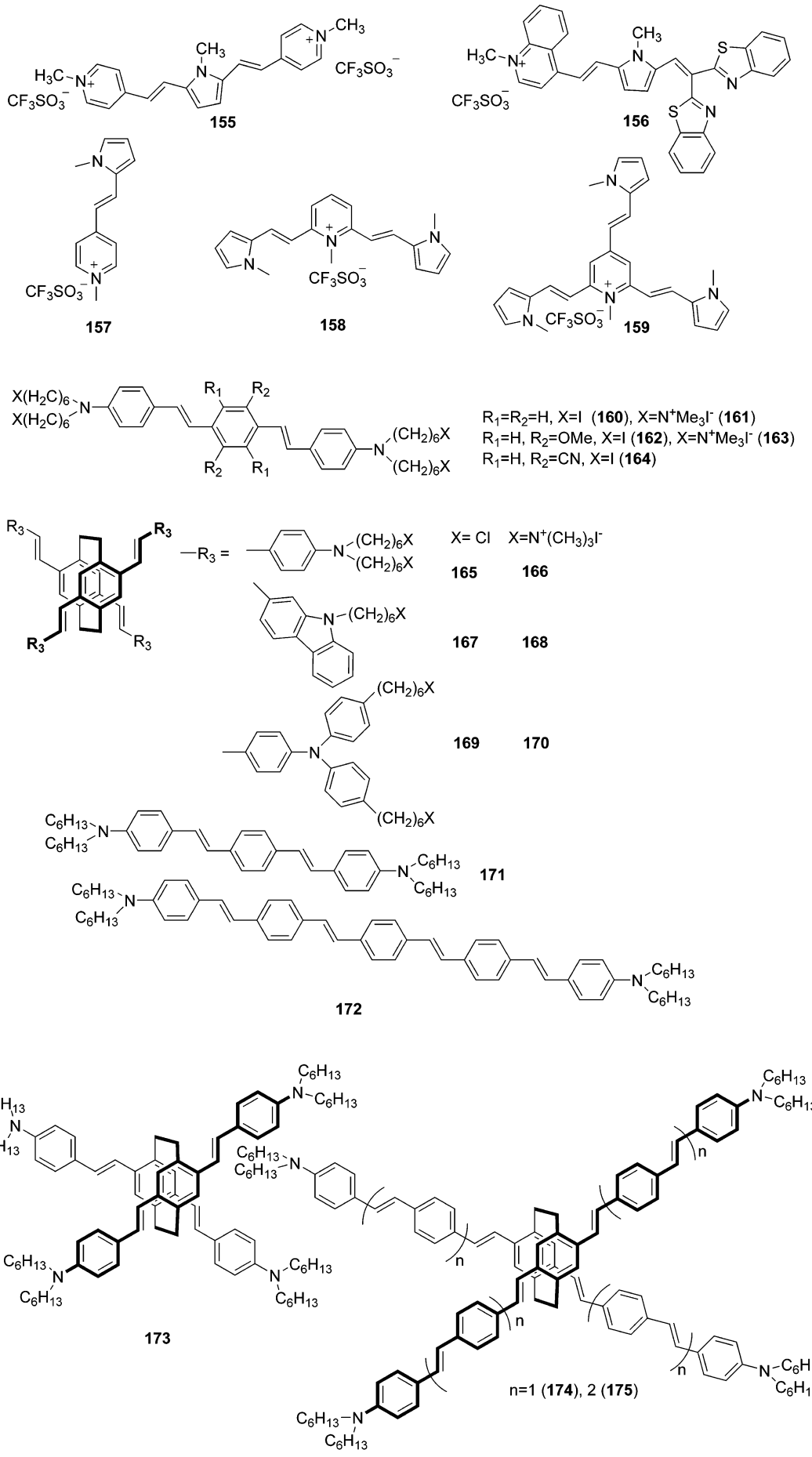

Table 7. 2PA Cross Section Values (σ_2) for Organic Molecules[a]

material	method	excitation wavelength/nm	solvent	σ_2/GM	other properties	ref
155	Z-scan, fs	790	DMSO	119	$\lambda_{abs} = 524$ nm, $\lambda_{em} = 620$ nm	71c
156	Z-scan, fs	790	DMSO	150	$\lambda_{abs} = 559$ nm, $\lambda_{em} = 670$ nm	111a
157	Z-scan, fs	790	DMSO	5	$\lambda_{abs} = 437$ nm, $\lambda_{em} = 523$ nm	111b
158	Z-scan, fs	790	DMSO	103	$\lambda_{abs} = 471$ nm, $\lambda_{em} = 554$ nm	111b
159	Z-scan, fs	790	DMSO	113	$\lambda_{abs} = 475$ nm, $\lambda_{em} = 596$ nm	111b
160	2PEF, fs	720	Tol	910	$\lambda_{abs} = 409$ nm, $\lambda_{em} = 449$ nm	37
161	2PEF, fs	720	H_2O	330	$\lambda_{abs} = 406$ nm, $\lambda_{em} = 558$ nm	37
162	2PEF, fs	725	Tol	890	$\lambda_{abs} = 427$ nm, $\lambda_{em} = 475$ nm	37
163	2PEF, fs	730	H_2O	360	$\lambda_{abs} = 423$ nm, $\lambda_{em} = 567$ nm	37
164	2PEF, fs	815	Tol	1710	$\lambda_{abs} = 485$ nm, $\lambda_{em} = 526$ nm	37
165	2PEF, fs	725	Tol	1290	$\lambda_{abs} = 434$ nm, $\lambda_{em} = 486$ nm	36
166	2PEF, fs	725	H_2O	370	$\lambda_{abs} = 435$ nm, $\lambda_{em} = 553$ nm	36
167	2PEF, fs	700	Tol	1690	$\lambda_{abs} = 420$ nm, $\lambda_{em} = 468$ nm	36
168	2PEF, fs	700	H_2O	700	$\lambda_{abs} = 410$ nm, $\lambda_{em} = 505$ nm	36
169	2PEF, fs	770	Tol	2080	$\lambda_{abs} = 441$ nm, $\lambda_{em} = 492$ nm	36
170	2PEF, fs	750	H_2O	690	$\lambda_{abs} = 431$ nm, $\lambda_{em} = 537$ nm	36
171	2PEF, fs & ns	720	Tol	870	$\lambda_{abs} = 412$ nm $\lambda_{em} = 453$ nm	169
172	2PEF, fs & ns	810	Tol	1450	$\lambda_{abs} = 435$ nm, $\lambda_{em} = 485$ nm	169
173	2PEF, fs & ns	720	Tol	1410	$\lambda_{abs} = 439$ nm, $\lambda_{em} = 490$ nm	169
174	2PEF, fs & ns	820	Tol	3430	$\lambda_{abs} = 457$ nm, $\lambda_{em} = 510$ nm	169
175	2PEF, fs & ns	830	Tol	3890	$\lambda_{abs} = 454$ nm, $\lambda_{em} = 495$ nm	169

[a] All the 2PA data are obtained by the two-photon excited fluorescence method (2PEF) or the Z-scan method. Nanosecond and femtosecond lasers were used for excitation.

ethyl)-1,3-dithiole.[246] The 2PA coefficients for this C_{60}-cycloadduct were determined at the excitation wavelength of 532 nm in benzene−toluene ($\beta = 27.35$ cm/GW), in benzene−alcohol ($\beta = 26.45$ cm/GW), and in an oligoetheracrylate matrix ($\beta = 26.7$ cm/GW). These values were all much higher than those of pristine C_{60} obtained under the same conditions: $\beta = 18.75$, 18.5, and 18.6 cm/GW, in that order.[247]

Employing the Bingel cyclopropanation reaction,[248] Chiang et al. reported the synthesis of the first highly two-photon active C_{60} derivative comprised of an A-sp^3-D conjugate structure, where the fullerene cage serves as an acceptor (A), the donor (D) is a diphenylaminofluorence, and a cyclopropylketo group provides an sp^3 connection. It has an effective 2PA cross section value ($\sigma_2 = 19\,600$ GM; 800 nm, 8 ns pulses).[249] In a subsequent work, using a long and branched alkyl chain, the resulting diad and triad showed greater effective cross sections (25 100 GM and 62 200 GM, respectively) at 800 nm, but the intrinsic cross section values were three orders of magnitude smaller (31 and 82 GM, respectively) at 780 nm, indicative of a very large contribution of excited-state absorption under nanosecond conditions.[250]

Zhao et al. reported the synthesis of a series of linear and branched multi-[60]fullerene-oligo(2,5-dilkoxyphenylene-ethynylene) compounds with C_{60}-end caps.[251] The two-photon property of a linear compound was characterized with a relatively large femtosecond cross section value of 140 ± 40 GM in DMSO at 800 nm using a differential Kerr effect (DOKE) technique.[252a] This is more than twice the value of the oligo(2,5-dilkoxyphenylene-ethynylene) bridge compound (65 ± 10 GM), indicating significant participation of the C_{60} cages in the nonlinear absorption process of the molecule.

4.6. Coordination and Organometallic Compounds

Metal complexes that are two-photon active can be broadly divided into two groups: (i) two-photon absorbing coordination compounds and (ii) two-photon absorbing organometallic compounds. While both coordination compounds and organometallics are hybrid systems comprised of a metal center covalently surrounded by organic ligands, the latter, by definition, contains at least one metal−carbon bond. The metal ions, including main group metals, transition metals, and lanthanides, can serve as either as a non-interacting center or a multidimensional template for increasing the molecular number density of two-photon active components (i.e., ligands), or as an important part of the structure to control the intramolecular charge-transfer process that drives the 2PA process. As templates, transition metal ions can assemble simple to more sophisticated ligands in a variety of multipolar arrangements resulting in interesting and tailorable electronic and optical properties, depending on the nature of the metal center and the energetics of the metal−ligand interactions, such as intraligand charge-transfer (ILCT) and metal−ligand charge-transfer (MLCT) processes. For example, a clever use of coordination chemistry is exemplified by the work of Pond et al. that invoked an excellent design incorporating an aza-crown-ether into a quadrupolar two-photon active chromophore to provide a controllable two-photon excited fluorescence. Thus, the coordination of a Mg(II) ion to the aza-crown-ether curtailed the electron-donating capacity of the nitrogen (aza-crown ether) to engage in the intramolecular charge transfer upon photoexcitation, as evidenced by the lowering of the σ_2 values by 50%.[159] In another instance, Zheng et al. observed that the σ_2 values of 1,10-phenanthroline-based π-conjugated 2PA ligands increased more than three times (from 165 GM to 578 GM) upon binding with a Ni(II) ion, and the fluorescence of the ligands could be quenched by certain metal ions.[81] Thus, the transition dynamics of two-photon excited states can be controlled by metal-ion-induced relaxation processes, providing unique opportunities for those applications when fluorescence has to be minimized.

4.6.1. Metal Dithiolenes

1,2-Dithiolene metal complexes are coordination compounds which contain at least a bidendate ligand formally

Chart 8. Structures for Organic Molecules Listed in Table 8

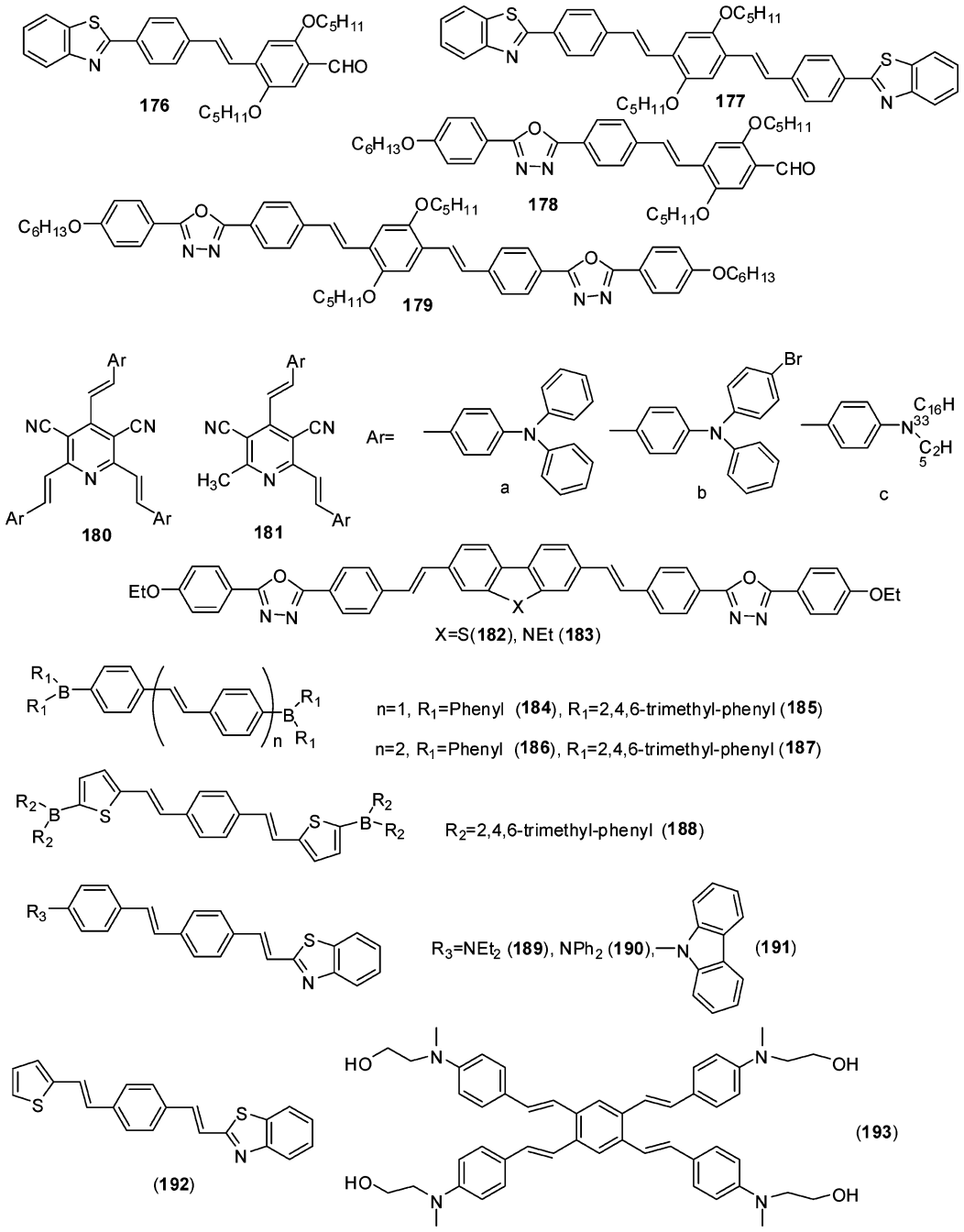

derived from the disubstituted 1,2-ethylenedithiol [R—C(S)═C(S)—R′].[253,254] Within this class of metal complexes, nickel bis(dithiolenes) are attractive nonlinear optical (NLO) materials because of the following reasons: (i) It is possible to tune the linear absorption band between about 700 and 1500 nm by judicious choice of the substituent groups on the dithiolene ligand.[255] This feature is particularly useful in selecting a material that shows near resonance enhancement for third-order NLO susceptibility throughout the range of wavelengths (i.e., 1.3−1.5 μm) of interest in telecommunications. (ii) They are very robust against laser damage, even at their near-IR absorption maxima, hence their utility as laser Q-switch dyes for Nd:YAG lasers.[256] (iii) They have been shown to possess large values of third-order nonlinear susceptibility ($\chi^{(3)}$),[257] and some unsymmetrical dithiolene−metal complexes also showed negative molecular first hyperpolarizability (β).[258] However, their two-photon absorptivity was a concern because of the early interest in them as promising materials for all-optical computing and switching applications,[259] where 2PA, in addition to linear absorption, must be minimized or completely eliminated to enhance the performance of the wave guides or optical fibers. The effective 2PA cross section values for nickel bis(dithiolenes) reported are in the range of 250−25 000 GM determined at 1064 nm[260] and 7500−19 000 GM at ∼1319 nm,[261] both with 100 ps laser pulses.

4.6.2. Pyridine-Based Multidentate Ligands

2,2′-Bipyridines, terpyridines, and 1,10-phenanthrolines are a family of π-deficient heterocyclics (polypyridines) that can bind to a wide range of transition metal ions via the nitrogen lone-pair electrons.

4.6.2.1. 1,10-Phenanthroline. Quadrupolar molecules with a 1,10-phenanthroline core and electron-donor terminal

Table 8. 2PA Cross Section Values (σ_2) for Organic Molecules[a]

material	method	excitation wavelength/nm	solvent	σ_2/GM	other properties	ref
176	2PEF, fs	788	$CHCl_3$	26	$\lambda_{abs} = 404$ nm, $\lambda_{em} = 463$ nm	69
177	2PEF, fs	788	$CHCl_3$	521	$\lambda_{abs} = 429$ nm, $\lambda_{em} = 494$ nm	69
178	2PEF, fs	788	$CHCl_3$	13	$\lambda_{abs} = 403$ nm, $\lambda_{em} = 464$ nm	69
179	2PEF, fs	788	$CHCl_3$	461	$\lambda_{abs} = 423$ nm, $\lambda_{em} = 482$ nm	69
180a	2PEF, fs	800	$CHCl_3$	187	$\lambda_{abs} = 480$ nm, $\lambda_{em} = 586$ nm	114
180b	2PEF, fs	800	$CHCl_3$	204	$\lambda_{abs} = 476$ nm, $\lambda_{em} = 575$ nm	114
181a			$CHCl_3$		$\lambda_{abs} = 471$ nm, $\lambda_{em} = 581$ nm	114
181b	2PEF, fs	800	$CHCl_3$	118	$\lambda_{abs} = 468$ nm, $\lambda_{em} = 570$ nm	114
181c	2PEF, fs	800	$CHCl_3$	109	$\lambda_{abs} = 482$ nm, $\lambda_{em} = 569$ nm	114
182	2PEF, fs	720	THF	299	$\lambda_{abs} = 347$ nm, $\lambda_{em} = 427$ nm	170
	2PEF, fs	720	CH_2Cl_2	100	$\lambda_{abs} = 347$ nm, $\lambda_{em} = 434$ nm	170
	2PEF, fs	720	DMF	377	$\lambda_{abs} = 348$ nm, $\lambda_{em} = 450$ nm	170
183	2PEF, fs	720	THF	348	$\lambda_{abs} = 358$ nm, $\lambda_{em} = 458$ nm	170
	2PEF, fs	720	CH_2Cl_2	167	$\lambda_{abs} = 353$ nm, $\lambda_{em} = 481$ nm	170
	2PEF, fs	720	DMF	454	$\lambda_{abs} = 354$ nm, $\lambda_{em} = 499$ nm	170
184	2PEF, fs	720	THF	75	$\lambda_{abs} = 389$ nm, $\lambda_{em} = 453$ nm	171
185	2PEF, fs	720	THF	41	$\lambda_{abs} = 372$ nm, $\lambda_{em} = 429$ nm	171
186	2PEF, fs	745	THF	920	$\lambda_{abs} = 412$ nm, $\lambda_{em} = 489$ nm	171
187	2PEF, fs	730	THF	835	$\lambda_{abs} = 397$ nm, $\lambda_{em} = 467$ nm	171
188	2PEF, fs	775	THF	1340	$\lambda_{abs} = 435$ nm, $\lambda_{em} = 515$ nm	171
189	2PEF, fs	800	Tol	116	$\lambda_{abs} = 428$ nm, $\lambda_{em} = 528$ nm	71d
	2PEF, fs	800	THF	206	$\lambda_{abs} = 425$ nm, $\lambda_{em} = 590$ nm	71d
190	2PEF, fs	800	Tol	190	$\lambda_{abs} = 417$ nm, $\lambda_{em} = 514$ nm	71d
	2PEF, fs	800	THF	221	$\lambda_{abs} = 412$ nm, $\lambda_{em} = 552$ nm	71d
191	2PEF, fs	800	Tol	99	$\lambda_{abs} = 387$ nm, $\lambda_{em} = 460$ nm	71d
	2PEF, fs	800	THF	118	$\lambda_{abs} = 384$ nm, $\lambda_{em} = 486$ nm	71d
192	2PEF, fs	800	Tol	42	$\lambda_{abs} = 388$ nm, $\lambda_{em} = 460$ nm	71d
	2PEF, fs	800	THF	65	$\lambda_{abs} = 380$ nm, $\lambda_{em} = 473$ nm	71d
193	2PEF, fs	760	DMF	97	$\lambda_{abs} = 391$ nm, $\lambda_{em} = 527$ nm	172

[a] All the 2PA data are obtained by the two-photon excited fluorescence method (2PEF) and femtosecond laser excitation.

groups such dihexylamino, hexyloxy, and *tert*-butylthiol groups were shown to possess quite large 2PA cross section values (165, 160, and 401 GM at the respective excitation wavelengths of 696, 758, and 788 nm). Furthermore, when each of these chromophores was coordinated to a nickel(II) ion via the nitrogen sites of the phenanthroline core, the resulting complexes preserve the 2PA responsiveness of the free bidentate ligands while the 2PA bands of the nickel(II) complexes were red-shifted relative to those of the free ligands. However, it is noteworthy that when two phenanthroline ligands with a stronger electron-donating dialkylamino group were coordinated to the Ni(II) ion, a decrease of ~20% in the 2PA cross section value was observed. This is in stark contrast to the enhancement of the 2PA response when similar Ni(II) chelates are formed from phenanthroline ligands and weaker electron donors such as alkyloxy and alkylthiol groups.[81]

4.6.2.2. 2,2′-Bipyridine. 2,2′-Bipyridines containing D−π components at the 4,4′ positions, where the π-linkage is C═C (styryl), C═N (imine), or N═N (azo) and D = dialkylamino groups, are known to coordinate well with a number of metal ions such as Ru(II), Re(I), Cu(II), and Zn(II) to form a variety of homoleptic and heteroleptic complexes.[262−264] The homoleptic complexes (ML_n), i.e., in which all ligands (L's) are identical, with either an octahedral or a tetrahedral geometry are of particular interest to second-order NLO materials research. Also known as octupoles, this special class of materials are attractive because they offer an improved transparency/optical nonlinearity tradeoff in comparison to the conventional dipolar molecules for $\chi^{(2)}$ applications.[48] Surprisingly, the experimental two-photon cross section values of these quadrupolar bipyridyl ligands and the associated octupolar metal complexes have not been reported. In a recent theoretical work that examined the one- and two-photon absorption properties of a series of homoleptic bipyridine Zn(II) and Cu(I) complexes (bipyridyl ligands are 4,4′-bis(dibutylaminostyryl)-[2,2′]-bipyridine and 4,4′-bis(diethylaminostyryl)-α,α′-dimethyl[2,2′]-bipyridine), the results indicated that these metal complexes have relatively large two-photon responses, 4−8 times larger than those of the free ligands.[265]

4.6.2.3. Terpyridine. Righetto et al. reported the synthesis and two-photon properties of various terpyridines, 4′-(C_6H_4-*p*-X)-2,2′:6′,2″-terpyridine where X = NBu_2 (TD1), $N(C_{16}H_{33})_2$ (TD_2), *trans*-CH═CH(C_6H_4)-*p*-$N(C_{16}H_{33})_2$ (TD_3), CH_3 (TD_4), NO_2 (TA), and related homoleptic and heteroleptic bis(terpyridine) cationic zinc(II) complexes were investigated by the femtosecond 2PEF method.[266] The 2PA cross section values for the free ligands characterized by the dipolar structure ranged from 76 to 105 GM measured at 720 or 815 nm. However, upon coordination to a cationic Zn(II) ion, a decrease in the 2PA response was observed. For example, one of the homoleptic complexes showed a value of 95 GM (at 815 nm), which corresponds to about half the total σ_2 value of two free ligands. An even larger reduction in the 2PA response was observed for the heteroleptic complexes (77 GM at 815 nm and 30 GM at 830 nm).

4.6.3. Other Transition-Metal Complexes

Wecksler et al. were the first to demonstrate the feasibility of utilizing the NIR two-photon excitation process to sensitize the nitric oxide (NO) release from a model system based on a dye-containing iron/sulfide/nitrosyl cluster, $Fe_2(\mu\text{-RS})_2(NO)_4$ (designated as Fluor-RSE, where RS = the 2-thioethyl ester of fluorescein).[267] The 2PA cross section of Fluor-RSE at 800 nm was found to be $\sigma_2 = 63 \pm 7$ GM via the femtosecond 2PEF technique. The σ_2 value (31.5 GM per ligand) was comparable to the cross section of 36 GM

Chart 9. Structures for Organic Molecules Listed in Table 9

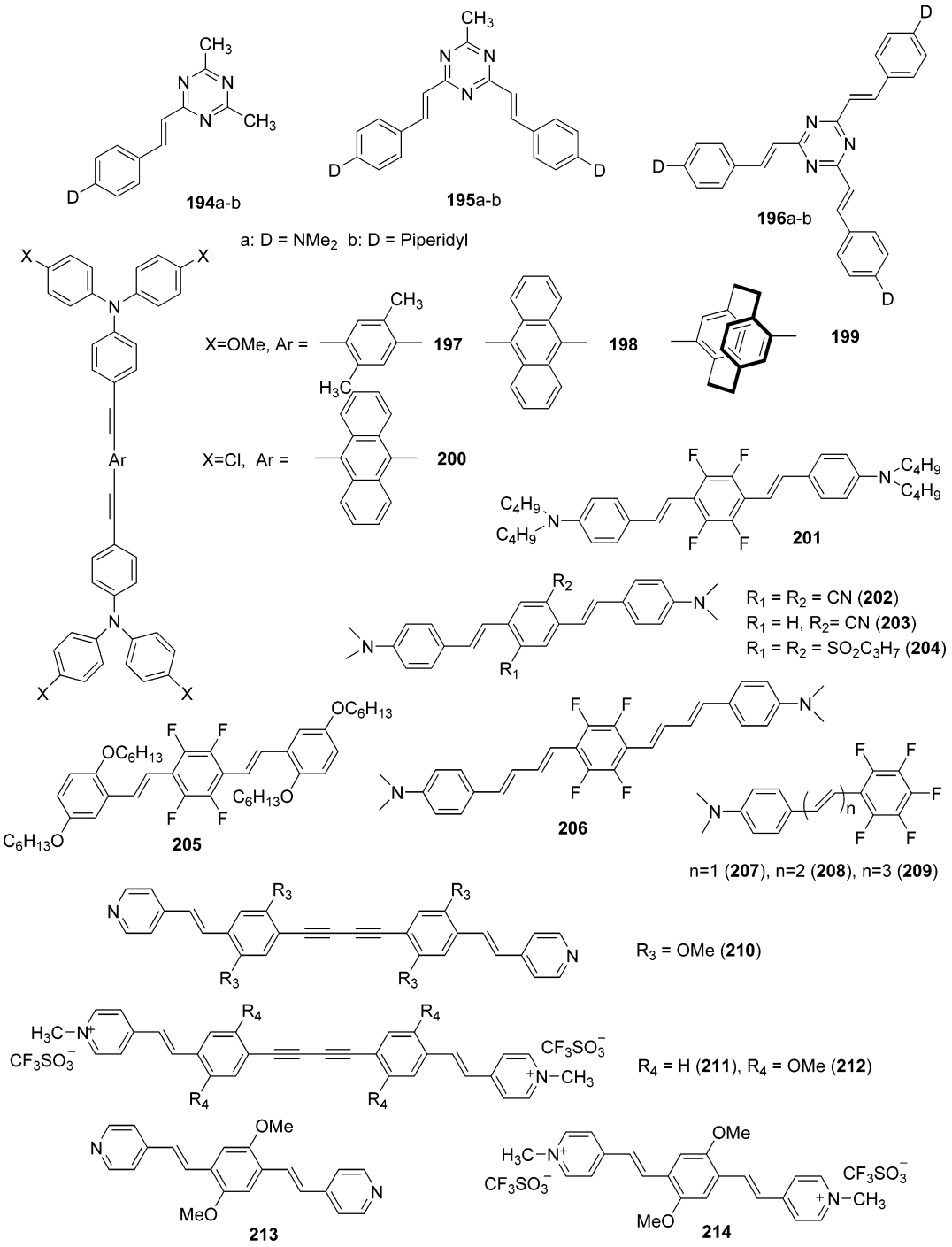

reported for fluorescein dye in pH 11 aqueous solution and of 32 ± 3 GM for Fluor-Et measured under similar conditions. This is expected since there are no direct electronic interactions between iron ions and the fluorescein-carrying sulfide ligands to modify the 2PA properties of the ligands.

Tian et al. reported the synthesis and two-photon properties of an interesting Ru(II)−Schiff base complex with an unusual coordinate mode.[268] This complex, $Ru[(bpy)_2L]PF_6$, where bpy = 2,2′-bipyridine and L was a *S*-dialkyl dithiocarbazate ligand, which was prepared from the condensation reaction 4-[*N*-hydroxyethyl-*N*-(methyl)amino]benzaldehyde and *S*-methyl dithiocarbazate, showed a relatively large effective 2PA cross section value (80 700 GM) upon two-photon excitation at 532 nm with 20 ns pulses. This value is more than twice that of the *S*-diamethyldithiocarbazate ligand (32 300 GM), suggesting the contribution of the $Ru(bpy)_2$ component, most likely via the enhanced excited-state absorption. Another interesting report by Das et al. indicated that while the bis-cinnamaldiminato Schiff base, which was derived from 1,2-phenylenediamine and 4-(dimethylamino)cinnnamaldehyde, did not show any two-photon absorptivity at 890 nm, upon chelating with Zn(II) or Cu(I) ions, the resulting mono- and bis-(Schiff base) complexes exhibited exceptional two-photon cross section values as high as 10 736 GM at the same wavelength determined by a femtosecond open-aperture *Z*-scan technique.[269] This work counteracts a precedent that metal coordination has led to considerable sensitivity reduction in the otherwise 2PA-active ligands. Clearly, more work is

Table 9. 2PA Cross Section Values (σ_2) for Organic Molecules[a]

material	method	excitation wavelength/nm	solvent	σ_2/GM	other properties	ref
194a	2PEF, fs	800	THF	343	λ_{abs} = 400 nm, λ_{em} = 486 nm	110b
194b	2PEF, fs	800	THF	488	λ_{abs} = 391 nm, λ_{em} = 488 nm	110b
195a	2PEF, fs	800	THF	1140	λ_{abs} = 416 nm, λ_{em} = 514 nm	110b
195b	2PEF, fs	800	THF	1345	λ_{abs} = 408 nm, λ_{em} = 526 nm	110b
196a	2PEF, fs	800	THF	2405	λ_{abs} = 418 nm, λ_{em} = 516 nm	110b
196b	2PEF, fs	800	THF	2523	λ_{abs} = 409 nm, λ_{em} = 530 nm	110b
197	2PEF, fs	712	Tol	980	λ_{abs} = 389 nm	173
198	2PEF, fs	842	Tol	400	λ_{abs} = 491 nm	173
199	2PEF, fs	728	Tol	280	λ_{abs} = 370 nm	173
200	2PEF, fs	809	Tol	550	λ_{abs} = 474 nm	173
201	2PEF, fs	760	Tol	1400	λ_{abs} = 430 nm, λ_{em} = 456 nm	61
202	2PEF, fs	816	Tol	3000	λ_{abs} = 471 nm, λ_{em} = 525 nm	61
203	2PEF, fs	740	Tol	260	λ_{abs} = 426 nm, λ_{em} = 483 nm	61
204	2PEF, fs	816	Tol	4100	λ_{abs} = 439 nm, λ_{em} = 528 nm	61
205	2PEF, fs	730	Tol	600	λ_{abs} = 386 nm, λ_{em} = 445 nm	61
206	2PEF, fs	780	Tol	1700	λ_{abs} = 453 nm, λ_{em} = 517 nm	61
207	2PEF, fs	750	Tol	120	λ_{abs} = 370 nm, λ_{em} = 439 nm	61
208	2PEF, fs	825	Tol	300	λ_{abs} = 396 nm, λ_{em} = 479 nm	61
209	2PEF, fs	850	Tol	500	λ_{abs} = 412 nm, λ_{em} = 525 nm	61
210	Z-scan, fs	694	DMSO	363	λ_{abs} = 421 nm	174
211	Z-scan, fs	720	DMSO	554	λ_{abs} = 397 nm	174
212	Z-scan, fs	764	DMSO	848	λ_{abs} = 467 nm	174
213	Z-scan, fs	751	DMSO	199	λ_{abs} = 405 nm	174
214	Z-scan, fs	751	DMSO	346	λ_{abs} = 462 nm	174

a: All 2PA data are obtained by femtosecond laser excitation and two-photon excited fluorescence (2PEF) method or Z-scan method.

needed in this area of 2PA materials research to better understand and correlate the influence of metal ions, the metal−ligand interactions, and other aspects of coordination chemistry in 2PA processes.

4.6.4. Lanthanide Complexes

In the history of MPA, a lanthanide-based material, namely, the CaF_2:Eu^{2+} crystal, was used to first experimentally validate the two-photon excitation process with its blue emission (425 nm) when excited by a ruby laser (694.3 nm).[4] As luminescent materials, lanthanide complexes are attractive for a number of reasons: (i) their visible emissions are quite long-lived; (ii) their absorption and emission can be tuned with the aid of appropriate photoactive ligands; (iii) their "heavy atom" effects can increase the intersystem crossing quantum yield, making the relaxation from their singlet (S_1) excited-state to the lowest triplet (T_1) state more efficient;[270] and (iv) the accessible energy-transfer path between the triplet states of photoactive ligands and the lanthanide ion can facilitate an efficient lanthanide-based upconversion emission via 2PA of the ligand. Thus, these photophysical properties should lend themselves to two-photon applications, especially frequency-upconverted imaging and related emission-based applications. However, there are only a few examples of lanthanide complexes in the literature that have been shown to be excitable via multiphoton processes, e.g., the europium (Eu^{3+}) and terbium (Tb^{3+}) complexes with nucleic acids, proteins, and fluorescent ligands as well as the Nd^{3+} and Yb^{3+} ions that were sensitized by a fluorescein-linked chelating agent.[271,272]

Luo et al. synthesized three terbium complexes containing multidentate ligands designated as L1, L2, and L3.[273] L1 (*N*,*N*′,*N*″-(nitrilotri-2,1-ethanediyl)tris[2,3-dimethoxybenzamide]) could be prepared from tris(2-aminoethyl)amine and methyl 2,3-dimethoxybenzoyl chloride,[274] L2 (*N*,*N*′-[1,2-ethanediylbis(imino-2,1-ethanediyl)]bis[2-hydroxybenzamide]) from diethylenetetraamine and methyl 2-hydroxybenzoate,[275] and L3 (tri[2-(salicyloylamino)ethyl]amine) from tris(2-aminoethyl)amine and methyl salicylate (methyl 2-hydroxybenzoate).[276] These terbium(III) complexes displayed bright green emission upon excitation with near-infrared (510−675 nm and 700−750 nm) nanosecond laser pulses, illustrating that an enhanced two-photon-induced lanthanide-based emission could be attained when suitable ligands were used as sensitizers. In addition, it is noteworthy that the results from separate, comparative photophysical experiments demonstrated that the 2PA property resides at the ligand only, and the subsequent transfer of upconverted energy from the ligands to Tb^{3+} was quite efficient, followed by bright green fluorescence.[273]

Fu et al.[277] reported on an efficient two-photon excitation−fluorescence energy transfer (TPE-FET) sensitization of Eu(III) luminescence in the [Eu(tta)$_3$dpbt] complex, where tta = thienyltrifluoroacetonate and dpbt = 2-(*N*,*N*-diethylanilin-4-yl)-4,6-bis(3,5-dimethylpyrazol-1-yl)-1,3,5-triazine. The 2PA cross section values of the free dpbt ligand and the resulting [Eu(tta)$_3$dpbt] complex were measured over the spectral region of 730−830 nm with femtosecond laser pulses, and the peak values were 185 and 157 GM, respectively. In addition to having a high luminescence quantum yield following one-photon-sensitization for [Eu(tta)$_3$dpbt] (Φ = 0.52 at λ_{em}= 614 nm),[278] this complex is unique also with regard to the high efficiency of two-photon sensitization and the high purity of the red emission. Since the one-photon sensitization of [Eu(tta)$_3$dpbt] by visible light was dominated by an efficient dpbt(S_1)-to-Eu(III) energy transfer,[278] it was postulated that the same mechanism of energy transfer was also operative upon two-photon excitation.

4.6.5. Ferrocene Derivatives

The ferrocene derivatives are thermally and photochemically stable and show a large optical nonlinearity.[279] Zheng et al.[280] reported the synthesis and characterization of two novel ferrocene derivatives containing a vinylene−phenylene−vinylene−fluorene linkage and diphenylamine or nitro groups at the opposite end to one of the cyclopentadienyl

Chart 10. Structures for Organic Molecules Listed in Table 10

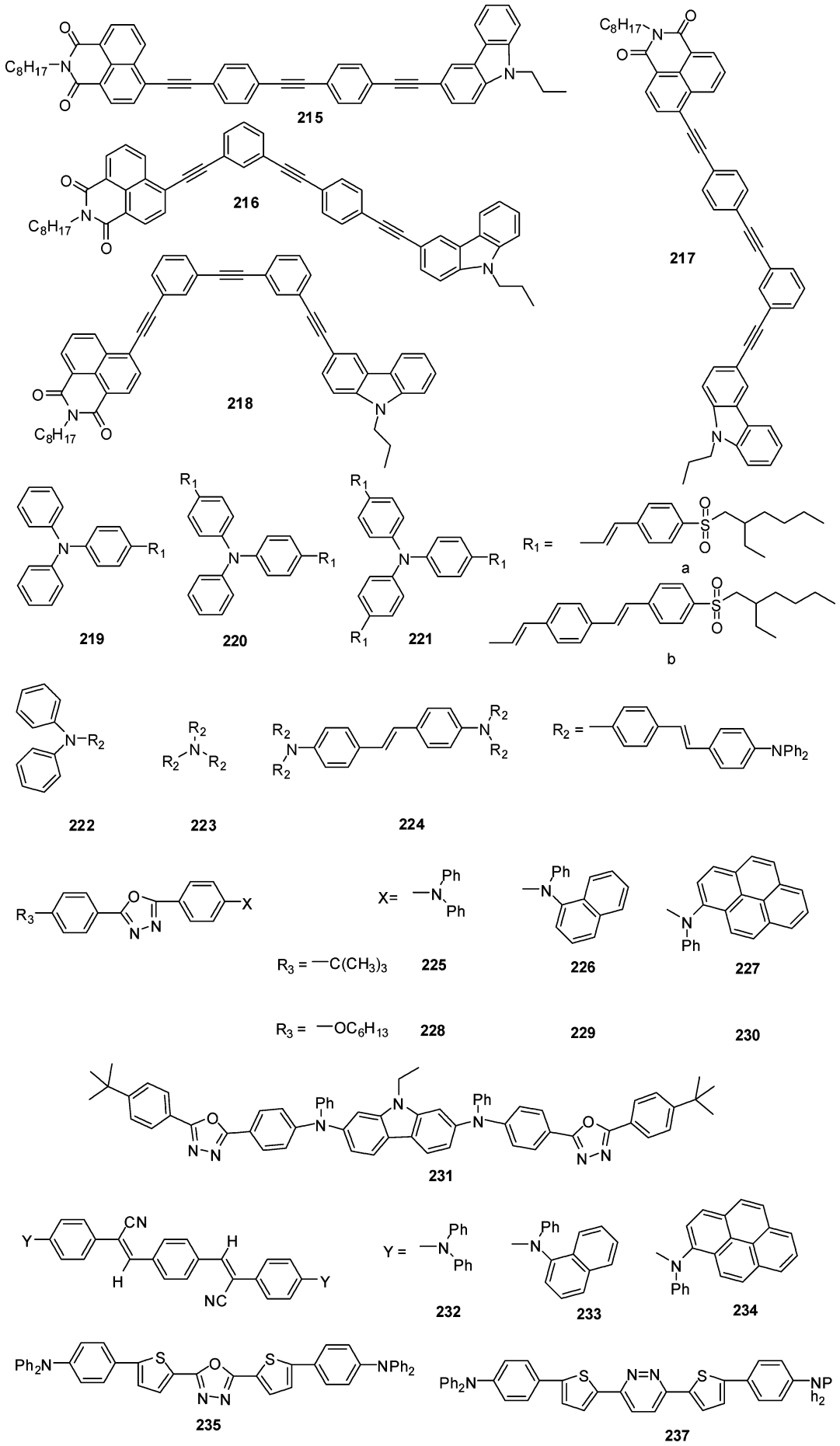

Chart 10 (Continued)

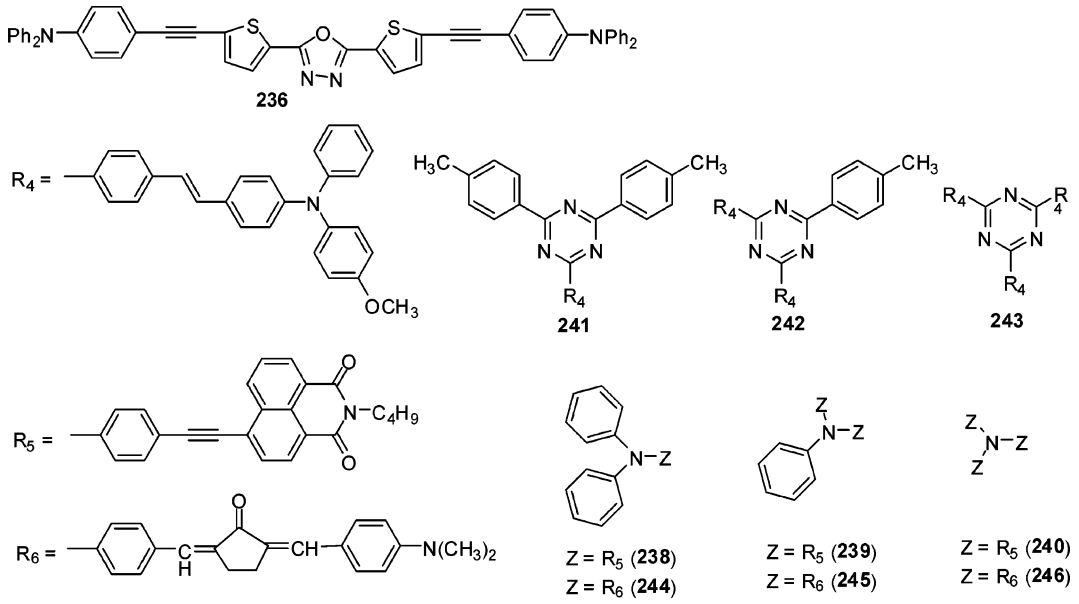

Table 10. 2PA Cross Section Values (σ_2) for Organic Molecules[a]

material	method	excitation wavelength/nm	solvent	σ_2/GM	other properties	ref
215	2PEF, fs	790	Tol	120	λ_{abs} = 390 nm, λ_{em} = ~450 nm	31
216	2PEF, fs	750	Tol	98	λ_{abs} = 374 nm	31
217	2PEF, fs	820	Tol	44	λ_{abs} = 405 nm	31
218	2PEF, fs	790	Tol	15	λ_{abs} = 391 nm, λ_{em} = ~410 nm	31
219a	NLT, ns	810	$CHCl_3$	1100	λ_{abs} = 390 nm, λ_{em} = 459 nm	64
219b	NLT, ns	860	$CHCl_3$	2700	λ_{abs} = 410 nm, λ_{em} = 482 nm	64
220a	NLT, ns	830	$CHCl_3$	1900	λ_{abs} = 412 nm, λ_{em} = 463 nm	64
220b	NLT, ns	820	$CHCl_3$	5600	λ_{abs} = 426 nm, λ_{em} = 486 nm	64
221a	NLT, ns	860	$CHCl_3$	4600	λ_{abs} = 412 nm, λ_{em} = 468 nm	64
221b	NLT, ns	860	$CHCl_3$	9400	λ_{abs} = 428 nm, λ_{em} = 491 nm	64
222	2PEF, fs	670		320	λ_{abs} = 389 nm	100
223	2PEF, fs	680		1300	λ_{abs} = 412 nm	100
224	2PEF, fs	694		2700	λ_{abs} = 417 nm	100
225	2PEF, fs	800	CH_2Cl_2	98	λ_{abs} = 354 nm, λ_{em} = 451 nm	175
226	2PEF, fs	800	CH_2Cl_2	104	λ_{abs} = 359 nm, λ_{em} = 454 nm	175
227	2PEF, fs	800	CH_2Cl_2	135	λ_{abs} = 380 nm, λ_{em} = 461 nm	175
228	2PEF, fs	800	CH_2Cl_2	141	λ_{abs} = 350 nm, λ_{em} = 440 nm	175
229	2PEF, fs	800	CH_2Cl_2	143	λ_{abs} = 358 nm, λ_{em} = 446 nm	175
230	2PEF, fs	800	CH_2Cl_2	249	λ_{abs} = 378 nm, λ_{em} = 462 nm	175
231	2PEF, fs	800	CH_2Cl_2	575	λ_{abs} = 386 nm, λ_{em} = 524 nm	175
232	2PEF, fs	800	CH_2Cl_2	254	λ_{abs} = 453 nm, λ_{em} = 611 nm	175
233	2PEF, fs	800	CH_2Cl_2	540	λ_{abs} = 457 nm, λ_{em} = 620 nm	175
234	2PEF, fs	800	CH_2Cl_2	1180	λ_{abs} = 461 nm, λ_{em} = 645 nm	175
235	2PEF, fs	800	CH_2Cl_2	1390	λ_{abs} = 409 nm, λ_{em} = 511 nm	175
236	2PEF, fs	800	CH_2Cl_2	997	λ_{abs} = 416 nm, λ_{em} = 525 nm	175
237	2PEF, fs	800	CH_2Cl_2	1442	λ_{abs} = 433 nm, λ_{em} = 536 nm	175
238	Z-scan, fs	780	Tol	107	λ_{abs} = 445 nm, λ_{em} = 530 nm	105
239	Z-scan, fs	780	Tol	360	λ_{abs} = 446 nm, λ_{em} = 516 nm	105
240	Z-scan, fs	780	Tol	250	λ_{abs} = 448 nm, λ_{em} = 502 nm	105
241	Z-scan, fs	800	$CHCl_3$	77	λ_{abs} = 418 nm, λ_{em} = 552 nm	110a
242	Z-scan, fs	800	$CHCl_3$	91	λ_{abs} = 425 nm, λ_{em} = 554 nm	110a
243	Z-scan, fs	800	$CHCl_3$	407	λ_{abs} = 430 nm, λ_{em} = 555 nm	110a
244	2PEF, fs	790	$CHCl_3$	781	λ_{abs} = 471 nm, λ_{em} = 546 nm	107
245	2PEF, fs	790	$CHCl_3$	2474	λ_{abs} = 491 nm, λ_{em} = 550 nm	107
246	2PEF, fs	790	$CHCl_3$	3298	λ_{abs} = 492 nm, λ_{em} = 553 nm	107

[a] The 2PA data are obtained from two-photon excited fluorescence (2PEF), nonlinear transmission (NLT), or Z-scan. A femtosecond laser or a nanosecond laser was used for excitation. The nanosecond values are overestimated in comparison with femtosecond values, due to the excited-state absorption (for details, see the first paragraph of section 4.2).

ligands. These ferrocene derivatives have relatively large two-photon (~105 GM at ~775 nm) and three-photon absorptions (2.12−3.00 × 10−25 cm^6 GW^{-2}; 1260−1600 nm) in the IR region as well as excellent thermal stabilities. The three-photon-absorption-based optical limiting properties of these two ferrocene derivatives were investigated by using sub-picosecond IR laser pulses.[280]

Rangel-Rojo et al.[281] prepared and studied the third-order optical nonlinearity of an interesting ferrocene derivative of a 2-amino-1,2,3-triazol-quinone system [2-(yliminomethyl-

Chart 11. Structures for Organic Molecules Listed in Table 11

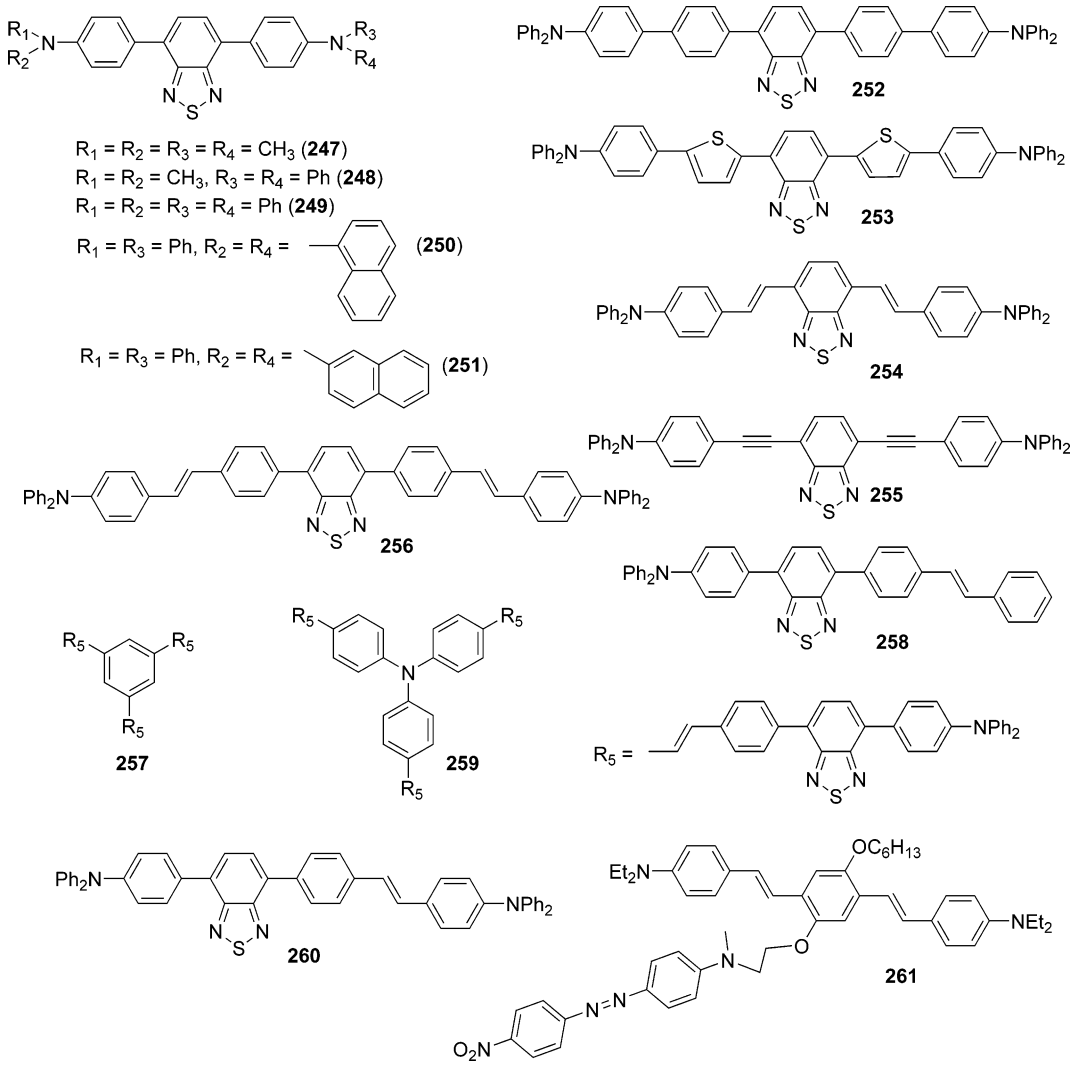

Table 11. 2PA Cross Section Values (σ_2) for Organic Molecules[a]

material	method	excitation wavelength/nm	solvent	σ_2/GM	other properties	ref
247	Z-scan, fs	760	Tol	120	λ_{abs} = 472 nm, λ_{em} = 624 nm	85
248	Z-scan, fs	780	Tol	120	λ_{abs} = 468 nm, λ_{em} = 612 nm	85
249	Z-scan, fs	780	Tol	130	λ_{abs} = 462 nm, λ_{em} = 592 nm	85
250	Z-scan, fs	780	Tol	120	λ_{abs} = 462 nm, λ_{em} = 588 nm	85
251	Z-scan, fs	780	Tol	110	λ_{abs} = 465 nm, λ_{em} = 591 nm	85
252	Z-scan, fs	780	Tol	200	λ_{abs} = 426 nm, λ_{em} = 550 nm	85
253	Z-scan, fs	780	Tol	280	λ_{abs} = 530 nm, λ_{em} = 661 nm	85
254	Z-scan, fs	780	Tol	330	λ_{abs} = 512 nm, λ_{em} = 617 nm	85
255	Z-scan, fs	780	Tol	200	λ_{abs} = 480 nm, λ_{em} = 568 nm	85
256	Z-scan, fs	780	Tol	330	λ_{abs} = 443 nm, λ_{em} = 564 nm	85
257	Z-scan, fs	720	Tol	780	λ_{abs} = 451 nm, λ_{em} = 577 nm	85
258	Z-scan, fs	720	Tol	170	λ_{abs} = 448 nm, λ_{em} = 577 nm	85
259	Z-scan, fs	780	Tol	800	λ_{abs} = 459 nm, λ_{em} = 583 nm	85
260	Z-scan, fs	780	Tol	230	λ_{abs} = 452 nm, λ_{em} = 584 nm	85
261	NLT, ns	730		2600		176
	NLT, ns	850		2600		176
	NLT, ns	980		800		176

[a] The 2PA data are obtained by the nonlinear transmission method (NLT) or the Z-scan method. A femtosecond laser or a nanosecond laser was used for excitation.

ferrocenyl)naptho-1,2,3-triazole-4,9-dione] in solution using the Z-scan technique with a tunable 10 ps laser source that allowed the resolution of the absorptive and refractive contributions to the nonlinearity at several wavelengths near resonance. It was concluded that the nonlinear response was attributed to the metal−ligand charge transfer that gave rise to the observed absorption features. The absorptive contribution switched from a saturable process (λ_{ex} 500−540 nm) to

Chart 12: Molecular Structures and Idealized Dipole Orientations

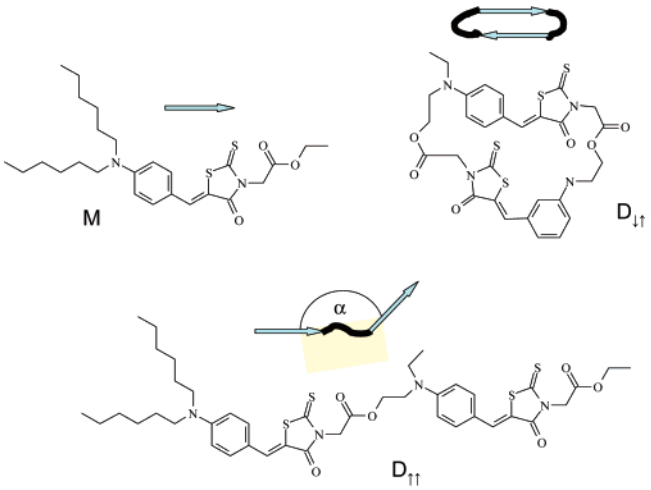

Chart 13: Molecular Structure of m-LPPP, Where $n \sim 12$

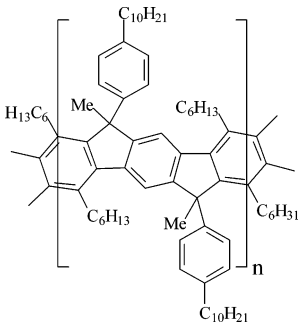

2PA (λ_{ex} 580−660 nm) as the excitation moved away from the maximum of the 2PA band. The two photon absorption was observed to peak at 580 nm ($\beta = 0.73 \pm 0.11$ cm/GW).

4.6.6. Alkynylruthenium Complexes

In their extensive work on organometallic complexes for nonlinear optics, Humphrey, Samoc, et al.[282,283] have synthesized and characterized many 1,2-bis(diphenylphosphine)-ethane-Ru(II)-based alkynylcomplexes that exhibited large two-photon responses with cross section values as high as 2100 GM.[283] These Ru(II) complexes are an interesting class of two-photon materials from the standpoint of electrochemical switching. Thus, the octupolar compound, 1,3,5-{*trans*-[RuCl(dppe)$_2$]C≡C-4-C$_6$H$_4$C≡C}$_3$C$_6$H$_3$ (**1**) could be reversibly oxidized in solution using an optically transparent thin-layer electrochemical cell, with the oxidation to $\mathbf{1}^{3+}$ resulting in the appearance of a strong absorption band at 11 200 cm^{-1} (893 nm), in contrast to the case for **1**, which is optically transparent at frequencies below 20 000 cm^{-1} (500 nm). The transient absorption (TA) data for **1** revealed efficient 2PA ($\sigma_2 \sim 10^3$ GM), whereas the transient absorption data for $\mathbf{1}^{3+}$ indicated saturable absorption (decay time ca. 1 ps). The switching of the third-order nonlinearity in the $\mathbf{1}/\mathbf{1}^{3+}$ pair represents the first demonstration of a femtosecond time-scale process that is being responsible for nonlinear electrochromism.[283d]

4.6.7. Platinum Acetylides

Platinum(II)−alkynyl complexes were first reported by Sonogashira and co-workers.[284] These molecules have an overall rigid-rod configuration, and the transition metal interacts with the π-electrons electrons of the carbon chain framework, leading to a more delocalized π-electron system. An assortment of Pt-acetylides has been synthesized, ranging from small molecules and oligomers to lyotropic liquid-crystalline polymers.[93,285] The organometallic platinum compounds have exhibited relatively large NLO effects and promising optical power limiting (OPL) properties. In particular, an example of a *trans*-arylethynyl platinum complex, bis((4-(phenylethynyl)phenyl)-ethynyl)bis(tributylphosphine) platinum(II), whose β value was first reported to be 0.34 cm/GW at 615 nm measured with 10 ps laser pulses, has been studied extensively for its OPL properties.[286] More recently, Vestberg et al. prepared a series of closely related *trans*-arylethynyl platinum complexes that were end-capped with 2,2-bis(methylol)propionic-acid-based dendrons.[288] The presence of large dendrons in these compounds was found to have the effect of hampering the quenching of phosphorescent states by oxygen, resulting in a considerably longer decay time of the phosphorescence (0.1−0.4 ms). More importantly, their results from two-photon-induced fluorescence and Z-scan (fs pulses at low pulse repetition frequency at approximately 720 nm) studies revealed that the 2PA cross section values of the *trans*-arylethynyl platinum complex and the related dendrimers are on the order of 0.01 cm/GW, substantially smaller than the previously reported value.[287] They also showed that Z-scans performed at a high pulse repetition frequency gave an apparent higher 2PA cross section value stemming from the population of excited triplet states, contributing to the incoherent MPA.[288]

4.7. Porphyrins and Metallophophyrins

Porphyrins and related tetrapyrrolic compounds (e.g., phthalocyanines) are macrocyclic π-systems composed of alternating four pyrrole-2,5-diyl units (or isoindole for phthalocyanine) with four methine (═CH−) bridges or four imine (═N−) bridges (for phthalocyanines). Porphyrin is an important structural component of many biological molecules such as chlorophyll, cytochrome *c*, hemeproteins, hemoglobin, etc., and it has been useful for decades as a tumor marker and a photosensitizer in one-photon-based photodynamic therapy (PDT).[289] In the past, while their reverse saturable absorption properties have been extensively investigated,[290] their 2PA properties were largely neglected, and in a few cases, where 2PA cross section values were measured, they were only on the order of 1−10 GM.[291] The pervasive drive and successes in advancing the 2PA efficiency of organic compounds via molecular engineering and rational synthesis recently spread to other classes of molecular and polymeric materials; porphyrins and, to a lesser extent, phthalocyanines are attractive target materials for such an exploitation, especially two-photon-based PDT.[291d,291e] Thus, within a relatively short time frame, the successes in structural modification and new insights, such as one-photon-resonance (Q-band) enhanced 2PA,[292] conjugative extension via meso−meso-linked vinylene[293] and butadiyne bridges,[294] and self-assembly driven by complimentary metal coordination,[295,296] have led to dramatic improvements in the 2PA cross section values for this classes of molecules. Furthermore, a recent work[298] indicated that expanding the size of the macrocyclic π systems can lead to molecular systems (core-modified aromatic, 42 π, decaphyrins) with intrinsic cross section values well over 100 000 GM (see Tables 12 and 13). However, since the reported Q-band enhanced 2PA systems have had their exceedingly large femto-second cross

Chart 14. Structures for Porphyrins, Metallophophyrins, and Other Metal Complexes Listed in Table 12

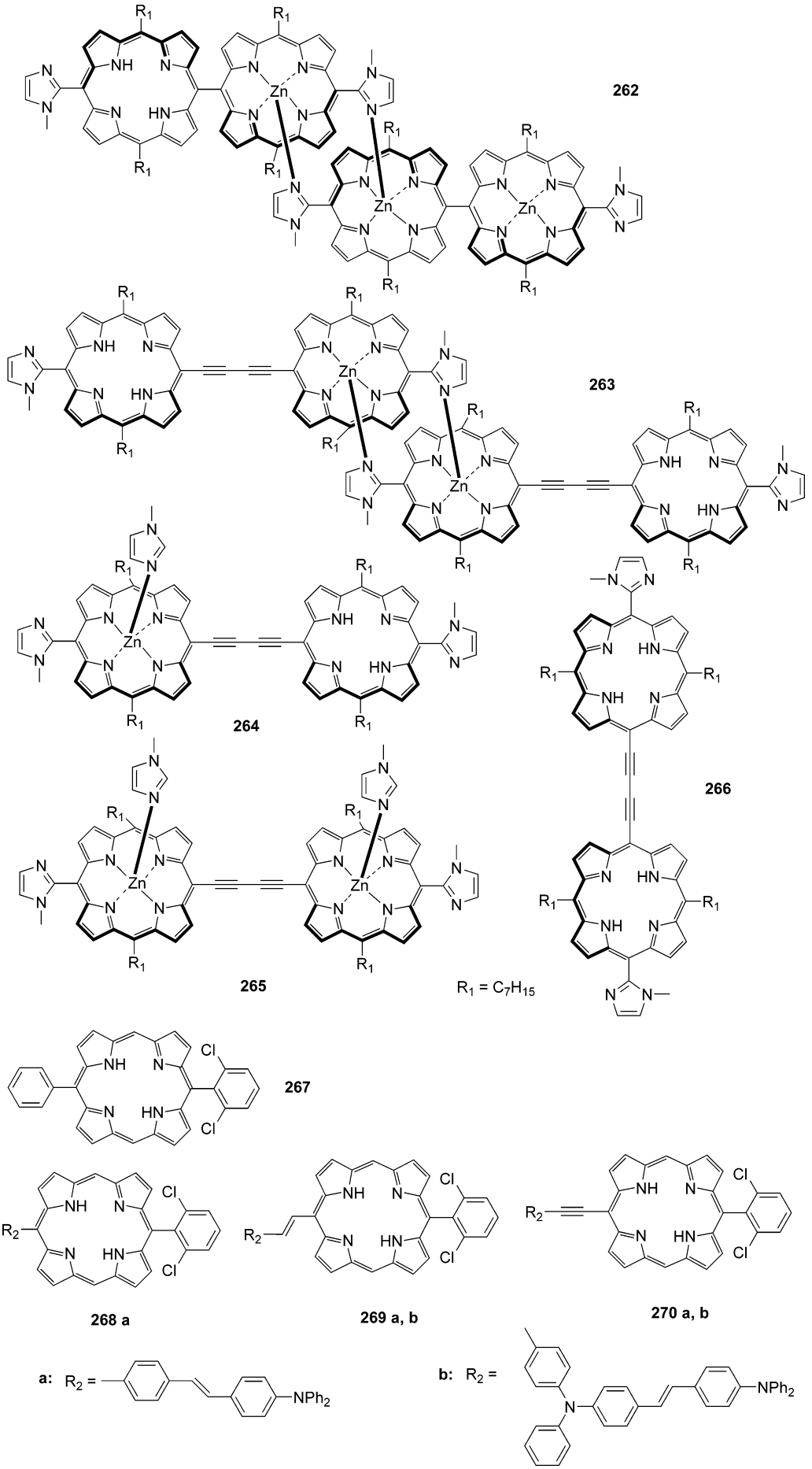

Chart 14 (Continued)

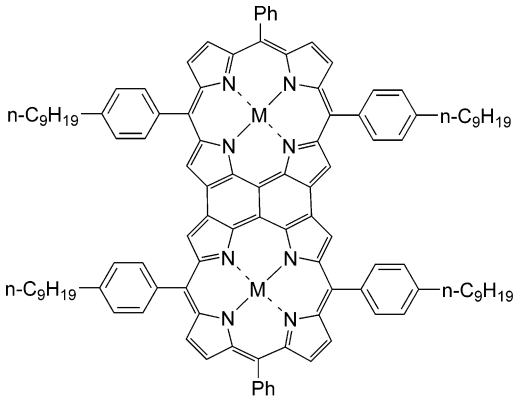

M = Zn (**271**), Cu (**272**), Ni (**273**), Metal Free (**274**)

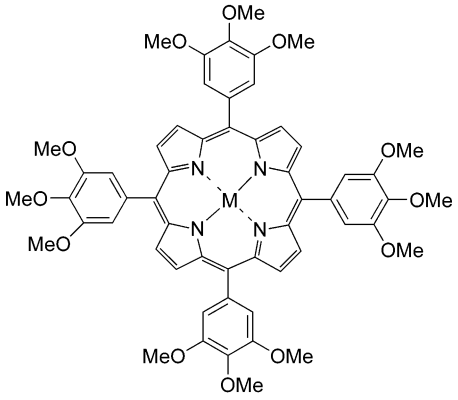

M = GaCl (III, **275**), InCl (III, **276**), TlCl (III, **277**), Sn (II, **278**), Pb (II, **279**)

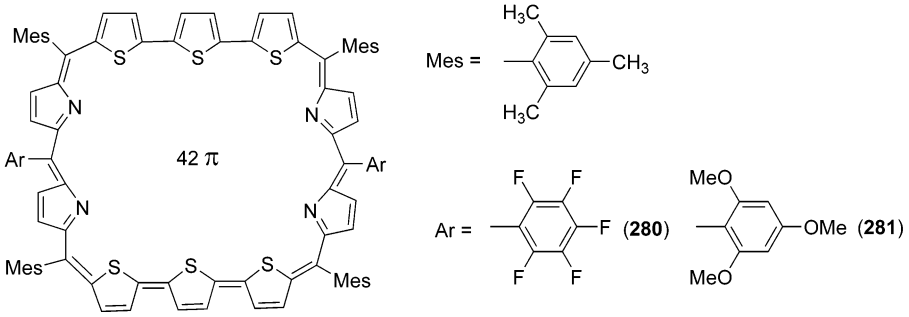

sections measured at wavelengths (usually around 800 nm) very near their Q bands, it should be kept in mind that, at these excitation wavelengths, these systems are not completely transparent to linear absorption, and the significant contributions by one-photon processes should be, if possible, quantified. In this context, it is not appropriate to compare these seemingly ultralarge cross section values with those of purely two-photon absorbing molecules.

4.8. Nanoparticles

Within the broad interest in nanostructured materials, there is increasing attention focused on the nonlinear optical properties of metal and semiconducting nanoparticles in life science research, especially the aspect of surface-plasmon enhancement that is important to fluorescence-based imaging applications.[306,307] From the materials standpoint, 2PA has been investigated so far for two-dimensional (2D) quantum wells,[308] one-dimensional (1D) quantum wires,[309] and quantum dots,[310−323] as well as for Au or Ag nanoparticles.[324] Historically, the third-order optical nonlinearities (2PA) of nanoparticles can be traced back to 1988, when Banyai et al. theoretically investigated the nonlinearities of GaAs quantum dots (QDs).[310] They predicted that two-photon resonance was energetically above the exciton resonance for quantum-dot radii, with values that were between the Bohr radii for the electron and the hole. Subsequently, the 2PA properties of quantum dots based on other semiconducting materials such as CdS,[311,313,317,318] InGaN/GaN,[315] CdTe,[319] InAs−GaAs,[320] and CdSe[323] as well as hybrid chitosan−ZnS quantum dots[322] were investigated. In 1989, the 2PA in GaAs/AlGaAs multiple quantum wells was first observed by Nithisoontorn et al.,[308] and 3 years later, Cingolani et al. reported on the polarization-dependent 2PA in GaAs/AlGaAs quantum wires.[309]

Besides quantum dots, 2D quantum wells, and 1D quantum wires, other types of nanocrystals have also been found to be multiphoton active. Fourkas et al.[324b] demonstrated that highly efficient and strong photoluminescence could be generated from the gold nanoparticles with diameters as small as a few nanometers upon excitation with sub-100 fs pulses of 790 nm light, and at the irradiance comparable to or less than those typically used for multiphoton imaging of fluorophore-tagged biological samples. Majchrowski et al. prepared nanocomposites from chromium(III)-doped yetternium−aluminu−borate (YAB:Cr) nanocrystallites and oligo(etheracrylate) polymer matrixes with NC concentrations varied from 0.2 to 7.9 wt %. They observed a temperature dependence (below 35 K) 2PA in these nanocomposites, and at the optimal concentration (3 wt %) and NC size (∼24 nm), a large β value of 30 ± 2 cm/GW was measured at ∼5 K. The Cr(III) dopant ions inside the studied NC appeared to play the crucial role in the observed nonlinear optical phenomena.[325] Cohanoschi et al.[324a] observed strong surface plasmon enhancement of two- and three-photon absorption of organic chromophores in an aqueous solution containing an activated gold colloid. Silver or gold nanoparticles, or quantum dots coated with a self-assembled layer of two-photon absorbing chromophores, have also been reported to have a large 2PA. Zhang et al.[326] found enhanced 2PA by combination of the large organic salt to CdS nanoclusters. Marder, Perry, and co-workers[58,327] also observed strong enhancement of the 2PA of organic molecules near silver nanoparticle fractal clusters, and this enhancement effect was manifested in the composite materials with very strong 2PA and two-photon-excited fluorescence properties.

Lal et al.[328a] reported the preparation, luminescent properties, and bioimaging applications of a novel "zinc sulfide

Table 12. 2PA Cross Section Values (σ_2) for Porphyrins, Metallophophyrins, and Other Metal Complexes[a]

material	method	excitation wavelength/nm	solvent	σ_2/GM	other properties[b]	ref
262	Z-scan, fs	964	$CHCl_3$	370		296
263	Z-scan, fs	887	$CHCl_3$	7600		296
264	Z-scan, fs	873	$CHCl_3$	1800		296
265	Z-scan, fs	873	$CHCl_3$	1200		296
266	Z-scan, fs	873	$CHCl_3$	1000		296
267	2PEF, fs	750	CH_2Cl_2	10	$\lambda_{abs} = 472$ nm, $\lambda_{em} = 624$ nm	298
268a	2PEF, fs	806	CH_2Cl_2	110	$\lambda_{abs} = 468$ nm, $\lambda_{em} = 612$ nm	298
269a	2PEF, fs	914 (816)	CH_2Cl_2	560 (480)	$\lambda_{abs} = 462$ nm, $\lambda_{em} = 592$ nm	298
269b	2PEF, fs	916 (826)	CH_2Cl_2	880 (810)	$\lambda_{abs} = 462$ nm, $\lambda_{em} = 588$ nm	298
270a	2PEF, fs	907 (820)	CH_2Cl_2	500 (730)	$\lambda_{abs} = 465$ nm, $\lambda_{em} = 591$ nm	298
270b	2PEF, fs	915 (803)	CH_2Cl_2	1100 (910)	$\lambda_{abs} = 426$ nm, $\lambda_{em} = 550$ nm	298
271	Z-scan, fs	800	Tol	14000		299
272	Z-scan, fs	800	Tol	12000		299
273	Z-scan, fs	800	Tol	15000		299
274	Z-scan, fs	800	Tol	13000		299
275	Z-scan, fs	840	boric acid glass	31	$\lambda_{abs} = 421$ nm, $\lambda_{em} = 596$ nm	300
		900		36		300
		1200		53		300
		1350		25		300
276	Z-scan, fs	840	boric acid glass	114	$\lambda_{abs} = 426$ nm, $\lambda_{em} = 602$ nm	300
		900		65		300
		1200		47		300
		1350		36		300
277	Z-scan, fs	840	boric acid glass	52	$\lambda_{abs} = 443$ nm, $\lambda_{em} = 692$ nm	300
		900		57		300
		1200		26		300
		1350		32		300
278	Z-scan, fs	840	boric acid glass	64	$\lambda_{abs} = 427$ nm, $\lambda_{em} = 601$ nm	300
		900		31		300
		1200		77		300
		1350		32		300
279	Z-scan, fs	840	boric acid glass	56	$\lambda_{abs} = 450$ nm, $\lambda_{em} = 715$ nm	300
		900		43		300
		1200		67		300
		1350		32		300
280	Z-scan, fs	780	CH_2Cl_2	108000	$\lambda_{abs} = 550$ nm	297
281	Z-scan, fs	780	CH_2Cl_2	106600	$\lambda_{abs} = 548$ nm	297

[a] All 2PA data are obtained by the two-photon excited fluorescence (2PEF) method or the Z-scan method. A femtosecond laser was used for excitation. [b] Sorret band (λ_{abs}) and emission wavelength (λ_{em}).

(core)−two-photon dye-silica (shell)" multilayered heterostructure. This method utilized reverse micelles synthesis involving multistep reactions, and led to composite nanoparticles with different sizes and morphology. The size of these composite nanoparticles was typically 15−30 nm. An increase in the luminescence intensity (similar to 70 times higher) and in the fluorescence lifetime was observed for the dye encapsulated within the silica nanobubble. Kim et al.[328b] reported dye-concentrated ORMOSIL nanoparticles, which showed a fluorescence-based ratiometric pH response, by one- and two-photon excitations. Recently, a novel class of two-photon dyes exhibiting enhanced fluorescence and 2PA activity by nanoaggregation was also reported by Kim et al.[328c]

4.9. Biomolecules and Derivatives

The two-photon cross section (mostly nanosecond) data of biological molecules such as bacteriorhodopsin (127−289 GM), β-carotene (720 GM, 35 ps pulses), chlorophyll-a (2 GM), nicotimide adenine (reduced formed, NADH; 340 GM), retinal, and derivatives (26−29 GM) were tabulated in Kershaw's review.[155] Recent investigations in this area have provided additional cross section data for a number of interesting biomolecules or their fluorogen-labeled derivatives: DNA (0.06 GM) and related nucleotides, guanosine 5′-monophosphate (0.7 GM) and uridine 5′-monophosphate (0.51 GM) measured at 532 nm with 28 ps pulses,[329] as well as 6MPA (4-amino-6-methyl-8-(2-deoxy-β-D-ribofuranosyl)-7(8H)-pteridone), a fluorescent analogue for adenine and guadine (3.4 GM at 659 nm),[330] the naphthalene-2,3-dicarboxyaldehyde derivative of glycine (∼0.5 GM at ∼840 nm),[331] and a fluorescamine derivative of leucine enkephalin (∼1.1 GM at 780 nm).[331] A noticeable development in this area is the very high 2PA excitation property of some biomaterials such as green fluorescence protein[332,333] (wild-type GFP ∼ 3 GM and enhanced GFP ∼ 180 GM at ∼800 nm), a phycoerythrobilin (PEB) phytofluor protein (known as Cph1(N514)-PEB, 20−30 GM at 792 nm),[334] and cytochrome *c* (∼1000 GM at 600 nm).[335] Thus, it appears that, with some possible exceptions that await verification, the nascent biomolecules have generally much smaller two-photon cross section values than those of synthetic organic 2PA materials.

5. Nonlinear Optical Characterizations of Multiphoton Active Materials

5.1. Selection of Excitation Wavelengths

For a given nonlinear absorbing material, the choice of the excitation wavelengths depends on the purpose of specific studies or applications. For novel-material-based studies, it

Chart 15. Structures for Porphyrins, Metallophophyrins, and Other Metal Complexes Listed in Table 13

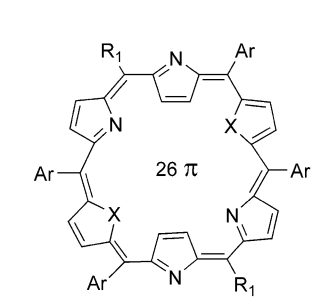

282

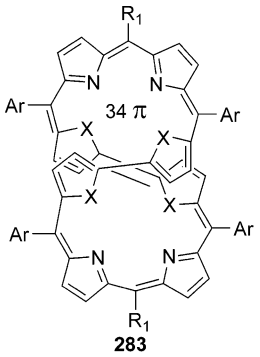

283

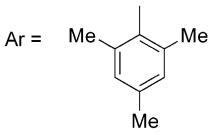

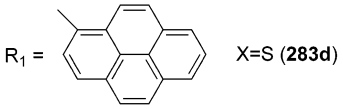

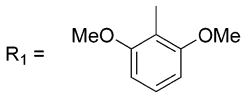

X= S (**282a**), Se (**282b**)

X= S (**282c**), Se (**282d**)

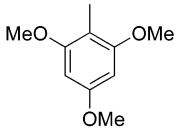

X= S (**282e**), Se (**283c**)

X= S (**282f**), S(**283a**), Se(**283b**)

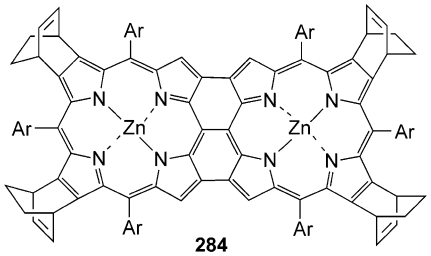

284

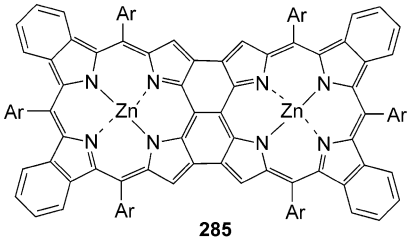

285

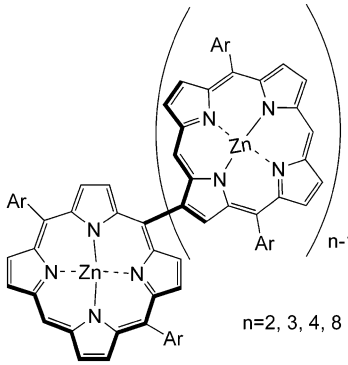

286-n_H

n=2, 3, 4, 8

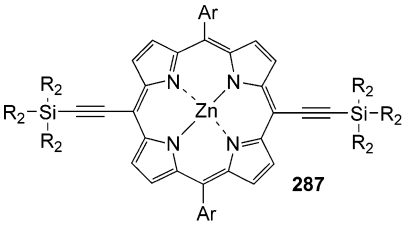

287

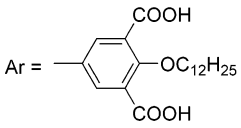

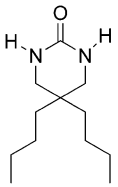

G

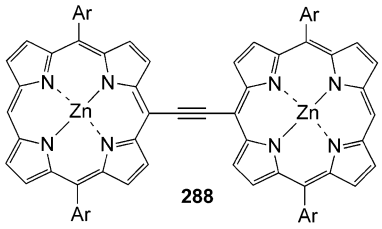

288

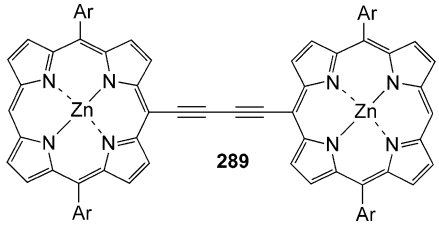

289

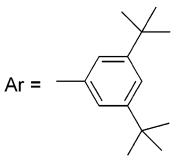

R_2 = n-Hexyl

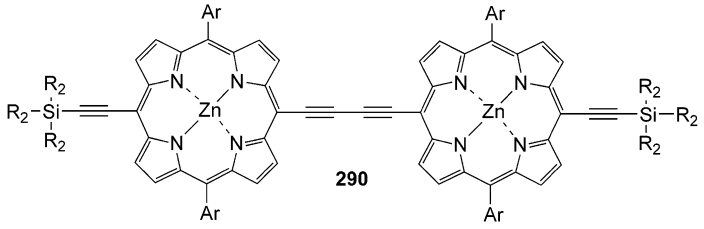

290

Chart 15 (Continued)

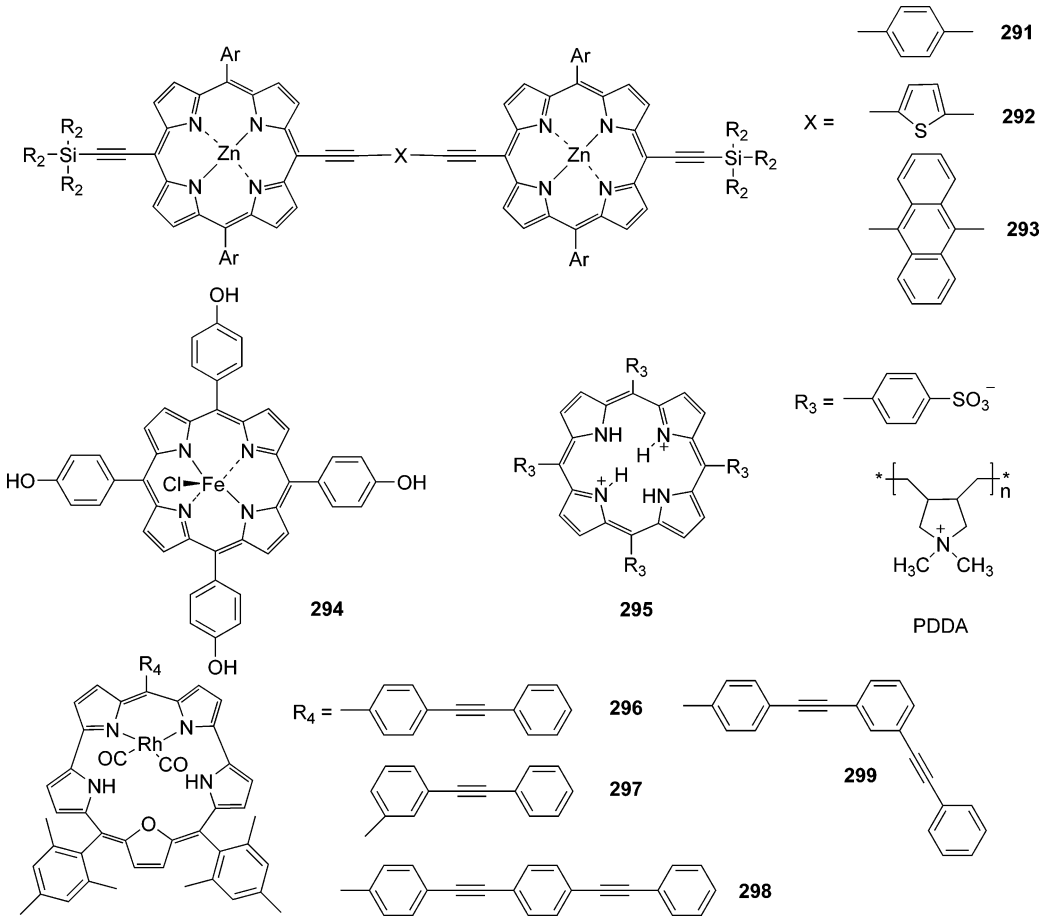

is important to know their nonlinear absorption spectral structures and then to choose suitable excitation wavelengths. Generally speaking, it is not an easy task to measure the complete MPA spectra for a given material (see subsection 5.4). For simplicity, Figure 4 shows a schematic diagram of the linear (one-photon) absorption spectral band centered on the wavelength position of λ_0, as well as the corresponding multi(2 and 3)-photon absorption bands for a given medium. Here, it should be noted that the selection rules, pathways of molecular transitions, resonance enhancements, and magnitudes of relevant matrix elements for one-photon and multiphoton processes may be generally different; therefore, even for a given material, the relative shapes of MPA spectra may differ from that of the corresponding one-photon absorption spectrum. For instance, for centrosymmetric molecules, the 2PA spectrum is inherently different from the one-photon absorption (1PA) spectrum because of the different selection rules (see subsection 2.3). For 3PA processes, the selection rules are the same as those for 1PA irrespective of the molecular symmetry, and the same bands should appear in the 3PA spectrum. However, the intensity and relative distribution of different spectral components still may differ from the latter. For these reasons, the peak (or central) wavelengths for the corresponding 2PA and 3PA bands may not be exactly located at the $2\lambda_0$ and $3\lambda_0$ positions. Based on very limited results of spectral comparison between 1PA and 2PA spectra for a given sample medium, it could be roughly assumed that the 2PA peak wavelength is close to or slightly shorter than the $2\lambda_0$ position. On the other hand, there is still a lack of experimental results of reliable comparisons among one- and three-photon as well as the one- and four-photon absorption spectra. Nevertheless, for a given sample medium, without knowing its MPA spectral structures, researchers may choose those excitation wavelengths located in the following spectral ranges for their MPA studies:

$$\lambda_0 \ll \lambda_{exc} \leq 2\lambda_0 \quad \text{(for 2PA)}$$

$$2\lambda_0 \ll \lambda_{exc} \leq 3\lambda_0 \quad \text{(for 3PA)}$$

$$3\lambda_0 \ll \lambda_{exc} \leq 4\lambda_0 \quad \text{(for 4PA)} \qquad (22)$$

There are several different types of coherent light sources that can provide the intense coherent radiation with suitable wavelengths for multiphoton related studies.

(1) *Pulsed or mode-locked lasers working in single (or several discrete) wavelength(s)*: such as Nd:YAG lasers (1064 nm, 532 nm), Ti:sapphire lasers (~800 nm), excimer lasers, and Raman lasers.

(2) *Pulsed lasers and optical parametric generators working in certain tunable spectral ranges*: such as tunable dye lasers, Ti:sapphire lasers, and laser beam-pumped optical parametric generators (OPGs) that are based on second-order nonlinear crystals.

(3) *Coherent white-light continuum generation*: An intense coherent white-light beam can be generated in various transparent nonlinear optical media (such as heavy water, quartz crystal, optical glasses, and fibers), excited by an input laser beam of high-peak power. This type of coherent light source with superbroad continuous spectral distribution is especially useful for MPA studies.

Table 13. 2PA Cross Section Values (σ_2) for Porphyrins, Metallophophyrins, and Other Metal Complexes[a]

material	method	excitation wavelength/nm	solvent	σ_2/GM	other properties	ref
282a	Z-scan, fs	780	CH_2Cl_2	2208		301
282b	Z-scan, fs	780	CH_2Cl_2	7800		301
282c	Z-scan, fs	780	CH_2Cl_2	3828		301
282d	Z-scan, fs	780	CH_2Cl_2	9060		301
282e	Z-scan, fs	780	CH_2Cl_2	4740		301
282f	Z-scan, fs	780	CH_2Cl_2	24000		301
283a	Z-scan, fs	780	CH_2Cl_2	81000		301
283b	Z-scan, fs	780	CH_2Cl_2	90600		301
283c	Z-scan, fs	780	CH_2Cl_2	67340		301
283d	Z-scan, fs	780	CH_2Cl_2	87694		301
284	Z-scan, fs	1250 (1260)	CH_2Cl_2[b]	11400 (10600)		302
285	Z-scan, fs	1260	CH_2Cl_2[b]	15400		302
287	2PEF, fs	833	CH_2Cl_2[c]	20	$\lambda_{abs} = 652$ nm (Q-band)	294
288	2PEF, fs	821		8200	$\lambda_{abs} = 730$ nm (Q-band)	294
289	2PEF, fs	830		5500	$\lambda_{abs} = 711$ nm (Q-band)	294
290	2PEF, fs	873		9100	$\lambda_{abs} = 756$ nm (Q-band)	294
291	2PEF, fs	859		3800	$\lambda_{abs} = 697$ nm (Q-band)	294
292	2PEF, fs	871		3100	$\lambda_{abs} = 725$ nm (Q-band)	294
293	2PEF, fs	838		9000	$\lambda_{abs} = 770$ nm (Q-band)	294
294		1150	/	80		303
286-n_H	Z-scan, fs	800	Tol/THF[d]	<100		304
286-2_H-G	Z-scan, fs	800		4500		304
286-3_H-G	Z-scan, fs	800		9600		304
286-4_H-G	Z-scan, fs	800		11800		304
286-8_H-G	Z-scan, fs	800		12800		304
295−20 bilayer film	Z-scan, fs	806	/	1700		305
295−50 bilayer film	Z-scan, fs	806		1100		305
295 water solution	Z-scan, fs	806		1000		305
296	Z-scan, fs	780	CH_2Cl_2	4496		297b
297	Z-scan, fs	780	CH_2Cl_2	1537		297b
298	Z-scan, fs	780	CH_2Cl_2	15525		297b
299	Z-scan, fs	780	CH_2Cl_2	10523		297b

[a] All 2PA data are obtained by the two-photon excited fluorescence (2PEF) method or the Z-scan method. A femtosecond laser was used for excitation. [b] CH_2Cl_2 containing 1% butylamine. [c] CH_2Cl_2 containing 1% pyridine. [d] Toluene/THF (9:1).

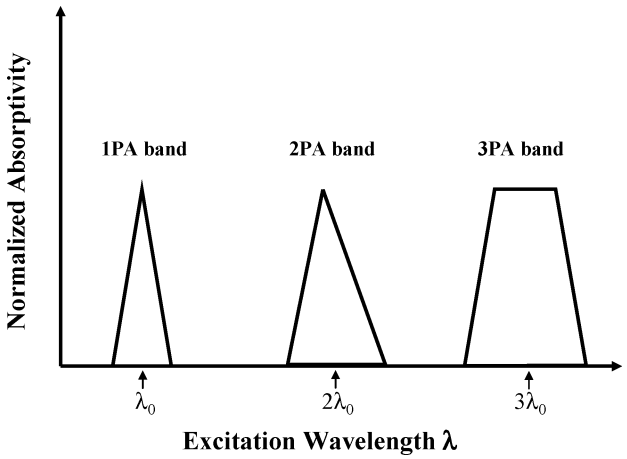

Figure 4. Schematic description of relative spectral positions and bandwidths for 1PA, 2PA, and 3PA bands. The relative shapes of these three absorptive bands do not have to be the same.

5.2. Measurements of MPA Cross Sections at Discrete Wavelengths

5.2.1. Nonlinear Transmission (NLT) Method

The most simple and straightforward method to experimentally determine the value of the MPA coefficient or cross section is to measure the nonlinear transmission of the sample as a function of the input intensity of an applied laser beam with a given wavelength. For example, if the linear (one-photon) absorption of a sample medium at the incident wavelength is negligible, the 2PA-induced nonlinear transmission for an input laser beam passing through the given medium can be expressed as follows (cf. eq 10):

$$T(I_0) = \frac{1}{1 + \beta(\lambda) I_0 l_0} \quad \text{(2PA)} \tag{23}$$

Here I_0 is the initial intensity of the incident light beam of wavelength λ and l_0 is the optical path length (thickness) of the sample. In eq 23, it was assumed that (i) the incident light beam possesses a uniform transverse intensity distribution and (ii) the beam's section is unchanged within the sample's path length. However, these two assumptions are not exactly held under most experimental conditions, under which the incident beam is usually focused on the center of a sample with thickness of about 0.5−2 cm. In this case, the focused laser beam has a nearly Gaussian transverse intensity distribution near the sample center.[336] With this correction, eq 23 can be modified as[337]

$$T(I_0) = \frac{\ln(1 + \beta(\lambda) I_0 l_0)}{\beta(\lambda) I_0 l_0} \quad \text{(2PA)} \tag{24}$$

For the same measured nonlinear transmission values, the estimated β value from eq 23 will be ~0.43 times smaller than the value estimated from eq 24, as shown in Figure 5. On the other hand, for a focused laser beam, the variation of beam size along the *z*-axis can be approximately described by a hyperbolic function, and the effective focal depth or the so-called Rayleigh length is determined by the focal length of a focusing lens as well as the spatial structures of

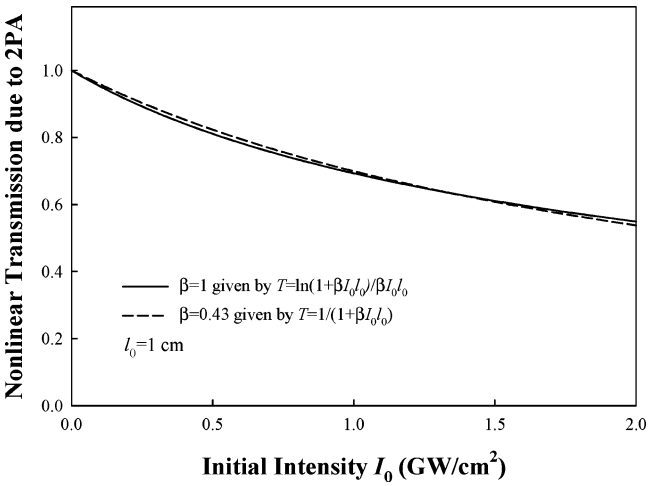

Figure 5. 2PA-induced nonlinear transmission as a function of the input light intensity. The solid line is the theoretical curve given by the formula with Gaussian transverse intensity correction and assumed β=1 cm/GW; the dashed line is the theoretical curve given by the original formula of 2PA with a uniform transverse intensity distribution and assumed β=0.43 cm/GW.

the laser beam. To meet the second assumption mentioned above, the effective focal depth of the focused laser beam should be comparable to the path length of the sample medium.

Based on the known values of I_0 and l_0 and the measured value of the nonlinear transmission $T(I_0)$, the value of the 2PA coefficient $\beta(\lambda)$ (in units of cm/GW) can be readily determined through eq 23 or eq 24. Moreover, if the concentration of the two-photon absorbing molecules is also known, the 2PA cross section σ_2' (in units of GW/cm^2) or σ_2 (in units of cm^4 s or GM) can be finally determined through eq 7 or eq 8.

Mentioned above is a simplest one-point measurement. To reduce the experimental uncertainty, one may conduct a multipoint measurement, i.e., to repeat the same measurement at several different I_0 levels, and then average over the measured values of $\beta(\lambda)$. If there are enough measured points, one may also make an experimental curve of nonlinear transmission as a function of incident intensity, and then fit the experimental data by using eq 23 or eq 24 with a best-fitting β value. In a multipoint measurement, the variation of the input intensity level can be done by two different methods. One is to fix the sample position and then vary the input intensity (or pulse energy) by using a variable optical attenuator; the other is to fix the input pulse energy level of a given focused laser beam and then change the distance from the sample to the focal point position. The second approach is also called the (open-aperture) Z-scan method.[338−340]

The same experimental setup and procedures mentioned here can also be applied to the measurements of 3PA and 4PA coefficients by using eqs 14 and 18, respectively. Then the corresponding 3PA and 4PA cross section values can be further determined based on the relationships expressed by eqs 13 and 17.

After measuring the nonlinear transmission, the determination of β depends on the local intensity I_0, which is not a directly measurable parameter. Usually, the energy and time duration of the input laser pulses are directly measurable, but the light intensity can be estimated only by knowing the size of the beam section inside the nonlinear medium. When a focused input laser beam is used, a reliable estimation of the real beam size inside the sample medium is quite difficult due to many possible reasons, such as, for example, (i) variation of the beam size before and after the focal point and (ii) self-focusing or self-defocusing of the laser beam across the sample medium. As the intensity is conversely proportional to the square of the beam size, the errors in the estimation of I_0 can be easily larger (or much larger) than 50−100%. Moreover, in some experimental setups, if the detector of the laser beam had a small effective detecting aperture (such as a photodiode detector or a detector of a larger area with a pinhole in front), or if the detector was far away from the sample position, a much bigger error might be introduced due to the change of the transverse intensity distribution of the laser beam at the detector's position, which could be caused by self-focusing, self-defocusing, a thermal lensing effect, or a thermal refractive-index disturbing effect. It should be noted that 2PA processes are always accompanied by induced refractive-index changes, as the former are described by the imaginary part and the latter described by the real part of the same third-order nonlinear susceptibility of $\chi^{(3)}$. Under these circumstances, the apparent changes of the detected optical signals may not be due to nonlinear transmission changes but mainly due to the variation of the spatial structures of the transmitted beam. This type of unreasonable setup in 2PA cross section measurements and in optical power limiting measurements can lead to severe artificial results. Even in an open-aperture *Z*-scan measurement, it is still essentially important to eliminate the possibility of these errors.

In general, to obtain a reliable result from the measurements of a 2PA coefficient and cross section, a detector with a larger area and without any attached pinhole should be adopted and placed not too far from the sample, and either a lens with a longer focal length (e.g., ≥10 cm) or a reverse telescope system should be employed to loosely focus the input laser beam. The applied local intensity at the focal position should not be too high to avoid possible self-focusing (or defocusing), local boiling, and/or other unexpected effects; the repetition rate of the input laser pulses should not be too high to reduce the thermal lensing effect. If the repetition rate of the input laser pulses is higher than 10−50 Hz, a chopper or electric shutter should be employed to reduce the thermal effect inside the sample medium.

5.2.2. Two-Photon Excited Fluorescence Method (2PEF)

In some cases, when an expensive ultrashort and high peak power laser source is not available, or the concentration of the tested samples cannot be high enough, the 2PA-induced nonlinear transmission change may be too small to measure. In such a case, an alternative method can be used to determine the 2PA cross section at a given excitation wavelength if the sample is highly fluorescent. This method is called the two-photon excited fluorescence (2PEF) technique,[341] which is based on a 2PA-induced fluorescence intensity measurement that is compared to a standard fluorescent sample, of which the 2PA cross section value $\sigma_2^s(\lambda_n)$ and the quantum yield of 2PA-induced fluorescence $\eta_{2PEF}^s(\lambda_n)$ at a given excitation wavelength (λ_n) are known. In this case, the measured 2PFE signal intensity of the standard sample solution can be simply expressed as

$$S_{2PEF}^s(\lambda_n) = A_\Sigma \eta_{2PEF}^s(\lambda_n)\sigma_2^s(\lambda_n) \qquad (25)$$

Here A_Σ is a phenomenological proportional coefficient that depends on the excitation light intensity and many other

experimental factors, including the optical setup, spectral sensitivity and aperture of the detector, sample concentration and thickness, etc. However, under the same experimental conditions except replacing the standard sample by a tested sample, the measured 2PEF signal intensity emitted from the latter can be expressed as

$$S_{2PEF}^{test}(\lambda_n) = A_\Sigma \eta_{2PEF}^{test}(\lambda_n)\sigma_2^{test}(\lambda_n) \quad (26)$$

Comparing eq 26 to eq 25 we have

$$\eta_{2PEF}^{test}(\lambda_n)\sigma_2^{test}(\lambda_n) = (S_{2PEF}^{test}/S_{2PEF}^{s})\eta_{2PEF}^{s}(\lambda_n)\sigma_2^{s}(\lambda_n) \quad (27)$$

The physical meaning of eq 27 is that if the four quantities on the right-hand side of the equation are known, we can determine the product of the two quantities on the left-hand side. In a most simplified case, if it can be assumed that $\eta_{2PEF}^{test} \approx \eta_{2PEF}^{s} \approx 1$, then eq 27 becomes

$$\sigma_2^{test}(\lambda_n) = (S_{2PEF}^{test}/S_{2PEF}^{s})\sigma_2^{s}(\lambda_n) \quad (28)$$

The major advantage of the 2PFE method is that, in conjunction with a highly sensitive photoelectric detector (photomultiplier or CCD array), even very weak fluorescence signals can be measured. Therefore, no high-power or high-energy pulsed laser source is needed, and a sample of low concentration [$\leq(10^{-3}-10^{-4})$ M] or of a small path length can be employed. The disadvantage of this method is that in general it can only determine the product of $\eta_{2PEF}^{test}(\lambda_n)\sigma_2^{test}(\lambda_n)$, not $\sigma_2^{test}(\lambda_n)$ alone. Logically, $\eta_{2PEF}^{test}(\lambda_n)$ could be determined only after $\sigma_2^{S}(\lambda_n)$ is known. From an experimental viewpoint, the absolute measurements of the quantum yield value for either $\eta_{2PEF}^{test}(\lambda_n)$ or $\eta_{2PEF}^{test}(\lambda_n)$ are quite complicated. To avoid this difficulty, sometimes researchers had to simply assume that the 2PA-induced fluorescence quantum yield is equal to the 1PA-induced fluorescence quantum yield.

5.3. Time-Regime Dependence of Measured Cross Section Values

During the late 1990s, researchers found that, even for the same nonlinearly absorbing medium excited at the same wavelength, the measured 2PA cross section values by using the nonlinear transmission method were dependent on the pulse duration of the applied laser beam. In particular, the apparent 2PA cross section values measured in the sub-picosecond or femtosecond regime for a given dye−solution sample could be one- or two-orders of magnitude smaller than that measured in the 5∼10 ns regime.[46,95,342,343] This huge difference of 2PA cross section values for the same molecular system might puzzle some researchers, as the cross section should be a molecular constant depending only on the wavelength, not the time duration of the applied light pulses. Although time-regime dependent results of MPA cross section measurements can strongly depend on specific experimental conditions and sample materials, some proposed explanations described below can be helpful for a better understanding in this specific issue.

5.3.1. MPA-Induced Excited-State Absorption

MPA-induced excited-state absorption is proposed to be one of the major possible mechanisms leading to a much greater effective (or apparent) MPA cross section value measured in the nanosecond regime, compared to the true cross section values measured in the sub-picosecond regime.[342,343] For simplicity, Figure 6 shows the schematic diagram of the energy-states structure representative for most multiphoton active organic molecular systems.[344] With two-photon (or three-photon) excitation, molecules in the lowest vibrational sublevel of the ground electronic singlet state (S_0) can be excited to a higher electronic singlet state (S_1 or S_n). These excited molecules have the tendency to rapidly relax to the lowest vibrational sublevel of S_1 through the internal conversion and vibrational relaxation. For commonly studied fluorescent organic chromophores, this fast relaxation process takes place within a time period of $\leq$1−10 ps. The lowest vibrational sublevel of S_1 is a metastable state exhibiting a lifetime of around 0.2−2 ns. Once molecules relax to this state, they have four possible pathways with which to leave it: (1) to emit fluorescence and return to the ground state, (2) to directly return to the ground state through a radiationless transition via internal conversion, (3) to relax to the triplet state T_1 that usually exhibits a much longer lifetime (e.g., 10^2 ns) than S_1, and (4) to be further excited to a higher excited-state through one-photon absorption. If the medium is highly fluorescent, i.e., the quantum yield of the fluorescence is close to 1, the second process can be neglected. The last process is called MPA-induced excited-state absorption (ESA), which may also take place for those molecules situated in the T_1 state. If the molecular population in the metastable excited-state is non-negligible and the 1PA cross section for a given input wavelength is much larger than the MPA cross section from the ground state, ESA-caused attenuation of the input light beam may become comparable to or even much greater than the MPA-induced attenuation. In these cases, the apparent MPA coefficient (or cross section) values determined by measuring the nonlinear transmission of the sample medium may be considerably or even significantly larger than the true values contributed from a pure MPA process.

It is obvious that the extent of influence by ESA on the nonlinear transmission measurement strongly depends on the state structures and transition properties of the sample medium and also on the parameters (wavelength, intensity level, and pulse duration) of the input laser beam. For a given sample medium and excitation wavelength, the ESA contribution to the measured nonlinear attenuation is merely determined by the pulse duration and the intensity level of the input laser beam. To elucidate this statement, we take two-photon excitation as an example and only consider two extreme situations. In the first case, we assume that the pulse duration is around 100−160 fs, such as the pulses from a Ti:sapphire laser device. In this situation, the pulse duration is so short that most of the two-photon excited molecules have not reached the lowest sublevel of S_1. Only after a time period of approximately 1−2 ps (internal conversion and vibrational relaxation time) can those excited molecules finally be accumulated in this metastable sublevel, while the input laser pulse is already gone. For this reason, it cannot cause absorption by molecules residing in this metastable state. In this case, the 2PA cross section values measured with sub-picosecond pulses are more close to the true values. In the second case, we assume that the input pulse duration (e.g., 5−10 ns) is considerably longer than the lifetime of the lowest sublevel of S_1 (e.g., 0.2−2 ns) and that a large number of excited molecules is accumulated and retained in that level. In this situation, the ESA process can repeatedly

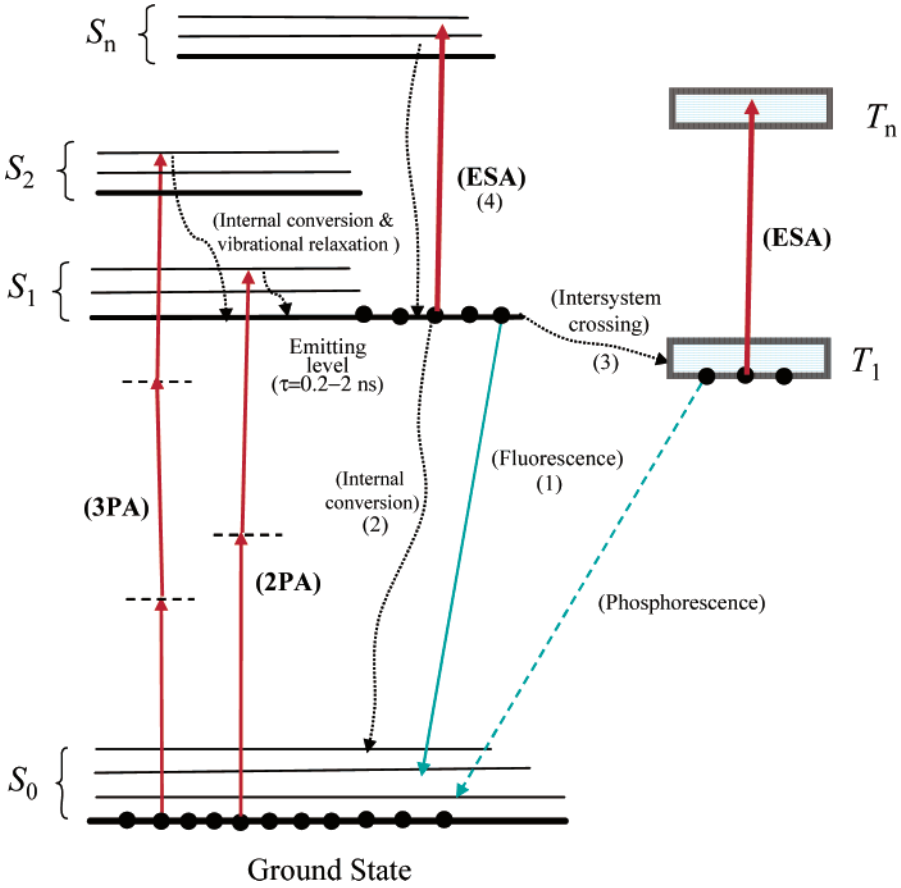

Figure 6. Schematic description of the state structure and MPA-induced transition pathways of an organic chromophore system. It is noted that there are four possible channels for the excited molecules to leave from the metastable emitting level. The dotted lines represent radiationless relaxations.

occur during the whole period of the input light pulse and becomes the mechanism that dominates the observed nonlinear attenuation of the input laser beam. This model explains why the effective or apparent 2PA cross section values measured in the nanosecond regime are significantly greater than those obtained with femtosecond laser pulses.

There are some experimental examples of 2PA- and 3PA-induced ESA studies.[94,200,345,346] Recently, Sutherland et al. have reported their quantitative results of ESA influence on the nonlinear transmission behavior of two-photon absorbing solutions measured in the nanosecond regime.[99] The investigated samples were solutions of three highly fluorescent AFX chromophores (AF240, AF350, and AF455) in THF, excited by 800 or 820 nm laser pulses of 3.2 ns duration. As the quantum yield of phosphorescence from the T_1 state is less than 7% for these three samples, the one-photon absorption from the lowest sublevel of S_1 may be the major source of ESA. Under these circumstances, the authors proposed an equivalent stepwise (2PA+1PA) three-photon absorption model and conducted the theoretical calculation based on the directly measurable parameters (including the true value of σ_2 measured in the sub-picosecond regime). The experimental results of nonlinear transmission as a function of the input pulse energy (or intensity) were in good agreement with that predicted from their theoretical calculation. As an example, Figure 7a shows the nonlinear transmission as a function of the input pulse energy for an AF455/THF sample (0.02 M, 1 mm thick); the hollow circles represent the measured data, the solid-line curves are predicted by the solution of an analytical theory with two given 2PA cross section values, and the dashed-line curves are predicted by the numerical solution of the related equations. Shown in Figure 7b are the nonlinear transmission curves of the same sample predicted by pure 2PA alone (dashed-line curve) and by 2PA+ESA together (solid-line curve), respectively. One can see that, at higher input levels, ESA becomes the dominant source responsible for the observed decrease of nonlinear transmission.

5.3.2. Stimulated Backscattering-Induced Nonlinear Attenuation

In measurements of the 2PA cross section in the nanosecond regime, He et al. have recently found that once the intensities or energies of the input laser pulses are above a certain threshold value, a backward stimulated Rayleigh−Bragg scattering (SRBS) takes place within the two-photon active medium.[347,348] In this case, energy from the input pump pulses will be transferred to backward stimulated scattering through the reflection from an induced standing-wave Bragg-grating in the nonlinearly absorbing medium. The efficiency of the energy transfer from the input pump beam to the backward stimulated scattering beam will get higher with increasing input intensity. Consequently, the measured nonlinear attenuation is not only due to pure MPA plus the ESA, but also due to stimulated backscattering. For this reason, the measured 2PA cross section value may deviate even more significantly from the true value for the pure 2PA process. As an example, Figure 8 shows the measured nonlinear transmission as a function of the input pulse energy in a 1 cm thick THF solution of an organic chromophore, PRL802, excited by a focused 532 nm laser beam of ~10 ns pulse duration.[347] In this figure, the hollow diamonds

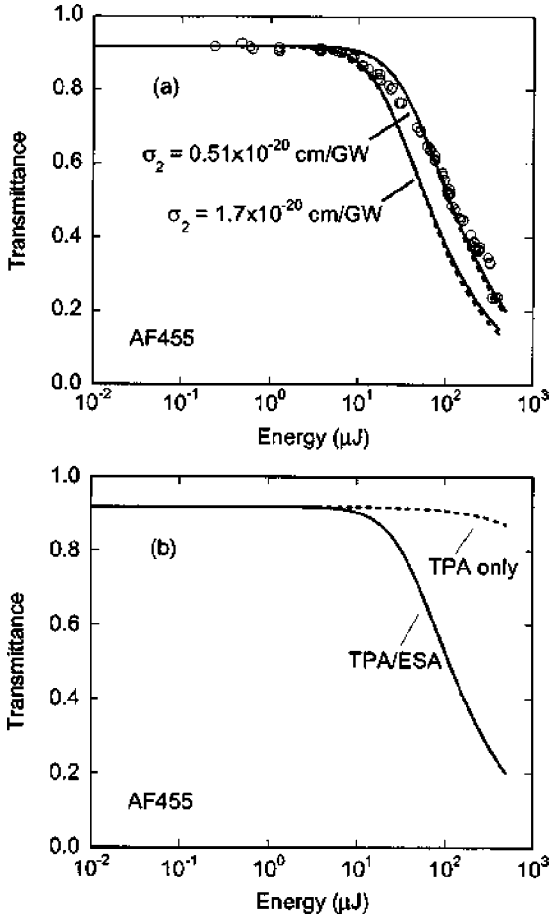

Figure 7. (a) Measured nonlinear transmission of AF455 in THF versus the input energy of 3.2 ns and 800 nm laser pulses, the solid lines are the fitting curves given by an analytical theory with two assumed 2PA cross section values, the dashed curves result from a numerical solution of the theory with the same two cross section values; (b) Nonlinear transmission curves of AF455 in THF due to pure 2PA contribution (dashed curve) and due to 2PA plus excited-state absorption (solid curve). Sample's concentration was 0.02 M, optical path length 1 mm. Reprinted with permission from ref 99. Copyright 2005 Optical Society of America.

represent the experimental data, while the dashed curve is a best fit to eq 21 using an effective 2PA coefficient of β = 9.46 cm/GW. However, this type of stimulated backscattering has been observed so far only in the nanosecond regime. In the sub-picosecond regime, the effective thickness of the induced Bragg grating is too short ($\leq$0.3 mm) because it is limited by the laser pulse length or coherent length; therefore, the backscattering is hard to stimulate. A more detailed discussion of stimulated Rayleigh−Bragg scattering will be given in section 6.

5.3.3. Saturation Effect of MPA in the Sub-picosecond Regime

The aforesaid two effects (ESA and stimulated backward scattering) may cause an additional nonlinear attenuation of the input laser beam. In other words, we are dealing with an equivalent 2PA-induced reverse-saturation effect in the nanosecond regime. On the contrary, in the sub-picosecond regime a saturation effect of the pure MPA process may be observed, which means that when the input laser intensity is higher than a certain value (so-called saturation intensity), the measured MPA coefficient values will decrease with a further increase of the input intensity values.[318,333,350] To

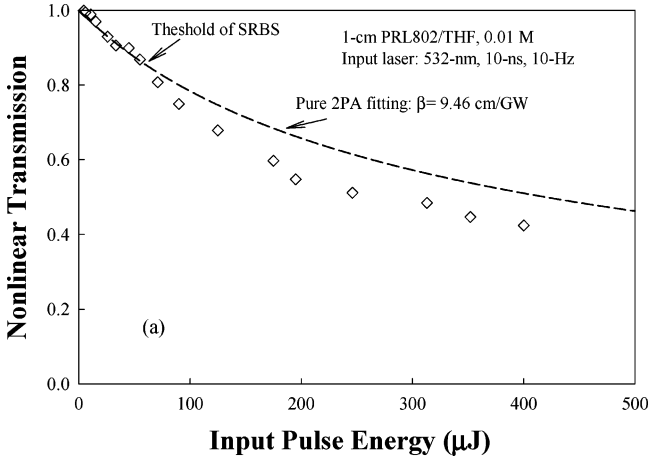

Figure 8. Measured nonlinear transmission versus the input energy of 10 ns, 532 nm laser pulses. The dashed curve is given by the 2PA formula with an assumed effective 2PA coefficient β=9.46 cm/GW. It is noted that once the input energy level is higher than a certain threshold value, the nonlinear transmission of the pump beam is getting lower due to backward stimulated Rayleigh-Bragg scattering. Reprinted with permission from ref 347. Copyright 2004 Optical Society of America.

explain the origin of the saturation effect, we should return to the expressions for MPA coefficients given in section 2, in which it is assumed that the MPA coefficients are simply proportional to the molecular density N_0. This assumption is acceptable only when the input light intensity is not too high and the depletion of the molecular population in the ground state can be neglected during the laser pulse duration. In a more rigorous manner for these expressions, N_0 should be replaced by $\Delta N = N_1 - N_2$, where N_1 is the population density in the ground state, while N_2 is the population density in upper states that become populated via 2PA. For a weak excitation, we may approximately assume that $N_2 \approx 0$ and $N_1 \approx N_0$. However, in the case of a very strong excitation, the depletion of N_1 is no longer negligible, which means that $(N_1 - N_2)$ will actually depend on the light intensity I_0. Then, for 2PA processes, eq 7 should be rewritten as[351]

$$\beta(I_0) = \frac{\sigma_2' N_0}{1 + (I_0/I_{s,2pa})^2} = \frac{\beta_0}{1 + (I_0/I_{s,2pa})^2} \qquad (29)$$

Here β_0 is the nonsaturation 2PA coefficient, which is independent of I_0, and $I_{s,2pa}$ is the saturation intensity of a given two-photon absorbing medium, at which the effective β value decreases to half of β_0. Combining this expression with the original eq 23, the nonlinear transmission becomes

$$T(I_0) = \frac{1}{1 + \beta_0 I_0 l_0/[1 + (I_0/I_{s,2pa})^2]} \quad \text{(2PA)} \qquad (30)$$

As an example, Figure 9 shows the measured nonlinear transmission for three two-photon absorbing chromophore solutions as a function of the input intensity of 775 nm, 160 fs laser pulses. In this figure, one can see that, at low input intensity levels, the experimental data can be well fitted without saturation (eq 23), whereas at high input levels the data can only be fitted by a theory (eq 30) that includes saturation. Based on this type of measurements and theoretical fitting, both the nonsaturation value of β_0 and the saturation intensity $I_{s,2pa}$ can be determined.[351]

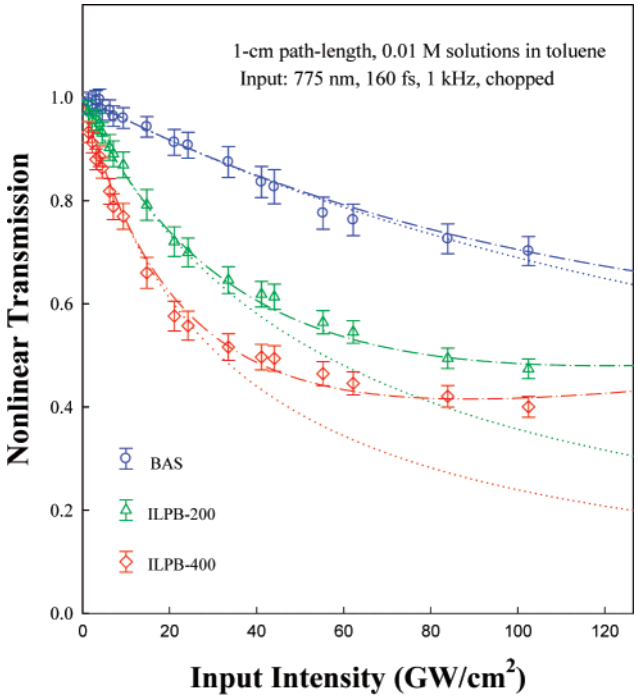

Figure 9. 2PA-induced nonlinear transmission versus the input light intensity for three chromophores (BAS, ILPB-200, and ILPB-400) in toluene. The dotted curves are the best fits given by the non-saturation theory, the dash-dotted curves are the best fits given by theory that includes saturation. Reused with permission from ref 351. Copyright 2007, American Institute of Physics.

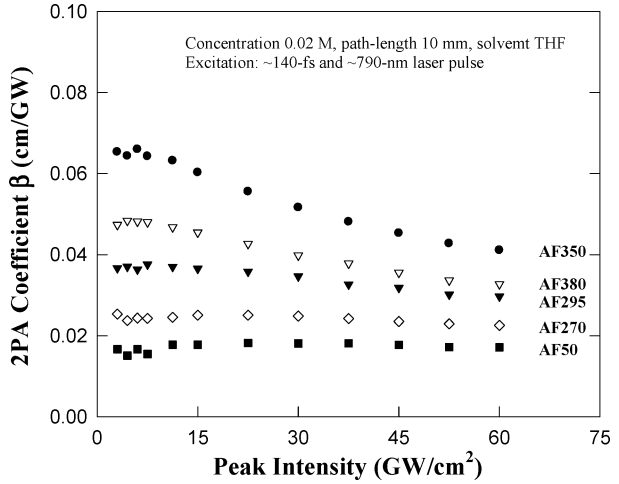

Figure 10. Measured 2PA coefficient values of five AFX chromophores in THF versus the input intensity of ~790 nm, ~140 fs laser pulses. It is noted that for AF350 and AF380 solution samples, the apparent β values are getting decreasing when the input intensity levels are higher than 10−15 GW/cm^2. Reused with permission from ref 352. Copyright 2004, American Institute of Physics.

As another example, shown in Figure 10 are the measured 2PA coefficient values of five AFX chromophores in THF versus the input intensity of ~790 nm, ~140 fs laser pulses. From the data shown in this figure, one can see that, among these five tested sample solutions, AF350 and AF380 manifest considerably larger β values compared to those of the other three compounds. However, these two compounds also exhibit much obvious saturation behavior when the input intensity levels are higher than 15−30 GW/cm^2.[352]

In the 3PA case, if the input light intensity is high enough, the same saturation effect can also be observed in nonlinear transmission measurements. With inclusion of the saturation effect, the original expression for the 3PA coefficient (eq 13) turns into[351]

$$\gamma(I_0) = \frac{\sigma_3'(\lambda)N_0}{1 + (I_0/I_{s,3pa})^3} = \frac{\gamma_0}{1 + (I_0/I_{s,3pa})^3} \quad \text{(3PA)} \quad (31)$$

Here γ_0 is the nonsaturation 3PA coefficient, and $I_{s,3pa}$ is the saturation intensity for a given three-photon absorbing medium. In this case, the previous expression of 3PA-induced nonlinear transmission (eq 14) changes to

$$T(I_0) = \frac{1}{\sqrt{1 + 2\gamma_0 I_0^2 l_0/[1 + (I_0/I_{s,3pa})^3]}} \quad \text{(3PA)} \quad (32)$$

Table 14. Data of Peak 2PA Wavelength (λ_{2PA}^{max}) and Maximum Cross Section (σ_2^{max}) Measured by Using the 2PEF Method for Six Bis(aminophenyl)polyene Compounds (Adapted from Ref 96)

	ns-measurements		ps-measurements	
compd	λ_{2PA}^{max} (nm)	σ_2^{max} (GM)	λ_{2PA}^{max} (nm)	σ_2^{max} (GM)
1	600	200	605	240
2	640	260	640	230
3	710	320	695	340
4	730	425	695	410
5	730	1300		
6			690	190

5.3.4. Results Based on the 2PEF Method

In some published papers, it was indicated that the two-photon excited fluorescence (2PEF) method yields 2PA cross section values in the nanosecond regime which are basically the same as those measured in the sub-picosecond regime.[28,96]

As an example of this type of results, Table 14 summarizes the data of the peak 2PA wavelength (λ_{2PA}^{max}) and cross section (σ_2^{max}) values of a series of bis(aminophenyl)polyene compound (1−6) solutions in toluene, which were measured by the 2PEF method with excitation pulses of 5 ns and 3 ps duration.[96] In this table one can see that the measured 2PA cross section values are nearly independent of the pulse durations. These apparently plausible results of 2PEF measurements may be reasonably explained. As mentioned previously, in the case of using the 2PEF method, the excitation levels and the sample concentration were much lower than that used for the NLT method; therefore, the stimulated backscattering and saturation effects can be excluded. On the other hand, even if the excited-state absorption (ESA) effect still takes place for nanosecond pulses, the fluorescence emission from the lowest level of the S_1 state (see Figure 6) will not gain from the ESA. It is noted that ESA only causes an additional (radiationless) loss and brings no contribution to the observed fluorescence signals. Owing to this reason, ESA does not have a significant influence on the 2PA cross section results measured by the 2PEF method in the nanosecond regime. However, when one measures the dependence of the fluorescence intensity on the excitation intensity, the ESA may cause a deviation from the square law; that is, the slope of the measured results in a logarithmic plot will be less than 2.

5.4. Measurements of MPA Spectra

Hitherto, we have only considered the measurement of the MPA coefficient or cross section at a single wavelength or

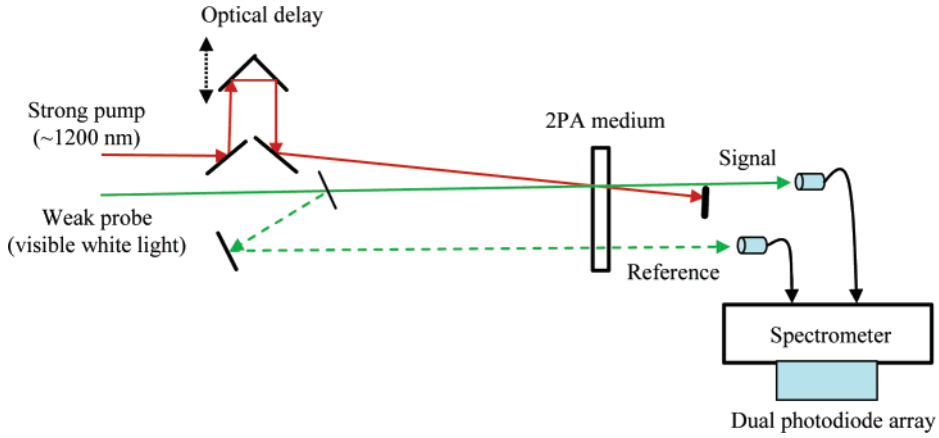

Figure 11. Optical layout for measuring nondegenerate 2PA spectra by using a two-beam configuration: a strong IR pump beam and a weak visible continuum beam.

several discrete wavelengths by using different methods. In order to obtain a complete MPA spectrum for a given sample medium, researchers have to repeat this type of measurement with a greater number of different wavelengths covering a broad enough spectral range. To do so, a tunable coherent light source can be utilized in conjunction with different approaches, such as direct nonlinear transmission (NLT) measurement,[199,353,354] open-aperture Z-scan measurement,[209,283b,355] multiphoton excited fluorescence measurement,[28,35,96,115,341,356] and the pump−probe two-beam approach.[357−359] Obviously, this kind of measurement is very sophisticated and highly time-consuming, as for each changed laser wavelength researchers have to remeasure the exact wavelength value, beam divergence, and pulse energy. There is another alternative and more efficient technique which uses a coherent white-light continuum beam to replace a tunable monochromatic laser source. This new approach may provide two major advantages. First, it is a continuous-spectrum measurement instead of a discrete-multiwavelength measurement. Second, it is a time-saving approach based on which a complete 2PA spectrum for a given sample medium can be recorded within a very short time period.

The white-light continuum generation is a nonlinear optical effect that can be efficiently produced in many transparent liquids and solids by using high peak-power ultrashort laser pulses of picosecond or femtosecond duration.[360] The mechanisms of continuum generation can be quite complicated, depending on the experimental conditions and the nonlinear media employed. Self-modulation-induced self-spectral-broadening, stimulated scattering, and four-photon parametric interactions are commonly recognized as major mechanisms contributing to the observed continuum generation. The generated continuum is a white-light coherent emission that features high directionality, a super-broad spectral band (usually covering the entire visible range and near IR range), a coherent phase-relationship among different spectral components, and high spectral intensity. Even in the early stage of continuum generation with picosecond laser pulses, this new type of coherent white-light source was employed to measure the transient linear absorption spectra of sample materials.[361] The major advantage of this application is the elimination of the need for spectral tunability and wavelength scanning.[165,362,363]

5.4.1. Nondegenerate 2PA Spectral Measurement Using the Pump−Probe Configuration

In 1999, Belfield, Negres, and their colleagues reported a novel approach to measure nondegenerate 2PA spectra by utilizing a pump−probe two-beam configuration, in which the strong pump was a monochromic IR laser beam and the weak probe was a white-light continuum beam.[55,364] As schematically shown in Figure 11, these two pulsed beams were overlapping in a two-photon absorbing sample with a small crossing angle. We assume that the very weak probe beam cannot produce degenerate 2PA by itself, but it can be nonlinearly attenuated through the simultaneous absorption of one photon from the monochromatic pump beam and one photon from the white-light probe beam. By recording the relative spectrum change of the probe beam with and without overlapping with the pump beam, one could finally obtain the relative spectrum of nondegenerate 2PA for the given sample medium. Assuming that the duration values of the pump pulses and the probe pulses are both in the subpicosecond regime, a temporal overlap is as important as the spatial overlap between these two beams, to ensure a nondegenerate 2PA along these two beams. For this reason, a variable optical delay line was needed. In the experiments, the pump beam was a 1220 nm output from an optical parametric generator (OPG), while the probe beam (white-light continuum) was generated in a 1.5 mm thick fused silica plate on which a 1400 nm laser beam from another OPG was focused. These two OPGs were pumped separately by 775 nm, 120 fs laser pulses from the same Ti:sapphire device.

In this case, a serious problem arises, which is related to the chirping effect taking place in continuum generation and the group-velocity dispersion (GVD) effect on the probe pulse's propagation through the optical elements. Owing to these two effects, even for a given continuum pulse that possesses a continuous spectral distribution over the visible spectral range, the arriving time in the center of a sample medium will be different for different spectral components of the continuum pulse. This means that, with a suitable optical delay, one can only ensure a temporal overlapping between the pump pulse and one specific spectral component from the probe pulse. Because of this reason, one has to repeat multipoint measurements with different time-delay values between these two beams, to ensure a sequential temporal overlapping with all spectral components of the probe pulse. By this way, the final nondegenerate 2PA spectrum with correction of chirping and GVD could be obtained for a given sample medium.[365] As an example, in Figure 12 the black triangles are the nondegenerate 2PA data of an alkyl-fluorene derivative solution sample in THF measured by the method described here, the hollow circles are the data from the sample measured by the 2PEF method,

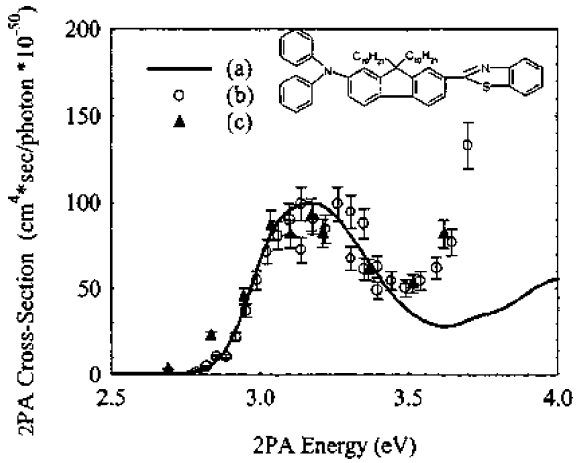

Figure 12. Nondegenerate 2PA spectral data of alkyl-fluorene derivative in THF versus energy of two photons (one from pump plus one from probe): (a) linear absorption curve, (b) data measured by 2PEF method, and (c) data measured by pump-continuum method with walk-off correction. Sample concentration 0.024 M, the path length 1 mm. Reprinted with permission from ref 365a. Copyright 2002 IEEE.

and the solid-line curve is the relative linear absorption spectrum.[365a] The chemical structure of the chromophore is shown in the top of this figure, the sample concentration was 0.024 M, and the path length was 1 mm.

5.4.2. Degenerate 2PA Spectral Measurement Using a Single Intense Continuum Beam

In 2002, He et al. reported another new approach to directly measure the degenerate 2PA spectra by using only one intense continuum beam.[73,366] The unique feature of this method is that a collimated and powerful white-light continuum (WLC) beam first passes through a spectral-dispersion element (prism or grating) and is then focused by a lens on the sample medium. Under this special arrangement, different spectral components of the WLC pulse will be separated inside the sample, nondegenerate 2PA between these different spectral components can be excluded, and only degenerate 2PA-induced nonlinear attenuation of these spectral components will be recorded. The major advantages of this method are its simplicity and reliability, as the above-mentioned chirping effect and GVD effect, related to continuum generation and propagation, have no influence on the 2PA spectral measurement. In addition, there is no critical requirement for spatial/temporal overlapping, as essentially needed in the two-beam (probe−pump) approach.

Figure 13 shows the optical setup for degenerate 2PA spectral measurements using an intense and spectrally dispersed WLC beam. Here, heavy water (D_2O) was chosen as the nonlinear transparent medium for providing continuum generation because of its high efficiency and stability compared to other commonly used solvents or liquids. The pump source for this continuum generation was a focused ultrashort pulsed laser beam provided by a Ti:sapphire laser oscillator/amplifier system with the following output parameters: pulse duration, ~150 fs; wavelength, ~790 nm; beam size, ~5 mm; divergence angle, ~0.3 mrad; repetition rate, 1 kHz. The output WLC beam was collimated via a lens, passed through an SF10-glass prism, and then focused via an $f = 10$ cm lens into the center of a 1 cm quartz cuvette filled with either a sample solution or a pure solvent. The intensity distribution of the dispersed spectral image at the sample position can be further imaged through a camera lens set on the surface of a CCD array controlled by a computer system. By comparing the recorded continuum spectrum passing through a chromophore solution sample to that passing through a pure solvent sample, the nonlinear attenuation of different spectral components due to the investigated chromophore can be readily determined. Furthermore, if the linear absorption in the measured spectral range is known or negligible, the relative nonlinear absorption spectrum due to degenerate 2PA can be finally obtained. After getting the relative degenerate 2PA spectral distribution curve for a given sample medium, one may measure the absolute value of the 2PA coefficient $\beta(\lambda_0)$ at a given wavelength λ_0 by the NLT method using a monochromatic laser beam, so that the complete 2PA spectral curve can be finally obtained at an absolute scale. It should be noted that the same technique can also be applied to nonfluorescent nonlinearly absorbing media, including pure solvents and solid samples. In that case, one just needs to compare the transmitted spectrum of a highly attenuated input continuum beam to that of an unattenuated strong input continuum beam. For the former, no 2PA takes place, while 2PA processes at different wavelengths will be generated for the latter. In this way, the residual linear attenuation influence can be automatically eliminated from the 2PA measurement.

As an example, shown in Figure 14 are the normalized degenerate 2PA spectra for five AFX chromophores (AF270, AF295, AF350, AF50, and AF380) in solution phase in THF,[352] measured with the single WLC beam configuration shown in Figure 13. The concentration and path length for all samples were 0.02 M and 1 cm, respectively. In the same figure, the solid-line curves are the normalized linear absorption spectral curves measured with a much lower concentration (0.0001 M). From Figure 14, one can see two noticeable features: (a) For AF-270, -295, and -350 samples, there is a similarity between the 2PA and linear absorption spectra. (b) For AF380, the 2PA spectrum is obviously different from the corresponding linear absorption spectrum, which exemplifies in this specific case the different selection rules for 1- and 2PA processes.

5.4.3. 3PA Spectral Measurement Results

In principle, all methods used for 2PA spectra measurements are also applicable to 3PA or even 4PA spectral measurements. In the latter two cases, of course, a much higher intensity (or peak power) of the coherent light source is required. In the following, we present two examples of 3PA spectral measurement that were obtained with two different technical approaches.

Drobizhev, Spangler et al. recently reported their 3PA spectral measurement results of three chromophores (TFA-01, TFA-02, and TFA-03), which belong to a series of fluorophores based on the tri(9,9-diethyl-9H-fluorenyl)amine unit. These results were obtained by using the three-photon excited fluorescence (3PEF) method.[115,356] The samples were chromophores in dichloromethane of concentration $\sim 10^{-4}$ M; the excitation source was the output beam from an OPG with a wavelength tunable from 1100 to 1600 nm, a pulse duration of ~100 fs, and a repetition rate of 1 kHz. Through comparison with a standard sample medium whose absolute value of 3PA cross section at a given wavelength was known, the absolute 3PA spectral data could be finally determined. As an example, the complete 3PA spectral data for a TFA-

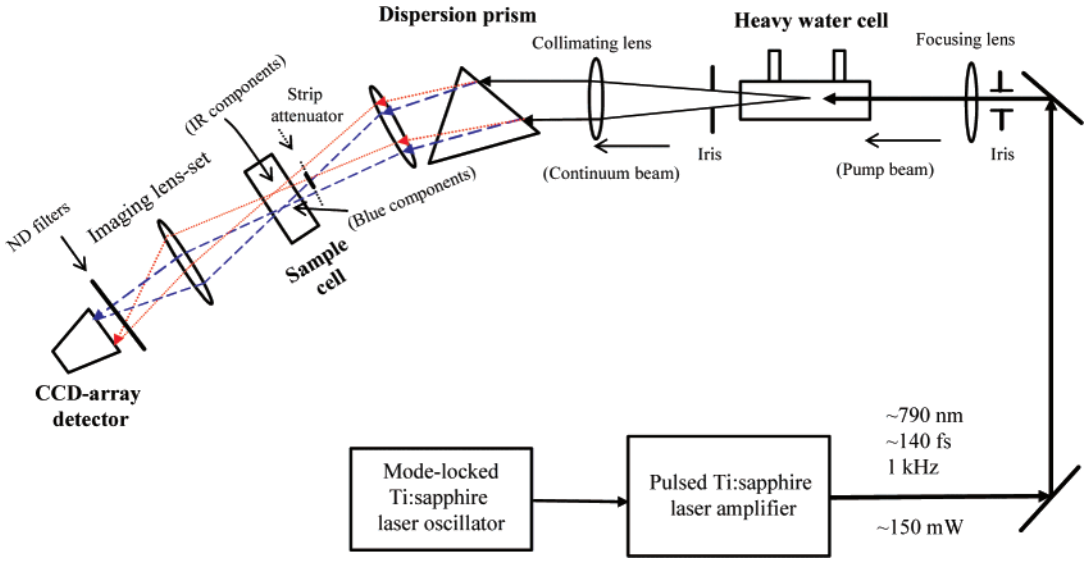

Figure 13. Experimental setup for degenerate 2PA spectral measurement using a single and spectrally dispersed white-light continuum beam. Reprinted with permission from ref 73. Copyright 2002 American Chemical Society.

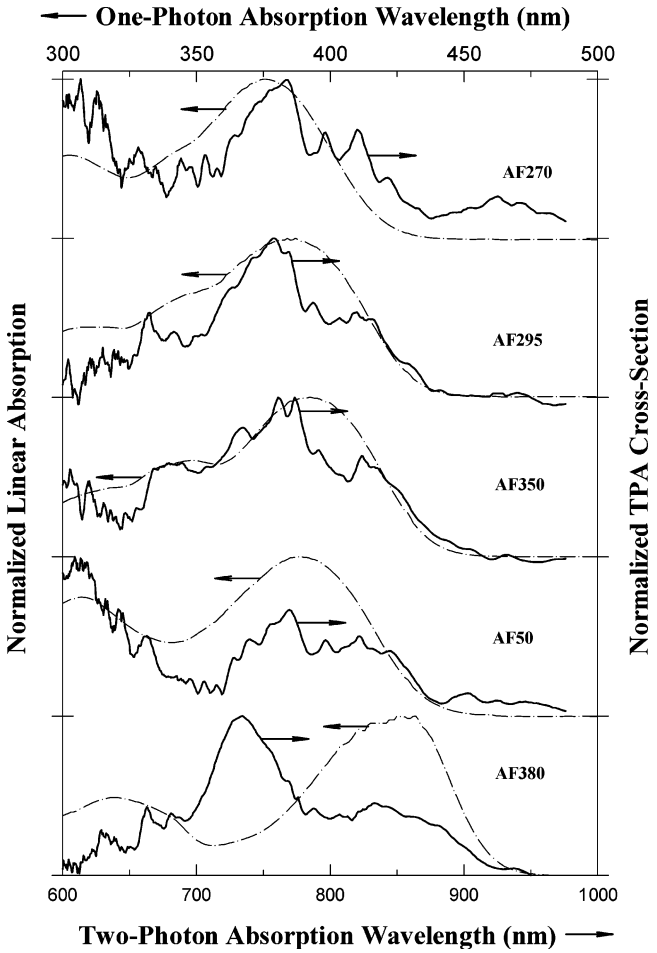

Figure 14. Normalized spectra of 2PA (solid-line curves) and 1PA (dash-dotted line curves) of five AFX chromophores in THF. Reused with permission from ref 352. Copyright 2004, American Institute of Physics.

03 sample solution are shown in Figure 15 by the full squares. The solid-line curve is the linear absorption spectrum. It can be seen that in this case the measured 3PA spectrum is generally following the 1PA spectrum.

Zheng et al. reported a cooperative enhancement of the 3PA cross section in a series of chromophores, going from

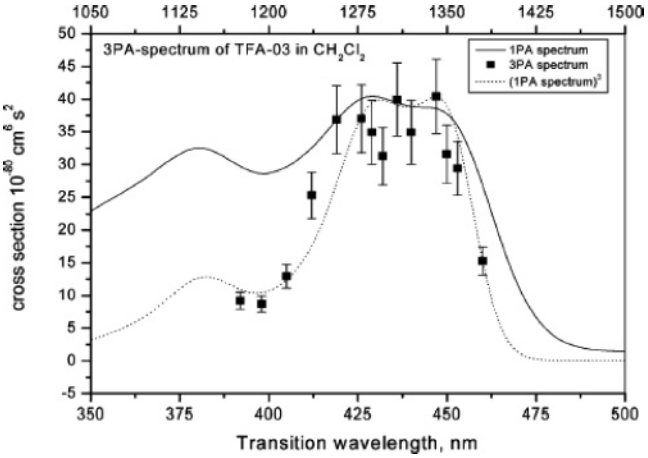

Figure 15. Measured 3PA spectral data of TFA-03 solution in CH_2Cl_2 by using the three-photon excited fluorescence (3PEF) method. The solid-line curve is the relative linear absorption spectrum. The dotted-line curve is the cube of the relative linear absorption spectrum. Reprinted with permission from ref 356b. Copyright 2005 American Chemical Society.

a one-branched to a three-branched and then to a dendritic structure.[367] These results were obtained by using the direct nonlinear transmission method. In 3PA measurements, the concentrations for the one-branched, the three-branched, and the dendritic chromophores were 0.02, 0.0067, and 0.0033 M in $CHCl_3$, respectively. The pump source for the 3PA measurement was a focused ultrashort pulsed laser beam from an optical parametric generator (OPG) with a wavelength tunable from 1100 to 1600 nm. The pulse duration and the repetition rate of the pump beam were 160 fs and 1 kHz, respectively. The output laser energy from the OPG was kept at ~1.0 μJ by using neutral density filters. As an example, the 3PA cross section values as a function of the input light wavelength for the dendritic chromophore are shown in Figure 16. The dashed line is a Gaussian fitting curve for the 3PA spectrum. As shown in Figure 16, the dendritic chromophore exhibits a 3PA peak value of 30.0×10^{-25} cm^6/GW^2 at the ~1200 nm position, which is about three times longer than the corresponding linear absorption peak wavelength.

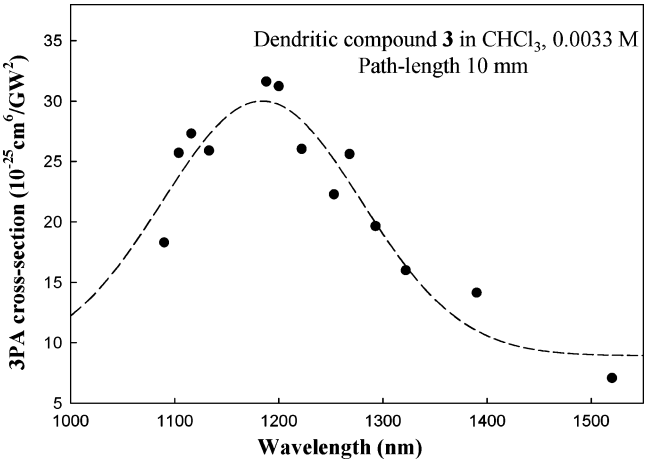

Figure 16. Measured 3PA cross section values of a π-conjugated dendritic chromophore solution in $CHCl_3$ versus the excitation wavelength by using NLT method. The dashed line is a Gaussian fitting curve. Reprinted with permission from ref 367. Copyright 2006 American Chemical Society.

5.5. Characterization of the MPA-Induced Fluorescence Emission

The majority of multiphoton active organic compounds investigated so far are fluorescent materials that can emit visible fluorescence excited by IR coherent radiation. Studies of properties and behaviors of this type of fluorescence emission may help researchers to have a better understanding about the transition pathways, selection rules, relaxation rates, excited-state lifetimes, and other useful information of multiphoton excitation processes. Characterizations of MPA-induced fluorescence from a given sample medium usually include (but are not limited to) the following measurements: emission spectrum, quantum yield, temporal (rising and decaying) behavior, excitation intensity dependence, concentration dependence, and polarization dependence.

5.5.1. Excitation Intensity Dependence of Fluorescence Emission

The measurement of the fluorescence emission intensity as a function of the input excitation intensity is particularly essential to identify the number (two, three, or four) of simultaneously absorbed photons involved in the elementary excitation process. In many published papers, the authors presented a square dependence of the fluorescence on the input intensity to prove the 2PA nature or a cubic dependence to prove the 3PA nature. Strictly speaking, even for a pure 2PA or 3PA process, the simple square or cubic law between the observed fluorescence signals and the input excitation intensity does not hold automatically. Instead, only under some specially arranged conditions, one may observe a simple square law or cubic law. To explain this, we have to return to some original equations given in section 2. For a pure 2PA process and according to eq 6, the total change of the intensity of the input beam will be

$$\Delta I = I_0 - I(l_0) = \frac{{I_0}^2 \beta l_0}{1 + I_0 \beta l_0} \tag{33}$$

It can be assumed that the molecular population number (ΔN) excited to the emitting level is proportional to ΔI; therefore, the signal intensity (I_{fluor}) of the detected fluorescence from the sample cell will be proportional to ΔN, and thus, we have

$$I_{fluor} \propto \Delta N \propto \Delta I \propto \frac{{I_0}^2 \beta l_0}{1 + I_0 \beta l_0} \quad \text{(2PA)} \tag{34}$$

It is obvious that in general there is no simple quadratic relationship between the fluorescence intensity and the input excitation light intensity. Only when $I_0 \beta l_0 \ll 1$, the following quadratic relationship is approximately valid.

$$I_{fluor} \propto {I_0}^2 \beta l_0 \tag{35}$$

In practice, to meet this requirement, the concentration and thickness of the sample medium should be quite small, and the input intensity should not be too high. Similarly, for a pure 3PA-induced fluorescence process, based on eq 12, we can write the total input intensity change of the input beam as

$$\Delta I = I_0 - I(l_0) = I_0 \left(1 - \frac{1}{\sqrt{1 + 2{I_0}^2 \gamma l_0}}\right) \tag{36}$$

Only when the condition of $2{I_0}^2 \gamma l_0 \ll 1$ is met, do we have the following approximate expression

$$I_{fluor} \propto \Delta I \approx I_0[1 - (1 - {I_0}^2 \gamma l_0)] \approx {I_0}^3 \gamma l_0 \quad \text{(3PA)} \tag{37}$$

In practice, to observe a cubic dependence, the values of sample concentration, thickness, and input intensity should not be too high.

As a recent example, Lin et al. have reported their results on 2PA and 3PA studies of a multibranched chromophore with symmetrical substitution.[163] The structural skeleton of this compound (**6**) is composed of a donor-π-donor (D-π-D) backbone in the center with two identical electron-pulling moieties (2,5-diphenyloxadiazole) extended outward from each donor site. Structural motifs similar to the central part of this compound have been demonstrated to show the enhanced MPA due to the symmetric charge transfer upon excitation. On the other hand, expanding the molecular dimensionality (from a quasi-1D linear structure to a 2D branched structure) through extension of the π-conjugation system on a molecule is expected to increase the number of effective π-electrons, which in turn may lead to an increased nonlinear absorptivity. Shown in Figure 17 are the measured data of the relative fluorescence intensity of compound **6** in $CHCl_3$ versus the relative input intensity of ~775 nm, ~160 fs laser pulses for two-photon excitation (2PE) (a) and of ~1300 nm, ~160 fs laser pulses for three-photon excitation (3PE) (b). The concentration and path length of the sample were $\sim 1 \times 10^{-3}$ M and 10 mm, respectively. The input intensity was varied in the 1−10 GW/cm^2 range for 2PE and in the 30−150 GW/cm^2 range for 3PE. From the results shown in Figure 17, one can see that, under these specific experimental conditions, the 2PE-induced fluorescence basically follows the square law, and the 3PE-induced fluorescence follows the cubic law.

5.5.2. Relative Spectral Distribution of MPA-Induced Fluorescence

For a given multiphoton absorbing and fluorescent organic chromophore sample, if the molecules excited via MPA are finally relaxed to the same metastable emitting state, i.e.,

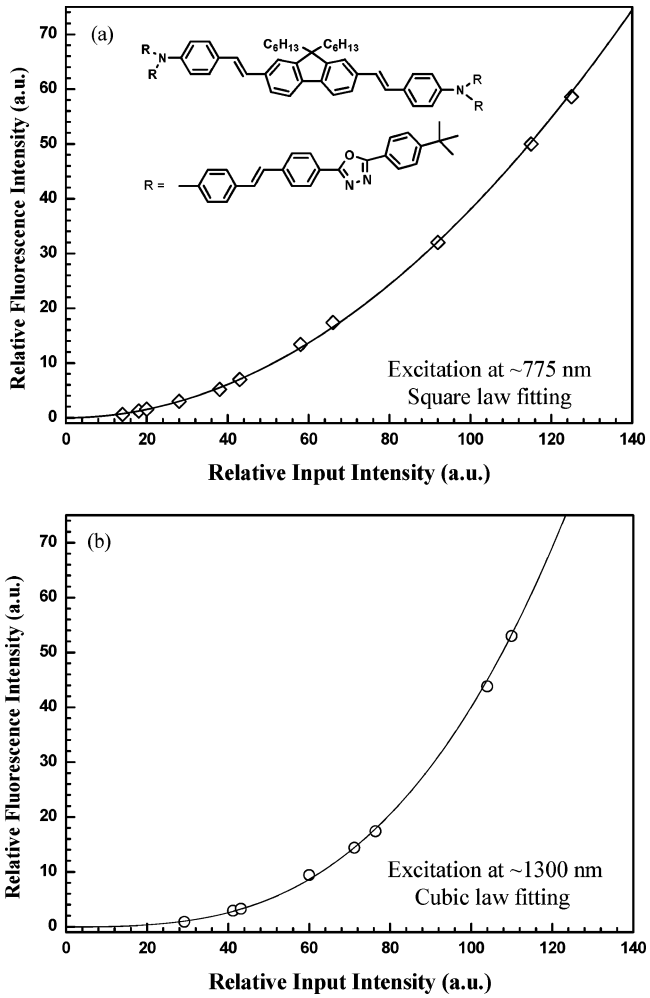

Figure 17. Measured intensity dependence of two-photon- (a) and three-photon- (b) induced fluorescence of compound **6** in $CHCl_3$ versus the relative input intensity of ~775 nm and ~1300 nm laser beams. The chemical structure of compound **6** is shown in the inset of (a). Sample concentration $\sim 1 \times 10^{-3}$ M, path length ~ 10 mm. From ref 163. Reproduced by permission of The Royal Society of Chemistry.

the lowest vibrational sublevel of S_1 as shown in Figure 6, the fluorescence spectral and decaying behaviors should be the same no matter how many photons are simultaneously absorbed for a single molecular transition. Many experimental results showed that the fluorescence emission spectra for a given medium excited by 1PA, 2PA, and 3PA are nearly the same.[46,163,351,368−370]

Sometimes, the concentration values of samples for multiphoton excitation measurements may be much higher than that for one-photon excitation; therefore, there may be some apparent difference in the blue edge of the emission spectra for high concentration samples, which is due to the reabsorption effect of the fluorescence signals with shorter wavelength components propagating within the sample medium.

5.5.3. Excitation Dynamics and Temporal Behavior of Fluorescence Emission

There are several approaches for investigating the dynamic and temporal behaviors of molecular transition and relaxation processes. Among them, the pump−probe technique using two-beam or multibeam configurations with slowly scanning optical delay is one of the most sophisticated and comprehensive methods to measure the dynamic properties related to MPA processes, such as radiationless transition rate or relaxation constants, excited-state absorption, reabsorption saturation, and excited-state lifetimes (e.g., refs 95 and 371). In these cases, the temporal resolution is essentially determined by the laser pulse width and the accuracy of the delay time scanning. Another more efficient and straightforward approach is to use a high-speed streak camera system, which can easily provide the information of multiphoton excited fluorescence delay, growth, and decay behaviors with a temporal resolution in the picosecond or sub-picosecond range (e.g., ref 46). Furthermore, in conjunction with a spectral dispersion system, the streak camera can measure the temporal behavior of different spectral components of fluorescence emission.

There are some other quite specialized methods that can be used to investigate the temporal behavior of fluorescence emission and ultrafast relaxation processes of molecular transitions, including the time-resolved fluorescence upconversion (sum-frequency) detection technique, the three-pulse photon-echo method, fluorescence anisotropy measurements, and transient excited-state absorption anisotropy measurements. Goodson, Varnavski, and co-workers have used these methods to investigate the transition dynamics and intramolecular energy migration processes in organic dendritic systems.[372,373] This type of dynamic spectroscopic technique can also be employed for studies of multiphoton excitation related processes.[374]

For some organic chromophores in solution phase, it was experimentally shown that the temporal decay and lifetime of one-, two-, and three-photon-induced fluorescence emission were nearly the same for a given sample medium.[46,163,351]

6. Applications of Multiphoton Active Materials

As mentioned in section 1, the rapidly expanding studies of multiphoton active materials are mainly promoted by the great potentials of various applications utilizing efficient multiphoton excitation. Some examples of these applications are frequency-upconversion lasing; optical power limiting, frequency-upconversion imaging and microscopy; optical microfabrication; optical data storage and processing; and multiphoton associated biological and medical applications. There are some common features always retained in these applications. First, a high-intensity coherent light source is needed to produce the necessary multiphoton excitation. Second, there is always a nonlinear relationship between the material's responses and the local light intensity. Here, the material's responses can be nonlinear transmission changes, fluorescence emission, population changes, refractive-index changes, etc. Third, there should be no linear (one-photon) absorption at the coherent light input wavelength for the multiphoton-active materials. Owing to the third feature, the excitation light beam can easily penetrate deeper into the materials or even pass through them. Moreover, if the input light beam is focused, near the focal point position, there is a quasi-Gaussian transverse intensity-distribution profile. Therefore, one may expect that the transverse distribution profile of the material's response will be much narrower or sharper than the former due to the second feature mentioned above. This means that a higher transverse resolution can be obtained. If the focal length is short enough, one could also get a higher longitudinal spatial resolution because of the same reason. Finally, as MPA is an instantaneous process

upon the input light action, an ultrafast response of the material can be expected in many applications.

6.1. Multiphoton Pumped (MPP) Frequency-Upconversion Lasing

The significance of MPP lasing studies is that it is a new approach to accomplish frequency-upconversion of coherent light. The other commonly used approaches of frequency upconversion are based either on sum-frequency or second-harmonic generation (SHG) in second-order nonlinear crystals or on third-harmonic generation (THG) in third-order nonlinear media. In all those cases, phase-matching requirements have to be fulfilled, which cannot be easily achieved except when very special techniques (such as birefringence in crystals or anomalous dispersion in isotropic materials) are employed. In contrast, MPP lasing can be realized in liquids, films, solid rods, optical fibers, and wave guides without phase-matching requirements. In addition, MPP lasing in dye-based systems exhibits the advantage of tunability within a quite broad spectral range.

From a long-term viewpoint, there is a definite trend to extend the lasing wavelengths into a much shorter spectral range (even to the vacuum UV or soft X-ray range), because extremely short lasing wavelengths will bring new advantages and promotions to various laser-based applications. In this important direction, MPP lasing can also play a vital role in the future, provided that the number of photons simultaneously absorbed from the pump beam (in the near IR or visible range) can be significantly increased.

6.1.1. General Features of MPP Lasing Materials and Devices

It is well-known that dye solutions and dye-doped solid materials are among the best lasing materials from the viewpoint of the low pump threshold requirement, high lasing efficiency, lasing wavelength tunability, low cost, and the ease of modification. The low pump threshold and high lasing efficiency are based on the so-called four-level lasing scheme and high quantum efficiency for the majority of commercial lasing dyes; the lasing wavelength tunability is ensured by the relatively broad spectral band of fluorescence emission for dye materials. Shortly after the advent of lasers, it was found that two- and even three-photon absorption-induced frequency-up-converted fluorescence in organic dye materials could be observed by using pulsed laser excitation.[375−379] Based on these phenomena, researchers can measure the pulse duration of ultrashort laser pulses by using two counter-propagating laser beams to create frequency-up-converted fluorescence fringes inside a dye solution.[377,379] Naturally, some researchers did also think of the possibility of two-photon pumped lasing in suitable materials if the pump laser intensity could be high enough to produce population inversion.

In practice, the earliest two-photon pumped (2PP) lasing was observed during the 1960s−1970s in several semiconductor crystals operating at low temperature.[380−384] Also, there were a few papers reporting two-photon excited stimulated emission in gas and metal vapor systems during the 1970s−1990s.[385−390] On the other hand, between the 1970s and 1993, there were several experimental reports on two-photon excited stimulated emission for commercial organic dye systems.[391−398] In these cases with no cavity enhancement, most of the observed output was the so-called amplified spontaneous emission (ASE) that usually was only characterized by spectral narrowing, not by high directionality. In 1995, He et al. reported 2PP cavity lasing with a narrow spectral line width and high directionality for solutions of a novel dye and for doped solid matrixes.[203] Since then, an increasing number of novel 2PP lasing dyes and cavity lasing configurations have been reported. The first three-photon pumped (3PP) lasing in a dye solution was reported in 2002.[399] Recently, four-photon pumped (4PP) lasing has been achieved in a series of new dye solutions.[400−402] In these two cases, a powerful ultrafast coherent light source tunable in the 1−2 μm range is necessary to provide high enough peak pump intensity in a dye-based gain medium.

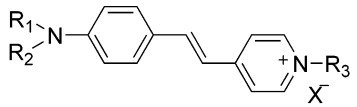

R_1= H, Alkyl, R_2= H, Alkyl, R_3 = Alkyl,
X = I, Br, BF_4, Tos, CF_3SO_3, etc

Figure 18. Generalized molecular structures of MPP lasing dyes.

To date, the number of reported novel MPP lasing dyes is below one tenth of the total number of reported novel two-photon absorbing chromophores. However, it should be noted that the major requirements for MPP lasing dyes are different from those for chromophores designed for other applications, where a larger MPA cross section is the most important consideration. Here, for the MPP lasing purpose, the most essential requirements for the lasing dyes are the ease of establishing population inversion and a higher lasing efficiency. Thus, it is important to realize that the best two-photon absorbing materials may not necessarily produce multiphoton pumped lasing. This may be the reason why only a small number of the reported novel multiphoton active chromophores can be employed for MPP lasing.

So far, we do not know exactly what specific parameters, molecular structures, and dynamic processes are the criteria to judge the MPP lasing capability of a dye. However, based on the reported experimental results, some common features of MPP lasing dyes can be briefly discussed. Hitherto, most MPP lasing dyes are salt-type asymmetric molecules consisting of a π-conjugated framework containing on one end an electron donor and on the other end an electron acceptor. Shown in Figure 18 is a general structure for this type of pull−push organic dyes. In this example, a dialkylamino group is used as an electron donor, and pyridium cation is used as an electron acceptor. Actually, other electron donors (alkyloxy groups, alkylthio groups, etc.)[400] or π-excessive heterocycles (substituted pyrroles, etc.)[407] can also be used for the preparation of a MPP lasing dye. As to the electron-acceptor end, one may replace the pyridium cation by other π-deficient heterocycles (substituted thiazoliums, benzothiazoliums, etc.)[414,415] or strong electron-withdrawing groups (alkylsulfonylphenyl groups, etc.).[399]

Figure 19 shows schematic diagrams of pump sources and the experimental setup for the MPP lasing study. Shown in Figure 19a are the pump sources for 2PP lasing in the nanosecond regime, which can be either a Q-switched Nd:YAG laser with 1064 nm output, or a frequency-doubled Q-switched Nd:YAG laser pumped dye laser system with ~800 nm output, or the same Nd:YAG laser pumped optical parametric generator (OPG) with coherent light output, tunable in a range from 700 to 1100 nm. In these cases, both the pump pulses and the 2PP lasing pulses are in the duration of nanoseconds. Moreover, shown in Figure 19b are the pump sources working in the femtosecond regime for the

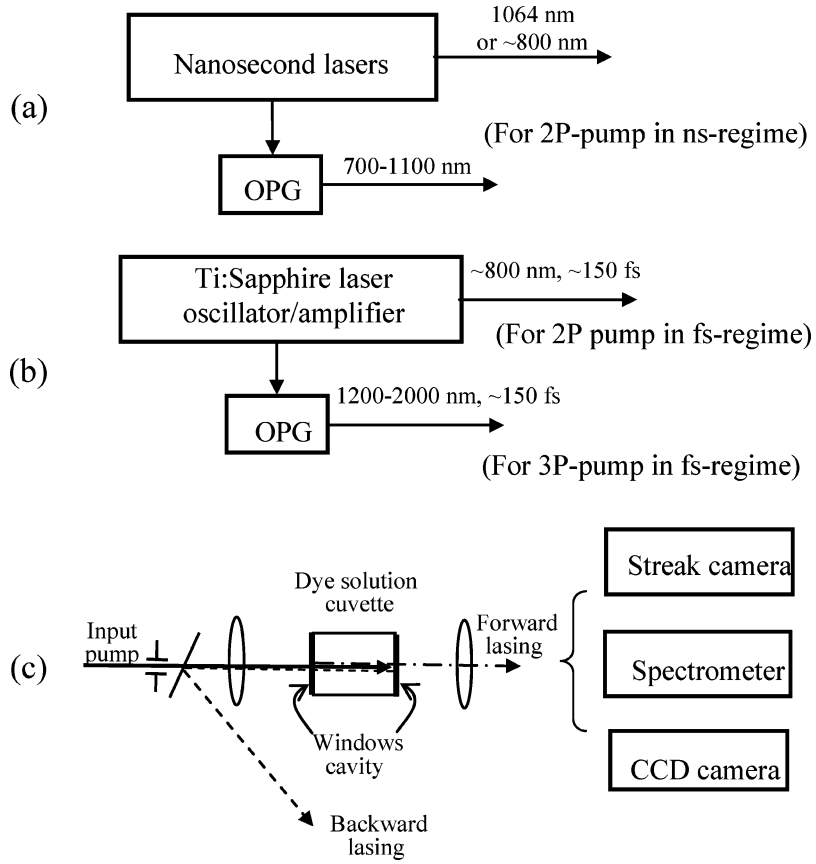

Figure 19. (a) Pump sources for 2PP lasing in the nanosecond regime; (b) Pump sources for MPP lasing in the femtosecond regime; (c) Experimental setup for MPP lasing and output characterization measurements.

MPP lasing purpose, which can be either a Ti:sapphire laser (oscillator/amplifier) system, with ~800 nm and ~150 fs output pulses, or an OPG system pumped by this laser, producing 1200−2000 nm tunable coherent light pulses. Among these two choices, the former can be utilized to achieve 2PP lasing, and the latter can be employed for 3PP lasing or 4PP lasing. In the case of femtosecond pulse excitation, the upconverted lasing pulses will still have a pulse duration of picoseconds, because the dye population inversion is maintained for a much longer time period (>10 ps) than the input pump pulse duration. Finally, shown in Figure 19c is a typical setup for MPP lasing and characterization. Typically, the input pump beam is focused into the center of a dye solution filled cuvette (or a dye-doped rod) of a length from several millimeters to one centimeter. Once the local pump intensity exceeds a certain threshold, an intense one-pass stimulated emission will be observed in both forward and backward directions, featuring drastic spectral narrowing as well as high directionality that is different from fluorescence emission or even ordinary ASE. In this case, the latter feature is automatically ensured by the extremely large geometrical ratio between the gain length and the transverse size of the focused pump beam. In the nanosecond pump cases, the lasing can be further enhanced by using two parallel optical windows of the cuvette or two end surfaces of a solid gain rod to provide an optical feedback to form a cavity. However, in the case of femtosecond excitation, the photon round time within this cavity is much longer than the pump pulse duration as well as the remaining time of the population inversion peak value, and no multipass cavity lasing can be expected; only cavityless lasing can be effectively generated. In the latter case, the high directionality of the output lasing beam is ensured by the focused pump beam geometry inside the gain medium.

The spectral narrowing of the lasing output can be easily measured by using a grating spectrometer; the spatial structures of the lasing output can be determined by near-field (near to the gain medium) and far-field (in the focal plane of a long focal-length lens) measurements using a CCD array camera. The temporal profile of the output lasing pulses can be recorded using an oscilloscope (with nanosecond resolution) or a streak camera system (with picosecond resolution).

6.1.2. Two-Photon Pumped (2PP) Cavity Lasing

Since 1995, a sizable number of novel organic chromophores have been developed, which can be used as highly efficient two-photon-pumped (2PP) lasing dyes. The following are the synthesized 2PP lasing dyes from different research groups: ASPT (1995),[203b,403] APSS (1995),[203a] ASPI (1996),[404] a series of ASSP dyes (total of 9 compounds) (2003),[405] and a series of PRL dyes (total of 10 compounds) (2005)[400] (from He and Prasad's group); M-PPE (1997)[406] and its four derivatives (2000)[407] (from Abbotto and Pagani's group); a series of ASPI derivatives (total of 11 compounds) (2000, 2002)[408−411] and three ASPT derivatives (2001)[412] (from Jiang's group); and some new organic compounds from other groups for 2PP lasing.[413−416]

The commonly used near-IR wavelengths for 2PP lasing in dye-based materials are 1064 nm and ~800 nm. Both 2PP cavity lasing and cavityless lasing can be easily achieved using various optical configurations of the gain medium, which can be a dye solution cell,[76a,417] a dye-doped solid rod,[418] a dye-doped gel-type medium,[419,420] a dye solution

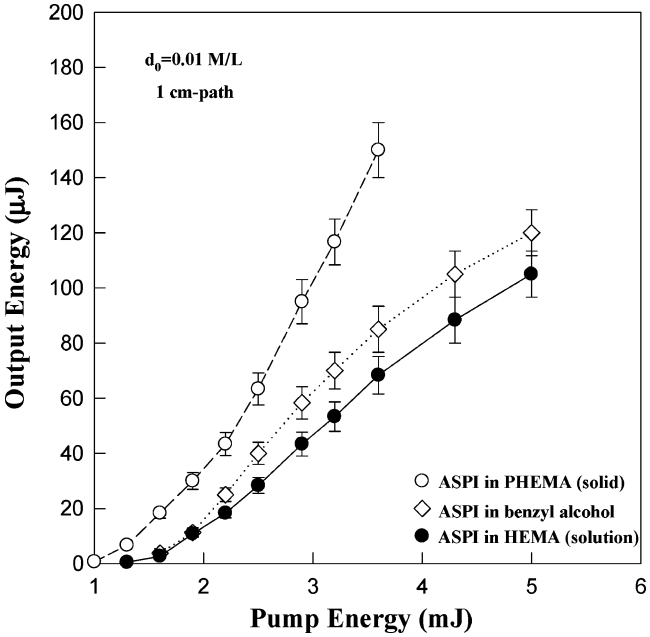

Figure 20. 2PP cavity lasing output energy from three ASPI-based gain media of same concentration versus the 1064 nm pump laser input energy. Reused with permission from ref 76a. Copyright 1997, American Institute of Physics.

filled liquid-core fiber,[203a] a dye-doped polymer-core fiber,[404] a thin film wave guide structure,[421,422] a microdroplet,[423] a photonic crystal structure,[180,424] a semiconductor quantum well structure,[425] or a nanoparticle-based gain medium.[426,427] In most of these cases, a high molar concentration (0.005−0.05 M) of dye is necessary, and the gain length of the lasing medium should be no less than several millimeters. For the latter reason, a longitudinal pump configuration is generally employed. If the dye-based gain medium is in a wave guide geometry (such as an optical fiber), one may expect a higher pump intensity and a much longer effective gain length. That was the partial reason why the first reported 2PP cavity lasing was demonstrated in a system involving a dye solution filled hollow fiber.[203a]

ASPI is one of the best 2PP lasing dyes reported so far, exhibiting the advantages of high solubility in polar solvents, low pump threshold, high lasing efficiency, and high photochemical stability. Shown in Figure 20 are the measured 2PP cavity lasing output energy values as a function of the input pump energy, from three gain media of the same length and concentration: ASPI in PHEMA (solid), ASPI in benzyl alcohol (solution), and ASPI in HEMA (solution).[76a] The maximum input pump energy value was limited by the optical damage inside the gain rod by the focused pump beam. From the data shown in Figure 20, one can see that, at the same pump level, a dye doped polymer rod could provide a considerably higher lasing efficiency. In this specific experiment, at a pump energy level of 3.6 mJ, the laser output energy from the ASPI-doped PHEMA rod was ∼0.15 mJ, and the overall energy transfer efficiency from the input pump to the output lasing was $\eta \approx 4.2\%$. On the other hand, at this pump level, the measured one-pass nonlinear absorption ratio was $\Delta \approx 0.25$; therefore, the net conversion efficiency from the absorbed pump energy to the output lasing energy was $\eta' = \eta/\Delta \approx 17\%$.

In some specific cases, it is desirable to make the lasing output wavelength tunable and have a spectral width as narrow as possible. In principle, various conventional

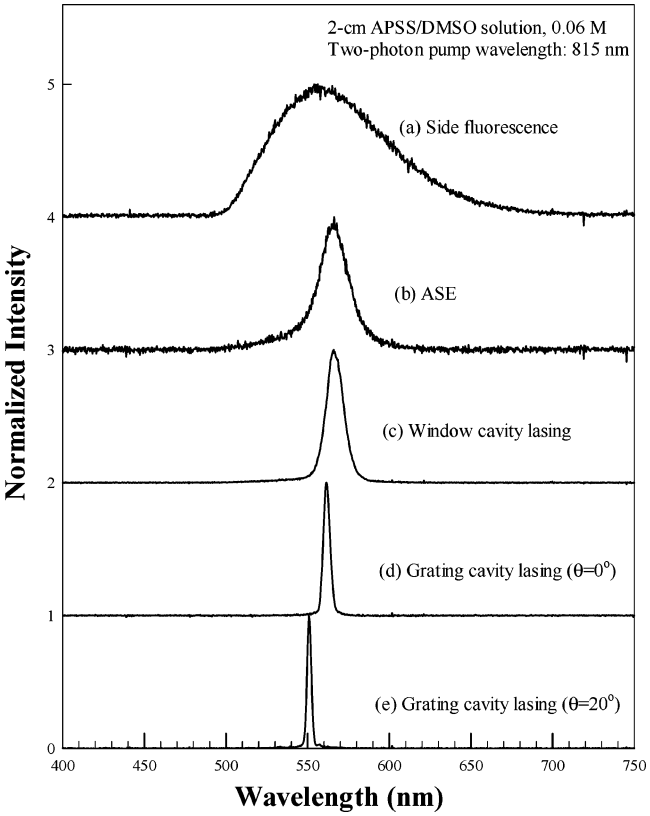

Figure 21. Spectral distribution for (a) two-photon-induced fluorescence, (b) 2PP cavityless stimulated emission or ASE, (c) cavity lasing formed by two windows of the cell, (d) cavity lasing with a feedback from a PDLC grating of θ=0°, and (e) cavity lasing with a feedback from a PDLC grating of θ=20°. The gain medium was APSS solution in DMSO pumped by ∼815 nm, ∼8 ns laser pulses. Reused with permission from ref 428. Copyright 2003, American Institute of Physics.

methods used for one-photon pumped tunable dye lasers can also be applied to 2PP laser devices.[428,429] There is a recent example in which a holographic polymer-dispersed liquid-crystal (H-PDLC) grating was employed as a feedback mirror as well as a lasing tuning element.[428] The gain medium was a 2 cm long APSS dye solution in DMSO, pumped with ∼815 nm, ∼8 ns pulses. Shown in Figure 21 are the measured spectral curves of the two-photon-induced fluorescence, the cavityless lasing, the cavity lasing with window reflection, and the tunable cavity lasing with a H-PDLC grating reflection, respectively. In this case, the spectral width for fluorescence was ∼82 nm, that for cavityless lasing was ∼20 nm, that for window cavity lasing was ∼13 nm, that for grating reflection lasing at $\theta = 0°$ was ∼5 nm, and, finally, that for grating reflection lasing at $\theta = 20°$ was 3 nm only. By changing the reflection angle of the grating, the output lasing wavelength can be smoothly tuned over a 25 nm range.

6.1.3. Three- and Four-Photon Pumped Lasing

In 2002 and 2005, He and Prasad's group reported unambiguous three-photon and four-photon pumped lasing with drastically narrowed spectral width and high directionality from novel organic dye-based solutions.[399−401] As mentioned before, in these cases, a powerful pulsed coherent light source, working in the 1.3−2 μm wavelength range and femtoseconds duration, was used to create population inversion and to provide a sufficient single-pass gain of

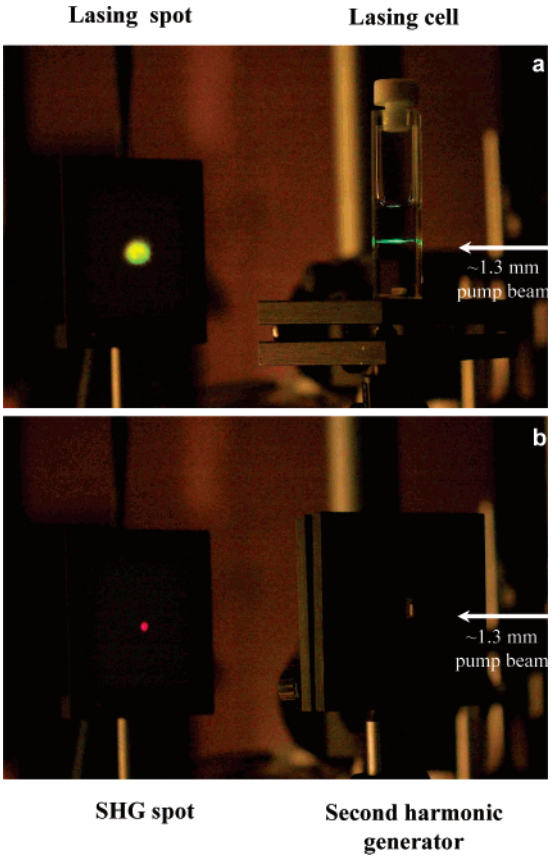

Figure 22. Photographs of (a) 3PP forward lasing from a 1 cm APSS solution in DMSO pumped by ~1.3 μm, ~150 fs pulses, and (b) second-harmonic generation (SHG) output beam from a BBO crystal. Both output beams show a high directionality or spatial coherence. Reprinted by permission from Macmillan Publishers Ltd: *Nature* (ref 399, http://www.nature.com), copyright 2002.

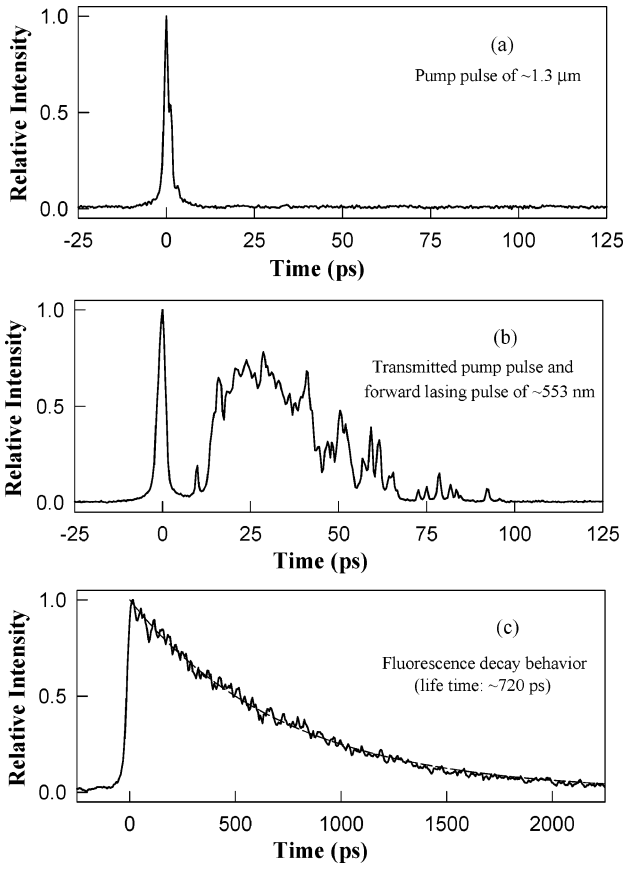

Figure 23. Temporal profiles of the 1.3 μm pump pulse (a), the transmitted pump pulse together with the 553 nm forward lasing pulse (b), and the three-photon-induced fluorescence decay (c). Reprinted by permission from Macmillan Publishers Ltd: *Nature* (ref 399, http://www.nature.com), copyright 2002.

stimulated emission. If the path length and the refractive index of a dye-based gain medium are 1 cm and 1.5, respectively, the photon round time of a cavity with nearly the same optical path length will be ~100 ps, which is much longer than the pump pulse duration (e.g., 100−500 fs) as well as the remaining period of the peak population inversion. For this reason, a multipass-based cavity enhancement is not expected; however, the high directionality of the one-pass cavityless lasing can still be obtained, owing to the focused pump beam configuration and nonlinear absorption property.

In general, good organic chromophores and materials for 2PP lasing are also good candidates for 3PP and 4PP lasing purposes.[399,401,430−432] For instance, APSS and ASPI are among the best 2PP lasing dyes; at the same time, they are also good chromophores for 3PP lasing.[399,430] Shown in Figure 22a is the photograph of the 3PP lasing output beam from a 1 cm long APSS solution cell pumped with ~1.3 μm, ~150 fs pump pulses, while in Figure 22b is the photograph of a second-harmonic generation (SHG) beam of the same pump beam passing through a BBO crystal. From these two photographs, one can see that both output beams have high directionality, indicating their spatial coherence property. Furthermore, Figure 23 shows the measured temporal profiles of the pump pulse, the forward 3PP lasing pulse, and the three-photon-induced fluorescence decay behavior, respectively, by using a streak camera of 2 ps resolution.[399] From Figure 23 one can see that there is a certain delay between the input pump pulse and the burst of forward stimulated emission. Furthermore, the forward stimulated emission pulse can last for a period of 50−70 ps, which is much shorter than the spontaneous fluorescence lifetime of ~720 ps. At an input pump energy level of ~1.5 μJ, the output lasing energy was ~17 nJ from a 1 cm dye solution of 0.06 M concentration, indicating an overall lasing efficiency of $\eta \approx 1.1\%$. At this pump level, the measured nonlinear transmission of the gain medium for the pump beam was ~0.47; therefore, the net 3PP lasing efficiency in this case should be $\eta' = \eta/0.47 \approx 2.1\%$. In another 3PP lasing experiment based on an ASPI solution in DMSO of 0.08 M concentration, pumped by ~1.5 μm laser pulses, the measured overall lasing efficiency was $\eta \approx 6.7\%$, and the corresponding net efficiency was $\eta' \approx 12\%$.[430]

Very recently, there has been a comprehensive experimental study of a series of newly synthesized chromophores (PRL-L1 to -L10) for two-, three-, and four-photon pumped lasing properties in solutions.[400] The chemical structures of these ten chromophores are shown in Figure 24. These are stilbazolium dyes having basically the same molecular backbone, but they differ either in their electron-donors or their electron-acceptors. Dialkylamino, alkyloxyl, and hydroxyl groups were chosen as electron donors. Various lasing wavelengths can be obtained from these dyes by changing the electron donating ability of the terminal groups on the stilbazolium backbone. Multiphoton pumped lasing can be achieved based on these dyes in solutions. At the same time, different electron donors or acceptors may influence dye interactions with a surrounding medium (solvent), which may affect their multiphoton pumped lasing properties. The

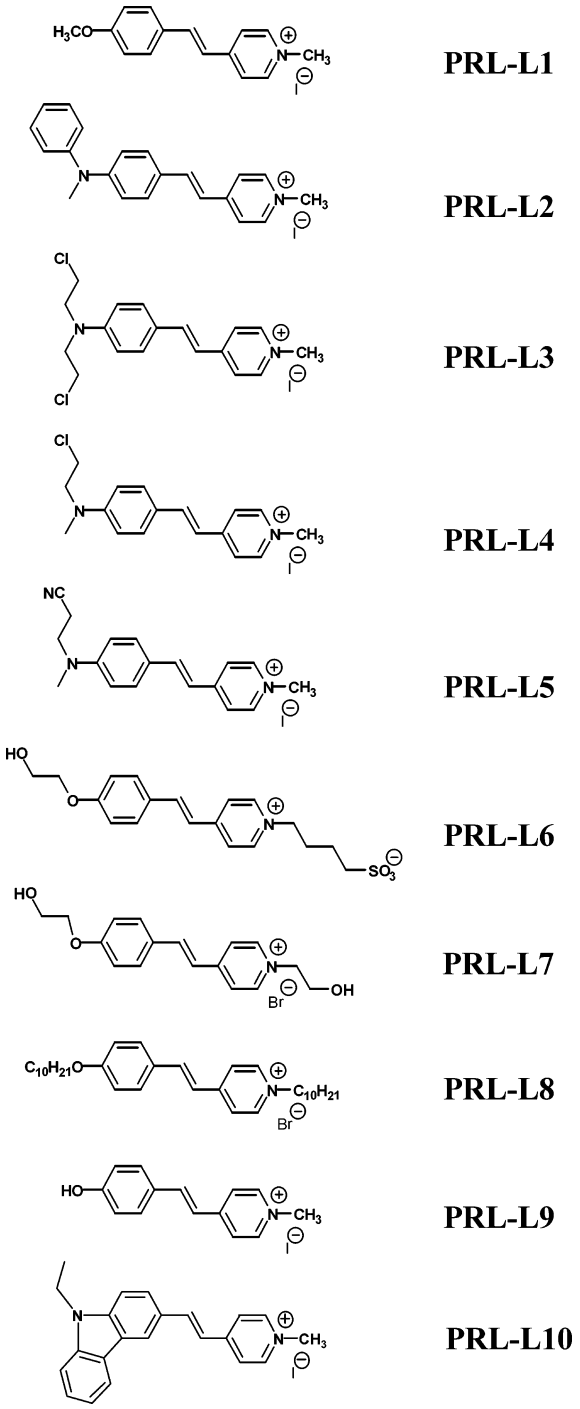

Figure 24. Chemical structures of newly synthesized ten stilbazolium dyes for multiphoton pumped lasing. Reprinted with permission from ref 400. Copyright 2005 Optical Society of America.

investigation of the lasing behavior in such a group of systematically varied molecular structures may help with the design and synthesis of future multiphoton active dye materials with better performance.

For simplicity and ease of comparison, three specific pump wavelengths were chosen for experiments with these dyes solutions: ~775 nm (for 2PP lasing), ~1320 nm (for 3PP lasing), and ~1890 nm (for 4PP lasing), with the same pulse duration of ~160 fs. The path length of the dye solution cell was 1 cm; the solvent for most dyes was DMSO for 2PP and 3PP lasing, or DMSO-d_6 for 4PP lasing. The dye concentration was mostly ~0.02 M. Under these conditions, most of these dye solutions showed 2PP and 3PP lasing, while three of them, i.e., PRL-L3, -L5, and -L10, could also be employed to achieve 4PP lasing. The measured key parameters of these ten lasing dye solutions are summarized in Table 15, from which one may note that the net 3PP lasing efficiency for PRL-L3 and PRL-L5 solutions of 0.02 M concentration was about 13%, while the overall 4PP lasing in the PRL-L3 solution was only about 0.12%. The latter value could be considerably improved if the concentration would be further increased.

During the lasing measurements of these dye solutions, an unexpected phenomenon was observed: there was a wavelength difference between the forward and the backward lasing output under 3PP and 4PP conditions. In these two cases, as shown in Table 15, the forward lasing wavelength was found to be shorter than the backward lasing wavelength by an amount of 17−21 nm for the PRL-L5 solution and by 26−31 nm for the PRL-L10 solution. As a visual demonstration of this effect, Figure 25 shows a photograph indicating the color difference between the forward and the backward lasing beams from a PRL-L3 solution under 4PP lasing conditions.

The other related fact is that, at the same pump level, the forward lasing output energy is always significantly greater than the backward lasing output energy under 3PP and 4PP conditions. For instance, for the PRL-L5 solution under 3PP lasing conditions, the measured ratio of the forward lasing energy to the backward lasing energy was about 10:1. These two effects that reflect the asymmetry between the two lasing output beams can be well explained by the latter experimental study and theoretical analysis.[371,433]

6.2. MPA-Based Optical Limiting, Stabilization, and Reshaping

An optical limiter is a special device, of which the optical transmissivity decreases when the input signal intensity increases. This kind of device can be used for protection of human eyes or optical sensors against high-intensity laser radiation-induced damage. Various nonlinear optical effects can be employed for the design and performance of optical limiters.[7,234,434−436] Although there is a great variety of optical limiting devices, most of them can be, in principle, classified into two broad categories: one is the energy-spreading type of device, and the other is the energy-absorbing type of device. The principle of the first type of device is based on an intensity-dependent change in the spatial structure of a laser beam passing through a nonlinear medium. At low-intensity levels, this change can be neglected and the whole laser beam can be detected through a properly placed aperture in front of a detector. At high-intensity levels, this change becomes so severe that only a small fraction of the transmitted beam can pass through the same aperture and be finally detected. In contrast, the operation of the second type of device is based on intensity-dependent nonlinear attenuation of the laser energy in a given nonlinear medium. In this case, the beam-structure change is not so important. In this review we only consider the second type of optical power limiting device, for which detecting the nonlinear absorption or transmission change is most important for the design of an optical setup. The ideal requirements for choosing a proper nonlinearly absorbing medium for optical limiting purposes can be described as follows: (i) there should be no linear absorption at the working wavelength range, so that the medium is highly transparent for weak input light signals;

Table 15. Multiphoton Pumped Lasing and Fluorescence Parameters for Solutions of Ten Dyes

dye	solvent conc (1 cm path length)	fluorescence lifetime τ[a] (ps)	lasing threshold[a] (μJ)	forward lasing wavelength[b] (nm)	backward lasing wavelength[b] (nm)	net lasing efficiency (%)
PRL-L1	DMSO/0.02 M	65 (2P)	0.46 (2P)	495 (2P)		
		85 (3P)				
	EG/0.04 M	70 (2P)				
		100 (3P)	1.5 (3P)	494 (3P)		
PRL-L2	DMSO/0.02 M	11 (2P)	no (2P)			
			1.5 (3P)	607 (3P)		
PRL-L3	DMSO/0.02 M	620 (2P)	1.2 (2P)	605 (2P)	606 (2P)	4.5 (2P)[c]
		680 (3P)	0.88 (3P)	579 (3P)	598 (3P)	13 (3P)[c]
			2 (4P)	580 (4P)	597 (4P)	0.12 (4P)[d]
PRL-L4	DMSO/0.02 M	200 (2P)	2.0 (2P)	618 (2P)	620 (2P)	
		225 (3P)	0.88 (3P)	594 (3P)	612 (3P)	
PRL-L5	DMSO/0.02 M	243 (2P)	1.2 (2P)	616 (2P)	618 (2P)	
		285 (3P)	0.66 (3P)	593 (3P)	611 (3P)	13 (3P)[c]
			2 (4P)	593 (4P)	607 (4P)	
PRL-L6	EG/0.01 M	110 (2P)	3.2 (2P)	502 (2P)		
		155 (3P)	4.1 (3P)	496 (3P)		
PRL-L7	EG/0.04 M	80 (2P)	1.9 (2P)	498 (2P)		
		110 (3P)	1.8 (3P)	490 (3P)		
PRL-L8	DMSO/0.02 M	110 (2P)	0.57 (2P)	511 (2P)		
		118 (3P)	no (3P)			
PRL-L9	DMSO/0.02 M	92 (2P)	0.46 (2P)	516 (2P)	519 (2P)	
		115 (3P)	no (3P)			
PRL-L10	DMSO/0.02 M		0.95 (2P)	595 (2P)	596 (2P)	
		1200 (3P)	1.2 (3P)	564 (3P)	594 (3P)	3.6 (3P)[e]
			3.9 (4P)	565 (4P)	591 (4P)	
(note)			(f = 10 cm)			(f = 5 cm)

[a] Uncertainty = ±10%. [b] Uncertainty = ±1.5 nm. [c] Concentration: 0.08 M. [d] Overall efficiency at 0.02 M concentration. [e] Concentration: 0.1 M.

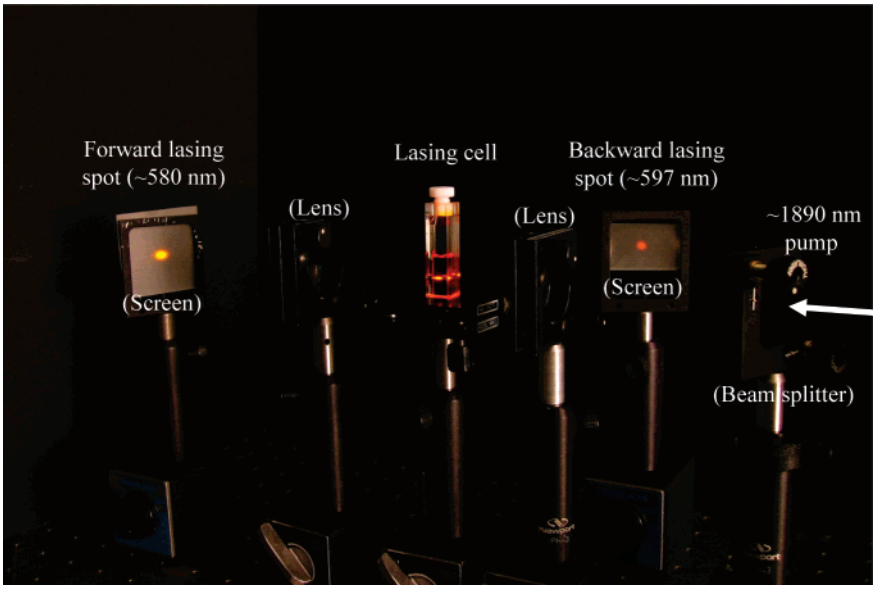

Figure 25. Photograph of the 4PP lasing in the PRL-L3 solution, exhibiting the different colors between the forward and backward lasing output beams.

(ii) there should be a strong dependence of the nonlinear transmission on the input light intensity, so that the medium is highly absorptive for intense laser signals; (iii) there should be a very fast temporal response of nonlinear transmission changes in the medium following the intensity change of the input signals; and (iv) the spatial quality of the light beam should be retained after passing through the nonlinear medium.

Two major nonlinear absorption processes can be employed for optical limiting: one is linear (one-photon) absorption initiated reverse saturable absorption (RSA), and the other is multiphoton absorption (MPA) and/or MPA-initiated excited-state absorption (ESA).[7,234] The working mechanism for the former is an initial one-photon absorption from the ground state followed by another one-photon absorption from the excited state. The major disadvantage of this type of optical limiting is that the initial linear absorption can impede the detection of a weaker input signal and degrade the beam quality. In this sense, the multiphoton absorbing medium is a much better choice for optical power limiting, because it basically fulfills all the requirements mentioned above. For the same reasons, the multiphoton absorbing medium can be highly useful not only for optical limiting but also for optical stabilization purposes. In many cases of applications (such as optical telecommunications and optical data processing), a random intensity fluctuation

of the laser signals is highly undesirable. If we let an intensity-fluctuating laser beam pass through a multiphoton absorbing medium, the intensity fluctuations of the transmitted beam will be considerably reduced, owing to the nonlinear transmission property of the medium. The same principle can also be applied for smoothing or reshaping the temporal and/or spatial profiles of intense coherent light signals. In all these cases, the common basis is that the nonlinear transmission of a multiphoton absorbing medium is getting lower when the input light intensity is getting higher, and vice versa.

6.2.1. 2PA-Based Optical Limiting

Semiconductor crystals were the solid materials used early for 2PA-based optical limiting studies starting from the mid-1980s by Van Stryland.[437−442] For these applications, the wavelengths of input laser beams were usually in the IR range, and the measured limiting effects might also be due to other mechanisms, such as induced free carriers absorption or nonlinear refraction. Even now, the study of nonlinear optical properties of semiconductor materials is still important for optical limiting and other applications.

It was well-known for a long time that many organic compounds exhibit the property of 2PA- and 2PA-induced fluorescence emission. However, enhanced efforts of using 2PA organic compounds for optical limiting purposes were initiated only in the mid-1990s.[71a,76a,342,443] Since then, various newly synthesized organic materials for optical limiting performance have been reported by many research groups around the world. In most cases, the investigated nonlinear absorbing materials were organic chromophores in the solution,[57,74,104,288,343,443−452] and dye-doped solid rods.[71a,76b] In some other cases, the two-photon absorbing materials for optical limiting measurements could also be organic crystals,[453,454] inorganic crystals[455] or a hybrid organic−inorganic crystal,[456] organic-liquid-core fiber array systems,[457−459] a polycrystalline solid film,[460] or an organic dye−C_{60} mixture in solution.[44] More recently, there have been some encouraging developments in new directions: one is the use of a neat liquid-crystal dye in its isotropic phase[184] as well as a neat liquid-dye salt[461,462] as more effective two-photon absorbing media because of their high molar concentrations; the other is the use of various nanoparticle activated systems in solutions or in solid matrixes.[321,324a,463−465]

In the simplest case, without considering induced scattering, refraction, and thermal lens effects, the nonlinear transmission T of a given two-photon absorbing medium for a focused laser beam is given by eq 24; therefore, the output intensity can be expressed as

$$I_{out} = I_0 T = \frac{\ln(1 + \beta I_0 l_0)}{\beta l_0} \quad (2PA) \qquad (38)$$

Here I_0 is the input light intensity, l_0 and β are the optical path length and 2PA coefficient of the medium, respectively. Researchers may use eq 24 or eq 38 to characterize the optical limiting performance of different 2PA materials. From eq 24, one can see that, for given values of I_0 and l_0, the nonlinear transmission is only determined by β, which is further proportional to the product of the 2PA cross section (σ_2) and the concentration of nonlinear absorbing molecules (without considering the saturation effect). The general rule is that, under the same experimental conditions (including the maximum input intensity level, path length, concentration, as well as specific optical setup), the sample material that exhibits the lowest nonlinear transmission will have the largest effective σ_2 value and, therefore, could be the best candidate for 2PA-based optical limiting performance. In this sense, the 2PA-based optical limiting measurement is the same as the 2PA cross section measurement using the nonlinear transmission method. However, in practice, it is very difficult to apply this rule to compare or evaluate those experimental results reported by different research groups under different experimental conditions. There are two major reasons which cause this difficulty. The first is that the nonlinear absorptivity of a given medium highly depends on the input pulse duration range, as discussed in subsection 5.3. The second is that, very often, the apparently obtained optical limiting effects are not only due to pure nonlinear absorption (2PA or 2PA plus ESA) but also due to other 2PA initiated processes, such as induced nonlinear scattering, nonlinear refraction, self-focusing or self-defocusing, and thermal-lens effect occurring in nonlinearly absorbing media. In all these cases, an apparent superior performance of optical limiting or an overestimated β (or σ_2) value may be artificially obtained.

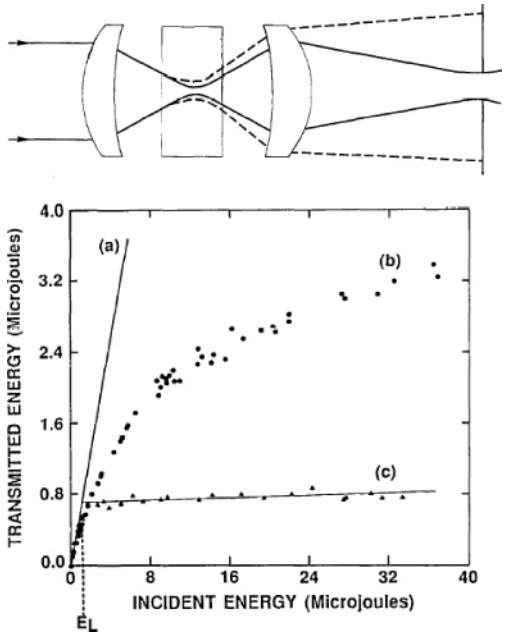

Figure 26. Top: Optical setup with an (effective) aperture before the detector for optical limiting measurement: solid lines (weak input beam) and dashed lines (strong input beam). Bottom: Input/output characteristics of a thick ZnSe rod, showing (a) the linear transmission, (b) the effect of 2PA (i.e., all energy collected), (c) the transmitted energy through an (effective) aperture (i.e., fluence in arbitrary units) as a function of the input energy of 532 nm, 30 ps laser pulses. Reprinted with permission from ref 441. Copyright 1988 Optical Society of America.

There was an excellent early experimental result presented by Van Stryland and co-workers, which clearly showed how nonlinear refraction and an effective aperture before the detector could cause a dramatically different optical limiting behavior for a given test sample.[441] In this experiment, the nonlinearly absorbing medium was a ZnSe semiconductor rod of 1 cm thickness, and the input was a focused 532 nm laser beam of 30 ps pulse duration. The optical setup for this measurement is shown in the top of Figure 26. At a very low input level, the whole transmitted beam could pass through an aperture with suitable diameter and be detected by a large-area detector. However, at a high input level, the

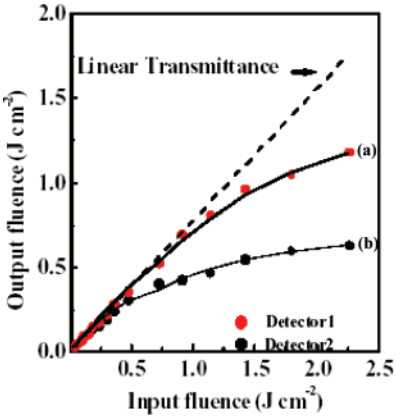

Figure 27. Measured optical limiting behavior of CdS nanoparticles in DMF: (a) the transmitted beam was totally received by Detector 1 through a larger-aperture lens placed near to the sample; (b) the transmitted beam was partially received by Detector 2 through a smaller aperture lens placed far away from the sample. An F/24 focusing geometry was used. Reprinted with permission from ref 465. Copyright 2005 Optical Society of America.

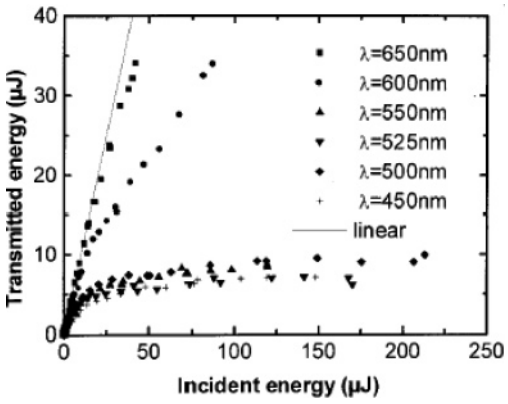

Figure 28. Measured optical limiting behavior of 2,2′-(9,9-dehexyl) bifluorene in chloroform (d_0=600 g/L) of 5 mm path length upon different wavelengths of 2.6 ns pulses. The thickness of the solution sample was ~5 mm, and the waist size of the input beam was ~30 μm by using an F/5 focusing geometry. Reused with permission from ref 449. Copyright 2001, American Institute of Physics.

spatial structure (divergence angle and beam size) of the transmitted beam changed due to nonlinear refraction caused by a 2PA-induced refractive-index change. As a result, only part of the transmitted beam could pass through the same aperture and be detected. Obviously, in this latter case, the apparent "attenuation" of the strong input beam was not only due to nonlinear absorption but also due to induced beam diffusion and the existing aperture. In the bottom of Figure 26, the transmitted pulse energy data of group b were measured by a large-area detector without placing any aperture, which could be fitted by a smoothly changing curve, whereas the data of group c were measured by the setup with an aperture placed in the front of the detector, as shown in the top of the same figure. In the latter case, one can see a sudden flattening or clamping of the output/input characteristic curve at a certain input level (indicated in Figure 26 by E_L). Although it looks like a perfect optical limiting performance, this type of result could be arbitrary and highly dependent on the size and position of the aperture.

In many practical cases, including open-aperture *Z*-scan measurements, even with no aperture placed in front of the detector, an effective aperture may still exist, if either the detector area or the size of the collecting-lens is not large enough compared to the size (or transverse distribution region) of the transmitted laser beam, which could be remarkably changed when a small *F*/number focusing system is adopted due to other nonlinear processes, such as induced refraction, scattering, self-focusing/defocusing, or a thermal-lensing effect. As a recent experimental example supporting the above statement, Figure 27 shows two measured output/input curves of an optical limiting device, using CdS nanoparticles in DMF as a nonlinear absorbing and scattering medium.[465] The average particle size was ~4.5 nm, the mixture ratio was CdS/DMF = 1/100, and the input was a 532 nm pulsed laser beam of 6 ns duration and 10-Hz repetition rate. The input beam was focused by an *F*/24 optical system providing a focal depth of ~3 mm. In Figure 27, curve a was measured by a larger-aperture collecting lens placed near the sample, and data were recorded by detector 1, whereas curve b was measured by placing a small-area collecting lens far from the sample and data were recorded by detector 2. In this case, the authors explained that curve a resulted mainly from 2PA, whereas curve b resulted from both 2PA and induced nonlinear scattering. Obviously, the data of curve b were dependent on the size and position of the second collecting lens.

In order to reduce or eliminate the influence from an effective aperture in nonlinear-absorption-based optical limiting experiments for fundamental research purposes, some measures can be taken to improve the reliability of the final results about the nonlinear absorptivity of the test material. These measures can be the following: (i) the use of a longer focusing length and a larger *F*/number to ensure a greater focal depth comparable to the sample thickness, (ii) the use of a detector with a detecting area remarkably larger than the detected beam size, placed near to the sample, and (iii) the use of a low repetition rate of input laser pulses via a chopper to reduce the thermal lensing effect.

In their early publications of optical limiting studies in the visible spectral range, Perry and co-workers indicated that the measured nonlinear absorption in the nanosecond regime was due to two-step combined processes, i.e., an initial 2PA process followed by an excited-state absorption (ESA) process.[342,445] Even so, in many practical cases of optical limiting experiments operating in the nanosecond regime, the nonlinear transmission curve (or output/input characteristic curve) for a given two-photon absorbing medium could still be approximately fitted with an *effective* 2PA coefficient β value.[57,71a,76b,342,443,461,462] On the other hand, based on the two-step nonlinear absorption model, Baldeck and co-workers indicated that the *effective* 2PA spectrum for a given medium measured in the nanosecond regime could be determined by the product of the pure 2PA spectrum and the one-photon ESA spectrum;[449,451] the former can be measured by using an upconversion fluorescence method, and the latter can be measured by using a pump−probe method. As an example of their studies, Figure 28 shows the measured optical limiting curves of a two-photon absorbing chromophore, 2,2′-(9,9-dehexyl)bifluorene in solution, excited with different wavelengths of input laser pulses of 2.6 ns duration.[449] The concentration of the chromophore in chloroform was 600 g/L, and the input beam was size-expanded through an inverse telescope system and then tightly focused via an F/5 configuration onto the center of a 5 mm solution cell, where the focal spot size was ~30 μm. In this case, the focal intensity was so strong that it might even damage the optical window. From Figure 28, one can see that, at a higher incident energy level, the input with

525 nm wavelength produced the lowest output, suggesting that the peak of the effective 2PA spectrum in the nanosecond regime could be located around this wavelength position. However, the authors also indicated that such measured effective nonlinear absorptivity was 2 orders of magnitude larger than the value expected by their theoretical calculation. It is possible that this discrepancy is due to the extremely small *F*/number focusing configuration, under which the focal depth of the input beam was extremely shorter than the sample thickness and the focal intensity was so strong that the local nonlinear absorption could initiate many other processes, such as bubbling in the liquid, self-focusing/defocusing, and other phenomena. As mentioned above, all these unexpected effects may lead to an apparently large nonlinear absorptivity of the test medium.

For all organic chromophore solutions or doped solid matrices used for optical limiting studies, the nonlinear absorptivity is directly proportional to the concentration of the absorbing molecules. In practice, the dye concentration values are usually limited to $10^{-2}-10^{-1}$ M in solution, as well as in doped solid matrices due to dye segregation at higher concentrations. Therefore, new types of organic nonlinear materials are desirable, which exhibit a much higher effective concentration of multiphoton absorbing molecules. These types of materials can be organic crystals consisting of molecules with nonlinearly absorbing chromophores, neat liquid crystals consisting of dye molecules, and neat dye liquid salts. There is a recent example of optical limiting studies in this new direction.[184] Shown in Figure 29 are the measured nonlinear transmission curve and the output/input characteristic curve of an optical limiter using a neat dye liquid crystal as the two-photon absorbing medium, excited by ~815 nm, ~5 ns laser pulses working at 10 Hz. The chemical structure of the dye molecules is shown in the top of the figure. The 1 cm path length cuvette was filled with the dye liquid crystal and heated to ~100 C° to keep the nonlinear medium in its isotropic phase. An *F*/100 focusing configuration was adopted. In Figure 29 the solid lines are the best fitting curves given by 2PA equations with an effective 2PA coefficient of $\beta = 6.25$ cm/GW.

6.2.2. 3PA-Based Optical Limiting

Three-photon absorbing materials can also be employed for optical limiting purposes. Moreover, owing to the cubic dependence of the nonlinear absorption on the local light intensity, the material may produce a very sharp change of nonlinear transmission with respect to the input intensity change. The other advantage of using a 3PA process to execute optical limiting operations is that the working wavelengths can be much longer and far away from the linear absorption band; therefore, the harmful linear absorption influence can be totally avoided. For a pure 3PA process, the nonlinear transmission of a medium is given by eq 14, and the output/input relationship can be described as

$$I_{out} = I_0 T = \frac{I_0}{\sqrt{1 + 2\gamma I_0^2 l_0}} \quad \text{(3PA)} \qquad (39)$$

Here, I_0 is the input intensity and γ and l_0 are the 3PA coefficient and thickness of the medium.

The earliest experimental result of 3PA-based optical limiting in a chromophore solution was reported in 1995. The samples were dye solutions operating with 1064 nm, 10 ns laser pulses.[466] In the recent decade, there have been an increasing number of papers published, which are related to 3PA-based optical limiting.[324a,462,463,467−472] In most cases, the nonlinear absorbing media were chromophores in solution although, in some other cases, the samples could be dye liquid salts,[114] as well as nanoparticle activated materials.[324a,463] The input laser wavelengths often used for 3PA optical limiting experiments were within the spectral range from ~1.0 to ~1.3 μm; the pulse duration is either in the 30−40 ps range or in the 100−160 fs range; the peak intensity of the focused laser beam varies from 10 to 400 GW/cm^2.

In 1995, He et al. reported a 3PA optical limiting demonstration based on an organic chromophore (BTTDOT)

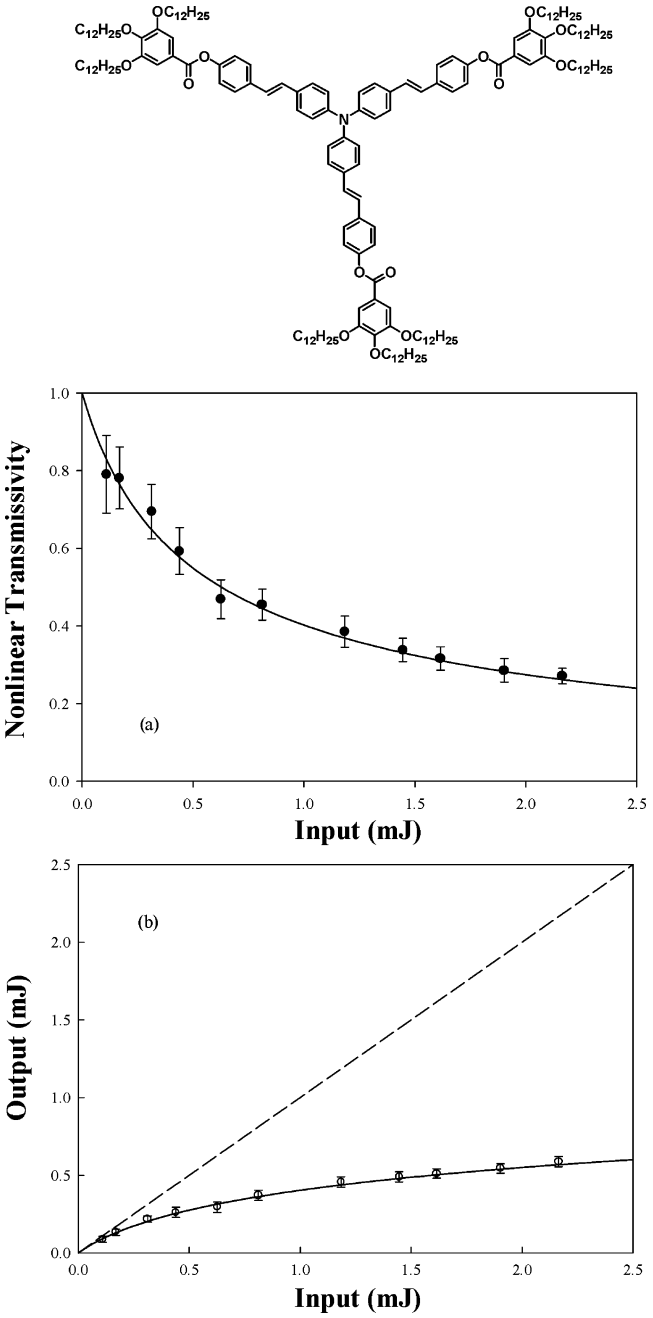

Figure 29. Measured nonlinear transmission data (a) and output pulse energy (b) versus the input energy of ~815 nm, ~5 ns laser pulses, passed through an F/100 focusing system and a 1 cm long neat dye liquid-crystal sample. The solid lines are the best fitting curves with an effective β=6.25 cm/GW. The chemical structure of the tested sample is shown at the top. Reused with permission from ref 184. Copyright 2003, American Institute of Physics.

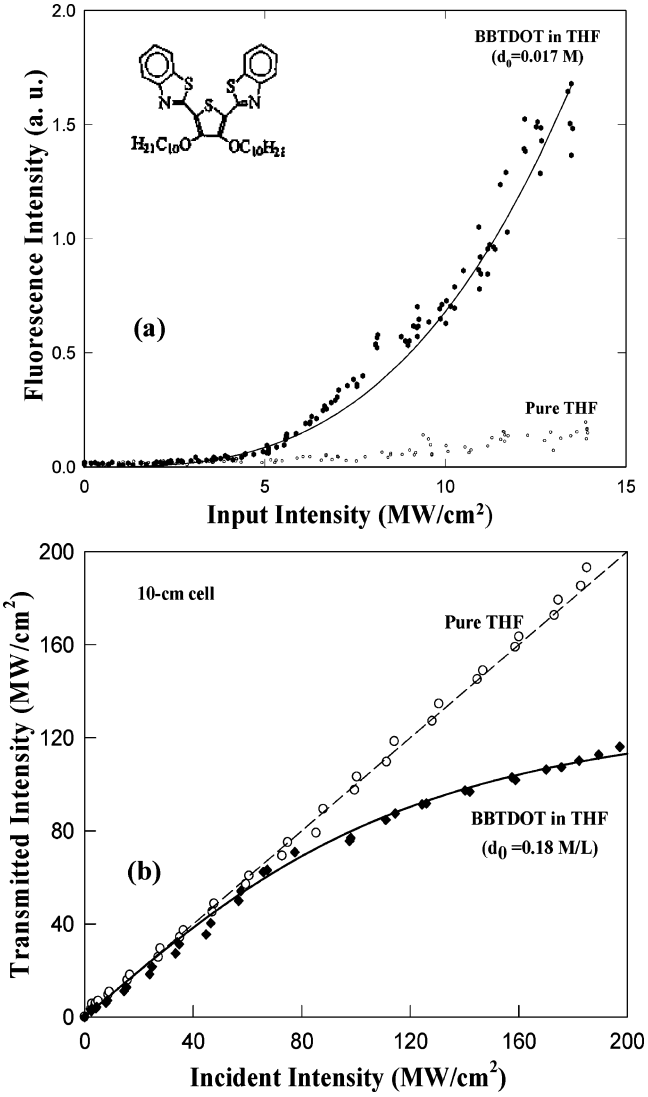

Figure 30. (a) Measured 3PA-induced ~450 nm fluorescence intensity of BBTDOT in THF versus the input intensity of the 1064 nm, 10 ns laser pulses; the solid line is the fitting curve given by a cubic law, and the chemical structure of BBTDOT is shown in the left top corner. (b) Measured output/input characteristic curve of a 10 cm long solution sample with using an F/50 focusing geometry; the solid line is the best fitting curve with an effective 3PA coefficient of γ=2.7 cm^3/ GW.^{2} Reprinted with permission from ref 466. Copyright 1995 Optical Society of America.

in THF;[466] the chemical structure of this chromophore is shown in the left top corner of Figure 30a. The major linear absorption band of this solution sample was located around 380 nm, and there was no linear absorption in the spectral range from 500 to 1100 nm. Upon excitation with 1064 nm, 10 ns laser pulses, the frequency-upconversion fluorescence band (centered in the 450 nm position) of this solution could be readily observed. For a solution sample of concentration $d_0 = 0.18$ M and under low excitation conditions ($\leq$15 MW/cm^2), the measured fluorescence intensity versus the input 1064 nm intensity could be well fitted by a cubic law, as shown in Figure 30a. For a 10 cm long solution sample of concentration $d_0 = 0.18$ M, the measured output/input data are shown in Figure 30b, indicating a typical 3PA-based optical limiting behavior; the solid line is the theoretical fitting curve given by eq 39 with an effective 3PA coefficient value of $\gamma = 2.7$ cm^3/GW.^{2} To obtain these results, a 10 mm diameter 1064 nm laser beam was focused via an $f =$ 50 cm lens, and the liquid cell was placed 15 cm after the focal plane to avoid any self-focusing/-defocusing effect.

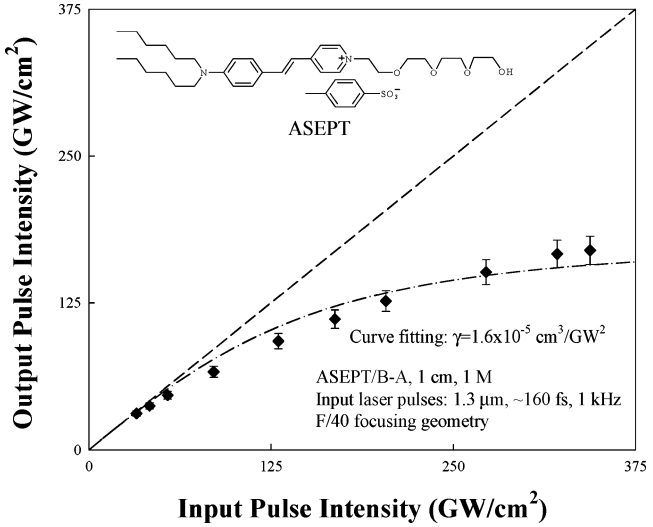

Figure 31. Measured 3PA-based optical limiting behavior of a 1 cm thick liquid dye salt sample (ASEPT diluted by benzyl alcohol) using ~1.3 μm, ~160 fs laser pulses; the dash-dotted line is the theoretical fitting curve with a 3PA coefficient value of γ=1.6 $\times$ 10^{-5} cm^3/ GW.^{2} An *F*/40 focusing geometry was used and the chemical structure of ASEPT is shown in the left top corner. Reprinted with permission from ref 462. Copyright 2005 IEEE.

As a recent example of a 3PA-based optical limiting experiment performed in the femtosecond-regime,[462] the nonlinear absorbing medium was a neat liquid dye salt slightly diluted with benzyl alcohol in a volume ratio of ~1/1, with an estimated molecular concentration of $d_0 \approx 1$ M. The chemical structure of this liquid dye salt (ASEPT) is shown in the left top corner of Figure 31. This sample medium exhibited a strong linear absorption band centered at ~500 nm and a linearly transparent window in the ~1.3 μm range; therefore, one may expect that an efficient 3PA excitation could be realized by using a strong IR radiation of ~1.3 μm. In this experiment, the input ~1.3 μm, ~160 fs pulsed beam was from an OPG device pumped by a Ti:sapphire laser system. Shown in Figure 31 are the measured output pulse intensity values of the laser beam passed through a 1 cm thick sample as a function of the input intensity; the dash-dotted line is the theoretical curve given by eq 39 with a best fitting parameter of $\gamma = 1.6 \times 10^{-5}$ cm^3/GW.^{2} It should be noted that though the materials giving the results shown in Figures 30 and 31 were different, the difference between the effective γ values measured in the nanosecond regime and in the femtosecond regime for these two samples still was too large in order of magnitude. This fact may imply that, in the nanosecond regime, a 3PA-initiated excited-state absorption (ESA) and/or other mechanisms could play important roles giving rise to a much higher nonlinear absorptivity than the pure 3PA process. Further studies of this issue are needed.

6.2.3. MPA-Based Optical Stabilization

The principle of optical stabilization can be described as follows: if an intensity-fluctuated laser beam passes through a multiphoton absorbing medium, the nonlinear transmission of the medium will be lower when the incident intensity increases, or in reverse, the nonlinear transmission of the medium will become higher when the input intensity is

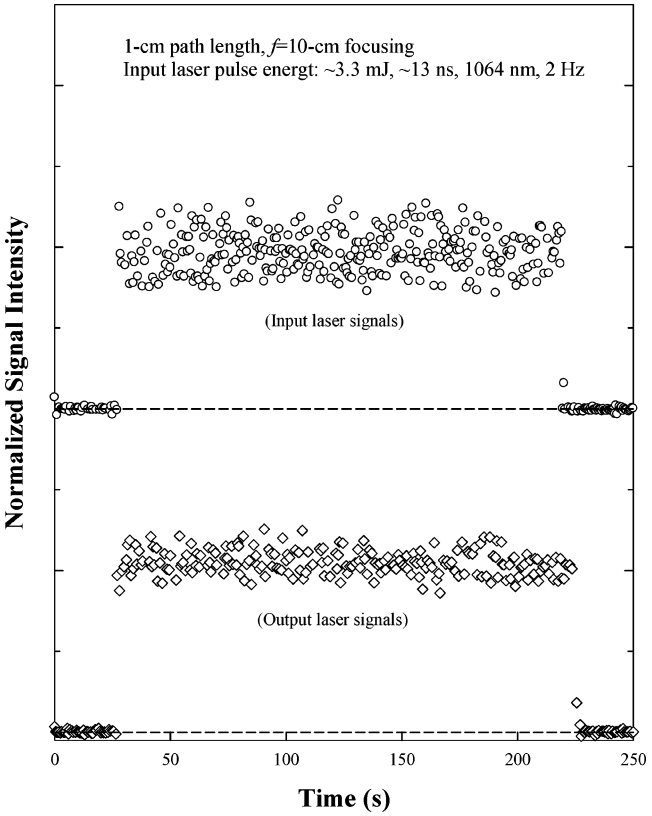

Figure 32. Measured relative laser pulse fluctuation for the input signals (upper trace), and for the output signals (lower trace) passed through a 1 cm long dye liquid salt (ASDPT) sample. Reprinted with permission from ref 461. Copyright 2005 Optical Society of America.

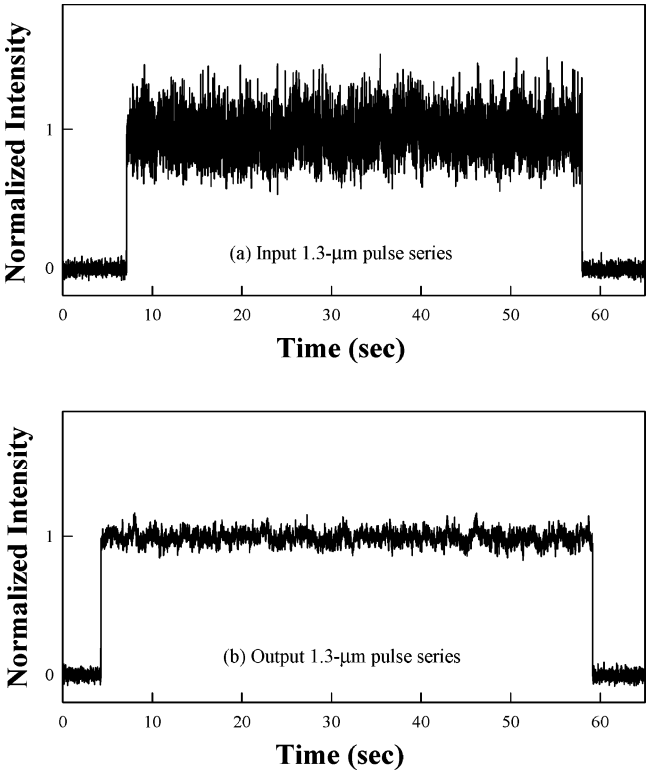

Figure 33. (a) Measured intensity-fluctuation profile for the input 1.3 μm, ~160 fs laser pulses of 1-kHz repetition rate; (b) Measured intensity-fluctuation profile for the output laser pulses passed through a 2 cm liquid dye salt (ASEPT) as the three-photon absorbing medium. Reprinted with permission from ref 462. Copyright 2005 IEEE.

temporarily reduced. Because of this reason, after passing through this type of medium, the intensity fluctuation of the transmitted laser beam will be automatically reduced.

The first experimental demonstration of optical stabilization based on a 2PA process was reported by He et al. in 1995, in which a 2.4 cm long dye (BBTDOT)-doped epoxy rod of $d_0 = 0.09$ M concentration was employed as the two-photon absorbing medium, and the input 602 nm, 0.5 ps pulsed laser beam was focused via an F/100 optical system onto the center of the epoxy rod.[71a] The relative peak intensity fluctuation of the input laser pulses with a repetition rate of 30 Hz was $\Delta \approx \pm 0.11$, whereas, after passing through the two-photon absorbing rod, the relative peak intensity fluctuation was reduced to $\Delta' \approx \pm 0.038$.

In a series of optical stabilization experiments reported later, the employed nonlinear absorbing media could be a chromophore solution,[473,474] a dye solution core optical fiber system,[475] a neat liquid-crystal dye system,[184] and a liquid dye salt system.[461,462]

A recent example of 2PA-based optical stabilization is using a 1 cm long dye liquid salt (ASDPT) sample as the nonlinear absorbing medium, operated with 1064 nm, ~13 ns laser pulses of 2-Hz repetition rate. The measured input and output intensity fluctuation profiles are shown in Figure 32.[461] To obtain these results, the input laser beam, from a Nd:YAG laser using a BDN-doped polymer sheet as the passive *Q*-switch element, was focused via an F/50 optical system onto the sample cell. As the shape of the input laser pulses roughly remained the same, the peak intensity fluctuation was mainly due to random variation of the pulse energy around its average value. In Figure 32 each point represents the measured relative energy value of a single pulse, which was recorded by a gated integrator, and the average input energy level was ~3.3 mJ. From this figure one can see that the input energy (intensity) fluctuation was $\Delta \approx \pm 0.25$ whereas the output fluctuation was $\Delta' \approx \pm 0.13$; that is, there was a 2-fold reduction in the relative fluctuation for the output pulse signals.

As mentioned in the beginning of the preceding subsection, the 3PA mechanism can also be applied to optical limiting and stabilization with an additional advantage of a cubic dependence of the nonlinear response of the material on the local intensity change of the beam. The first experimental demonstration of 3PA-based optical stabilization was reported in 2005,[462] in which a 2 cm long liquid dye salt (ASEPT, see the inset of Figure 31) sample was employed as a three-photon absorbing medium; the input 1.3 μm and ~160 fs laser pulses of 1-kHz repetition rate and 2.5 mm beam size were from a OPG device pumped by a Ti:sapphire laser system. Shown in Figure 33 are the measured intensity fluctuation profiles of the input and the output pulse signals recorded by a gated integrator (Boxcar), where each measured point represents the average value over 8 pulses, and the total measured points were ~7500 over an exposure period of ~60 s. The average input pulse energy (or intensity) level was ~4 μJ (or ~500 GW/cm^2). From Figure 33, one can see that, after averaging 8 pulses, the recorded relative fluctuation of the input signals was $\Delta \approx \pm 0.33$, whereas for the output signals the fluctuation was reduced to $\Delta' \approx \pm 0.08$. Thus, this is strong experimental evidence of a drastic improvement of the intensity stability of laser pulses after passing through a 3PA medium.

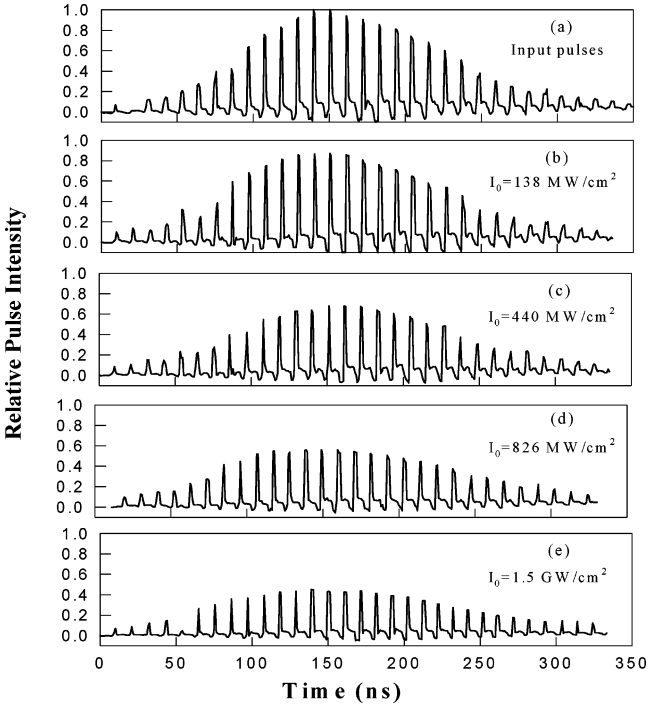

Figure 34. Measured relative pulse intensity distributions for (a) the input pulse train and (b)−(e) the output pulse trains passed through a 20 cm long ASPI/DMSO filled hollow fiber system at various input peak intensity levels. Reprinted with permission from ref 475. Copyright 1997 Optical Society of America.

6.2.4. MPA-Based Optical Reshaping

The same MPA mechanisms can also be utilized for reshaping the temporal and/or spatial profiles of a pulsed laser beam or, in another case, for smoothing a random spatial intensity fluctuation across the beam's diameter. In all these types of applications, the only requirement is to have a high-intensity laser beam to pass through a multiphoton absorbing medium.

In the earliest experiment of showing the 2PA-based optical reshaping effect, the nonlinear absorbing medium was a solution of ASPI dye in dimethyl sulfoxide (DMSO) with a concentration of $d_0 = 0.05$ M, filled into a 20 cm long hollow fiber system to increase the effective interaction length.[475] The input laser beam consisted of a series of 1064 nm pulse trains generated by a *Q*-switched and mode-locked Nd:YAG laser device, operating at a mode-locked frequency of 100 MHz and a Q-switched frequency of 500 Hz; each pulse train contained ∼30 subpulses of ∼130 ps pulse duration. Shown in Figure 34 are the measured profiles for (a) the input pulse train and for (b−e) the output pulse train after passing through the nonlinear absorptive 2PA liquid filled hollow fiber system at different input peak pulse intensity (I_0) levels. One can easily see that when the input peak intensity increased from 138 MW/cm^2 to 1.5 GW/cm^2, the envelope of the transmitted pulse train became flatter and broader in the central region of the train. This is a straightforward demonstration of an optical reshaping effect on the temporal profile of a laser pulse train, based on the 2PA mechanism.

To show how a multiphoton absorbing medium can be employed for reshaping the spatial intensity distribution of an intense laser beam, we shall discuss another experimental example, in which a focused and spatially modulated laser field could be reshaped or smoothed after passing through a nonlinear absorbing medium.[46] The 810 nm, 7 ns laser beam from a pulsed dye laser system was first split into two beams and then refocused with a small crossing angle onto the center of a 1 cm path length liquid cell to produce a transversely modulated intensity distribution. The two-photon absorbing medium used for this experiment was an AF350 dye solution in THF of concentration $d_0 = 0.033$ M. Shown in Figure 35a is the measured transverse intensity distribution of the laser beams at the focal plane position after passing through a 1 cm liquid cell filled with pure THF solvent that had no 2PA at 810 nm radiation, whereas shown in Figure 35b is the measured transverse intensity distribution of the laser beams after passing through the same cell filled with dye solution. Comparing these two spatial profiles, one can see that the modulation depth changed from ∼67% for the former to ∼39% for the latter. Under these conditions, the measured effective 2PA coefficient value for AF350/THF was $\beta = 30$ cm/GW. For comparison, shown in Figure 35c is an assumed initial transverse intensity distribution of a laser field at the focal plane, which is formed by a proper Gaussian function multiplying an interference pattern function with a modulation depth of ∼67%. After passing through a 1 cm two-photon absorbing medium of $\beta = 30$ cm/GW, the predicted intensity distribution of the transmitted laser field is shown in Figure 35d. Comparing Figure 35b and d, one can see that the measured results are in good agreement with the theoretical simulation. The above demonstration implies the feasibility of using a multiphoton absorbing medium to reduce the spatial intensity fluctuation of laser fields.

6.3. MPA-Based Stimulated Scattering

Stimulated scattering of coherent light is one of the major subjects in nonlinear optics and quantum electronics. Although several types (Raman, Brillouin, Rayleigh-wing, and thermal Rayleigh) of stimulated scattering were discovered in the 1960s, stimulated scattering related studies have remained highly active over the past several decades because of fundamental research interests and the potentials of application.[5−7] First, stimulated scattering is one of the most effective physical approaches for generating frequency-shifted coherent light emission. Second, stimulated scattering is one of the most effective approaches for generating optical phase-conjugation waves that possess special properties to overcome the distortion/aberration influences from a gain or propagation medium.[7] In addition, studies of various stimulated scattering effects can provide new knowledge and useful information about the interaction between nonlinear scattering media and intense coherent light fields.

To date, for all known stimulated scattering effects, there is always a frequency shift between the stimulated scattering beam and the pump laser beam. For example, the frequency shift values are large (10^2-10^3 cm^{-1}) for most stimulated Raman scattering processes that generally involve molecular vibrational transitions. For backward stimulated Brillouin scattering in liquid and solid media, these values are quite small ($10^{-1}-1$ cm^{-1}), corresponding to the frequencies of opto-electrostriction-induced hypersonic waves. Here, we introduce a new type of stimulated scattering, the so-called stimulated Rayleigh−Bragg scattering, which is different from all other known stimulated scattering effects in the following two ways: (i) there is no frequency shift between the input pump laser beam and the backward stimulated scattering beam, and (ii) it can only be observed in a multiphoton absorbing medium.[347,348]

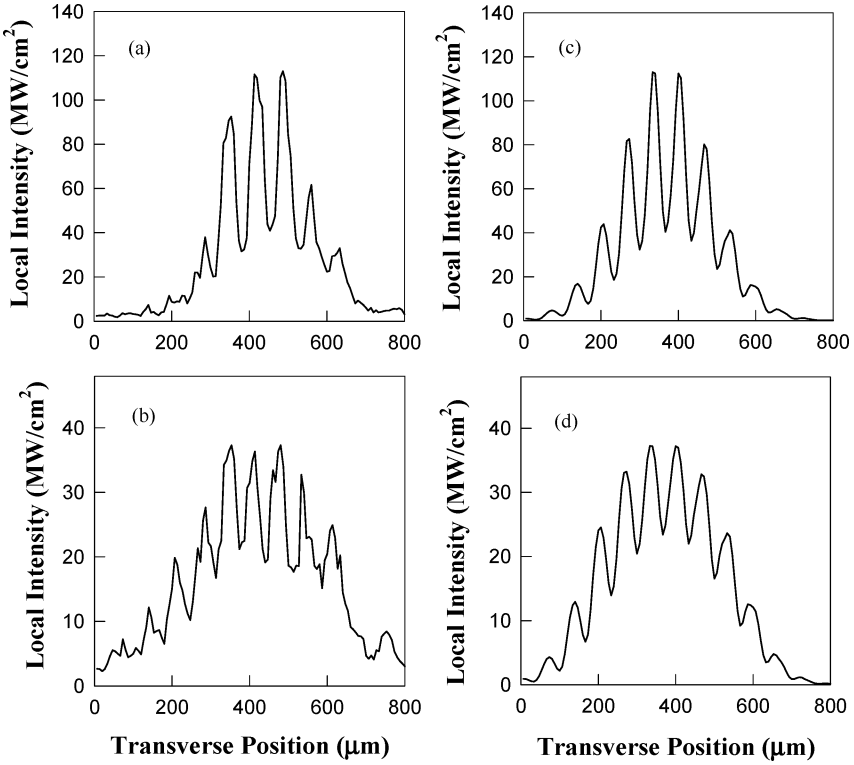

Figure 35. Measured transverse intensity distributions of the 810 nm laser beams passed through (a) a 1 cm pure THF sample and (b) a 1 cm AF350/THF solution sample. Theoretically assumed input transverse intensity distribution (c) and the computer-simulated output intensity distribution of the laser beam passed through a 1 cm two-photon absorbing medium of β=30 cm/GW. Reprinted with permission from ref 46. Copyright 2000 American Chemical Society.

The terminology "stimulated Rayleigh−Bragg scattering" contains two meanings: first, the stimulated scattering originates from the spontaneous Rayleigh scattering; second, a positive feedback for the initial backward Rayleigh scattering signals can be provided by a Bragg grating formed in a multiphoton absorbing medium. Actually, from a historical point of view, the discovery of this new stimulated scattering effect was inherently related to the characterization studies of two-photon active materials. When measuring the effective 2PA coefficient (β) of some two-photon active chromophore solutions by using the nonlinear transmission method in the nanosecond regime, it was found that at a given wavelength, the measured effective β value for a given solution sample was not a constant. Specifically, when the input intensity of nanosecond laser pulses is higher than a certain (threshold) value, the apparent effective β value suddenly becomes higher with a further increase of the input laser intensity. This unexpected increase of the effective 2PA coefficient can be explained, if it is assumed that there are some additional nonlinear processes, which take partial energy from the input laser pulses. One recognized process is 2PA initiated excited-state absorption, as discussed before; the other can be a backward stimulated scattering process enhanced by 2PA. The experimental observation from the backward direction of the input laser beam verified the existence of a highly directional stimulated scattering when the input pump intensity is higher than a certain threshold value.

6.3.1. 2PA-Excited Stimulated Rayleigh–Bragg Scattering (SRBS)

The scattering medium employed for the first experimental demonstration of SRBS is a two-photon absorbing dye solution: PRL802 in THF of spectroscopic grade.[347] This

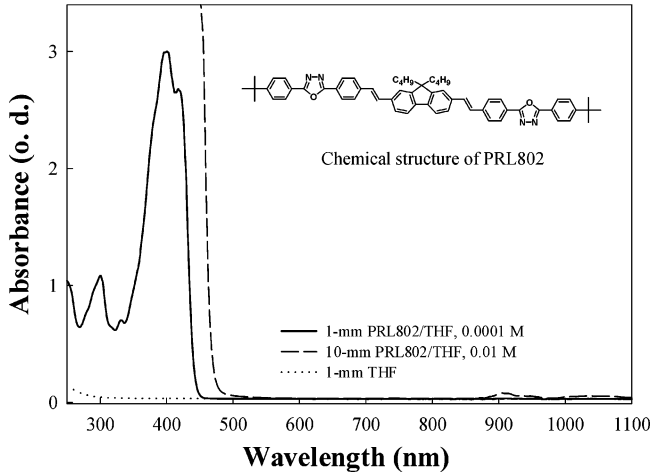

Figure 36. Linear absorption spectral curves for solutions of PRL802 in THF and for the pure solvent THF. The chemical structure of the solute is shown in the inset. Reprinted with permission from ref 347. Copyright 2004 Optical Society of America.

dye is one of a series of novel two-photon absorbing chromophores synthesized for 2PA-based optical limiting and frequency-upconversion lasing purposes. The chemical structure of the dye molecule and the linear absorption spectra for two solutions with different concentrations and pass lengths are shown in Figure 36, from which one can see that there is no linear absorption for PRL 802/THF in the spectral range from 520 to 875 nm.

The pump laser beam of 532 nm was provided by a Q-switched and frequency-doubled Nd:YAG laser system that utilized a saturable BDN dye-doped acetate sheet (from Kodak) as a passive Q-switching element to produce a

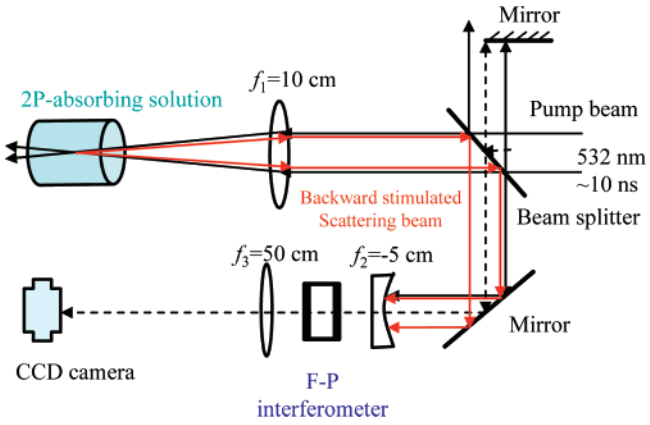

Figure 37. Experimental setup for observation of backward stimulated Rayleigh-Bragg scattering (SRBS) from a two-photon absorbing dye solution. Reprinted with permission from ref 347. Copyright 2004 Optical Society of America.

narrower lasing spectral line width. The measured parameters of the 532 nm pump laser beam were ~0.08 cm^{-1} spectral width, ~10 ns pulse duration, ~3.5 mm beam size, and 5-Hz repetition rate. As shown in Figure 37, the input 532 nm laser beam was focused via an $f = 10$ cm lens onto the center of a 1 cm long glass cell filled with a PRL802/THF solution of 0.01 M concentration. The incident angle of the input pump beam on the liquid cell was around 10−15° to avoid any reflection influence from the two optical windows of this cell. Under these experimental conditions, the 2PA-induced upconversion fluorescence of ~475 nm from the sample solution could be readily seen.

It was found that once the input laser energy (or intensity) exceeded a certain threshold value (~60 μJ or ~40 MW/cm^2), a highly directional and backward stimulated scattering beam could be observed. To identify the spectral property of the observed stimulated scattering, a Fabry−Perot (F−P) interferometer of 1 cm spacing was used in conjunction with an $f = 50$ cm lens and a CCD camera. The F−P measurements showed that there was no frequency shift between the pump beam and the backward stimulated scattering beam within the spectral resolution of the system (0.025 cm^{-1}).

Shown in Figure 38 are the measured backward stimulated scattering pulse energy values as a function of the input pump pulse energy. Under this experimental condition, at a pump level of ~400 μJ, the output backward stimulated scattering energy was ~65 μJ; therefore, the overall output/input energy conversion efficiency was ~16%.

6.3.2. Physical Model of SRBS in a MPA Medium

To explain the generation of the observed frequency unshifted backward stimulated scattering in a two-photon absorbing medium, a Bragg-grating reflection model is proposed.[347,348] It is known that for any type of stimulated scattering the following two basic requirements must be met: (i) there should be an original seed signal, usually from the corresponding spontaneous scattering, and (ii) there should be a gain (positive feedback) mechanism that ensures further amplification of the original seed signals. In the two-photon excitation case, the backward propagating spontaneous Rayleigh scattering can be recognized as original seed signals, which can interfere with the forward propagating pump beam to form a standing wave with a periodic spatial intensity distribution. This intensity modulation may further

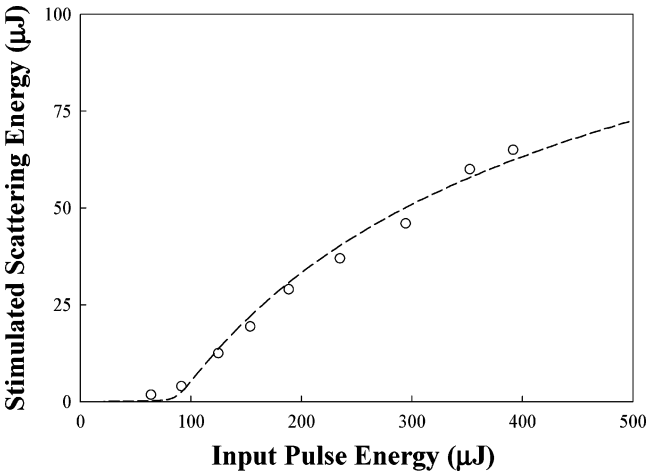

Figure 38. Measured output pulse energy of backward stimulated scattering versus the input pump pulse energy. An F/28 focusing geometry was used. The dashed line is the theoretical fitting curve given by a Bragg grating reflection model. Reprinted with permission from ref 348 (http://link.aps.org/abstract/PRA/v71/p063810). Copyright 2005 by the American Physical Society.

induce an intensity-dependent refractive-index change and create a stationary Bragg grating. Such formed Bragg grating produces a nonzero reflectivity for both the strong forward pump beam and the very weak backward scattering beam. However, the absolute value of the energy reflected from the pump beam to the scattering beam will be much greater than that from the backward scattering beam to the pump beam. The net result is that the initial backward scattering seed signals become stronger along with their backward propagation, as schematically shown in Figure 39.[349]

Moreover, a slightly enhanced backward scattering seed beam will improve the modulation depth of the Bragg grating and consequently increase the reflectivity of this grating, which means more energy will transfer from the pump beam to the backward scattering beam. These processes may finally make the backward scattering signals amplified or stimulated. One can realize that there is a typical positive feedback provided by a stationary Bragg grating formed by two counter-propagating beams. Upon this assumption, 2PA may play a particularly important role in the following two ways. First, accompanying 2PA, there is a resonantly enhanced refractive-index change that is necessary for forming an effective Bragg grating. Second, 2PA leads to certain attenuation only on the strong pump beam, not on the much weaker seed scattering beam, due to the quadratic intensity dependence. In contrast, for a linear absorbing medium, the linear attenuation ratio is the same for both the strong pump beam and the weak scattering beam, which may prohibit the latter to be finally stimulated. That can explain why the effect of stimulated Rayleigh−Bragg scattering is much easier to be observed in a two-photon absorbing medium than in a linear absorbing medium.

A specially designed experiment of a two-counter-propagating-beam formed grating in a two-photon absorbing dye solution has been conducted.[348] The measured dynamic behavior of a Bragg grating and its reflection property are quantitatively consistent with the predictions from the suggested grating reflection model. Based on this model, a quantitative theory was given and could be used for fitting the experimental results shown in Figure 38.

It is obvious that the above-mentioned principle of generating SRBS in a two-photon absorbing medium is also

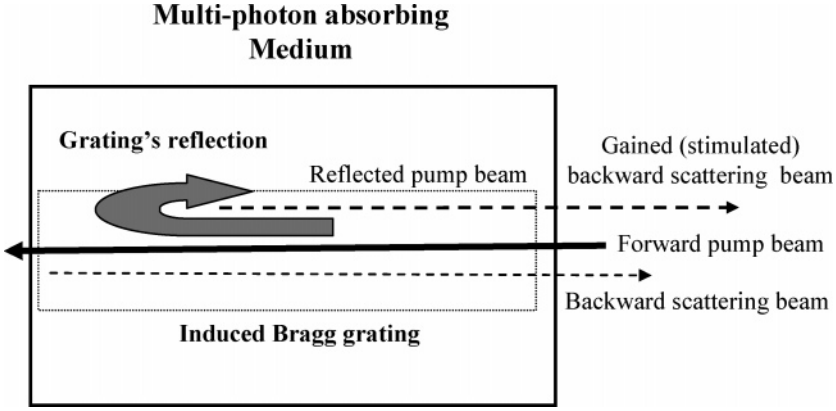

Figure 39. A schematic diagram showing that the 2PA-enhanced Bragg grating provides a positive feedback to the backward Rayleigh scattering. Reprinted with permission from ref 349. Copyright 2007 Optical Society of America.

applicable to generate the same type of stimulated scattering in a three- or four-photon absorbing medium. More recently, a highly efficient SRBS has been generated in a three-photon absorbing chromophore solution (PRL-OT04 in chloroform), pumped by 1064 nm laser pulses of nanosecond duration.[349] The conversion efficiency from the input pump energy to the output backward stimulated scattering energy was $\eta =$ 26%. In addition to that, a superior optical phase-conjugation property of the backward SRBS beam has been experimentally demonstrated by employing two different optical setups. In both cases, a specially introduced aberration influence of 4−5 mrad can be basically removed by the backward SRBS beam that retains a much smaller beam divergence of $\leq$0.4 mrad.

6.3.3. Applications of SRBS in a MPA Medium

Compared to all other known stimulated scattering effects, SRBS possesses the following two unique features. First, it has been experimentally shown that, under the same experimental conditions in the nanosecond regime, the pump threshold value (in pulse energy or intensity) for generating SRBS in a given two- or three-photon absorbing dye solution can be considerably lower than that for generating stimulated Brillouin scattering (SBS) or stimulated Raman scattering in the pure solvent with the same path length. Second, for SRBS there is no frequency shift between the forward pump laser beam and the backward stimulated scattering. Moreover, there are two additional features inherently related to SRBS processes. One is the great variety of MPA materials that can be utilized for SRBS generation; the other is the superior optical phase-conjugation capability of a backward SRBS beam owing to a greater refractive-index change enhanced by MPA processes. All aforementioned features are favorable for application considerations. The following are some possible applications based on the SRBS technique and MPA materials:[476]

(1) *Phase-Conjugate Feedback Element (Reflector) in a Laser Oscillator/Amplifier System*. The SRBS device can be utilized as a phase-conjugate reflector, which is an equivalent cavity mirror capable of generating a backward stimulated scattering beam without frequency-shift, and, therefore, can compensate the distortion or aberration influence from the gain or propagation medium.[349]

(2) *Cooperative Reflector in Conjunction with a Target System for Laser Tracking, Aiming, Autofocusing, and Lidar Operations*. The working principle is basically the same as mentioned above.

(3) *Laser Pulse Compressor System*. Owing to the threshold requirement, the pulse duration of the backward SRBS pulse can be considerably narrower than the input pump laser pulse, so that a compressed narrow laser pulse can be obtained from a laser oscillator and/or amplifier system.

(4) *Laser Power Limiter and Stabilizer Systems*. Since the SRBS is relatively easy to generate in the nanosecond regime, it will cause an additional nonlinear attenuation of the input laser beam and, therefore, can be useful for optical limiting and stabilization applications.

It is noteworthy that currently researchers are pursuing their efforts to realize lasing in ultrashort-wavelength spectral ranges, including the X-ray range. It is known that, in these spectral ranges, a highly reflective mirror or material may not be easy to obtain for the cavity feedback purpose. However, on the other hand, it is also known that the cross section of Rayleigh scattering is proportional to the fourth power of the input light frequency. Therefore, the principle of backward SRBS may be more efficiently applied to future ultrashort-wavelength (including X-ray) laser systems, playing the role of an optical feedback element or an equivalent phase-conjugate cavity mirror.

6.4. Multiphoton Excitation (MPE)-Based Laser Scanning Microscopy

6.4.1. MPE-Based Confocal Microscopy

6.4.1.1. Advantages of Multiphoton Confocal Microscopy. For a conventional one-photon-excitation-based fluorescence microscope, the fluorescence intensity of a sample at a given position is linearly proportional to the local intensity of the excitation light. There are some limitations related to this type of microscopy. First, if both the excitation light and the fluorescence emission signal are in the visible range, the scattering of the former from the sample may generate a strong and undesirable background to the latter. Second, the linear absorption takes place everywhere along the propagation length of the excitation light inside the sample, which may lead to a poor longitudinal (*z*-axis) resolution. In addition, sometimes the visible excitation light cannot penetrate the sample medium due to strong linear absorption in the surface or in a shallow layer of the sample; therefore, the sample's internal structure cannot be explored.

In multiphoton microscopy, a fluorophore (or fluorochrome) is excited by MPA as discussed in previous sections, and the resulting up-conversion fluorescence is used to obtain

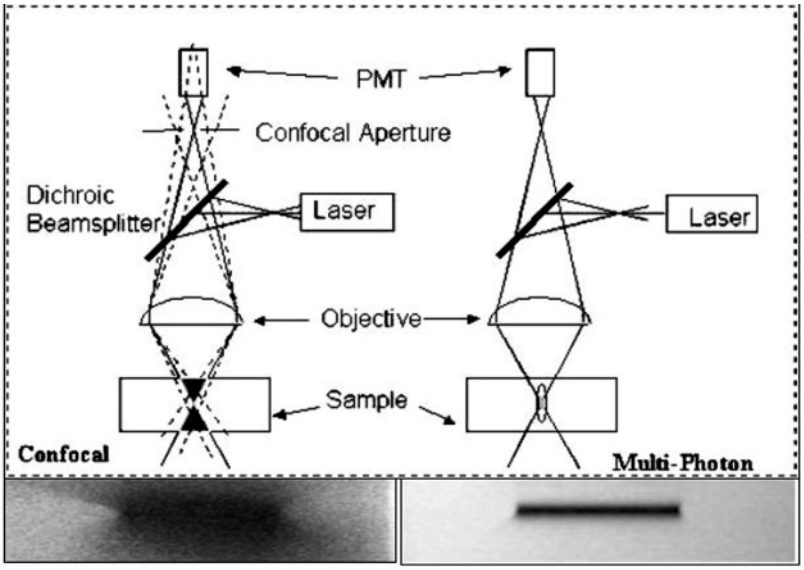

Figure 40. Comparison of ordinary one-photon confocal imaging (left) and two-photon imaging (right) showing the volume difference of excitation and the resultant photobleaching image in a dye doped polymer sample.

an image of the fluorophore doped sample. The first demonstration of two-photon excitation-based frequency-upconversion microscopy was reported by Webb and his co-worker in 1990.[477] Six years later, three-photon excitation-based laser scanning microscopy was also successfully demonstrated by Hell et al. and Webb et al.[478] However, since three-photon excitation requires much higher peak power and focused intensity of the laser beam, only two-photon microscopy has emerged as a more popular and powerful microscopy technique. Two-photon laser scanning microscopy can use a pulsed laser of longer visible or near IR wavelength as an excitation source and can produce frequency-upconverted fluorescence in the visible spectral region. Therefore, two-photon microscopy extends the range of dynamic processes by opening the entire visible spectral region for simultaneous multicolor imaging.[479] It is preferable to use ultrashort laser pulses (i.e., picoseconds or femtoseconds duration from mode-locked lasers), whereby the average power can be kept very low to minimize any thermal damage of the sample. A Ti:sapphire laser which produces very short (100−150 fs) pulses of light around 800 nm (at a repetition rate of ∼80 MHz), with a very large peak power value (∼50 kW), is a popular choice for two-photon microscopy studies.

Although conventional optical microscopy has been a vital tool for the study of biological systems as well as material science, for the last three centuries only with the invention of confocal microscopy in 1957 by Minsky,[480] the capability to obtain a 3D image was achieved. Further, with the development of the modern laser scanning confocal microscope, this technique has found application in all areas of biological as well as materials research. Even though confocal microscopy provides a high-resolution optical sectioning capability, it has some inherent problems.[481,482] Since the confocal aperture reduces the fluorescence signal level, one needs a higher excitation power, which can increase the possibility of photobleaching. Furthermore, in one-photon confocal microscopy, linear excitation is used to obtain fluorescence. In this case, the excitation of fluorescence occurs along the exciting cone of light, thus increasing the chance of photobleaching a large area. Another problem is that most fluorophores used for bioimaging are excited by one-photon absorption in the UV or blue light region. At these wavelengths, light is highly attenuated in a tissue due to strong linear absorption and scattering, limiting the depth access. Furthermore, UV or blue light excitation also gives rise to an undesired autofluorescence background. These problems can be overcome or minimized with the use of two-photon excitation.[483−485]

In two-photon laser scanning microscopy (TPLSM), which uses a tightly focused excitation beam, the region outside the focus has much less risk of being excited. This eliminates the substantial "out-of-focus" fluorescence, often induced by one-photon excitation when used without a confocal aperture. TPLSM thus provides an inherent optical sectioning ability without using any confocal aperture. As shown in Figure 40, two-photon excitation can also greatly reduce the spatial range of photobleaching, as only the region at the focused point can be excited. This feature is derived from the fact that two-photon excitation is quadratically dependent on the intensity and hence highly localized at the focal point at which the intensity is the greatest.

Compared to short wavelength excitation in the UV−visible range, the excitation beam with longer wavelength in the near IR region may have negligible linear absorption and scattering and, therefore, can penetrate much deeper into a tissue sample. The elimination of UV also improves the viability of a cell (or tissue) and permits more scans to obtain a better 3D image. From the instrumentation perspective, the conversion of a conventional scanning laser microscope into a TPLSM is straightforward. One only needs to change a few optical elements. The ordinary dichroic mirror is to be replaced by a mirror to reflect near IR or red excitation wavelengths.

In addition to the sectioning capability, less photodamage, and a deeper penetration, the resolution is another factor that contributes to the potential of TPLSM. According to the Rayleigh criterion for one-photon imaging, the image resolution (minimum spot size) is limited by the diffraction related to an objective lens, i.e.,

$$a_0 = 1.22\lambda/(n \sin \theta_0) = 1.22\lambda/\mathrm{NA} \qquad (40)$$

Here, λ is the illumination wavelength, n is the refractive index in the object space, θ_0 is the acceptance angle of the

lens, and $n \sin \theta_0 = \mathrm{NA}$ is also called the numerical aperture (NA) for the objective. One may reach a larger NA value by using an oil-immersion objective; even so, the available NA is still around the values of 0.8−1.4. For this reason, the resolution of a laser focusing system is limited by the applied wavelength.

When comparing two-photon excitation with one-photon excitation of a given fluorophore-associated sample, two-photon excitation apparently should yield worse resolution because it utilizes a significantly longer wavelength. However, other factors, such as the nonlinear dependence of the fluorescence emission on the local spatial intensity distribution of the two-photon excitation, as well as the out-of-focus fluorescence in one-photon excitation, may affect the achievable resolution. Generally, the strength of TPLSM does not lie in an improvement of resolution but in the other advantages described above.

6.4.1.2. Instrumentation for Two-Photon Confocal Microscopy. Currently, most confocal microscopy manufacturers offer a multiphoton/two-photon option by coupling their imaging system with an ultrashort pulse laser source, such as a Ti:sapphire laser system. Typically, in conventional confocal microscopy, a continuous-wave (CW) laser beam (from an argon or krypton/argon laser source) is coupled to a single mode fiber and delivered into the confocal laser microscope scan-head. The laser power in the range of microwatts is enough to obtain one-photon excited fluorescence in the sample plane for confocal imaging. In multiphoton microscopy, the situation is more complex. One requires a high (kW to MW) beam power from a near-IR pulsed laser to obtain simultaneous absorption of two (or more) photons and to produce significant fluorescence for imaging. If such a high power would be delivered continuously, it would induce thermal destruction of the samples, especially biological samples. This problem can be overcome through the use of ultrashort laser pulses to provide a high-peak power, while keeping a modest average power. Although a shorter pulse width can provide a higher two-photon-induced fluorescence output, there is a practical limitation due to the duration-broadening of ultrashort pulses introduced by the microscope optics. It has been determined that the optimal laser pulse width for two-photon imaging is in the range of 70−200 fs.[486] Typically, high repetition rate lasers (40−100 MHz) are considered to be optimal for two-photon microscopy, as lower repetition rate lasers increase the image acquisition time in a raster scanning imaging system. In some other cases, high repetition rate picosecond lasers[487,488] and continuous wave lasers[489−493] have also been demonstrated to be useful for two-photon microscopy. A typical two-photon confocal microscope works with an ultrashort laser system; the laser beam is coupled into a galvanometer-based scanner device mounted on an upright or inverted optical microscope. Such a laser beam is raster-scanned at the focal plane using galvanometers. In order to obtain a 3D image, the focal plane is changed by translating the sample stage vertically, using a stepper motor or using a piezoelectric stage. The raster-scanned data from each focal plane are obtained and stored in a computer, and can be used to reconstruct the 3D image of the sample.

As an example for typical two-photon imaging, 3D reconstruction of a retinal ganglion cell stained with the water soluble two-photon dye APSS is shown in Figure 41. This image was acquired with a commercial Bio-Rad confocal microscope, adapted for two-photon imaging. An 800 nm laser beam of ∼90 fs pulse duration, 82-MHz repetition rate, and 15-mW average power at the sample plane was used to excite the two-photon fluorescence. The fluorescence signal around 490−550 nm was collected using band-pass filters.

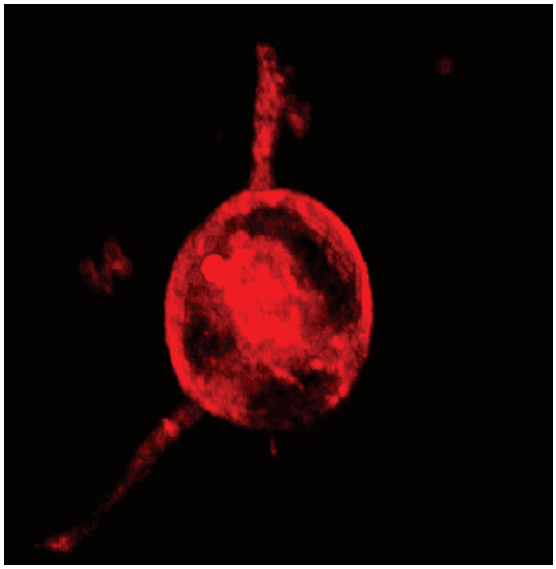

Figure 41. 3D reconstruction of a retinal ganglion cell stained with the water soluble two-photon dye, APSS. This image was acquired with a Bio-Rad confocal microscope (MRC-1024), adapted for two-photon imaging. The fluorescence signal at around 490−550 nm was collected using band-pass filters.

Many of the fluorescent dyes commonly used for imaging, as well as quantum dots and some endogenous biomolecules, have been found to have significant two-photon-induced fluorescence capability[28,43,306,331,494−504] and have been used for successful multiphoton bioimaging.

6.4.1.3. Applications of Two-Photon Confocal Microscopy. Since the first demonstration by Webb's group over a decade ago,[477,505] two-photon microscopy has been applied to a variety of imaging tasks and has now become one of the most important tools in fluorescence microscopy of thick tissue and in live animals. Biologists have used it to measure calcium dynamics deep in brain slices[506−513] and for *in-vivo* imaging.[514−520] Two-photon microscopy has proved invaluable to cancer researchers for *in-vivo* studies of angiogenesis,[521−523] to immunologists for investigating lymphocyte trafficking,[524−526] and for monitoring of embryos.[527,528] There are reports of using this technique for material characterization as well.[479,529,530] Many detailed reviews on two-photon imaging applications can be found elsewhere.[531−536]

Two-photon laser scanning microscopy can readily be used to monitor the cellular entry pattern of a drug, by coupling a two-photon fluorescent probe to the drug. In the studies cited here, researchers used optical tracking of a fluorescently labeled chemotherapeutic agent to monitor its cellular uptake and to understand the mechanism of chemotherapy.[67,537,538] Chemotherapy is commonly used in the treatment of cancers. However, the mechanism of action of many of these agents is not well understood. In this chemotherapeutic approach, pioneered by Schally and co-workers, drug targeting is used based upon the selectivity of luteinizing hormone-releasing hormone analogues for specific binding sites in tumor tissues.[539,540] An example is AN-152, developed in Schally's lab, which consists of an agonistic analogue of luteinizing hormone-releasing hormone, [D-Lys^6] LH-RH, conjugated to a cytotoxic agent, doxorubicin, as shown in Figure 42.[67]

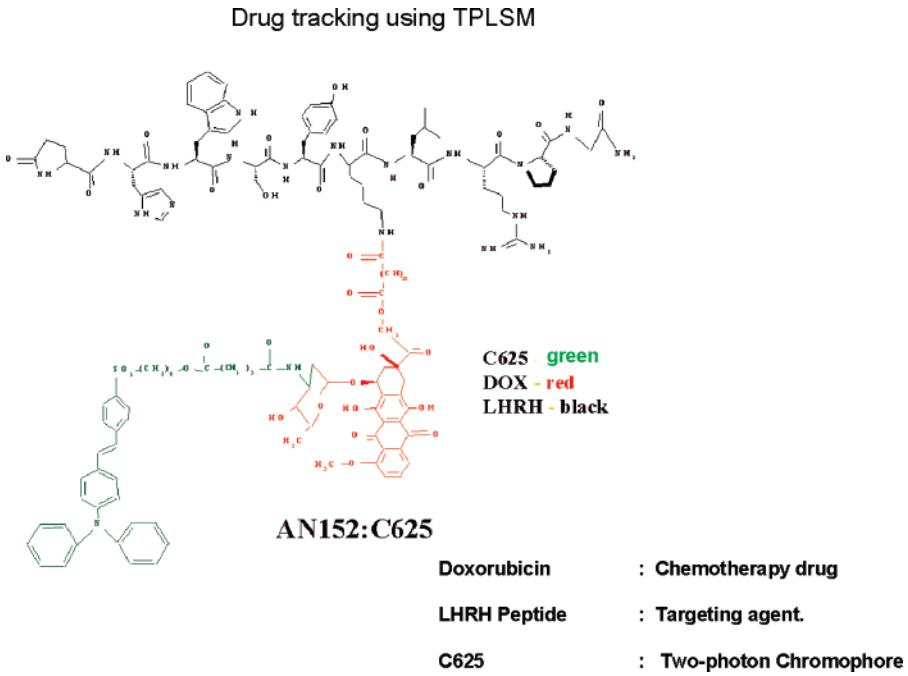

Figure 42. The structure of chemotherapeutic drug-carrier (LH-RH peptide)-dye conjugate. Two-photon images of MCF-7 cells showing the intake of drug into cell over a time period of 50 min. (For details see ref 67).

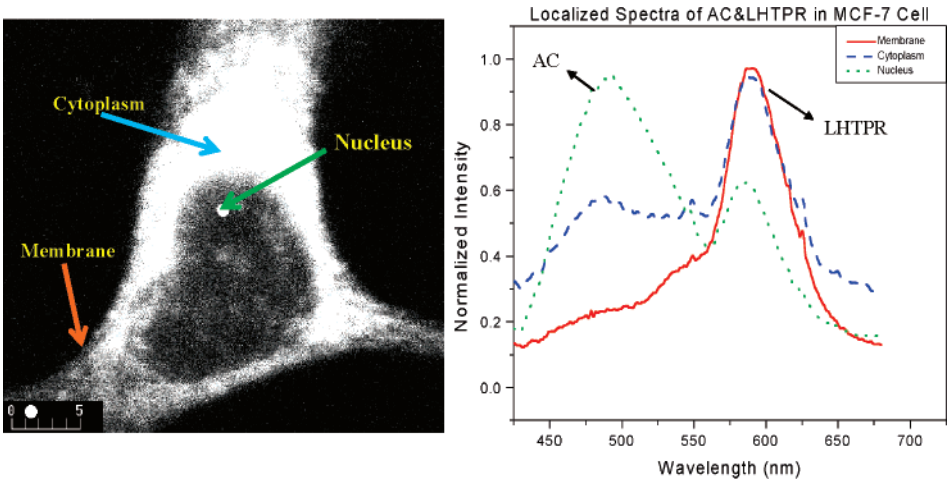

Figure 43. Left panel shows the two-photon fluorescence image of a breast cancer cell treated with AN-152:C625 (drug labeled with the green emitting dye C625) and [D-Lys^6]LH-RH:TPR(the peptide carrier labeled with the red emitting dye TPR). Right panel shows the localized spectra obtained from different parts of the cell indicated by the arrows in the image. (For details see ref 538).

In order to utilize two-photon confocal microscopy to produce a 3D image of the biological cellular process, a two-photon fluorophore (as a marker or tracer) was attached to AN-152, with the help of which internalization of AN-152 was monitored. The results of this investigation visually showed the receptor-mediated entry of AN-152 into the cell cytoplasm and subsequently into the nucleus of a MCF-7 breast cancer cell. It was found that AN-152 entered the cell nucleus, supporting the assumption that the mechanism of the antiproliferative activity of doxorubicin is potentially due to its entry into the nucleus and its action on the Topo-isomerase II−DNA complex.

Localized spectroscopy was also used, in conjunction with imaging, to elucidate the mechanism of this targeting chemotherapeutic agent (AN-152) in living cancer cells.[538] Two different two-photon fluorescent probes, with different fluorescence emission, were coupled to AN-152 and [D-Lys^6]-LH-RH separately. Multicolor fluorescence from the chemotherapeutic agent (AN-152) and the peptide (LH-RH) inside the different parts of the cell (nuclei and cytoplasm) were ratiometrically studied. AN-152 and the LH-RH peptide carrier showed different intracellular spectral profiles. These results are shown in Figure 43. Ratiometric studies showed that AN-152 could enter the nucleus more easily than LH-RH itself. This study confirmed the fact that the LH-RH peptide was helping the drug enter the cell, but the doxorubicin unit was responsible for entry into the nucleus and subsequent cell death. This study illustrates the utility of fluororescently labeled drugs for imaging and probing cellular processes induced by drug interactions.

6.4.2. MPE-Based Near-Field Microscopy

6.4.2.1. Basic Principle of Near-Field Optical Microscopy. According to the Rayleigh criterion, the spatial resolution of a conventional optical microscope is determined by eq 40, which suggests that reducing the excitation wavelength, working in a high-index medium, and increasing the aperture angle can improve the resolution. However, even

in the best case for a conventional optical microscope, it is still not possible to spatially resolve two objects that are separated at a distance significantly smaller than the excitation wavelength. Near-field optical microscopy can overcome this limitation and provide a spatial resolution much shorter than the excitation wavelength.

Consider an object of limited size d, placed in a plane $(x,y,0)$, and with a transfer function $f(x,y,0)$. The spatial frequency spectrum of the object, $F(u,v)$, is a Fourier transform of $f(x,y,0)$ and contains frequencies from zero to infinity due to the limited size of the object. When a plane wave, $E(x,y,0)$, illuminates the object, the emerging spatial wave, $U(u,v)$, is the convolution of the angular spectrum of the incident wave, $E(u,v)$, and that of the object, $F(u,v)$. Since $E(x,y,0)$ is a uniform plane wave, its corresponding Fourier transform $E(u,v)$ is a δ function, and therefore $U(u,v) = F(u,v)$ at the object plane. When the field propagates into a free space, the spatial frequency spectrum at a distance z with respect to the object can be obtained from the Helmholtz equation and is given by

$$F(u,v;z) = F(u,v)\exp\left(i\frac{2\pi}{\lambda}z\sqrt{1-(u\lambda)^2-(v\lambda)^2}\right) \quad (41)$$

Equation 41 indicates that the low spatial frequency components, which are in the frequency domain $(u^2 + v^2) < 1/\lambda^2$, can propagate with a phase delay in a direction normal to the object plane and can be detected by a detector at a distance more than one wavelength from the object. These waves comprise wave vectors with real components in the propagation direction and are called "propagating waves". However, the high spatial frequency components, which are in the frequency domain $(u^2 + v^2) > 1/\lambda^2$, can only propagate along the object surface and decay exponentially in the perpendicular direction. These waves comprise wave vectors with imaginary components in the propagation direction and are called "nonpropagating waves" or "evanescent waves". It is thus clear that an object with a limited size diffracts both propagating and evanescent waves. However, in conventional optical microscopy, only propagating waves that contain spatial frequencies larger than the wavelength λ are detected, but evanescent waves that contain the information about subwavelength details of the object are lost.

Since the confinement of the evanescent field is on the subwavelength scale, the collection of evanescent waves requires the detector to be close to the object, not farther away than a wavelength of the incident light, and this region is referred to as the "near-field zone". The concept of near-field optics was suggested in 1928;[541] however, the technical difficulties could not be overcome at that time. To achieve an optical resolution beyond the diffraction limit, the probe has to be brought within the near-field of the object. With the invention of scanning tunneling microscopy (STM), sample and probe manipulation with sub-nanometer precision are available. The technologies associated with STM can be extended to a host of other probes. This makes it possible to position, control, and raster-scan a probe in the near-field above the sample surface, while forming an optical image point by point. The probe acts as either a light source or a detector, and the spatial resolution is determined by the probe size and the probe−sample distance. Such a technique is referred to as near-field scanning optical microscopy (NSOM).[542−545]

6.4.2.2. Instrumentation of Near-Field Microscopy. Basically, there are two different modes of operation for

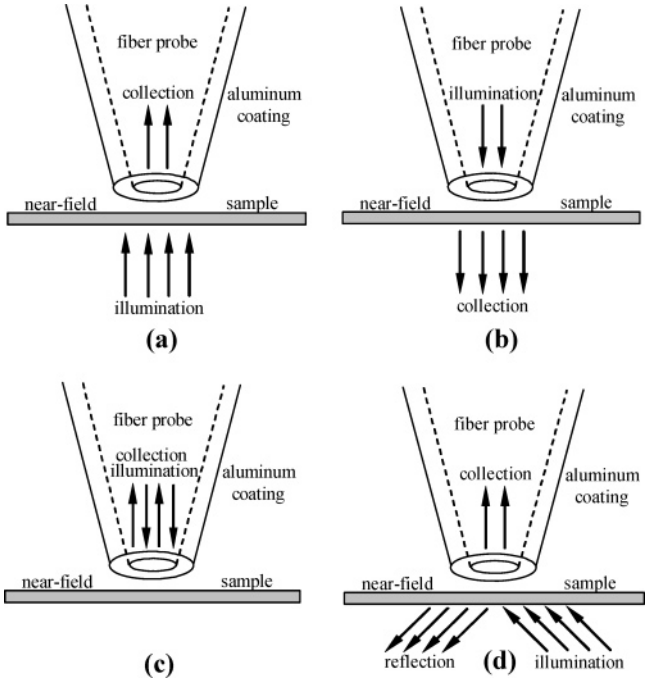

Figure 44. Configurations used in NSOM: (a) collection mode, (b) illunimation mode, (c) collection/illumination mode, and (d) PSTM.

NSOM: collection mode and illumination mode, as shown in parts a and b, respectively, of Figure 44. In the collection mode, the probe collects the light in the near-field of the sample, whereas, in illumination mode, the excitation light is transmitted through the probe and illuminates the sample in the near-field. The combination of collection mode and illumination mode NSOM is shown in Figure 44c, in which both the sample illumination and collection are performed in the near-field of the sample. In addition, there is another collection mode that is based on the near-field detection of evanescent waves above the sample, which is illuminated under total internal reflection. This approach is referred to as photon scanning tunneling microscopy (PSTM),[546,547] as shown in Figure 44d.

The basic setup of NSOM contains a light source, collection optics, and a detector. Thus, to clarify near-field optical imaging, the electromagnetic radiation is first generated by the interactions of the applied excitation field with the object, and then it is transferred through a single-mode fiber probe in collection-mode NSOM or through a high NA microscope objective in illumination-mode NSOM and finally detected with a photosensitive instrument such as a photomultiplier tube (PMT), a charge-coupled device (CCD), or an avalanche photodiode (APD). In the absence of scanning, the probe is held stationary in the near-field with respect to the sample, which is useful for the localized spectroscopic measurements. In a scan, the probe moves relative to the sample. The detected information is measured at each scan point, and an image is obtained with the transference of the local information at each point. The shear-force feedback technique is usually used for distance regulation to keep the optical probe at a constant distance from the sample surface.[548,549]

6.4.2.3. Applications of Multiphoton Near-Field Microscopy. Multiphoton excitation microscopy is a nonlinear optical imaging technique that has the advantages of effective rejection of background, reduced volume of photobleaching, and depth discrimination. These advantages can also benefit

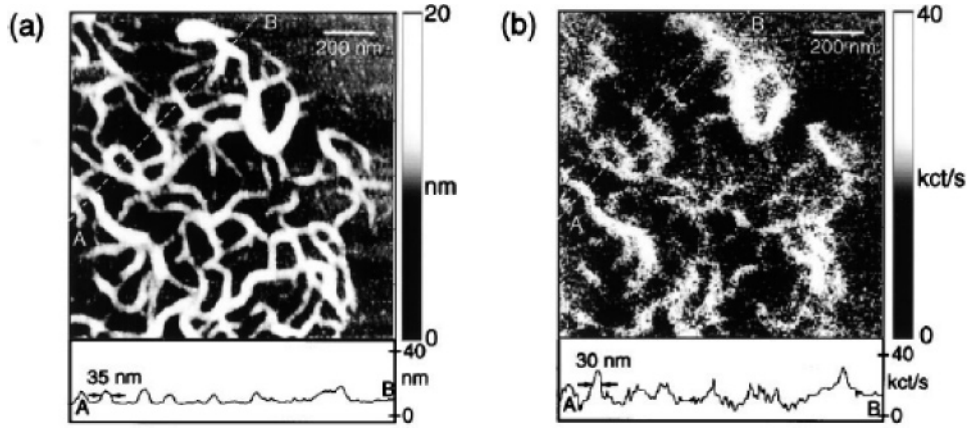

Figure 45. Simultaneous topographic image (a) and two-photon fluorescence image (b) of J-aggregates of PIC dye in a PVC film. The topographic cross section along the dashed line (A-B) has a particular feature of 35 nm fwhm (indicated by arrows) and a corresponding 30 nm fwhm in the emission cross section. Reprinted with permission from ref 559 (http://link.aps.org/abstract/PRL/v82/p4014). Copyright 1999 by the American Physical Society.

near-field optical microscopy. For example, using one-photon excitation to obtain a near-field image of an extended sample is difficult due to the limited depth of excitation field. Multiphoton excitation, however, limits the excitation to a small volume in the vicinity of the probe, thus providing a means to suppress optical excitation of samples far below the molecules of interest. Such feasibility was first demonstrated by near-field two-photon excitation of Rhodamine B molecules with 800 nm, 100 fs laser pulses, using an uncoated, tapered optical fiber as a probe, and the resulting images of two-photon-induced fluorescence showed a resolution of ~175 nm.[550] Shortly after this work, three-photon excitation was extended to near-field optical microscopy to image fluorescence of DNA dyes with sub-wavelength resolution.[551] Since then, multiphoton near-field microscopy has been widely developed and used to study organic, metallic, semiconducting, and biological materials.[491,552−557]

One major issue in multiphoton near-field excitation arises from the limited optical throughput from the near-field probe. This is due to the propagation cutoff of the wave guide mode in fibers with restricted apertures. To overcome these limitations, several approaches have been developed. One approach is to utilize an apertureless near-field probe and illuminate the probe with femtosecond laser pulses. Light polarized along the sharp axis of a metallic tip induces surface plasmons so that a strong enhancement of the electromagnetic field in the local vicinity of the tip is induced.[558,559] By using apertureless near-field optical microscopy, two-photon fluorescence imaging of photosynthetic membranes as well as *J*-aggregates of pseudoisocyanine (PIC) dye was demonstrated with a spatial resolution of ~20 nm.[559] As an example, parts a and b of Figure 45 show the simultaneous images of the topography and the two-photon excited near-field fluorescence for *J*-aggregates of PIC dye molecules in a polyvinyl sulfate (PVS) film. The arrows in the topography cross section indicate a feature with a fwhm of 35 nm, while the corresponding feature in the emission cross section has a fwhm of 30 nm. This latter image demonstrates the superior spatial resolution of the two-photon excitation approach.

Another approach is to utilize collection-mode NSOM[560,561] or PSTM,[562,563] in which the sample is illuminated in the far field and the fluorescence signal is collected in the near field. The capability of delivering high excitation intensities associated with collection-mode near-field optical microscopy

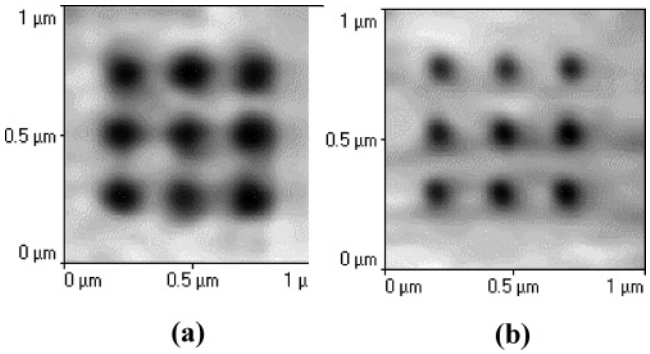

Figure 46. Near-field one-photon (a) and two-photon (b) bleached data bits. Reprinted with permission from ref 565. Copyright 2001 Optical Society of America.

benefits near-field probing of multiphoton excitation and other nonlinear effects, especially for the materials that have high damage thresholds. This approach was demonstrated for two-photon fluorescence imaging of nonlinear organic and inorganic nanomaterials with subdiffraction limited resolution.

Multiphoton near-field optical microscopy not only is a powerful tool for nanomaterial characterization but also has potential applications in nano-photolithography and high-density optical data storage. One of the principles of two-photon optical storage or photolithography is that a recording medium exhibits photobleaching after two-photon excitation. Compared with near-field one-photon recording, in which photobleaching is a linear process and occurs in the entire zone of illumination, the quadratic dependence on the excitation intensity of two-photon excitation limits the effective excitation to a smaller volume and enables light confinement in the near-field of the probe. Therefore, a much higher storage density can be achieved with near-field two-photon excitation. In a series of experiments, recorded domains down to ~70 nm have been obtained with two-photon excitation.[564−566]

Figure 46 shows an example of photobleaching of an organic dye in a plastic medium.[565] By using a metal-coated fiber probe, photobleaching was accomplished with near-field one-photon excitation at 400 nm and two-photon excitation at 800 nm, respectively. With one-photon excitation, the photobleached spot size is ~140 nm. However, smaller spot sizes of 70 nm could be produced with two-photon excitation. Considering an adjacent spacing of 290

nm between two neighboring spots, this corresponds to a storage density of 1.5 Gbit/cm^2.[564] The same technique was also used to write gratings with a line density as high as 62 500 line/cm.

In a different demonstration, when apertureless near-field optical microscopy was used, the local field enhancement at the extremity of a metallic tip could lead to two-photon excited polymerization in a commercial photoresist, SU-8. Photolithographic features down to ~70 nm were thus obtained.[566]

In conclusion, near-field multiphoton optical microscopy offers exciting opportunities for both fundamental research and practical applications. The studies presented in this subsection focus on near-field two-photon and three-photon imaging as well as their application for ultrahigh density optical storage. These studies demonstrated the advantages of high-contrast, high-resolution, and site specific imaging and spectroscopy.

6.5. MPE-Based Data Storage and Microfabrication

6.5.1. Common Features of MPE for Data Storage and Microfabrication

In the past several decades, a focused laser beam has been utilized for data recording and reading as well as for material processing and fabrication. In most of these applications, the basic mechanism concerning the interaction between the laser radiation and the materials is one-photon absorption or other linear optical processes. In all cases, the available data storage density or the precision of optical machining is essentially limited by the resolution of a laser focusing system. It is known that the resolution of a focusing system is determined by the minimum size of the focal spot the system can provide, which is simply the product of the beam divergence angle and the focal length. In an ideal situation, if the beam divergence angle reaches its diffraction limit, the available minimum focal spot size is determined by eq 40, i.e., limited in a wavelength range of the used laser beam.

It is easy to make materials that are highly one-photon absorbing; hence, a low-intensity laser beam is enough for optical data recording or storage. In this case, the intensity attenuation of the laser beam along the propagation direction inside a recording medium follows the exponential law. According to this law, if the recording medium is highly one-photon absorptive, the incident focused laser beam can only penetrate into a shallow layer near the material surface, in which 2D information can be recorded. Owing to the nature of one-photon interaction, the material response to the incident local laser intensity manifests a linear relationship, and therefore, the lateral reactive range of the material is basically determined by the spot size of the focused laser beam. Based on this fact, the maximum 2D data-storage density in a linear absorbing medium surface is limited to ~10^8 bits/cm^2 for laser wavelengths in the visible or near-IR range. Furthermore, if the recording medium is a slightly one-photon absorbing thick film or plate, a focused laser beam will easily penetrate the whole thickness of the medium, which means that a multilayer recording along the beam's propagation direction inside the medium is not available. For the same reason, a focused laser beam can only be employed to fabricate a 2D structure but not a 3D structure.

The physical picture of MPA-based optical data storage and fabrication is remarkably different from that mentioned above for one-photon interaction. In this new case, much higher focused laser intensity is needed while the materials for recording or fabrication should be highly multiphoton active. The material response is proportional to the square of local light intensity for a 2PA mechanism or to the cubic of local intensity for a 3PA mechanism. These nonlinear relationships imply a very unique feature of the interaction between a tightly focused laser beam and a multiphoton absorbing medium: that is the highly localized reactive range of the nonlinear medium in respect to the focal laser intensity distribution profile. To illustrate this special feature, intrinsically related to multiphoton interaction, the normalized lateral intensity profile in the focal plane is expressed in Figure 47 by a Gaussian function $I(r)$ (solid-line curve) with an assumed characteristic spot radius of $r_0 = 0.5$ μm, while the profiles of the square and cubic of this function are expressed by a dashed-line curve and a dot-dashed-line curve, respectively. As outlined above, the material response will be determined by the curve of $I^2(r)$ for a 2PA process or by the curve of $I^3(r)$ for a 3PA process. It is obvious from Figure 47 that the full-width of the solid-line curve determined at $1/e$ points is $2r_0 = 1$ μm, whereas the full-width in the same definition is ~0.7 μm for the dashed-line curve and ~0.6 μm for the dot-dashed line curve, respectively. Based on this picture, one can realize that in a multiphoton active medium the reactive range can be smaller than the incident laser focal spot size in the recoding ($x-y$) plane.

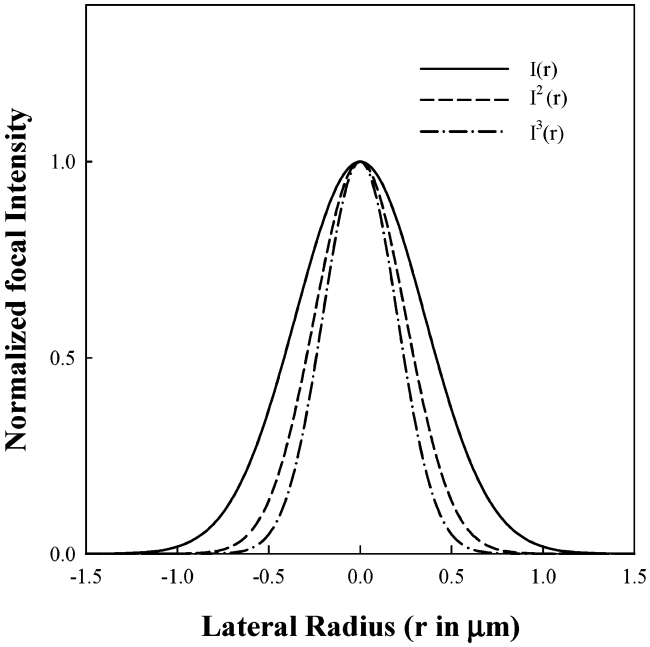

Figure 47. Profiles of the normalized focal intensity distribution function $I(r)$ (solid line), the function $I^2(r)$ (dashed line), and the function $I^3(r)$ (dot-dashed line). The solid-line curve represents a Gaussian lateral intensity distribution at the focal plane with a characteristic focal spot size of 1 μm.

Furthermore, the same conclusion is also applicable to the material response along the z-axial direction. It is commonly known that, for the focusing optical system, a shorter focal length can provide a shorter focal depth of the beam. In the common cases of optical data storage and microfabrication, a microscope objective with very short focal length is utilized and, therefore, a much shorter focal depth of the tightly focused laser beam can be expected along the z-direction. Just for illustration purposes, we show in Figure 48 the spatial profiles of two focused beams as a function of the z-distance

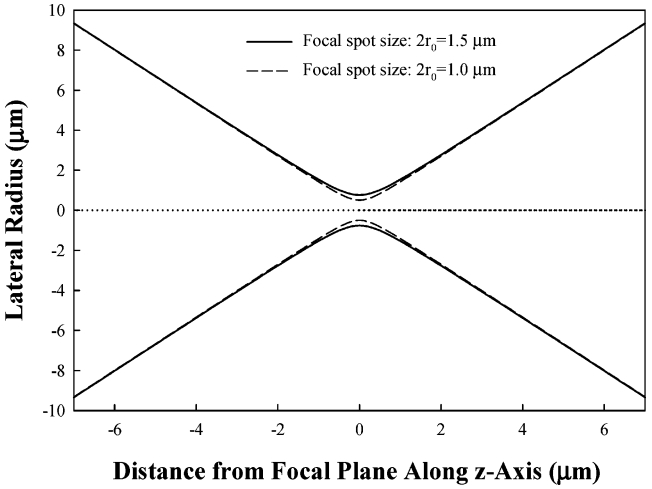

Figure 48. Variation of the beam size along the propagation direction for two beams with different focal spot sizes.

from the focal plane, where the thick (black) solid-line curves show a focal spot size of 1.5 μm while the thin (red) solid-line curves show a focal spot size of 1.0 μm. In obtaining these curves, the NA = 0.8 value of a focusing objective is adopted and a hyperbolic shape of the beam configuration near the focal region is assumed.[336]

From Figure 48 one can see that the beam with the smaller focal spot size possesses a shorter focal depth or a faster beam size change before or after reaching the focal point. More specifically speaking, if we define the focal depth as the distance between two positions along the *z*-axis at which the transverse beam size is two times larger than the focal spot size, the focal depth value will be estimated as $\Delta z_f \approx 2.0$ μm from the beam having a focal spot size of $2r_0 = 1.5$ μm, and $\Delta z_f \approx 1.4$ μm for the beam having a focal spot size of $2r_0 = 1.0$ μm, respectively. These estimations mean that under an optimum focusing condition, the focal depth can be controlled at a value slightly larger than the focal spot size. Moreover, in the case of multiphoton interaction, the effective reactive range in 3D ($x-y-z$) space can be further confined due to the nonlinear dependence of the material response on the local light intensity.

Finally, another important feature of using multiphoton techniques to record optical data is that the incident laser beam can be focused on any designed depth of the recording medium, This advantage is ensured by two facts: (i) there is no linear absorption of the medium for the laser wavelength chosen for multiphoton interaction, and (ii) only the local intensity near the focal point region will be high enough to cause nonlinear absorption or other nonlinear responses inside the medium. Based on this feature, multilayer optical data recording or 3D microfabrication can be easily achieved in a thick film or a bulk made of multiphoton absorbing materials. If we assume the bit spacing in a single recorded layer is $\sim$1 μm and the distance between two neighboring layers is $\sim$1.5 μm, then one may reach a volume density of $\sim 6.7 \times 10^{11}$ bits/cm^3 for 3D data storage that is not possible from the one-photon technique.

6.5.2. Three-Dimensional Data Storage in Two-Photon Active Materials

It is a significant progress to realize 3D data storage in a two-photon active medium, which has mainly been achieved over the past 10 years.[567,568] However, the earliest experimental demonstration of 3D data storage was presented by

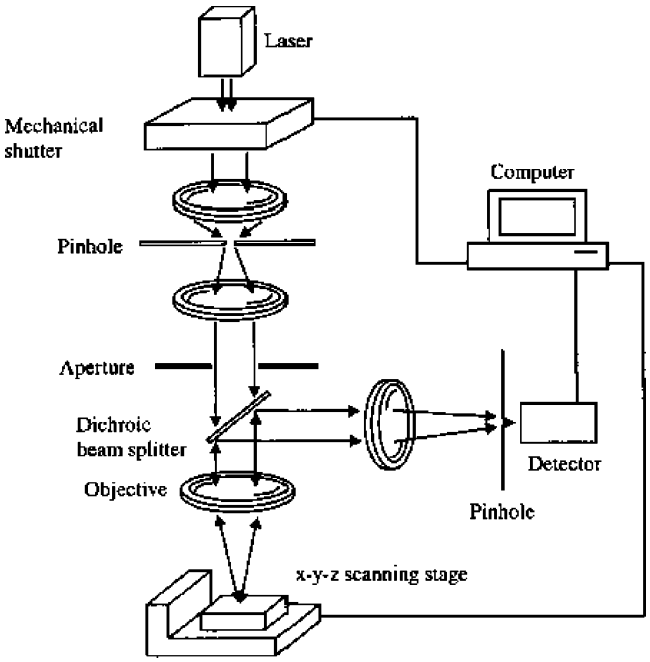

Figure 49. Schematic diagram of the two-photon confocal microscope used to record and read 3D data bits in a photobleaching polymer. Reprinted with permission from ref 576. Copyright 1999 Optical Society of America.

Parthenopoulos and Rentzepis in 1989.[569,570] In this pioneering work, a photochromic organic molecule-doped polymer bulk was used as the recording medium, and two perpendicularly crossed laser beams (532 nm + 532 nm, or 532 nm + 1064 nm, 25 ps pulse duration) were used as writing beams to create a two-photon-induced chemical change of the organic molecules at the destined location within the polymer sample. After two-photon excitation in the recording spot, the chromatic molecules changed their energy structure and absorption−emission property; by using other two crossed laser beams with longer wavelength (1064 nm + 1064 nm) as reading beams, the recorded spot could be read out by detecting the two-reading-beams-induced fluorescence emission. Shortly after this work, in 1991, Strickler and Webb reported another technical approach in which a single tightly focused laser beam ($\sim$620 nm wavelength and $\sim$100 fs pulse duration) was used to enhance the polymerization process via a 2PA mechanism inside a UV-preirradiated 100 mm thick photopolymer film.[571] In the focal position (recorded bit location), the density and refractive index were different from the unradiated area. This writing-beam-induced refractive-index change could be read out by using another reading beam (488 nm with low intensity) through the so-called differential interference contrast microscopy technique. The significance of this work was to provide an example for realizing volume (25 layers) data storage by using only one intense laser beam. Since the mid 1990s, the advancement in the research area of 3D data storage has been driven by Kawata's group,[567,572−575] Gu's group,[576−580] Prasad's group,[581−583] Rentzepis' group,[584,585] Belfield's group,[568,586] as well as some other groups.[587−594]

Usually, a complete 3D data storage system consists of the following: (i) a multiphoton active recording medium, (ii) a data-writing laser beam and focusing optics, (iii) $x-y-z$ scanning mechanisms, and (iv) a data-reading laser beam and related optics. The recording medium can be a thick film or a thin slab made of a solid matrix (polymer, sol−gel glass, or crystal) containing multiphoton active centers (dye

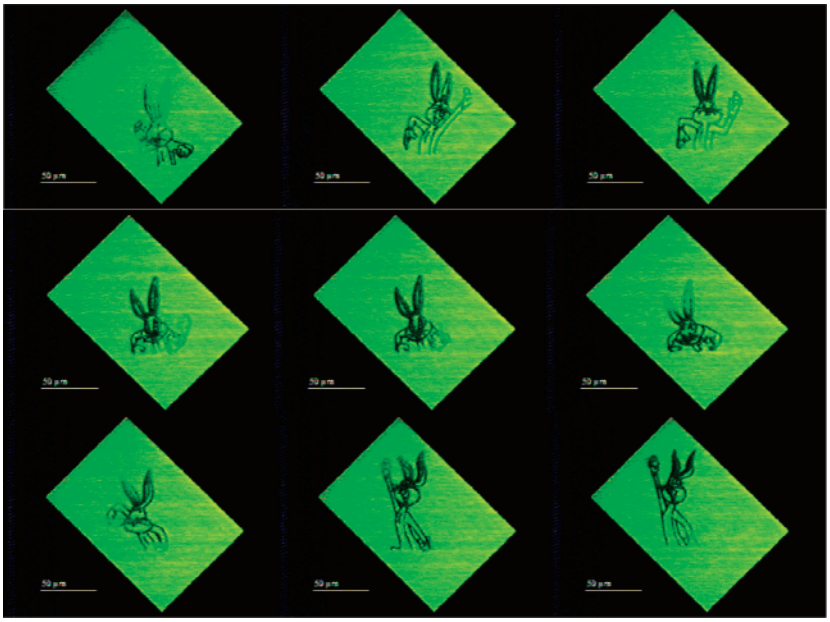

Figure 50. Nine frames of an animated movie stored at different depths in a two-photon dye doped polymer block. The spacing between adjacent layers is 5 μm, and the transverse scale bar is 50 μm. Reprinted with permission from ref 582. Copyright 1996 American Chemical Society.

molecules, impurities, or nanoparticles). The writing beam is usually a pulsed laser beam of ~800 nm wavelength and 100−150 fs duration from a mode-locked Ti:sapphire laser system for two-photon excitation. The focusing optics is a microscopic objective with a larger NA value (0.8−1.4). The 3D recording is ensured by a computer controlled scanning system to change the focal position of the writing beam inside the recording medium; in a simple case, the latter can be mounted upon an $x-y-z$ translation piezostage. The choices of reading-beam wavelength, power level, and the reading manner depend on the specific mechanism of the writing-beam-induced physical/chemical changes of the medium in the recorded bits positions. As an example, Figure 49 shows a typical experimental setup for a 2PA-based 3D data writing and reading system.

In most cases to date, the recording media have been various two-photon active organic chromophore-doped polymers, in which the intense writing laser beam could produce some types of property changes of the material in the focal spot region through different mechanisms. The following are the major mechanisms used for 2PA-based 3D data storage: (a) photochromic reaction that may lead to the induced changes of absorption, fluorescence, and/or refractive index;[573,578,588,594] (b) photobleaching reaction that may lead to a change of absorption or fluorescence;[576,581,587,592] (c) photorefractive reaction in a photorefractive polymer or crystal;[572,574,577] (d) photopolymerization reaction[571,589] and some other photochemical reactions leading to optical property changes.[583,584,586] In some cases, researchers may also utilize the anisotropy of certain optical properties induced by two-photon excitation to record and read out optical data.[579−592] More recently, some novel materials have been reported for 2PA-based data storage, such as densely packed semiconductor nanocrystal solid films and Au-nanoparticle doped sol−gel glass films.[575,580]

Shown in Figure 50 is an early experimental achievement of multilayer 3D data storage in a two-photon active dye-doped polymer block, working in a photobleaching mechanism by Prasad's group. The two-photon absorbing dye was APSS, which was doped into a transparent polymer [poly-

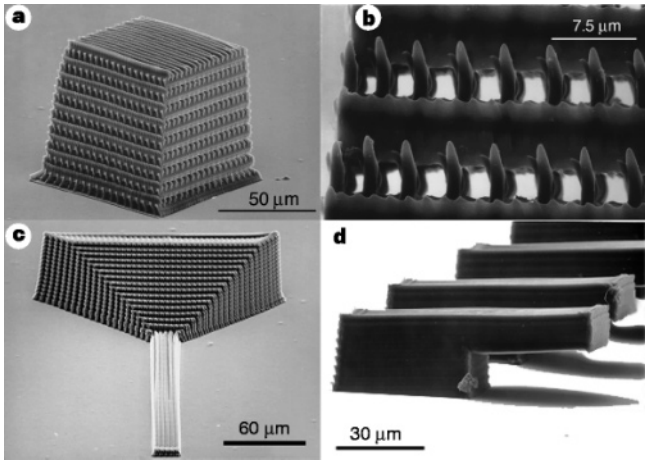

Figure 51. 3D microstructures produced by two-photon-initiated polymerization. **a**, Photonic band gap structure. **b**, Magnified top-view of structure in **a**. **c**, Tapered waveguide structure. **d**, Array of cantilevers. Reprinted by permission from Macmillan Publishers Ltd: *Nature* (ref 600, http://www.nature.com), copyright 1999.

(hydroxyethyl methacrylate)] block of 3 × 3 × 3 mm size. The writing laser beam of ~800 nm wavelength was from a Ti:sapphire laser working with a confocal laser scanning microscope. In the writing beam focused bit position, 2PA processes could bleach the fluorescence capability of the dye molecules and then produced a "dark" spot compared to unirradiated areas when scanned by a reading beam of the same wavelength.

The key issue to increase the 3D data storage density is to reduce both the lateral bit spacing and the axial layer spacing in a given recording medium. In ref 572 the reported density value was 33 Gbits/cm^3 in a photorefractive crystal medium, 205 Gbits/cm^3 in a polymer dispersed liquid crystals medium,[579] and ~300 Gbits/cm^3 in a photopolymerization medium.[571] Moreover, based on the lateral and axial sizes of the recorded bits, the authors of refs 581 and 583 estimated that a 10^{12} bits/cm^3 or 1000 Gbits/cm^3 density value could be achieved in their systems.

Figure 52. Micro gear-wheel affixed to a shaft. The gear wheel is freely movable. Reprinted with permission from ref 605. Copyright 2000 Optical Society of America.

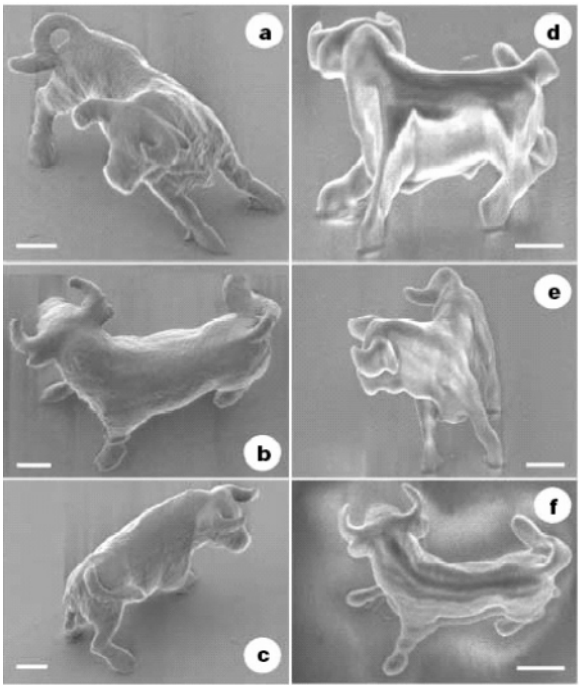

Figure 53. a−c, Bull sculpture produced by raster scanning; the process took 180 min **d−f,** The surface of the bull was defined by 2PA (that is, surface-profile scanning) and was then solidified internally by illumination under a mercury lamp, reducing the 2PA-scanning time to 13 min. Reprinted by permission from Macmillan Publishers Ltd: *Nature* (ref 597, http://www.nature.com), copyright 2001.

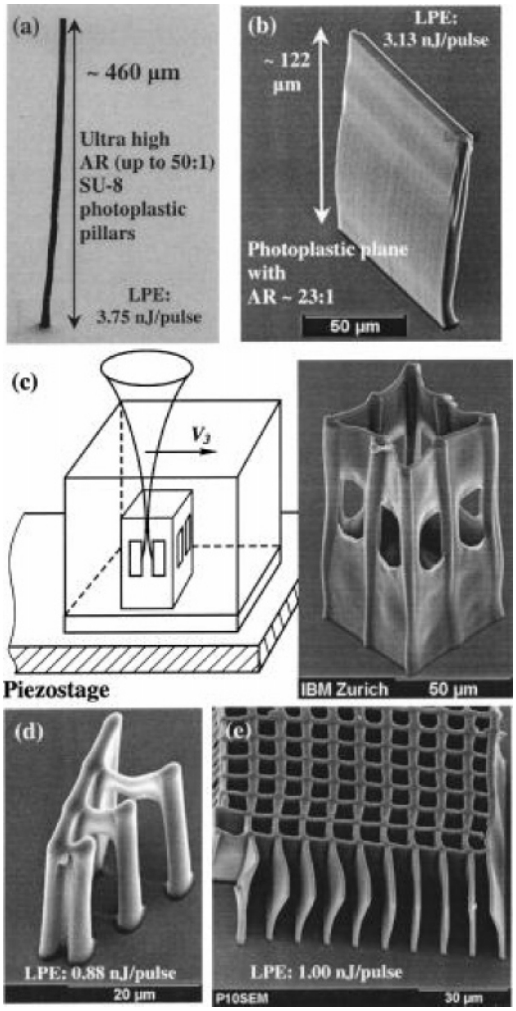

Figure 54. Examples of real 3D microfabrication using the 2PA technique with a low numerical aperture objective. SEM micrographs showing (a) a mechanically rigid, ultrahigh-AR (up to 50:1) photoplastic pillar measuring ~460 μm high, (b) a vertical photoplastic plane measuring ~122 μm high with an aspect ratio of up to 23:1, (c) a 132 × 50 × 50 μm^3 cage structure made from high-AR pillars and planes, (d) suspended photoplastic bridges of various lengths from 5 μm to 15 μm long, and (e) attempts in realizing an photonic crystal structure with a periodicity of ~10 μm. The diagram on the left-hand side of (c) shows the general schematic of exploiting different scanning speeds for the shutter mechanism. Reprinted with permission from ref 615. Copyright 2004, American Institute of Physics.

6.5.3. Two-Photon Polymerization-Based Three-Dimensional Microfabrication

The features of high spatial confinement of multiphoton interactions and the penetrating capability of a focused laser beam can be used to create 3D microstructures or to fabricate micromachines with a subdiffraction-limit spatial resolution. The emergence of this so-called 3D microfabrication is one of the latest achievements of multiphoton-based application techniques.[595,568] This new technique is essentially a multiphoton-interaction-based 3D photolithography. In the past 10 years, numerous excellent studies in this research area have been done by the following research groups, including Kawata's group,[595−599] Marder and Perry's group,[600−603] Sun's group,[604,605] Belfield and Van Stryland's group,[568,606] Baldeck's group,[607,608] Lee's group,[609,610] and many others.[611−620]

The first experimental demonstration of a two-photon-induced polymerization process to produce a 3D polymer part with microstructure was reported by Kawata et al. in 1997.[596] In this work, the sample medium was a commercial resin (SCR-500) containing a UV-sensitive photoinitiator, urethane acrylate monomer, and urethane acrylate oligomers; the incident was a 790 nm, 200 fs pulsed laser beam focused by a 0.85-NA objective. After laser exposure and 2PA-induced polymerization, the resultant solidified polymer structures were extracted by removing the unsolidified resin with ethanol. Another important year for two-photon microfabrication development was 1999, in which several groups published their research works with different features. Among them, Cumpston et al. presented their high-quality 3D microstructure from two-photon polymer resins films; the photos of their products are shown in Figure 51;[600] Sun et al. reported their 3D photonic crystal structures through two-photon-induced polymerization in a resin medium. The microstructures consisted of 20 layers of solidified microrods with 0.6−2.0 μm diameter and 1.2−1.4 μm spacing;[604] Joshi

et al. reported fabrication of 3D optical wave guide circuitry in a two-photon polymerizable optical resin.[611]

To avoid the drift and distortion of components in microfabrication processes, it was proposed to utilize a pre-exposure technique (with a xenon lamp) to increase the viscosity of resins and let the solidified elements be tightly confined at the laser exposed sites; Figure 52 shows a movable microgear-wheel fabricated using this technique with a spatial resolution of ~0.5 μm.[605]

In 2001, Kawata et al. reported their 3D fabrication of several microstructures with a much higher spatial resolution (~0.12 μm) in a commercially available resin, consisting of urethane acrylate monomers and oligomers as well as 2PA-active photoinitiators.[597] By pinpoint scanning the laser focus according to preprogrammed patterns, designs can be faithfully replicated to form real structures. One of the microstructures they made was a computer designed 10 μm long and 7 μm high microbull. Figure 53 shows scanning electron micrographs of "microbull" sculptures through 2PA-induced photopolymerization processes.

From a chemist's point of view, one of the key issues for 3D microfabrication is the design and synthesis of highly 2PA-active photoinitiators in appropriate photopolymerizable systems, which may lead to higher polymerization efficiency while requiring a lower laser beam intensity or power level.[598,601−603,606,608,612,616,620−623]

Finally, as one more example of a recent study on 2PA-based 3D fabrication, Teh et al. demonstrated that, even by using a low numerical aperture optics (10×, 0.3 NA objective), the rapid microfabrication of photoplastic pillars, planes, and cage structures with an ultrahigh aspect ratio (AR) could be achieved, based on SU-8 resin/resist films of thickness from 500 to 975 μm.[615] Shown in Figure 54 are the scanning electronic microscope (SEM) micrographs of these microstructures.

7. Concluding Remarks

The early studies of multiphoton processes and multiphoton active materials started at the beginning of the 1960s, immediately after the invention of lasers. Up to the end of the 1980s, most studies in this area were focused on two-photon spectroscopy of simple atomic and molecular gaseous systems, organic solvents and compounds, as well as inorganic crystals and semiconductors. All these studies have brought a great deal of new information and knowledge on the electronic, vibrational, and even rotational states of the investigated atomic and molecular systems. Since the 1990s, researchers' efforts have turned to developing various highly efficient two-photon active materials and to seeking for their applications. It seems that 1995−2006 was a boom decade for multiphoton related research, and more than 3000 papers in this area were published within this period.

For the characterization of a given multiphoton absorbing material, the most essential task is to measure the multiphoton absorption (MPA) coefficient, which is a concentration dependent parameter, and to determine the MPA cross section value, which does not depend on the concentration of the nonlinear absorbing material. Since MPA generally requires high or very high local intensity of the input laser beam, many different physical processes (such as excited-state absorption, a saturation effect, stimulated backscattering, self-focusing or self-defocusing, a thermal lensing effect, etc.) may also occur together with a pure MPA process. Under these circumstances, the measured results may strongly depend on the method used, the laser pulse duration and intensity levels, optical setup designs, and other experimental conditions. Because of these reasons, sometimes the finally reported values of cross section measurements may be greatly overestimated. This situation makes it difficult to compare cross section values reported by different research groups under different conditions. To improve this situation and to obtain more reliable results in future MPA cross section measurements, researchers should have a reasonable design of optical setup and appropriate control of experimental conditions to avoid self-focusing or defocusing and thermal-lensing effects. One also should try to eliminate contributions from other nonlinear attenuation effects, including (but not limited to) excited-state absorption and stimulated backscattering.

In the past decade, significant progresses have been made in the design and synthesis of two-photon absorbing materials with a very large cross section. Although it is still possible to further enhance the molecular 2PA cross section value by using an optimized molecular design strategy, for certain applications the two-photon-property requirement has basically been met with the new available materials. Recently, it has become clear that, for the two-photon technology to realize its full potential, the development of more two-photon-active chromophores, together with the no-less-important secondary properties such as processability, biocompatibility, photostability, and durability that depend on specific applications, will play a vital role. For example, for lasing and optical limiting applications, the photostability becomes a very important requirement besides the large 2PA capability. And for two-photon biological imaging applications, a chromophore with a large 2PA cross section value and a high fluorescence quantum yield is necessary in order to achieve a better signal-to-noise ratio. At the same time, this chromophore should also have other secondary properties such as biocompatibility and cellular selectivity. Moreover, in two-photon photodynamic-therapy applications, the two-photon materials should have a high quantum yield for two-photon-induced singlet oxygen (^{1}O) generation, low dark cytotoxicity, as well as cancer cells selectivity. Therefore, when designing the next generation of two-photon (or multiphoton) materials, one should not only consider their two-photon absorptivity but also tailor their secondary properties to meet their specific applications.

In this review, several major applications of multiphoton excitation (MPE) and multiphoton active materials were briefly described. Among them, multiphoton pumped lasing has provided an effective approach to achieve tunable frequency up-conversion of coherent light without the phase-matching requirement. MPA-based optical limiting exhibits the advantages of negligible initial attenuation for a weak signal and high dynamic attenuation for a strong signal; therefore, it can be used for protection of optical sensors or human eyes from laser radiation-induced damage. MPA-based optical stabilization and reshaping can find their special applications in optical telecommunications and optical data processing. MPE-based laser scanning microscopes have manifested the 3D imaging capability with a superior spatial resolution. The same MPE principles can be also utilized for optical data storage and microfabrication. For data storage, the data density stored in a bulk medium or a thick film can be significantly increased; for microfabrication, a 3D micropart or microdevice can be fabricated in a mul-

tiphoton active material by using a scanning and focused laser beam.

Finally, it should be pointed out that it is impossible to mention here all multiphoton related applications because of the limitations of scope and length of this review. For example, the principles and techniques of MPE have provided many special approaches for fundamental research and practical applications in biology and medicine. It is expected that the multiphoton technology will have very bright prospects through the further efforts of researchers.

8. Acknowledgments

The authors wish to acknowledge those colleagues who have written part of this review article: Dr. Haridas E. Pudavar (multiphoton excited confocal microscopy), Dr. Yuzhen Shen (multiphoton excited near-field microscopy), and Dr. Alexander Baev (quantum chemical modeling of multiphoton absorption). The critical reading of our manuscript by Patrick Schneider, Rune Mosbacher, and Haiyan Qin is highly appreciated. We are indebted to those authors whose works have been quoted in this review. We are also grateful to many authors and publishers for the permission to reproduce their figures in this review. Finally, we owe a great deal of gratitude to the reviewers of this article; their critical comments and suggestions were highly constructive and helpful. This work was support by the Directorate of Chemistry and Life Sciences of the U.S. Air Force Office of Scientific Research (AFOSR), Washington, D.C., and by the National Science Foundation (DMR-0307282).

9. References

(1) Goppert-Mayer, M. *Ann. Phys.* **1931**, *9*, 273.
(2) Dirac, P. A. M. *Proc. R. Soc. London* **1927**, *A114*, 243.
(3) Maiman, T. H. *Nature* **1960**, *187*, 493.
(4) Kaiser, W.; Garrett, C. G. B. *Phys. Rev. Lett*. **1961**, *7*, 229.
(5) Shen, Y. R. *The Principles of Nonlinear Optics*; Wiley: New York, 1984.
(6) Boyd, R. W. *Nonlinear Optics*, 2nd ed.; Academic: San Diego, CA, 2002.
(7) He, G. S.; Liu, S. H. *Physics of Nonlinear Optics*; World Scientific: Singapore, 2000.
(8) Sutherland, R. L. *Handbook of Nonlinear Optics*; Marcel Dekker: New York, 1998.
(9) Prasad, P. N. *Introduction to Biophotonics*; John Wiley: New York, 2003.
(10) Prasad, P. N. *Nanophotonics*; John Wiley: New York, 2004.
(11) Worlock, J. M. In *Laser Handbook*; Arecchi, F. T., Schulz-DuBois, E. O., Eds.; North-Holland: 1972; Vol. 2, pp 1323−1369.
(12) (a) Hochstrasser, R. M.; Sung, H.-N.; Wessel, J. E. *J. Chem. Phys*. **1973**, *58*, 4694. (b) Hochstrasser, R. M.; Sung, H.-N.; Wessel, J. E. *J. Am. Chem. Soc*. **1973**, *95*, 8179. (c) Hochstrasser, R. M.; Sung, H. N.; Wessel, J. E. *Chem. Phys. Lett*. **1974**, *24*, 168. (d) Hochstrasser, R. M.; Sung, H. N.; Wessel, J. E. *Chem. Phys. Lett*. **1974**, *24*, 7. (e) Bray, R. G.; Hochstrasser, R. M. *Mol. Phys*. **1976**, *31*, 1199. (f) Hochstrasser, R. M.; Sung, H. N. *J. Chem. Phys*. **1977**, *66*, 3276. (g) Hochstrasser, R. M.; Klimcak, C. M.; Meredith, G. R. *J. Chem. Phys*. **1979**, *70*, 870. (h) Mehreteab, A.; Andrews, J. R.; Smith, A. B., III; Hochstrasser, R. M. *J. Phys. Chem*. **1982**, *86*, 888. (i) Thorne, J. R. G.; Ohsako, Y.; Zeigler, J. M.; Hochstrasser, R. M. *Chem. Phys. Lett*. **1989**, *162*, 455.
(13) (a) Monson, P. R.; McClain, W. M. *J. Chem. Phys*. **1970**, *53*, 29. (b) McClain, W. M. *J. Chem. Phys*. **1971**, *55*, 2798. (c) Monson, P. R.; McClain, W. M. *J. Chem. Phys*. **1972**, *56*, 4817. (d) McClain, W. M. *J. Chem. Phys*. **1973**, *58*, 324. (e) McClain, W. M. *Acc. Chem. Res*. **1974**, *7*, 129. (f) Drucker, R. P.; McClain, W. M. *J. Chem. Phys*. **1974**, *61*, 2609. (g) Friedrich, D. M.; McClain, W. M. *Chem. Phys. Lett*. **1975**, *32*, 541. (h) Anderson, R. J. M.; Holtom, G. R.; McClain, W. M. *J. Chem. Phys*. **1979**, *70*, 4310. (i) Friedrich, D. M.; McClain, W. M. *Annu. Rev. Phys. Chem*. **1980**, *31*, 559. (j) Vasudev, R.; Stachelek, T. M.; McClain, W. M.; Woerdman, J. P. *Opt. Commun*. **1981**, *38*, 149. (k) Vasudev, R.; McClain, W. M. *J. Mol. Spectrosc*. **1981**, *89*, 125.
(14) (a) Birge, R. R.; Bennett, J. A.; Fang, H. L. B.; Leroi, G. E. *Springer Ser. Chem. Phys.* **1978**, *3*, 347. (b) Birge, R. R.; Bennett, J. A.; Pierce, B. M.; Thomas, T. M. *J. Am. Chem. Soc*. **1978**, *100*, 1533. (c) Bennett, J. A.; Birge, R. R. *J. Chem. Phys*. **1980**, *73*, 4234. (d) Birge, R. R.; Bennett, J. A.; Hubbard, L. M.; Fang, H. L.; Pierce, B. M.; Kliger, D. S.; Leroi, G. E. *J. Am. Chem. Soc*. **1982**, *104*, 2519. (e) Birge, R. R.; Pierce, B. M.; Murray, L. P. *NATO ASI Ser., Ser. C* **1984**, *139*, 473. (f) Birge, R. R.; Murray, L. P.; Pierce, B. M.; Akita, H.; Balogh-Nair, V.; Findsen, L. A.; Nakanishi, K. *Proc. Nat. Acad. Sci. U.S.A.* **1985**, *82*, 4117. (g) Murray, L. P.; Birge, R. R. *Can. J. Chem*. **1985**, *63*, 1967.
(15) (a) Asscher, M.; Haas, Y. *Chem. Phys. Lett*. **1978**, *59*, 231. (b) Asscher, M.; Haas, Y.; Roellig, M. P.; Houston, P. L. *J. Chem. Phys*. **1980**, *72*, 768. (c) Haas, Y.; Asscher, M. *Adv. Chem. Phys*. **1981**, *47*, 17. (d) Sirkin, E. R.; Asscher, M.; Haas, Y. *Chem. Phys. Lett*. **1982**, *86*, 265. (e) Catanzarite, J. H.; Haas, Y.; Reisler, H.; Wittig, C. *J. Chem. Phys*. **1983**, *78*, 5506. (f) Ruhman, S.; Haas, Y.; Laukemper, J.; Preuss, M.; Stein, H.; Feldmann, D.; Welge, K. H. *J. Phys. Chem*. **1984**, *88*, 5162. (g) Zilberg, S.; Haas, Y.; Shaik, S. *J. Phys. Chem*. **1995**, *99*, 16558. (h) Belau, L.; Haas, Y. *Chem. Phys. Lett*. **2001**, *333*, 297.
(16) (a) Hohlneicher, G.; Dick, B. *J. Chem. Phys*. **1979**, *70*, 5427. (b) Dick, B.; Hohlneicher, G. *Theor. Chim. Acta* **1979**, *53*, 221. (c) Dick, B.; Hohlneicher, G. *Chem. Phys. Lett*. **1981**, *84*, 471. (d) Dick, B.; Hohlneicher, G. *J. Chem. Phys*. **1982**, *76*, 5755. (e) Dick, B.; Hohlneicher, G. *Chem. Phys. Lett*. **1983**, *97*, 324. (f) Dick, B.; Hohlneicher, G. *Chem. Phys*. **1985**, *94*, 131. (g) Gutmann, M.; Gudipati, M.; Schoenzart, P. F.; Hohlneicher, G. *J. Phys. Chem*. **1992**, *96*, 2433. (h) Wolf, J.; Hohlneicher, G. *Chem. Phys*. **1994**, *181*, 185. (i) Hohlneicher, G.; Wrzal, R.; Lenoir, D.; Frank, R. *J. Phys. Chem. A* **1999**, *103*, 8969.
(17) (a) Wunsch, L.; Neusser, H. J.; Schlag, E. W. *Chem. Phys. Lett*. **1975**, *31*, 433. (b) Wunsch, L.; Neusser, H. J.; Schlag, E. W. *Chem. Phys. Lett*. **1976**, *38*, 216. (c) Boesl, U.; Neusser, H. J.; Schlag, E. W. *Chem. Phys.* **1976**, *15*, 167. (d) Wunsch, L.; Metz, F.; Neusser, H. J.; Schlag, E. W. *J. Chem. Phys*. **1977**, *66*, 386. (e) Hampf, W.; Neusser, H. J.; Schlag, E. W. *Chem. Phys. Lett*. **1977**, *46*, 406. (f) Robey, M. J.; Schlag, E. W. *Chem. Phys*. **1978**, *30*, 9. (g) Boesl, U.; Neusser, H. J.; Schlag, E. W. *Chem. Phys*. **1981**, *55*, 193.
(18) (a) Dinges, R.; Froehlich, D.; Staginnus, B.; Staude, W. *Phys. Rev. Lett*. **1970**, *25*, 922. (b) Froehlich, D.; Treusch, J.; Kottler, W. *Phys. Rev. Lett*. **1972**, *29*, 1603. (c) Dinges, R.; Froehlich, D. *Solid State Commun*. **1976**, *19*, 61. (d) Froehlich, D.; Kenklies, R.; Helbig, R. *Phys. Rev. Lett*. **1978**, *41*, 1750. (e) Froehlich, D.; Reimann, K.; Wille, R. *Europhys. Lett*. **1987**, *3*, 853. (f) Froehlich, D.; Wille, R.; Schlapp, W.; Weimann, G. *Phys. Rev. Lett*. **1988**, *61*, 1878.
(19) (a) Hänsch, T. W.; Harvey, K. C.; Meisel, G.; Schawlow, A. L. *Opt. Commun*. **1974**, *1*, 50. (b) Hänsch, T. W.; Lee, S. A.; Wallenstein, R.; Wieman, C. *Phys. Rev. Lett*. **1975**, *34*, 307. (c) Lee, S. A.; Wallenstein, R.; Hänsch, T. W. *Phys. Rev. Lett*. **1975**, *35*, 1262. (d) Lombardi, J. R.; Wallenstein, R.; Hänsch, T. W.; Friedrich, D. M. *J. Chem. Phys*. **1976**, *65*, 2357. (e) Beausoleil, R. G.; Hänsch, T. W. *Phys. Rev. A* **1986**, *33*, 1661. (f) Zimmermann, C.; Kallenbach, R.; Hänsch, T. W. *Phys. Rev. Lett*. **1990**, *65*, 571.
(20) (a) Cagnac, B.; Grynberg, G.; Biraben, F. *J. Phys. (Paris)* **1973**, *34*, 845. (b) Biraben, F.; Cagnac, B.; Grynberg, G. *Phys. Rev. Lett*. **1974**, *32*, 643. (c) Biraben, F.; Giacobino, E.; Grynberg, G. *Phys. Rev. A* **1975**, *12*, 2444. (d) Grynberg, G.; Biraben, F.; Bassini, M.; Cagnac, B. *Phys. Rev. Lett*. **1976**, *37*, 283. (e) Bassini, M.; Biraben, F.; Cagnac, B.; Grynberg, G. *Opt. Commun*. **1977**, *21*, 263.
(21) (a) Levenson, M. D.; Bloembergen, N. *Phys. Rev. Lett*. **1974**, *32*, 645. (b) Bloembergen, N.; Levenson, M. D.; Salour, M. M. *Phys. Rev. Lett*. **1974**, *32*, 867. (c) Levenson, M. D. *Phys. Rev. A* **1976**, *13*, 2314. (d) Harper, C. D.; Wheatley, S. E.; Levenson, M. D. *J. Opt. Soc. Am*. **1977**, *67*, 579. (e) Zapka, W.; Levenson, M. D.; Schellenberg, F. M.; Tam, A. C.; Bjorklund, G. C. *Opt. Lett*. **1983**, *8*, 27.
(22) Heitler, W. *The Quantum Theory of Radiation*, 3rd ed.; Oxford University: London, 1954.
(23) Marcuse, D. *Principles of Quantum Electronics*; Academic: New York, 1980.
(24) Craig, D. P.; Thirunamachandran, T. *Molecular Quantum Electrodynamics*; Academic: London, 1984.
(25) Jagatap, B. N.; Meath, W. J. *J. Opt. Soc. Am. B* **2002**, *19*, 2673.
(26) Arbitrarily, we consider 2PA molecules with femtosecond cross section values of ≥100 GM and nanosecond cross section values of ≥10 000 GM to be large.
(27) (a) Ramakrishna, G.; Goodson, T., III. *J. Phys. Chem. A* **2007**, *111*, 993. (b) Nguyen, K. A.; Rogers, J. E.; Slagle, J. E.; Day, P. N.; Kannan, R.; Tan, L.-S.; Fleitz, P. A.; Pachter, R. *J. Phys. Chem. A* **2006**, *110*, 13172. (c) Porres, L.; Charlot, M.; Entwistle, C. D.; Beeby, A.; Marder, T. B.; Blanchard-Desce, M. *Proc. SPIE—Int. Soc. Opt. Eng*. **2005**, *5934*, 1.

(28) Albota, M.; Beljonne, D.; Bredas, J. L.; Ehrlich, J. E.; Fu, J. Y.; Heikal, A. A.; Hess, S. E.; Kogej, T.; Levin, M. D.; Marder, S. R.; McCord-Maughon, D.; Perry, J. W.; Rockel, H.; Rumi, M.; Subramaniam, G.; Webb, W. W.; Wu, X. L.; Xu, C. *Science* **1998**, *281*, 1653.

(29) Marder, S. R.; Torruellas, W. E.; Blanchard-Desce, M.; Ricci, V.; Stegeman, G. I.; Gilmour, S.; Bredas, J. L.; Li, J.; Bublitz, G. U.; Boxer, S. G. *Science* **1997**, *276*, 1233.

(30) (a) Norman, P.; Luo, Y.; Ågren, H. *Chem. Phys. Lett*. **1998**, *296*, 8. (b) Norman, P.; Luo, Y.; Ågren, H. *Opt. Commun*. **1999**, *168*, 297.

(31) Lee, S.; Thomas, K. R. J.; Thayumanavan, S.; Bardeen, C. J. *J. Phys. Chem. A* **2005**, *109*, 9767.

(32) Bartkowiak, W.; Zalesny, R.; Leszczynski, J. *Chem. Phys*. **2003**, *287*, 103.

(33) Barzoukas, M.; Blanchard-Desce, M. *J. Chem. Phys*. **2000**, *113*, 3951.

(34) Norman, P.; Luo, Y.; Agren, H. *J. Chem. Phys*. **1999**, *111*, 7758.

(35) Drobizhev, M.; Karotki, A.; Rebane, A.; Spangler, C. W. *Opt. Lett*. **2001**, *26*, 1081.

(36) Woo, H. Y.; Liu, B.; Kohler, B.; Korystov, D.; Mikhailovsky, A.; Bazan, G. C. *J. Am. Chem. Soc*. **2005**, *127*, 14721.

(37) Woo, H. Y.; Korystov, D.; Mikhailovsky, A.; Nguyen, T.-Q.; Bazan, G. C. *J. Am. Chem. Soc*. **2005**, *127*, 13794.

(38) Baur, J. W.; Alexander, M. D. J.; Banach, M.; Denny, L. R.; Reinhardt, B. A.; Vaia, R. A.; Fleitz, P. A.; Kirkpatrick, S. M. *Chem. Mater*. **1999**, *11*, 2899.

(39) Kamada, K.; Ohta, K.; Iwase, Y.; Kondo, K. *Chem. Phys. Lett*. **2003**, *372*, 386.

(40) Drobizhev, M.; Stepanenko, Y.; Dzenis, Y.; Karotki, A.; Rebane, A.; Taylor, P. N.; Anderson, H. L. *J. Am. Chem. Soc*. **2004**, *126*, 15352.

(41) Reinhardt, B. A. *Photonics Sci. News* **1999**, *4*, 21.

(42) Marder, S. R. *Chem. Commun*. **2006**, 131.

(43) Reinhardt, B. A.; Brott, L. L.; Clarson, S. J.; Dillard, A. G.; Bhatt, J. C.; Kannan, R.; Yuan, L.; He, G. S.; Prasad, P. N. *Chem. Mater*. **1998**, *10*, 1863.

(44) AF-380 was first reported in: Joshi, M. P.; Swiatkiewicz, J.; Xu, F.; Prasad, P. N.; Reinhardt, B. A.; Kannan, R. *Opt. Lett*. **1998**, *23*, 1742. For the reason of patent-filing requirements, the molecular structure of AF-380 was not revealed in this paper. This paper preceded the earliest example of octupolar 2PA molecules reported from other group, e.g.: Cho, B. R.; Son, K. H.; Lee, S. H.; Song, Y.-S.; Lee, Y.-K.; Jeon, S.-J.; Choi, J. H.; Lee, H.; Cho, M. *J. Am. Chem. Soc*. **2001**, *123*, 10039.

(45) Kannan, R.; Reinhardt, B. A.; Tan, L.-S. U.S. Patent 6,300,502, October 9, 2001.

(46) He, G. S.; Swiatkiewicz, J.; Jiang, Y.; Prasad, P. N.; Reinhardt, B. A.; Tan, L.-S.; Kannan, R. *J. Phys. Chem. A* **2000**, *104*, 4805.

(47) Chung, S.-J.; Kim, K.-S.; Lin, T.-C.; He, G. S.; Swiatkiewicz, J.; Prasad, P. N. *J. Phys. Chem. B* **1999**, *103*, 10741.

(48) Zyss, J.; Ledoux, I. *Chem. Rev*. **1994**, *94*, 77.

(49) Spangler, C. W.; Elandaloussi, E. H.; Reeves, B. *Polym. Prepr*. **2000**, *41*, 789.

(50) McDonagh, A. M.; Humphrey, M. G.; Samoc, M.; Luther-Davies, B. *Organometallics* **1999**, *18*, 5195.

(51) Kogel, T.; Beljonne, D.; Meyers, F.; Perry, J. W.; Marder, S. R.; Breda, J. L. *Chem. Phys. Lett*. **1998**, *298*, 1.

(52) Baev, A.; Prasad, P. N.; Samoc, M. *J. Chem. Phys*. **2005**, *122*, 224309/1.

(53) Zhou, X.; Ren, A.-M.; Feng, J.-K.; Liu, X.-J. *Chem. Phys. Lett*. **2002**, *362*, 541.

(54) Katan, C.; Terenziani, F.; Mongin, O.; Werts, M. H. V.; Porres, L.; Pons, T.; Mertz, J.; Tretiak, S.; Blanchard-Desce, M. *J. Phys. Chem. A* **2005**, *109*, 3024.

(55) Belfield, K. D.; Hagan, D. J.; Van Stryland, E. W.; Schafer, K. J.; Negres, R. A. *Org. Lett*. **1999**, *1*, 1575.

(56) De Boni, L.; Rodrigues, J. J. J.; dos Santos, D. S. J.; Silva, C. H. T. P.; Balogh, D. T.; O. N. Oliveira, J.; Zilio, S. C.; Misoguti, L.; Mendonça, C. R. *Chem. Phys. Lett*. **2002**, *361*, 209.

(57) Lin, T.-C.; He, G. S.; Prasad, P. N.; Tan, L.-S. *J. Mater. Chem*. **2004**, *14*, 982.

(58) Stellacci, F.; Bauer, C. A.; Meyer-Friedrichsen, T.; Wenseleers, W.; Marder, S. R.; Perry, J. W. *J. Am. Chem. Soc*. **2003**, *125*, 328.

(59) Ventelon, L.; Moreaux, L.; Mertz, J.; Blanchard-Desce, M. *Synth. Met*. **2002**, *127*, 17.

(60) Aujard, I.; Benbrahim, C.; Gouget, M.; Ruel, O.; Baudin, J.-B.; Neveu, P.; Jullien, L. *Chem.—Eur. J*. **2006**, *12*, 6865.

(61) Strehmel, B.; Sarker, A. M.; Detert, H. *ChemPhysChem* **2003**, *4*, 249.

(62) Porres, L.; Mongin, O.; Katan, C.; Charlot, M.; Pons, T.; Mertz, J.; Blanchard-Desce, M. *Org. Lett*. **2004**, *6*, 47.

(63) Le Droumaguet, C.; Mongin, O.; Werts, M. H. V.; Blanchard-Desce, M. *Chem. Commun*. **2005**, 2802.

(64) Lee, H. J.; Sohn, J.; Hwang, J.; Park, S. Y.; Choi, H.; Cha, M. *Chem. Mater*. **2004**, *16*, 456.

(65) Riehl, D.; Izard, N.; Vivien, L.; Anglaret, E.; Doris, E.; Menard, C.; Mioskowski, C.; Porres, L.; Mongin, O.; Charlot, M.; Blanchard-Desce, M.; Anemian, R.; Mulatier, J.-C.; Barsu, C.; Andraud, C. *Proc. SPIE—Int. Soc. Opt. Eng*. **2003**, *5211*, 124.

(66) Bhawalkar, J. D.; He, G. S.; Park, C. K.; Zhao, C. F.; Ruland, G.; Prasad, P. N. *Opt. Commun*. **1996**, *124*, 33.

(67) Wang, X.; Krebs, L. J.; Al-Nuri, M.; Pudavar, H. E.; Ghosal, S.; Liebow, C.; Nagy, A. A.; Schally, A. V.; Prasad, P. N. *Proc. Natl. Acad. Sci. U.S.A*. **1999**, *96*, 11081.

(68) Huang, Z.-L.; Lei, H.; Li, N.; Qiu, Z.-R.; Wang, H.-Z.; Guo, J.-D.; Luo, Y.; Zhong, Z.-P.; Liu, X.-F.; Zhou, Z.-H. *J. Mater. Chem*. **2003**, *13*, 708.

(69) Shao, P.; Huang, B.; Chen, L.; Liu, Z.; Qin, J.; Gong, H.; Ding, S.; Wang, Q. *J. Mater. Chem*. **2005**, *15*, 4502.

(70) Kannan, R.; He, G. S.; Yuan, L.; Xu, F.; Prasad, P. N.; Dombroskie, A. G.; Reinhardt, B. A.; Baur, J. W.; Vaia, R. A.; Tan, L.-S. *Chem. Mater*. **2001**, *13*, 1896.

(71) (a) He, G. S.; Gvishi, R.; Prasad, P. N.; Reinhardt, B. A. *Opt. Commun*. **1995**, *117*, 133. (b) Belfield, K. D.; Schafer, K. J.; Mourad, W.; Reinhardt, B. A. *J. Org. Chem*. **2000**, *65*, 4475. (c) Abbotto, A.; Beverina, L.; Bozio, R.; Facchetti, A.; Ferrante, C.; Pagani, G. A.; Pedron, D.; Signorini, R. *Org. Lett*. **2002**, *4*, 1495. (d) Cao, D.-X.; Fang, Q.; Wang, D.; Liu, Z.-Q.; Xue, G.; Xu, G.-B.; Yu, W.-T. *Eur. J. Org. Chem*. **2003**, *2003*, 3628.

(72) Kim, O.-K.; Lee, K.-S.; Woo, H. Y.; Kim, K.-S.; He, G. S.; Swiatkiewicz, J.; Prasad, P. N. *Chem. Mater*. **2000**, *12*, 284.

(73) He, G. S.; Lin, T.-C.; Prasad, P. N.; Kannan, R.; Vaia, R. A.; Tan, L.-S. *J. Phys. Chem. B* **2002**, *106*, 11081.

(74) Charlot, M.; Izard, N.; Mongin, O.; Riehl, D.; Blanchard-Desce, M. *Chem. Phys. Lett*. **2006**, *417*, 297.

(75) Parent, M.; Mongin, O.; Kamada, K.; Katan, C.; Blanchard-Desce, M. *Chem. Commun*. **2005**, 2029.

(76) (a) He, G. S.; Yuan, L.; Cui, Y.; Li, M.; Prasad, P. N. *J. Appl. Phys*. **1997**, *81*, 2529. (b) He, G. S.; Bhawalkar, J. D.; Zhao, C. F.; Prasad, P. N. *Appl. Phys. Lett*. **1995**, *67*, 2433.

(77) Kawamata, J.; Akiba, M.; Tani, T.; Harada, A.; Inagaki, Y. *Chem. Lett*. **2004**, *33*, 448.

(78) Wu, L.-Z.; Tang, X.-J.; Jiang, M.-H.; Tung, C.-H. *Chem. Phys. Lett*. **1999**, *315*, 379.

(79) Porrès, L.; Mongin, O.; Blanchard-Desce, M. *Tetrahedron Lett*. **2006**, *47*, 1913.

(80) (a) Ventelon, L.; Blanchard-Desce, M.; Moreaux, L.; Mertz, J. *Chem. Commun*. **1999**, 2055—2056. (b) Ventelon, L.; Charier, S.; Moreaux, L.; Mertz, J.; Blanchard-Desce, M. *Angew. Chem., Int. Ed*. **2001**, *40*, 2098.

(81) Zheng, Q.; He, G. S.; Prasad, P. N. *J. Mater. Chem*. **2005**, *15*, 579.

(82) Yang, W. J.; Kim, D. Y.; Jeong, M.-Y.; Kim, H. M.; Jeon, S.-J.; Cho, B. R. *Chem. Commun*. **2003**, 2618.

(83) Kim, H. M.; Yang, W. J.; Kim, C. H.; Park, W.-H.; Jeon, S.-J.; Cho, B. R. *Chem.—Eur. J*. **2005**, *11*, 6386.

(84) Liu, S.; Lin, K. S.; Churikov, V. M.; Su, Y. Z.; Lin, J. T.; Huang, T.-H.; Hsu, C. C. *Chem. Phys. Lett*. **2004**, *390*, 433.

(85) Kato, S.-i.; Matsumoto, T.; Shigeiwa, M.; Gorohmaru, H.; Maeda, S.; Ishi-i, T.; Mataka, S. *Chem.—Eur. J*. **2006**, *12*, 2303.

(86) Woo, H. Y.; Hong, J. W.; Liu, B.; Mikhailovsky, A.; Korystov, D.; Bazan, G. C. *J. Am. Chem. Soc*. **2005**, *127*, 820.

(87) Ehrlich, J. E.; Wu, X. L.; Lee, I. Y. S.; Heikal, A. A.; Hu, Z. Y.; Rockel, H.; Marder, S. R.; Perry, J. W. *Mater. Res. Soc. Symp. Proc*. **1997**, *479*, 9.

(88) Kleinschmidt, J.; Rentsch, S.; Tottleben, W.; Wilhelmi, B. *Chem. Phys. Lett*. **1974**, *24*, 133.

(89) Zhao, M.; Cui, Y.; Samoc, M.; Prasad, P. N.; Unroe, M. R.; Reinhardt, B. A. *J. Chem. Phys*. **1991**, *95*, 3991.

(90) Sutherland, R. L.; Rea, E.; Natarajan, L. V.; Pottenger, T.; Fleitz, P. A. *J. Chem. Phys*. **1993**, *98*, 2593.

(91) Palffy-Muhoray, P.; Yuan, H. J.; Li, L.; Lee, M. A.; DeSalvo, J. R.; Wei, T. H.; Sheik-Bahae, M.; Hagan, D. J.; Stryland, E. W. V. *Mol. Cryst. Liq. Cryst*. **1991**, *207*, 291.

(92) Said, A. A.; Wamsley, C.; Hagan, D. J.; Stryland, E. W. V.; Reinhardt, B. A.; Roderer, P.; Dillard, A. G. *Chem. Phys. Lett*. **1994**, *228*, 646.

(93) Guha, S.; Kang, K.; Porter, P.; Roach, J. F.; Remy, D. E.; Aranda, F. J.; Rao, D. V. G. L. N. *Opt. Lett*. **1992**, *17*, 264.

(94) Oulianov, D. A.; Tomov, I. V.; Dvornikov, A. S.; Rentzepis, P. M. *Opt. Commun*. **2001**, *191*, 235.

(95) Swiatkiewicz, J.; Prasad, P. N.; Reinhardt, B. A. *Opt. Commun*. **1998**, *157*, 135.

(96) Rumi, M.; Ehrlich, J. E.; Heikal, A. A.; Perry, J. W.; Barlow, S.; Hu, Z.; McCord-Maughon, D.; Parker, T. C.; Rockel, H.; Thayumanavan, S.; Marder, S. R.; Beljonne, D.; Brédas, J.-L. *J. Am. Chem. Soc*. **2000**, *122*, 9500.

(97) Das, G. P.; Vaia, R.; Yeates, A. T.; Dudis, D. S. *Synth. Met.* **2000**, *116*, 281.
(98) Das, G. P.; Yeates, A. T.; Dudis, D. S. *J. Opt. Soc. Am. B* **1997**, *14*, 2325.
(99) Sutherland, R. L.; Brant, M. C.; Heinrichs, J.; Rogers, J. E.; Slagle, J. E.; McLean, D. G.; Fleitz, P. A. *J. Opt. Soc. Am. B* **2005**, *22*, 1939.
(100) Drobizhev, M.; Karotki, A.; Dzenis, Y.; Rebane, A.; Suo, Z.; Spangler, C. W. *J. Phys. Chem.* B **2003**, *107*, 7540.
(101) Wei, P.; Bi, X.; Wu, Z.; Xu, Z. *Org. Lett.* **2005**, *7*, 3199.
(102) Chung, S.-J.; Lin, T.-C.; Kim, K.-S.; He, G. S.; Swiatkiewicz, J.; Prasad, P. N.; Baker, G. A.; Bright, F. V. *Chem. Mater.* **2001**, *13*, 4071.
(103) Yoo, J.; Yang, S. K.; Jeong, M.-Y.; Ahn, H. C.; Jeon, S.-J.; Cho, B. R. *Org. Lett.* **2003**, *5*, 645.
(104) Mongin, O.; Porrès, L.; Katan, C.; Pons, T.; Mertz, J.; Blanchard-Desce, M. *Tetrahedron Lett.* **2003**, *44*, 8121.
(105) Li, J.; Meng, F.; Tian, H.; Mi, J.; Ji, W. *Chem. Lett.* **2005**, *34*, 922.
(106) Yang, W. J.; Kim, D. Y.; Kim, C. H.; Jeong, M.-Y.; Lee, S. K.; Jeon, S.-J.; Cho, B. R. *Org. Lett.* **2004**, *6*, 1389.
(107) Wu, J.; Zhao, Y.; Li, X.; Shi, M.; Wu, F.; Fang, X. *New J. Chem.* **2006**, *30*, 1098.
(108) Huang, Z.; Wang, X.; Li, B.; Lv, C.; Xu, J.; Jiang, W.; Tao, X.; Qian, S.; Cui, Y.; Yang, P. *Opt. Mater.* **2007**, *29*, 1084.
(109) Kannan, R.; He, G. S.; Lin, T.-C.; Prasad, P. N.; Vaia, R. A.; Tan, L.-S. *Chem. Mater.* **2004**, *16*, 185.
(110) (a) Meng, F.; Li, B.; Qian, S.; Chen, K.; Tian, H. *Chem. Lett.* **2004**, *33*, 470. (b) Cui, Y.-Z.; Fang, Q.; Xue, G.; Xu, G.-B.; Yin, L.; Yu, W.-T. *Chem. Lett.* **2005**, *34*, 644. (c) Li, B.; Tong, R.; Zhu, R.; Meng, F.; Tian, H.; Qian, S. *J. Phys. Chem. B* **2005**, *109*, 10705.
(111) (a) Abbotto, A.; Beverina, L.; Bozio, R.; Facchetti, A.; Ferrante, C.; Pagani, G. A.; Pedron, D.; Signorini, R. *Chem. Commun.* **2003**, 2144. (b) Abbotto, A.; Beverina, L.; Bradamante, S.; Facchetti, A.; Pagani, G. A.; Bozio, R.; Ferrante, C.; Pedron, D.; Signorini, R. *Synth. Met.* **2003**, *139*, 795.
(112) (a) Cho, B. R.; Son, K. H.; Lee, S. H.; Song, Y.-S.; Lee, Y.-K.; Jeon, S.-J.; Choi, J. H.; Lee, H.; Cho, M. *J. Am. Chem. Soc.* **2001**, *123*, 10039. (b) Cho, B. R.; Piao, M. J.; Son, K. H.; Lee, S. H.; Yoon, S. J.; Jeon, S.-J.; Cho, M. *Chem.—Eur. J.* **2002**, *8*, 3907. (c) Yang, W. J.; Kim, C. H.; Jeong, M.-Y.; Lee, S. K.; Piao, M. J.; Jeon, S.-J.; Cho, B. R. *Chem. Mater.* **2004**, *16*, 2783.
(113) Zheng, Q.; He, G. S.; Prasad, P. N. *Chem. Mater.* **2005**, *17*, 6004.
(114) Wang, H.; Li, Z.; Shao, P.; Liang, Y.; Wang, H.; Qin, J.; Gong, Q. *New J. Chem.* **2005**, *29*, 792.
(115) Drobizhev, M.; Rebane, A.; Suo, Z.; Spangler, C. W. *J. Lumin.* **2005**, *111*, 291.
(116) Kuzyk, M. G. *J. Chem. Phys.* **2003**, *119*, 8327.
(117) Kohn, W.; Sham, L. J. *Phys. Rev. A* **1965**, *140*, 1133.
(118) Olsen, J.; Jørgensen, P. *J. Chem. Phys.* **1985**, *82*, 3235.
(119) Hättig, C.; Christiansen, O.; Jørgensen, P. *J. Chem. Phys.* **1998**, *108*, 8355.
(120) Pantell, R.; Praedere, F.; Hanus, J.; Schott, M.; Puthoff, H. *J. Chem. Phys.* **1967**, *46* 3507.
(121) Moccia, R.; Rizzo, A. *J. Phys. B: At. Mol. Phys.* **1985**, *18*, 3319.
(122) Wang, C.-K.; Macak, P.; Luo, Y.; Ågren, H. *J. Chem. Phys.* **2001**, *114*, 9813.
(123) Norman, P.; Cronstrand, P.; Ericsson, J. *Chem. Phys.* **2002**, *285*, 207.
(124) Luo, Y.; Ågren, H.; Vahtras, O.; Jørgensen, P. *Chem. Phys. Lett.* **1993**, *204*, 587.
(125) (a) Sundholm, D.; Rizzo, A.; Jørgensen, P. *J. Chem. Phys.* **1994**, *101*, 4931. (b) Sundholm, D.; Olsen, J.; Jørgensen, P. *J. Chem. Phys.* **1995**, *102*, 4143.
(126) Paterson, M. J.; Christiansen, O.; Pawlowski, F.; Jørgensen, P.; Hättig, C.; Helgaker, T.; Sałek, P. *J. Chem. Phys.* **2006**, *124*, 054322.
(127) Sałek, P.; Vahtras, O.; Guo, J.; Luo, Y.; Helgaker, T.; Ågren, H. *Chem. Phys. Lett.* **2003**, *374*, 446.
(128) Masunov, A.; Tretiak, S. *J. Phys. Chem. B* **2004**, *108*, 899.
(129) Day, P. N.; Nguyen, K. A.; Pachter, R. *J. Phys. Chem. B* **2006**, *125*, 094103.
(130) Baev, A.; Sałek, P.; Gel'mukhanov, F.; Ågren, H. *J. Phys. Chem. B* **2006**, *110*, 5379.
(131) Luo, Y.; Ågren, H.; Knuts, S.; Minaev, B. F.; Jørgensen, P. *Chem. Phys. Lett.* **1993**, *209*, 513.
(132) Luo, Y.; Norman, P.; Macak, P.; Ågren, H. *J. Phys. Chem. A* **2000**, *104*, 4718.
(133) Wang, C.-K.; Zhao, K.; Su, Y.; Ren, Y.; Zhao, X.; Luo, Y. *J. Chem. Phys.* **2003**, *119*, 1208.
(134) Frediani, L.; Rinkevicius, Z.; Ågren, H. *J. Chem. Phys.* **2005**, *122*, 244104.
(135) Meyers, F.; Marder, S. R.; Pierce, B. M.; Brédas, J. L. *J. Am. Chem. Soc.* **1994**, *116*, 10703.
(136) (a) Zojer, E.; Beljonne, D.; Kogej, T.; Vogel, H.; Marder, S. R.; Perry, J. W.; Brédas, J. L. *J. Chem. Phys.* **2002**, *116*, 3646. (b) Zojer, E.; Wenseleers, W.; Halik, M.; Grasso, C.; Barlow, S.; Perry, J. W.; Marder, S. R.; Brédas, J.-L. *ChemPhysChem* **2004**, *5*, 982.
(137) Cronstrand, P.; Luo, Y.; Ågren, H. *Chem. Phys. Lett.* **2002**, *352*, 262.
(138) Macak, P.; Luo, Y.; Norman, P.; Ågren, H. *J. Chem. Phys.* **2000**, *113*, 7055.
(139) Gel'mukhanov, F.; Baev, A.; Macak, P.; Luo, Y.; Ågren, H. *J. Opt. Soc. Am. B* **2002**, *19*, 937.
(140) Baev, A.; Gel'mukhanov, F.; Macak, P.; Luo, Y.; Ågren, H. *Chem. Phys.* **2002**, *117*, 6214.
(141) Baev, A.; Gel'mukhanov, F.; Kimberg, V.; Ågren, H. *J. Phys. B: At. Mol. Opt. Phys.* **2003**, *36*, 3761.
(142) Baev, A.; Gel'mukhanov, F.; Rubio-Pons, O.; Cronstrand, P.; Ågren, H. *J. Opt. Soc. Am. B* **2005**, *22*, 385.
(143) Baev, A.; Kimberg, V.; Polyutov, S.; Gel'mukhanov, F.; Ågren, H. *J. Opt. Soc. Am. B* **2004**, *21*, 384.
(144) Polyutov, S.; Minkov, I.; Gel'mukhanov, F.; Ågren, H. *J. Phys. Chem. A* **2005**, *109*, 9507.
(145) Baev, A.; Norman, P.; Henriksson, J.; Ågren, H. *J. Phys. Chem. B* **2006**, *110*, 20912.
(146) (a) Das, G. P.; Yeates, A. T.; Dudis, D. S. *Chem. Phys. Lett.* **2002**, *361*, 71. (b) Das, G. P.; Yeates, A. T.; Dudis, D. S. *Chem. Phys. Lett.* **2004**, *393*, 76.
(147) (a) Zhou, X.; Ren, A.-M.; Feng, J.-K.; Liu, X.-J. *Chem. Phys. Lett.* **2004**, *385*, 149. (b) Zhou, X.; Feng, J-K.; Ren, A.-M. *Synth. Met.* **2005**, *155*, 615.
(148) (a) Liu, X.-J.; Feng, J.-K.; Ren, A.-M.; Cheng, H.; Zhou, X. *J. Chem. Phys.* **2004**, *121*, 8253. (b) Zhang, X.-B.; Feng, J.-K.; Ren, A.-M.; Sun, C.-C. *THEOCHEM* **2006**, *767*, 165.
(149) (a) Allcock, P.; Andrews, D. L. *J. Chem. Phys.* **1998**, *108*, 3089. (b) Allcock, P.; Jenkins, R. D.; Andrews, D. L. *Phys. Rev. A* **2000**, *61*, 023812/1.
(150) (a) Andrews, D. L.; Bradshaw, D. S. *J. Chem. Phys.* **2004**, *121*, 2445. (b) Jenkins, R. D.; Andrews, D. L. *Photochem. Photobiol. Sci.* **2004**, *3*, 39. (c) Bradshaw, D. S.; Andrews, D. L. *Chem. Phys. Lett.* **2006**, *430*, 191.
(151) Yee, J. H. *Phys. Rev. B* **1972**, *5*, 449.
(152) Mitra, S. S.; Judell, N. H. K.; Vaidyanathan, A.; Guenther, A. H. *Opt. Lett.* **1982**, *7*, 307.
(153) Pasquarello, A.; Andreani, L. C. *Phys. Rev. B* **1990**, *41*, 12230.
(154) Zhu, L.; Yang, X.; Yi, Y.; Xuan, P.; Shuai, Z.; Chen, D.; Zojer, E.; Bredas, J.-L.; Beljonne, D. *J. Chem. Phys.* **2004**, *121*, 11060.
(155) Kershaw, S. In *Characterization Techniques and Tabulations for Organic Nonlinear Optical Materials*; Kuzyk, M. G., Dirk, C. W., Eds.; Marcel Dekker, Inc.: New York, 1998; pp 515—654.
(156) Subramaniam, G.; Andras, J.; Brodhead, J.; Gill, R.; Slaska, M. *MCLC S&T A: Mol. Cryst. Liq. Cryst.* **2001**, *365*, 33.
(157) Pond, S. J. K.; Rumi, M.; Levin, M. D.; Parker, T. C.; Beljonne, D.; Day, M. W.; Bredas, J. L.; Marder, S. R.; Perry, J. W. *J. Phys. Chem. A* **2002**, *106*, 11470.
(158) Halik, M.; Wenseleers, W.; Grasso, C.; Stellacci, F.; Zojer, E.; Barlow, S.; Bredas, J.-L.; Perry, J. W.; Marder, S. R. *Chem. Commun.* **2003**, 1490.
(159) Pond, S. J. K.; Tsutsumi, O.; Rumi, M.; Kwon, O.; Zojer, E.; Bredas, J. L.; Marder, S. R.; Perry, J. W. *J. Am. Chem. Soc.* **2004**, *126*, 9291.
(160) Chung, S. J.; Rumi, M.; Alain, V.; Barlow, S.; Perry, J. W.; Marder, S. R. *J. Am. Chem. Soc.* **2005**, *127*, 10844.
(161) Beverina, L.; Fu, J.; Leclercq, A.; Zojer, E.; Pacher, P.; Barlow, S.; VanStryland, E. W.; Hagan, D. J.; Bredas, J. L.; Marder, S. R. *J. Am. Chem. Soc.* **2005**, *127*, 7282.
(162) Mongin, O.; Brunel, J.; Porres, L.; Blanchard-Desce, M. *Tetrahedron Lett.* **2003**, *44*, 2813.
(163) Lin, T.-C.; He, G. S.; Zheng, Q.; Prasad, P. N. *J. Mater. Chem.* **2006**, *16*, 2490.
(164) Belfield, K. D.; Morales, A. R.; Kang, B. S.; Hales, J. M.; Hagan, D. J.; VanStryland, E. W.; Chapela, V. M.; Percino, J. *Chem. Mater.* **2004**, *16*, 4634.
(165) Belfield, K. D.; Morales, A. R.; Hales, J. M.; Hagan, D. J.; VanStryland, E. W.; Chapela, V. M.; Percino, J. *Chem. Mater.* **2004**, *16*, 2267.
(166) Yao, S.; Belfield, K. D. *J. Org. Chem.* **2005**, *70*, 5126.
(167) Lee, S. K.; Yang, W. J.; Choi, J. J.; Kim, C. H.; Jeon, S. J.; Cho, B. R. *Org. Lett.* **2005**, *7*, 323.
(168) Yang, W. J.; Kim, D. Y.; Jeong, M.-Y.; Kim, H. M.; Lee, Y. K.; Fang, X.; Jeon, S.-J.; Cho, B. R. *Chem.—Eur. J.* **2005**, *11*, 4191.
(169) Bartholomew, G. P.; Rumi, M.; Pond, S. J. K.; Perry, J. W.; Tretiak, S.; Bazan, G. C. *J. Am. Chem. Soc.* **2004**, *126*, 11529.
(170) Wang, X.; Yang, P.; Jiang, W.; Xu, G.; Guo, X. *Opt. Mater.* **2005**, *27*, 1163.
(171) Liu, Z. Q.; Fang, Q.; Cao, D. X.; Wang, D.; Xu, G. B. *Org. Lett.* **2004**, *6*, 2933.
(172) Wang, L.; Tao, X.-T.; Yang, J.-X.; Xu, G.-B.; Ren, Y.; Liu, Y.; Yan, Y.-X.; Liu, Z.; Jiang, M.-H. *Synth. Met.* **2006**, *156*, 141.

(173) Strehmel, B.; Amthor, S.; Schelter, J.; Lambert, C. *ChemPhysChem* **2005**, *6*, 893.
(174) Iwase, Y.; Kamada, K.; Ohta, K.; Kondo, K. *J. Mater. Chem.* **2003**, *13*, 1575.
(175) Huang, P.-H.; Shen, J.-Y.; Pu, S.-C.; Wen, Y.-S.; Lin, J. T.; Chuo, P.-T.; Yeh, M.-C. P. *J. Mater. Chem.* **2006**, *16*, 850.
(176) Zhang, J.; Cui, Y.; Wang, M.; Liu, J. *Chem. Commun.* **2002**, *21*, 2526.
(177) Yuan, H. J.; Li, L.; Palffy-Muhoray, P. *Proc. SPIE—Int. Soc. Opt. Eng.* **1990**, *1307*, 363.
(178) Yuan, H. J.; Li, L.; Palffy-Muhoray, P. *Mol. Cryst. Liq. Cryst.* **1991**, *199*, 223.
(179) Soileau, M. J.; Van Stryland, E. W.; Guha, S. *Proc. SPIE—Int. Soc. Opt. Eng.* **1987**, *682*, 135.
(180) Shirota, K.; Sun, H.-B.; Kawata, S. *Appl. Phys. Lett.* **2004**, *84*, 1632.
(181) McEwan, K.; Hollins, R. *Proc. SPIE—Int. Soc. Opt. Eng.* **1994**, *2229*, 122.
(182) Soileau, M. J.; Van Stryland, E. W.; Guha, S.; Sharp, E. J.; Wood, G. L.; Pohlmann, J. L. W. *Mol. Cryst. Liq. Cryst.* **1987**, *143*, 139.
(183) Lincker, F.; Bourgun, P.; Masson, P.; Didier, P.; Guidoni, L.; Bigot, J.-Y.; Nicoud, J.-F.; Donnio, B.; Guillon, D. *Org. Lett.* **2005**, *7*, 1505.
(184) He, G. S.; Lin, T.-C.; Prasad, P. N.; Cho, C.-C.; Yu, L.-J. *Appl. Phys. Lett.* **2003**, *82*, 4717.
(185) Khoo, I.-C.; Diaz, A.; Wood, M. V.; Chen, P. H. *IEEE J. Sel. Top. Quantum Electron* **2001**, *7*, 760.
(186) Rao, D. N.; Chopra, P.; Ghoshal, S. K.; Swiatkiewicz, J.; Prasad, P. N. *J. Chem. Phys.* **1986**, *84*, 7049.
(187) Lindle, J. R.; Bartoli, F. J.; Hoffman, C. A.; Kim, O. K.; Lee, Y. S.; Shirk, J. S.; Kafafi, Z. H. *Appl. Phys. Lett.* **1990**, *56*, 712.
(188) Yu, L.; Chen, M.; Dalton, L. R. *Chem. Mater.* **1990**, *2*, 649.
(189) (a) Perepichka, I. F.; Perepichka, D. F.; Meng, H.; Wudl, F. *Adv. Mater.* **2005**, *17*, 2281. (b) Barbarella, G.; Melucci, M.; Sotgiu, G. *Adv. Mater.* **2005**, *17*, 1581.
(190) (a) Lee, C. Y. C.; Swiatkiewicz, J.; Prasad, P. N.; Mehta, R.; Bai, S. J. *Polymer* **1991**, *32*, 1195. (b) Dotrong, M.; Mehta, R.; Balchin, G. A.; Tomlinson, R. C.; Sinsky, M.; Lee, C. Y. C.; Evers, R. C. *J. Polym. Sci., Part A: Polym. Chem.* **1993**, *31*, 723.
(191) Agrawal, A. K.; Jenekhe, S. A.; Vanherzeele, H.; Meth, J. S. *J. Phys. Chem.* **1992**, *96*, 2837.
(192) Kimball, B. R.; Nakashima, M.; Roach, J. F.; Jaglowski, A. J.; Aranda, F. J.; Rao, D. V. G. L. N. *Proc. SPIE—Int. Soc. Opt. Eng.* **1996**, *2853*, 190.
(193) Yu, L.; Dalton, L. R. *Macromolecules* **1990**, *23*, 3439.
(194) Prasad, P. N.; Willians, D. J. *Introduction to Nonlinear Optical Effects in Molecules and Polymers*; Wiley-Interscience: New York, 1991; Chapter 10.
(195) (a) Sauteret, C.; Hermann, J. P.; Frey, R.; Pradere, F.; Ducuing, J.; Baughman, R. H.; Chance, R. R. *Phys. Rev. Lett.* **1976**, *36*, 956. (b) Rustagi, K. C.; Ducuing, J. *Opt. Commun.* **1974**, *10*, 258. (c) Hermann, J. P.; Ricard, D.; Ducuing, J. *Appl. Phys. Lett.* **1973**, *23*, 178.
(196) Chance, R. R.; Shand, M. L.; Hogg, C.; Silbey, R. *Phys. Rev. B* **1980**, *22*, 3540.
(197) Nunzi, J. M.; Grec, D. *J. Appl. Phys.* **1987**, *62*, 2198.
(198) Pender, W. A.; Boyle, A. J.; Lambkin, P.; Blau, W. J.; Mazaheri, K.; Westland, D. J.; Skarda, V.; Sparpaglione, M. *Appl. Phys. Lett.* **1995**, *66*, 786.
(199) Banfi, G.; Fortusini, D.; Dainesi, P.; Grando, D.; Sottini, S. *J. Chem. Phys.* **1998**, *108*, 4319.
(200) Polyakov, S.; Yoshino, F.; Liu, M.; Stegeman, G. *Phys. Rev. B* **2004**, *69*, 115421/1.
(201) Terenziani, F.; Morone, Marika, Gmouh; Blanchard-Desce, M. *ChemPhysChem* **2006**, *7*, 685.
(202) (a) Lenz, R. W.; Han, C. C.; Lux, M. *Polymer* **1989**, *30*, 1041. (b) Jin, J. I.; Lee, Y. H.; Shim, H. K. *Macromolecules* **1993**, *26*, 1805. (c) Jin, J. I.; Park, C. K.; Shim, H. K. *Macromolecules* **1993**, *26*, 1799.
(203) (a) He, G. S.; Bhawalkar, J. D.; Zhao, C. F.; Park, C.-K.; Prasad, P. N. *Opt. Lett.* **1995**, *20*, 2393. (b) He, G. S.; Zhao, C. F.; Bhawalkar, J. D.; Prasad, P. N. *Appl. Phys. Lett.* **1995**, *67*, 3703.
(204) Samoc, A.; Samoc, M.; Woodruff, M.; Luther-Davies, B. *Opt. Lett.* **1995**, *20*, 1241.
(205) (a) Gagnon, D. R.; Capistran, J. D.; Karasz, F. E.; Lenz, R. W.; Antoun, S. *Polymer* **1987**, *28*, 567. (b) Burn, P. L.; Bradley, D. D. C.; Friend, R. H.; Halliday, D. A.; Holmes, A. B.; Jackson, R. W.; Kraft, A. *J. Chem. Soc., Perkin Trans. 1* **1992**, 3225.
(206) Lemmer, U.; Fischer, R.; Feldmann, J.; Mahrt, R. F.; Yang, J.; Greiner, A.; Baessler, H.; Goebel, E. O.; Heesel, H.; et al. *Chem. Phys. Lett.* **1993**, *203*, 28.
(207) Pang, Y.; Samoc, M.; Prasad, P. N. *J. Chem. Phys.* **1991**, *94*, 5282.
(208) Baker, C. J.; Gelsen, O. M.; Bradley, D. D. C. *Chem. Phys. Lett.* **1993**, *201*, 127.
(209) De Boni, L.; Andrade, A. A.; Correa, D. S.; Balogh, D. T.; Zilio, S. C.; Misoguti, L.; Mendonca, C. R. *J. Phys. Chem. B* **2004**, *108*, 5221.
(210) Chung, S. J.; Maciel, G. S.; Pudavar, H. E.; Lin, T. C.; He, G. S.; Swiatkiewicz, J.; Prasad, P. N.; Lee, D. W.; Jin, J. I. *J. Phys. Chem. A* **2002**, *106*, 7512.
(211) Oliveira, S. L.; Correa, D. S.; De Boni, L.; Misoguti, L.; Zilio, S. C.; Mendonca, C. R. *Appl. Phys. Lett.* **2006**, *88*, 021911/1.
(212) Meyer, R. K.; Benner, R. E.; Vardeny, Z. V.; Liess, M.; Ozaki, M.; Yoshino, K.; Ding, Y.; Barton, T. *Synth. Met.* **1997**, *84*, 549.
(213) Lee, G. J.; Kim, K.; Jin, J.-I. *Opt. Commun.* **2002**, *203*, 151.
(214) He, G. S.; Weder, C.; Smith, P.; Prasad, P. N. *IEEE J. Quantum Electron.* **1998**, *34*, 2279.
(215) Hein, J.; Bergner, H.; Lenzner, M.; Rentsch, S. *Chem. Phys.* **1994**, *179*, 543.
(216) Periasamy, N.; Danieli, R.; Ruani, G.; Zamboni, R.; Taliani, C. *Phys. Rev. Lett.* **1992**, *68*, 919.
(217) Thienpont, H.; Rikken, G. L. J. A.; Meijer, E. W.; Ten Hoeve, W.; Wynberg, H. *Phys. Rev. Lett.* **1990**, *65*, 2141.
(218) Zhao, M. T.; Singh, B. P.; Prasad, P. N. *J. Chem. Phys.* **1988**, *89*, 5535.
(219) Beljonne, D.; Breda, J. L. *J. Opt. Soc. Am. B* **1994**, *11*, 1380.
(220) (a) Pfeffer, N.; Raimond, P.; Charra, F.; Nunzi, J.-M. *Chem. Phys. Lett.* **1993**, *201*, 357. (b) Pfeffer, N.; Charra, F.; Nunzi, J. M. *Opt. Lett.* **1991**, *16*, 1987.
(221) Hohenau, A.; Cagran, C.; Kranzelbinder, G.; Scherf, U.; Leising, G. *Adv. Mater.* **2001**, *13*, 1303.
(222) Samoc, M.; Samoc, A.; Luther-Davies, B.; Scherf, U. *Synth. Met.* **1997**, *87*, 197.
(223) Harrison, M. G.; Urbasch, G.; Mahrt, R. F.; Giessen, H.; Bassler, H.; Scherf, U. *Chem. Phys. Lett.* **1999**, *313*, 755.
(224) Liu, J.; Zhu, H.; Hu, Y.; Sun, D.; Li, F.; Sun, M. *Proc. SPIE—Int. Soc. Opt. Eng.* **2000**, *3939*, 252.
(225) Belfield, K. D.; Yao, S.; Morales, A. R.; Hales, J. M.; Hagan, D. J.; Van Stryland, E. W.; Chapela, V. M.; Percino, J. *Polym. Adv. Technol.* **2005**, *16*, 150.
(226) Adronov, A.; Frechet, J. M. J.; He, G. S.; Kim, K. S.; Chung, S. J.; Swiatkiewicz, J.; Prasad, P. N. *Chem. Mater.* **2000**, *12*, 2838.
(227) He, G. S.; Lin, T.-C.; Cui, Y.; Prasad, P. N.; Brousmiche, D. W.; Serin, J. M.; Frechet, J. M. J. *Opt. Lett.* **2003**, *28*, 768.
(228) (a) Brousmiche, D. W.; Serin, J. M.; Frechet, J. M. J.; He, G. S.; Lin, T. C.; Chung, S. J.; Prasad, P. N. *J. Am. Chem. Soc.* **2003**, *125*, 1448. (b) Brousmiche, D. W.; Serin, J. M.; Frechet, J. M. J.; He, G. S.; Lin, T. C.; Chung, S. J.; Prasad, P. N.; Kannan, R.; Tan, L. S. *J. Phys. Chem. B* **2004**, *108*, 8592.
(229) Hua, J. L.; Li, B.; Meng, F. S.; Ding, F.; Qian, S. X.; Tian, H. *Polymer* **2004**, *45*, 7143.
(230) (a) He, Q.; Bai, F.; Yang, J.; Lin, H.; Huang, H.; Yu, G.; Li, Y. *Thin Solid Films* **2002**, *417*, 183. (b) He, Q.; Huang, H.; Sun, Q.; Lin, H.; Yang, J.; Bai, F. *Polym. Adv. Technol.* **2004**, *15*, 43. (c) Li, C.; Liu, C.; Li, Q.; Gong, Q. *Chem. Phys. Lett.* **2004**, *400*, 569.
(231) Meng, F.; Liu, C.; Hua, J.; Cao, Y.; Chen, K.; Tian, H. *Eur. Polym. J.* **2003**, *39*, 1325.
(232) Mi, J.; Zhu, R.; You, G.; Li, B.; Liu, W.; Qian, S.; Meng, F.; Tian, H. *Mater. Sci. Forum* **2005**, *480−481*, 27.
(233) Tutt, L. W.; Kost, A. *Nature* **1992**, *356*, 225.
(234) Tutt, L. W.; Boggess, T. F. *Prog. Quantum Electron.* **1993**, *17*, 299.
(235) Drenser, K. A.; Larsen, R. J.; Strohkendl, F. P.; Dalton, L. R. *J. Phys. Chem. A* **1999**, *103*, 2290.
(236) Han, Y.; Zhang, W.; Gao, X.; Cui, Y.; Xia, Y.; Gu, G.; Zang, W.; Du, Y.; Feng, D. *Appl. Phys. Lett.* **1993**, *63*, 447.
(237) Lindle, J. R.; Pong, R. G. S.; Bartoli, F. J.; Kafafi, Z. H. *Phys. Rev. B* **1993**, *48*, 9447.
(238) Bezel, I. V.; Chekalin, S. V.; Matveets, Y. A.; Stepanov, A. G.; Yartsev, A. P.; Letokhov, V. S. *Chem. Phys. Lett.* **1994**, *218*, 475.
(239) Zhou, X.; Ren, A.-M.; Feng, J.-K. *THEOCHEM* **2004**, *680*, 237.
(240) Zhou, X.; Ren, A.-M.; Feng, J.-K.; Liu, X.-J. *Chin. J. Chem.* **2004**, *22*, 653.
(241) Rao, S. V.; Rao, D. N.; Akkara, J. A.; DeCristofano, B. S.; Rao, D. V. G. L. N. *Chem. Phys. Lett.* **1998**, *297*, 491.
(242) Strohkendl, F. P.; Axenson, T. J.; Larsen, R. J.; Dalton, L. R.; Hellwarth, R. W.; Kafafi, Z. H. *Proc SPIE—Int. Soc. Opt. Eng.* **1997**, *3142*, 2.
(243) Strohkendl, F. P.; Axenson, T. J.; Larsen, R. J.; Dalton, L. R.; Hellwarth, R. W.; Kafafi, Z. H. *J. Phys. Chem. B* **1997**, *101*, 8802.
(244) Strohkendl, F. P.; Axenson, T. J.; Larsen, R. J.; Dalton, L. R.; Hellwarth, R. W.; Kafafi, Z. H. *Chem. Phys. Lett.* **1999**, *245*, 285.
(245) (a) Liu, Z.-B.; Tian, J.-G.; Zang, W.-P.; Zhou, W.-Y.; Zhang, C.-P.; Zheng, J.-Y.; Zhou, Y.-C.; Xu, H. *Appl. Opt.* **2003**, *42*, 7072. (b) Meneghetti, M.; Fantinel, F.; Bozio, R. *Synth. Met.* **2003**, *137*, 1495. (c) Kohlman, R.; Klimov, V.; Grigorova, M.; Shi, X.; Mattes, B. R.; McBranch, D.; Wang, H.; Wudl, F.; Nogues, J. L.; Moreshead, W. *Proc. SPIE—Int. Soc. Opt. Eng.* **1997**, *3142*, 72.

(246) Boulle, C. M. C.; Bainville, M.; Gorgues, A.; Hudhomme, P.; Orduna, J.; Garin, J. *Tetrahedron Lett.* **1997**, *38*, 81.

(247) (a) Sahraoui, B.; Kityk, I. V.; Phu, X. N.; Hudhomme, P.; Gorgues, A. *Phys. Rev. B* **1999**, *59*, 9229. (b) Sahraoui, B.; Phu, X. N.; Kityk, I. V.; Hudhomme, P.; Gorgues, A. *MCLC S&T, Sect. B: Nonlin. Opt.* **1999**, *21*, 543. (c) Sahraoui, B.; Kityk, I. V.; Bielieninik, J.; Hudhomme, P.; Gorgues, A. *Opt. Mater.* **1999**, *13*, 349. (d) Sahraoui, B.; Kityk, I. V.; Bielieninik, J.; Hudhomme, P.; Gorgues, A. *Mater. Lett.* **1999**, *41*, 164.

(248) Bingel, C. *Chem. Ber.* **1993**, *126*, 1957.

(249) Chiang, L. Y.; Padmawar, P. A.; Canteenwala, T.; Tan, L.-S.; He, G. S.; Kannan, R.; Vaia, R.; Lin, T.-C.; Zheng, Q.; Prasad, P. N. *Chem. Commun.* **2002**, 1854.

(250) Padmawar, P. A.; Rogers, J. E.; He, G. S.; Chiang, L. Y.; Canteenwala, T.; Tan, L.-S.; Zheng, Q.; Slagle, J. E.; McLean, D. G.; Fleitz, P. A.; Prasad, P. N. *Chem. Mater.* **2006**, *18*, 4065.

(251) Zhao, Y.; Shirai, Y.; Slepkov, A. D.; Cheng, L.; Alemany, L. B.; Sasaki, T.; Hegmann, F. A.; Tour, J. M. *Chem.—Eur. J.* **2005**, *11*, 3643.

(252) (a) Slepkov, Aaron D.; Hegmann, Frank A.; Kamada, Kenji; Zhao, Yuming; Tykwinski, Rik R. *J. Opt. A: Pure Appl. Opt.* **2002**, *4*, S207. (b) Slepkov, A. D.; Hegmann, F. A.; Zhao, Y.; Tykwinski, R. R.; Kamada, K. *J. Chem. Phys.* **2002**, *116*, 3834.

(253) McCleverty, J. A. *Prog. Inorg. Chem.* **1968**, *10*, 49.

(254) Schrauzer, G. N. *Acc. Chem. Res.* **1969**, *2*, 72.

(255) (a) Muller-Westerhoff, U. T.; Vance, B.; Yoon, D. I. *Tetrahedron* **1991**, *47*, 909. (b) Hill, C. A. S.; Underhill, A. E.; Charlton, A.; Winter, C. S.; Oliver, S. N.; Rush, J. D. *Proc. SPIE—Int. Soc. Opt. Eng.* **1993**, *1775*, 43.

(256) Reynolds, G. A.; Drexhage, K. H. *J. Appl. Phys.* **1975**, *46*, 4852.

(257) Hill, C. A. S.; Charlton, A.; Underhill, A. E.; Malik, K. M. A.; Hursthouse, M. B.; Karaulov, A. I.; Oliver, S. N.; Kershaw, S. V. *J. Chem. Soc., Dalton Trans.* **1995**, 587.

(258) (a) Cummings, S. D.; Cheng, L.-T.; Eisenberg, R. *Chem. Mater.* **1997**, *9*, 440. (b) Chen, C. T.; Liao, S. Y.; Lin, K. J.; Lai, L. L. *Adv. Mater.* **1998**, *10*, 334. (c) Dai, J.; Bian, G.-Q.; Wang, X.; Xu, Q.-F.; Zhou, M.-Y.; Munakata, M.; Maekawa, M.; Tong, M.-H.; Sun, Z.-R.; Zeng, H.-P. *J. Am. Chem. Soc.* **2000**, *122*, 11007.

(259) (a) Winter, C. S.; Hill, C. A. S.; Underhill, A. E. *Appl. Phys. Lett.* **1991**, *58*, 107. (b) Zuo, J.-L.; Yao, T.-M.; You, F.; You, X.-Z.; Fun, H.-K.; Yip, B.-C. *J. Mater. Chem.* **1996**, *6*, 1633. (c) Ushijima, H.; Kawasaki, T.; Kamata, T.; Kodzasa, T.; Matsuda, H.; Fukaya, T.; Fujii, Y.; Mizukami, F. *Mol. Cryst. Liq. Cryst. S&T Sect. A: Mol. Cryst. Liq. Cryst.* **1996**, *286*, 597.

(260) Winter, C. S.; Manning, R. J.; Oliver, S. N.; Hill, C. A. S. *Opt. Commun.* **1992**, *90*, 139.

(261) (a) Kershaw, S. V. *Optoelectron. Prop. Inorg. Compd.* **1999**, 349. (b) Kershaw, S. V.; Oliver, S. N.; Manning, R. J.; Rush, J. D.; Hill, C. A.; Underhill, A. E.; Charlton. *Proc. SPIE—Int. Soc. Opt. Eng.* **1993**, *2025*, 388.

(262) (a) Le Bouder, T.; Maury, O.; Bondon, A.; Costuas, K.; Amouyal, E.; Ledoux, I.; Zyss, J.; Le Bozec, H. *J. Am. Chem. Soc.* **2003**, *125*, 12284. (b) Juris, A.; Campagna, S.; Bidd, I.; Lehn, J. M.; Ziessel, R. *Inorg. Chem.* **1988**, *27*, 4007. (c) Le Bouder, T.; Viau, L.; Guegan, J.-P.; Maury, O.; Le Bozec, H. *Eur. J. Org. Chem.* **2002**, 3024. (d) Le Bozec, H.; Le Bouder, T.; Maury, O.; Bondon, A.; Ledoux, I.; Deveau, S.; Zyss, J. *Adv. Mater.* **2001**, *13*, 1677.

(263) (a) Maury, O.; Lacour, J.; Le Bozec, H. *Eur. J. Inorg. Chem.* **2001**, 201. (b) Hilton, A.; Renouard, T.; Maury, O.; Le Bozec, H.; Ledoux, I.; Zyss, J. *Chem. Commun.* **1999**, 2521.

(264) Ziessel, R.; Juris, A.; Venturi, M. *Inorg. Chem.* **1998**, *37*, 5061.

(265) Liu, X.-J.; Feng, J.-K.; Ren, A.-M.; Cheng, H.; Zhou, X. *J. Chem. Phys.* **2004**, *120*, 11493.

(266) Righetto, S.; Rondena, S.; Locatelli, D.; Roberto, D.; Tessore, F.; Ugo, R.; Quici, S.; Roma, S.; Korystov, D.; Srdanov, V. I. *J. Mater. Chem.* **2006**, *16*, 1439.

(267) Wecksler, S. R.; Mikhailovsky, A.; Korystov, D.; Ford, P. C. *J. Am. Chem. Soc.* **2006**, *128*, 3831.

(268) (a) Zhang, M.-L.; Tian, Y.-P.; Zhang, X.-J.; Wu, J.-Y.; Zhang, S.-Y.; Wang, D.; Jiang, M.-H.; Chantrapromm, S.; Fun, H.-K. *Transition Met. Chem.* **2004**, *29*, 596. (b) Tian, Y.-P.; Zhang, M.-L.; Hu, Z.-J.; Hu, H.-M.; Wu, J.-Y.; Zhang, X.-J.; Zhang, S.-Y.; Tao, X.-T.; Jiang, M.-H.; Chen, H.-P.; Chantrapromma, S.; Fun, H.-K. *Transition Met. Chem.* **2005**, *30*, 778.

(269) Das, S.; Nag, A.; Goswami, D.; Bharadwaj, P. K. *J. Am. Chem. Soc.* **2006**, *128*, 402.

(270) Maciel, G. S.; Kim, K.-S.; Chung, S.-J.; Swiatkiewicz, J.; He, G. S.; Prasad, P. N. *J. Phys. Chem. B* **2001**, *105*, 3155.

(271) Piszczek, G.; Maliwal, B. P.; Gryczynski, I.; Dattelbaum, J.; Lakowicz, J. R. *J. Fluoresc.* **2001**, *11*, 101.

(272) Piszczek, G.; Gryczynski, I.; Maliwal, B. P.; Lakowicz, J. R. *J. Fluoresc.* **2002**, *12*, 15.

(273) Luo, L.; Lai, W. P.-W.; Wong, K.-L.; Wong, W.-T.; Li, K.-F.; Cheah, K.-W. *Chem. Phys. Lett.* **2004**, *398*, 372.

(274) (a) Wong, K.-L.; Law, G.-L.; Kwok, W.-M.; Wong, W.-T.; Phillips, D. L. *Angew. Chem., Int. Ed.* **2005**, *44*, 3436. (b) Rodgers, S. J.; Lee, C. W.; Ng, C. Y.; Raymond, K. N. *Inorg. Chem.* **1987**, *26*, 1622. (c) Po-Wan Lai, W.; Wong, W.-T. *New J. Chem.* **2000**, *24*, 943.

(275) Chandra, S. K.; Chakravorty, A. *Inorg. Chem.* **1992**, *31*, 760.

(276) Cohen, S. M.; Meyer, M.; Raymond, K. N. *J. Am. Chem. Soc.* **1998**, *120*, 6277.

(277) Fu, L.-M.; Wen, X.-F.; Ai, X.-C.; Sun, Y.; Wu, Y.-S.; Zhang, J.-P.; Wang, Y. *Angew. Chem., Int. Ed.* **2005**, *44*, 747.

(278) Yang, C.; Fu, L.-M.; Wang, Y.; Zhang, J.-P.; Wong, W.-T.; Ai, X.-C.; Qiao, Y.-F.; Zou, B.-S.; Gui, L.-L. *Angew. Chem., Int. Ed.* **2004**, *43*, 5010.

(279) (a) Tsuboya, N.; Hamasaki, R.; Ito, M.; Mitsuishi, M.; Miyashita, T.; Yamamoto, Y. *J. Mater. Chem.* **2003**, *13*, 511. (b) Yuan, W.; Sun, L.; Tang, H.; Wen, Y.; Jiang, G.; Huang, W.; Jiang, L.; Song, Y.; Tian, H.; Zhu, D. *Adv. Mater.* **2005**, *17*, 156.

(280) Zheng, Q.; He, G. S.; Lu, C.; Prasad, P. N. *J. Mater. Chem.* **2005**, *15*, 3488.

(281) Rangel-Rojo, R.; Kimura, K.; Matsuda, H.; Mendez-Rojas, M. A.; Watson, W. H. *Opt. Commun.* **2003**, *228*, 181.

(282) Powell, C. E.; Humphrey, M. G. *Coord. Chem. Rev.* **2004**, *248*, 725.

(283) (a) Hurst, S. K.; Cifuentes, M. P.; Morrall, J. P. L.; Lucas, N. T.; Whittall, I. R.; Humphrey, M. G.; Asselberghs, I.; Persoons, A.; Samoc, M.; Luther-Davies, B.; Willis, A. C. *Organometallics* **2001**, *20*, 4664. (b) Powell, C. E.; Morrall, J. P.; Ward, S. A.; Cifuentes, M. P.; Notaras, E. G. A.; Samoc, M.; Humphrey, M. G. *J. Am. Chem. Soc.* **2004**, *126*, 12234. (c) Powell, C. E.; Cifuentes, M. P.; Morrall, J. P.; Stranger, R.; Humphrey, M. G.; Samoc, M.; Luther-Davies, B.; Heath, G. A. *J. Am. Chem. Soc.* **2003**, *125*, 602. (d) Powell, C. E.; Humphrey, M. G.; Morrall, J. P.; Samoc, M.; Luther-Davies, B. *J. Phys. Chem. A* **2003**, *107*, 11264. (e) Hurst, S. K.; Lucas, N. T.; Humphrey, M. G.; Isoshima, T.; Wostyn, K.; Asselberghs, I.; Clays, K.; Persoons, A.; Samoc, M.; Luther-Davies, B. *Inorg. Chim. Acta* **2003**, *350*, 62. (f) Hurst, S. K.; Humphrey, M. G.; Morrall, J. P.; Cifuentes, M. P.; Samoc, M.; Luther-Davies, B.; Heath, G. A.; Willis, A. C. *J. Organomet. Chem.* **2003**, *670*, 56. (g) Hurst, S. K.; Cifuentes, M. P.; McDonagh, A. M.; Humphrey, M. G.; Samoc, M.; Luther-Davies, B.; Asselberghs, I.; Persoons, A. *J. Organomet. Chem.* **2002**, *642*, 259. (h) Hurst, S. K.; Humphrey, M. G.; Isoshima, T.; Wostyn, K.; Asselberghs, I.; Clays, K.; Persoons, A.; Samoc, M.; Luther-Davies, B. *Organometallics* **2002**, *21*, 2024.

(284) (a) Hagihara, N.; Sonogashira, K.; Takahashi, S. In *Advances in Polymer Science and Speciality Polymers*; Springer: Berlin/Heidelberg, 1981; Vol. 41, pp 149—179. (b) Sonogashira, K.; Fujikura, Y.; Yatake, T.; Toyoshima, N.; Takahashi, S.; Hagihara, N. *J. Organomet. Chem.* **1978**, *145*, 101.

(285) (a) Nguyen, P.; Lesley, G.; Marder, T. B.; Ledoux, I.; Zyss, J. *Chem. Mater.* **1997**, *9*, 406. (b) Casalboni, M.; Sarcinelli, F.; Pizzoferrato, R.; D'Amato, R.; Furlani, A.; Russo, M. V. *Chem. Phys. Lett.* **2000**, *319*, 107. (c) Lewis, J.; Long, N. J.; Raithby, P. R.; Shields, G. P.; Wong, W.-Y.; Younus, M. *J. Chem. Soc., Dalton Trans.* **1997**, 4283. (d) Bruce, M. I.; Davy, J.; Hall, B. C.; Van Galen, Y. J.; Skelton, B. W.; White, A. H. *Appl. Organomet. Chem.* **2002**, *16*, 559. (e) Khan, M. S.; Schwartz, D. J.; Pasha, N. A.; Kakkar, A. K.; Lin, B.; Raithby, P. R.; Lewis, J. *Z. Anorg. Allg. Chem.* **1992**, *616*, 121. (f) Haskins-Glusac, K.; Ghiviriga, I.; Abboud, K. A.; Schanze, K. S. *J. Phys. Chem. B* **2004**, *108*, 4969. (g) Chawdhury, N.; Koehler, A.; Friend, R. H.; Younus, M.; Long, N. J.; Raithby, P. R.; Lewis, J. *Macromolecules* **1998**, *31*, 722. (h) D'Amato, R.; Furlani, A.; Colapietro, M.; Portalone, G.; Casalboni, M.; Falconieri, M.; Russo, M. V. *J. Organomet. Chem.* **2001**, *627*, 13. (i) Desroches, C.; Lopes, C.; Kessler, V.; Parola, S. *Dalton Trans.* **2003**, 2085. (j) Sun, W.; Wu, Z.-X.; Yang, Q.-Z.; Wu, L.-Z.; Tung, C.-H. *Appl. Phys. Lett.* **2003**, *82*, 850.

(286) McKay, T. J.; Staromlynska, J.; Wilson, P.; Davy, J. *J. Appl. Phys.* **1999**, *85*, 1337.

(287) Staromlynska, J.; McKay, T. J.; Wilson, P. *J. Appl. Phys.* **2000**, *88*, 1726.

(288) Vestberg, R.; Westlund, R.; Eriksson, A.; Lopes, C.; Carlsson, M.; Eliasson, B.; Glimsdal, E.; Lindgren, M.; Malmstroem, E. *Macromolecules* **2006**, *39*, 2238.

(289) (a) Bonnett, R. *Chem. Soc. Rev.* **1995**, *24*, 19. (b) Prasad, P. N. *Introduction to Biophotonics*; Wiley-Interscience: Hoboken, NJ, 2003; Chapter 12 and references therein.

(290) Perry, J. W. Organic and metal-containing reverse saturable absorbers for optical limiters. In *Nonlinear Optics of Organic Molecules and Polymers*; Nalwa, H. S., Miyata, S., Eds.; CRC: Boca Raton, FL, 1997; pp 813—840.

(291) (a) Vsevolodov, N. N.; Kostikov, A. P.; Kayushin, L. P.; Gorbatenkov, V. I. *Biofizika* **1973**, *18*, 755. (b) Meshalkin, Y. P.; Chunosova, S.

S. *Quant. Electron.* **2005**, *35*, 527. (c) Goyan, R. L.; Cramb, D. T. *Photochem. Photobiol.* **2000**, *72*, 821. (d) Dichtel, W. R.; Serin, J. M.; Edder, C.; Frechet, J. M. J.; Matuszewski, M.; Tan, L. S.; Ohulchanskyy, T. Y.; Prasad, P. N. *J. Am. Chem. Soc.* **2004**, *126*, 5380. (e) Oar, M. A.; Serin, J. M.; Dichtel, W. R.; Frechet, J. M. J.; Ohulchanskyy, T. Y.; Prasad, P. N. *Chem. Mater.* **2005**, *17*, 2267.

(292) (a) Drobizhev, M.; Karotki, A.; Kruk, M.; Rebane, A. *Chem. Phys. Lett.* **2002**, *355*, 175. (b) Drobizhev, M.; Karotki, A.; Kruk, M.; Mamardashvili, N. Z.; Rebane, A. *Chem. Phys. Lett.* **2002**, *361*, 504. (c) Karotki, A.; Drobizhev, M.; Kruk, M.; Spangler, C.; Nickel, E.; Mamardashvili, N.; Rebane, A. *J. Opt. Soc. Am. B* **2003**, *20*, 321. (d) Drobizhev, M.; Karotki, A.; Kruk, M.; Krivokapic, A.; Anderson, H. L.; Rebane, A. *Chem. Phys. Lett.* **2003**, *370*, 690. (It should be pointed out that such one-photon resonance (Q-band) enhanced 2PA is not the same as all the other 2PA processes discussed in this review. In the excitation spectral region of 710−810 nm of these porphyrins, the two-photon absorptivity is resonantly enhanced due to the nearby Q(0−0) one-photon transition serving as a near-resonance intermediate state, whereas linear absorption is essentially nonexistent in the excitation range in strictly two-photon absorbing chromophores.)

(293) Frampton, M. J.; Akdas, H.; Cowley, A. R.; Rogers, J. E.; Slagle, J. E.; Fleitz, P. A.; Drobizhev, M.; Rebane, A.; Anderson, H. L. *Org. Lett.* **2005**, *7*, 5365.

(294) (a) Karotki, A.; Drobizhev, M.; Dzenis, Y.; Taylor, P. N.; Anderson, H. L.; Rebane, A. *Phys. Chem. Chem. Phys.* **2004**, *6*, 7. (b) Drobizhev, M.; Stepanenko, Y.; Dzenis, Y.; Karotki, A.; Rebane, A.; Taylor, P. N.; Anderson, H. L. *J. Phys. Chem. B* **2005**, *109*, 7223.

(295) Ogawa, K.; Ohashi, A.; Kobuke, Y.; Kamada, K.; Ohta, K. *J. Phys. Chem. B* **2005**, *109*, 22003.

(296) Ogawa, K.; Ohashi, A.; Kobuke, Y.; Kamada, K.; Ohta, K. *J. Am. Chem. Soc.* **2003**, *125*, 13356.

(297) (a) Rath, H.; Prabhuraja, V.; Chandrashekar, T. K.; Nag, A.; Goswami, D.; Joshi, B. S. *Org. Lett.* **2006**, *8*, 2325. (b) Misra, R.; Kumar, R.; Chandrashekar, T. K.; Nag, A.; Goswami, D. *Org. Lett.* **2006**, *8* (4), 629.

(298) Drobizhev, M.; Meng, F.; Rebane, A.; Stepanenko, Y.; Nickel, E.; Spangler, C. W. *J. Phys. Chem. B* **2006**, *110*, 9802.

(299) Kim, D. Y.; Ahn, T. K.; Kwon, J. H.; Kim, D.; Ikeue, T.; Aratani, N.; Osuka, A.; Shigeiwa, M.; Maeda, S. *J. Phys. Chem. A* **2005**, *109*, 2996.

(300) Wen, T. C.; Hwang, L. C.; Lin, W. Y.; Chen, C. H.; Wu, C. H. *Chem. Phys.* **2003**, *286*, 293.

(301) Rath, H.; Sankar, J.; PrabhuRaja, V.; Chandrashekar, T. K.; Nag, A.; Goswami, D. *J. Am. Chem. Soc.* **2005**, *127*, 11608.

(302) Inokuma, Y.; Ono, N.; Uno, H.; Kim, D. Y.; Noh, S. B.; Kim, D.; Osuka, A. *Chem. Commun.* **2005**, 3782.

(303) Humphrey, J.; Kuciauskas, D. *J. Phys. Chem. B* **2004**, *108*, 12016.

(304) Ikeda, C.; Yoon, Z. S.; Park, M.; Inoue, H.; Kim, D.; Osuka, A. *J. Am. Chem. Soc.* **2005**, *127*, 534.

(305) Collini, E.; Ferrante, C.; Bozio, R.; Lodi, A.; Ponterini, G. *J. Mater. Chem.* **2006**, *16*, 1573.

(306) Larson Daniel, R.; Zipfel Warren, R.; Williams Rebecca, M.; Clark Stephen, W.; Bruchez Marcel, P.; Wise Frank, W.; Webb Watt, W. *Science* **2003**, *300*, 1434.

(307) Yao, J.; Larson, D. R.; Vishwasrao, H. D.; Zipfel, W. R.; Webb, W. W. *Proc. Natl. Acad. Sci. U.S.A.* **2005**, *102*, 14284.

(308) Nithisoontorn, M.; Unterrainer, K.; Michaelis, S.; Sawaki, N.; Gornik, E.; Kano, H. *Phys. Rev. Lett.* **1989**, *62*, 3078.

(309) Cingolani, R.; Lepore, M.; Tommasi, R.; Catalano, I. M.; Lage, H.; Heitmann, D.; Ploog, K.; Shimizu, A.; Sakaki, H.; Ogawa, T. *Phys. Rev. Lett.* **1992**, *69*, 1276.

(310) Banyai, L.; Lindberg, M.; Koch, S. W. *Opt. Lett.* **1988**, *13*, 212.

(311) Etienne, M.; Biney, A.; Walser, A. D.; Dorsinville, R.; Bauer, D. L. V.; Balogh-Nair, V. *Appl. Phys. Lett.* **2005**, *87*, 181913/1.

(312) Gao, Y.; Huong, N. Q.; Birman, J. L.; Potasek, M. J. *J. Appl. Phys.* **2004**, *96*, 4839.

(313) He, J.; Mi, J.; Li, H.; Ji, W. *J. Phys. Chem. B* **2005**, *109*, 19184.

(314) Herda, R.; Hakulinen, T.; Suomalainen, S.; Okhotnikov, O. G. *Appl. Phys. Lett.* **2005**, *87*, 211105/1.

(315) Jarjour, A. F.; Green, A. M.; Parker, T. J.; Taylor, R. A.; Oliver, R. A.; Briggs, G. A. D.; Kappers, M. J.; Humphreys, C. J.; Martin, R. W.; Watson, I. M. *Physica E* **2006**, *32*, 119.

(316) Ju, H.; Uskov, A. V.; Noetzel, R.; Li, Z.; Molina Vazquez, J.; Lenstra, D.; Khoe, G. D.; Dorren, H. J. S. *Appl. Phys. B* **2006**, *82*, 615.

(317) Kang, K. I.; McGinnis, B. P.; Sandalphon; Hu, Y. Z.; Koch, S. W.; Peyghambarian, N.; Mysyrowicz, A.; Liu, L. C.; Risbud, S. H. *Phys. Rev. B* **1992**, *45*, 3465.

(318) Lami, J.-F.; Gilliot, P.; Hirlimann, C. *Phys. Rev. Lett.* **1996**, *77*, 1632.

(319) Padilha, L. A.; Fu, J.; Hagan, D. J.; Van Stryland, E. W.; Cesar, C. L.; Barbosa, L. C.; Cruz, C. H. B. *Opt. Exp.* **2005**, *13*, 6460.

(320) Paskov, P. P.; Holtz, P. O.; Monemar, B.; Garcia, J. M.; Schoenfeld, W. V.; Petroff, P. M. *Appl. Phys. Lett.* **2000**, *77*, 812.

(321) Li, Q.; Liu, C.; Liu, Z.; Gong, Q. *Opt. Exp.* **2005**, *13*, 1833.

(322) Wang, X. D. Y.; Ding, S.; Fan, L.; Shi, X.; Wang, Q.; Xiong, G. *Physica E* **2005**, *30*, 96.

(323) Ispasoiu, R. G.; Jin, Y.; Lee, J.; Papadimitrakopoulos, F.; Goodson, T., III. *Nano Lett.* **2002**, *2*, 127.

(324) (a) Cohanoschi, I.; Hernandez, F. E. *J. Phys. Chem. B* **2005**, *109*, 14506. (b) Farrer, R. A.; Butterfield, F. L.; Chen, V. W.; Fourkas, J. T. *Nano Lett.* **2005**, *5*, 1139.

(325) Majchrowski, A.; Ebothe, J.; Fuks-Janczarek, I.; Makowska-Janusik, M.; Sahraoui, B.; Kityk, I. V. *Opt. Mater.* **2005**, *27*, 675.

(326) Zhang, X. J.; Tian, Y. P.; Jin, F.; Wu, J. Y.; Xie, Y.; Tao, X. T.; Jiang, M. H. *Cryst. Growth Des.* **2005**, *5*, 565.

(327) Wenseleers, W. S. F.; Meyer-Friedrichsen, T.; Mangel, T.; Bauer, C. A.; Pond, S. J. K.; Marder, S. R.; Perry, J. W. *J. Phys. Chem. B* **2002**. *106*, 6853.

(328) (a) Lal, M.; Levy, L.; Kim, K. S.; He, G. S.; Wang, X.; Min, Y. H.; Pakatchi, S.; Prasad, P. N *Chem. Mater.* **2000**, *12*, 2632−2639. (b) Kim, S.; Pudavar, H. E.; Prasad, P. N. *Chem. Commun.* **2006**, 2071−2073. (c) Kim, S.; Zheng, Q.; He, G. S.; Bharali, D. J.; Pudavar, H. E.; Baev, A.; Prasad, P. N. *Adv. Funct. Mater.* **2006**, *16*, 2317.

(329) Gut, I. G.; Hefetz, Y.; Kochevar, I. E.; Hillenkamp, F. *J. Phys. Chem.* **1993**, *97*, 5171.

(330) Stanley, R. J.; Hou, Z.; Yang, A.; Hawkins, M. E. *J. Phys. Chem.* **2005**, *109*, 3690.

(331) Shear, J. B.; Brown, E. B.; Webb, W. W. *Anal. Chem.* **1996**, *68*, 1778.

(332) Xu, C.; Zipfel, W.; Shear, J. B.; Williams, R. M.; Webb, W. W. *Proc. Natl. Acad. Sci. U.S.A.* **1996**, *93*, 10763.

(333) Kirkpatrick, S. M.; Naik, R. R.; Stone, M. O. *J. Phys. Chem. B* **2001**, *105*, 2867.

(334) Gryczynski, I.; Piszczek, G.; Lakowicz, J. R.; Lagarias, J. C. *J. Photochem. Photobiol., A* **2002**, *150*, 13.

(335) Andrade, A. A.; Barbosa Neto, N. M.; Misoguti, L.; De Boni, L.; Zilio, S. C.; Mendonca, C. R. *Chem. Phys. Lett.* **2004**, *390*, 506.

(336) Yariv, A. *Optical Electronics*, 3rd ed.; Holt, Rinehart & Winston: New York, 1985; pp 28−34.

(337) Boggess, T. F.; Bohnert, K. M.; Mansour, K.; Moss, S. C.; Boyd, I. W.; Smirl, A. L. *IEEE J. Quantum Electron.* **1986**, *QE-22*, 360.

(338) Van Stryland, E. W.; Sheik-Bahae, M. *Opt. Eng.* **1998**, *60*, 655.

(339) (a) Yu, B.; Zhu, C.; Gan, F.; Wu, X.; Zhang, G.; Tang, G.; Chen, W. *Opt. Mater.* **1997**, *8*, 249. (b) Attias, A.-J.; Cavalli, C.; Lemaitre, N.; Cherioux, F.; Maillotte, H.; Ledoux, I.; Zyss, J. *J. Opt. A: Pure Appl. Opt.* **2002**, *4*, S212−S220.

(340) (a) Guo, S.-L.; Xu, L.; Wang, H.-T.; You, X.-Z.; Ming, N. B. *Opt. Quantum Electron.* **2003**, *35*, 693. (b) Gopinath, J. T.; Soljacic, M.; Ippen, E. P.; Fuflyigin, V. N.; King, W. A.; Shurgalin, M. *J. Appl. Phys.* **2004**, *96*, 6931.

(341) (a) Xu, C.; Webb, W. W. *J. Opt. Soc. Am. B* **1996**, *13*, 481. (b) Aslanidi, E. B.; Tikhonov, E. A. *Opt. Spectrosc.* **1974**, *37*, 446.

(342) Ehrlich, J. E.; Wu, X. L.; Lee, I.-Y. S.; Hu, Z.-Y.; Rockel, H.; Marder, S. R.; Perry, J. W. *Opt. Lett.* **1997**, *22*, 1843.

(343) Perry, J. W.; Barlow, S.; Ehrlich, J. E.; Heikal, A. A.; Hu, Z.-Y.; Lee, L.-Y. S.; Mansour, K.; Marder, S. R.; Rockel, H.; Rumi, M.; Thayumanavan, S.; Wu, X. L. *Nonlinear Opt.* **1999**, *21*, 225.

(344) Lakowicz, J. R. *Principles of Fluorescent Spectroscopy*; Kluwer Academic/Plenum: New York, 1999; Chapters 5 and 6.

(345) (a) Thomas, J.; Anija, M.; Cyriac, J.; Pradeep, T.; Philip, R. *Chem. Phys. Lett.* **2005**, *403*, 308. (b) Schiccheri, N.; Meneghetti, M. *J. Phys. Chem. A* **2005**, *109*, 4643.

(346) Penzkofer, A.; Falkenstein, W. *Opt. Commun.* **1976**, *16*, 247.

(347) He, G. S.; Lin, T.-C.; Prasad, P. N. *Opt. Exp.* **2004**, *12*, 5952.

(348) He, G. S.; Lu, C.; Zheng, Q.; Prasad, P. N.; Zerom, P.; Boyd, R. W.; Samoc, M. *Phys. Rev. A* **2005**, *71*, 063810/1.

(349) He, G. S.; Zheng, Q.; Prasad, P. N. *J. Opt. Soc. Am.* B **2007**, *24*, 1166.

(350) Schroeder, R.; Ullrich, B. *Opt. Lett.* **2002**, *27*, 1285.

(351) He, G. S.; Zheng, Q.; Baev, A.; Prasad, P. N. *J. Appl. Phys.* **2007**, *101*, 083108.

(352) He, G. S.; Lin, T.-C.; Dai, J.; Prasad, P. N.; Kannan, R.; Dombroskie, A. G.; Vaia, R. A.; Tan, L.-S. *J. Chem. Phys.* **2004**, *120*, 5275.

(353) Wang, X.; Wang, D.; Zhou, G.; Yu, W.; Zhou, Y.; Fang, Q.; Jiang, M. *J. Mater. Chem.* **2001**, *11*, 1600.

(354) Lei, H.; Huang, Z. L.; Wang, H. Z.; Tang, X. J.; Wu, L. Z.; Zhou, G. Y.; Wang, D.; Tian, Y. B. *Chem. Phys. Lett.* **2002**, *352*, 240.

(355) Cha, M.; Torruellas, W. E.; Stegeman, G. I.; Horsthuis, W. H. G.; Mohlmann, G. R.; Meth, J. *Appl. Phys. Lett.* **1994**, *65*, 2648.

(356) (a) Drobizhev, M.; Karotki, A.; Kruk, M.; Dzenis, Yu.; Rebane, A.; Suo, Z.; Spangler, C. W. *J. Phys. Chem. B* **2004**, *108*, 4221. (b) Suo, Z.; Drobizhev, M.; Spangler, C. W.; Christensson, N.; Rebane, A. *Org. Lett.* **2005**, *7*, 4807.

(357) Swofford, R. L.; McClain, W. M. *Rev. Sci. Instrum.* **1975**, *46*, 246.

(358) Gass, P. A.; Abram, I.; Raj, R.; Schott, M. *J. Chem. Phys.* **1994**, *100*, 88.

(359) Feneyrou, P.; Doclot, O.; Block, D.; Baldeck, P. L.; Delysse, S.; Nunzi, J. M. *Opt. Lett*. **1997**, *22*, 1132.
(360) (a) Alfano, R. R.; Shapiro, S. L. *Phys. Rev. Lett*. **1970**, *24*, 584. (b) Alfano, R. R., Ed. *The Supercontinuum Laser Sources*; Springer-Verlag: New York, 1989.
(361) Busch, G. E.; Jones, R. P.; Rentzepis, P. M. *Chem. Phys. Lett*. **1973**, *18*, 178.
(362) Balu, M.; Hales, J.; Hagan, D. J.; Van, Stryland, E. W. *Opt. Exp*. **2004**, *12*, 3820.
(363) Collini, E.; Ferrante, C.; Bozio, R. *J. Phys. Chem. B* **2005**, *109*, 2.
(364) Negres, R. A.; Van Stryland, E. W.; Hagan, D. J.; Belfield, K. D.; Schafer, K. J.; Przhonska, O. V.; Reinhardt, B. A. *Proc. SPIE—Int. Soc. Opt. Eng*. **1999**, *3796*, 88.
(365) (a) Negres, R. A.; Hales, J. M.; Kobyakov, A.; Hagan, D. J.; Van Stryland, E. W. *IEEE J. Quantum Electron.* **2002**, *38*, 1205. (b) Negres, R. A.; Hales, J. M.; Kobyakov, A.; Hagan, D. J.; Van Stryland, E. W. *Opt. Lett*. **2002**, *27*, 270.
(366) He, G. S.; Lin, T.-C.; Prasad, P. N. *Opt. Exp.* **2002**, *10*, 566.
(367) Zheng, Q.; He, G. S.; Baev, A.; Prasad, P. N. *J. Phys. Chem. B* **2006**, *110*, 14604.
(368) Hernandez, F. E.; Belfield, K. D.; Cohanoschi, I. *Chem. Phys. Lett*. **2004**, *391*, 22.
(369) Cohanoschi, I.; Belfield, K. D.; Hernandez, F. E. *Chem. Phys. Lett*. **2005**, *406*, 462.
(370) Wang, Y.; Tai, O. Y.-H.; Wang, C. H.; Jen, A. K.-Y. *J. Chem. Phys*. **2004**, *121*, 7901.
(371) He, G. S.; Lu, C.; Zheng, Q.; Baev, A.; Samoc, M.; Prasad, P. N. *Phys. Rev. A* **2006**, *73*, 033815/1.
(372) (a) Goodson, T., III. *Acc. Chem. Res*. **2005**, *38*, 99. (b) Lahankar, S. A.; West, R.; Varnavski, O.; Xie, X.; Goodson, T., III; Sukhomlinova, L.; Twieg, R. *J. Chem. Phys*. **2004**, *120*, 337.
(373) (a) Varnavski, O.; Leanov, A.; Liu, L.; Takacs, J.; Goodson, T., III. *Phys. Rev. B* **2000**, *61*, 12732. (b) Varnavski, O.; Samuel, I. D. W.; Palsson, L.-O.; Beavington, R.; Burn, P. L.; Goodson, T., III. *J. Chem. Phys*. **2002**, *116*, 8893. (c) Varnavski, O.; Goodson, T., III; Sukhomlinova, L.; Twieg, R. *J. Phys. Chem. B* **2004**, *108*, 10484.
(374) Wang, Y.; He, G. S.; Prasad, P. N.; Goodson, T., III. *J. Am. Chem. Soc*. **2005**, *127*, 10128.
(375) Peticolas, W. L.; Goldsborough, J. P.; Rieckhoff, K. E. J. *Phys. Rev. Lett*. **1963**, *10*, 43.
(376) Peticolas, W. L.; Rieckhoff, K. E. *J. Chem. Phys*. **1963**, *39*, 1347.
(377) Rentzepis, P. M.; Mitschele, C. J.; Saxman, A. C. *Appl. Phys. Lett.* **1970**, *17*, 122.
(378) Seldon, A. C.; Coll, R. H. *Nature (London), Phys. Sci.* **1971**, *229*, 210.
(379) Giordmaine, J. A.; Rentzepis, Shapiro, S. L.; Wecht, K. W. *Appl. Phys. Lett*. **1967**, *11*, 216.
(380) Basov, N. G.; Grasyuk, A. G.; Zubarev, I. G.; Katulin, V. A. *JETP Lett.* **1965**, *1*, 118.
(381) Basov, N. G.; Grasyuk, A. Z.; Zubarev, I. G.; Katulin, V. A. *Soviet Physics-Solid State* **1966**, *7*, 2932.
(382) Patel, C. K. N.; Fleury, P. A.; Slusher, R. E.; Frisch, H. L. *Phys. Rev. Lett*. **1966**, *16*, 971.
(383) Manlief, S. K.; Palik, E. D. *Appl. Phys. Lett*. **1973**, *22*, 443.
(384) Yoshida. T.; Miyazaki. K.; Fujisawa, K. Japanese *J. Appl. Phys*. **1975**, *14*, 1987.
(385) Bloom, D. M.; Yardley, J. T.; Young, J. F.; Harris, S. E. *Appl. Phys. Lett*. **1974**, *24*, 427.
(386) Willenberg, G. D.; Weiss, C. O.; Jones, H. *Appl. Phys. Lett*. **1980**, *37*, 133.
(387) Goldstone, J.; Jacoby, M.; Harris, D.; Stone, J. *Laser Focus World* **1991**, *27*, 27.
(388) Miller, John C. *Phys. Rev. A* **1989**, *40*, 6969.
(389) Auyeung, R. C. Y.; Cooper, D. G.; Kim, S.; Feldman, B. J. *Opt. Commun*. **1990**, *79*, 207.
(390) Tserepi, A. D.; Wurzberg, E.; Miller. T. A. *Chem. Phys. Lett*. **1997**, *265*, 297.
(391) Rapp, W.; Gronau, B. *Chem. Phys. Lett*. **1971**, *8*, 529.
(392) Topp, M. R.; Rentzepis, P. M. *Phys. Rev. A* **1971**, *3*, 358.
(393) Rubinov, A. N.; Richardson, M. C.; Sala, K.; Alcock, A. J. *Appl. Phys. Lett*. **1975**, *27*, 358.
(394) Prokhorenko, V. I.; Tikhonov, E. A.; Shpak, M. T. *Sov. J. Quantum Electron*. **1981**, *11*, 139.
(395) Qiu, P.; Penzkofer, A. *Appl. Phys. B* **1989**, *48*, 115.
(396) Zaporozhchenko, V. A.; Kachinskii, A. V.; Korol'kov, M. V.; Chenkhlov, O. V. *Sov. J. Quantum. Electron*. **1989**, *19*, 1179.
(397) Kwok, A. S.; Serpenguzel, A.; Hsieh, W. F.; Chang, R. K.; Gillespie, J. B. *Opt. Lett*. **1992**, *17*, 1435.
(398) Mukherjee, A. *Appl. Phys. Lett*. **1993**, *62*, 3423.
(399) He, G. S.; Markowicz, P. P; Lin, T.-C.; Prasad, P. N. *Nature* (London), **2002**, *415*, 767.
(400) He, G. S.; Lin, T.-C.; Chung, S.-J.; Zheng, Q.; Lu, C.; Cui, Y.; Prasad, P. N. *J. Opt. Soc. Am. B* **2005**, *22*, 2219.
(401) Markowicz, P. P.; He, G. S.; Prasad, P. N. *Opt. Lett*. **2005**, *30*, 1369.
(402) Fan, H.-H.; Wang, H.-Z.; Tian, Y.-P.; *Chin. Phys. Lett.* **2005**, *22*, 1152.
(403) Zhao, C. F.; He, G. S.; Bhawalkar, J. D.; Park, C.-K, Prasad, P. N. *Chem. Mater*. **1995**, *7*, 1979.
(404) He, G. S.; Bhawalkar, J. D.; Zhao, C. F.; Park, C.-K.; Prasad, P. N. *Appl. Phys. Lett*. **1996**, *68*, 3549.
(405) Zheng, Q.; He, G. S.; Lin, T.-C.; Prasad, P. N. *J. Mater. Chem*. **2003**, *13*, 2499.
(406) He, G. S.; Yuan, L.; Prasad, P. N.; Abbotto, A.; Facchetti, A.; Pagani, G. A. *Opt. Commun.* **1997**, *140*, 49.
(407) Abbotto, A.; Beverina, L.; Bozio, R.; Bradamante, S.; Ferrante, C.; Pagani, G. A.; Signorini, R. *Adv. Mater.* **2000**, *12*, 1963.
(408) Wang, X.-M.; Zhou, Y.-F, Yu, W.-T.; Wang, C.; Fang, Q.; Jiang, M.-H.; Lei, H.; Wang, H.-Z. *J. Mater. Chem*. **2000**, *10*, 2698.
(409) Ren, Y.; Fang, Q.; Yu, W.-T.; Lei, H.; Tian, Y.-P.; Jiang, M.-H.; Yang, Q.-C.; Mak, T. C. W. *J. Mater. Chem*. **2000**, *10*, 2025.
(410) Wang, H. Z.; Lei, H.; Wei, Z. C.; Zhao, F. L.; Zheng, X. G.; Xu, N. S.; Wang, X. M.; Ren, Y.; Tian, Y. P.; Fang, Q.; Jiang, M. H. *Chem. Phys. Lett*. **2000**, *324*, 349.
(411) Wang, X.; Wang, D.; Jiang, W.; Jiang, M. *Opt. Mater*. **2002**, *20*, 217.
(412) Zhou, Y.-F.; Meng, F. Q.; Zhao, X.; Xu, D.; Jiang, M.-H. *J. Phys. Chem. Solids* **2001**, *62*, 1145.
(413) Fakis, M.; Polyzos, J.; Tsigaridas, G.; Parthenios, J.; Fragos, A.; Giannetas, V.; Persephonis, P.; Mikroyannidis, J. *Chem. Phys. Lett*. **2000**, *323*, 111.
(414) Tang, X.-J.; Wu, L.-Z.; Zhang, L.-P.; Tung, C.-H. *Chem. Phys. Lett*. **2002**, *356*, 573.
(415) Tang, X.-J.; Wu, L.-Z.; Zhang, L.-P.; Tung, C.-H. *Phys. Chem. Chem. Phys.* **2002**, *4*, 5744.
(416) Pikas, D. J.; Kirkpatrick, S. M.; Tewksbury, E.; Brott, L. L.; Naik, R. R.; Stone, M. O.; Dennis, W. M. *J. Phys. Chem. B* **2002**, *106*, 4831.
(417) He, G. S.; Signorini, R.; Prasad, P. N. *Appl. Opt*. **1998**, *37*, 5720.
(418) He, G. S.; Bhawalkar, J. D.; Zhao, C.; Prasad, P. N. *IEEE J. Quantum Electron*. **1996**, *32*, 749.
(419) Lai, M.; Pakatchi, S.; He, G. S.; Kim, K. S.; Prasad, P. N. *Chem. Mater*. **1999**, *11*, 3012.
(420) He, G. S.; Zheng, Q.; Prasad, P. N.; Grote, J. G.; Hopkins, F. K. *Opt. Lett*. **2006**, *31*, 359.
(421) He, G. S.; Signorini, R.; Prasad, P. N. *IEEE J. Quantum Electron*. **1998**, *34*, 7.
(422) Ye, C.; Wang, J.; Lo, D. *Appl. Phys. B* **2004**, *78*, 539.
(423) Anand, M.; Dharmadhikari, A. K.; Dharmadhikari, J. A.; Mishra, A.; Mathur, D.; Krishnamurthy, M. *Chem. Phys. Lett*, **2003**, *372*, 263.
(424) Bauer, C.; Schnabel, B.; Kley, E.-B.; Scherf, U.; Giessen, H.; Mahrt, F, *Adv. Mater*. **2002**, *14*, 673.
(425) Maro, C.; Lepore, M.; Cingolani, R.; Tommasi, R.; Ferrara, M.; Catalano, I. M.; Ploog, K.; Fischer, A. *Phys. Rev. B* **1991**, *44*, 8384.
(426) Nayfeh, M. H.; Barry, N.; Therrien, J.; Akcakir, O.; Gratton, E.; Belomoin, G. *Appl. Phys. Lett*. **2001**, *78*, 1131.
(427) Zhang, X.; Tian, Y.; Jin, F.; Wu, J.; Xie, Y.; Tao, X.; Jiang, M. *Cryst. Growth Des.* **2005**, *5*, 565.
(428) He, G. S.; Lin, T.-C.; Hsiao, V. K. S.; Cartwright, A. N.; Prasad, P. N.; Natarajan, L. V.; Tondiglia, V. P.; Jakubiak, R.; Vaia, R. A.; Bunning, T. J. *Appl. Phys. Lett*. **2003**, *83*, 2733.
(429) Wang, J.; Ye, C.; Chen, F.; Shi, L.; Lo, D. *Journal of Optics A: Pure and Applied Optics* **2005**, *7*, 261.
(430) He, G. S.; Dai, J.; Lin, T.-C.; Markowicz, P. P.; Prasad, P. N. *Opt. Lett*. **2003**, *28*, 719.
(431) He, G. S.; Helgeson, R.; Lin, T.-C.; Zheng, Q.; Wudl, F.; Prasad, P. N. *IEEE J. Quantum Electron*. **2003**, *39*, 1003.
(432) Yang, Q.; Lin, S.; Xu, L.; Yang, F.; Yang, Y.; Pan, L.; Sun, C.; Li, Y.; Sun, G.; Jiang, Z. *Appl. Phys. B* **2005**, *80*, 953.
(433) Kimberg, V.; Polyutov, S.; Gel'mukhanov, F.; Ågren, H.; Baev, A.; Zheng, Q.; He, G. S. *Phys. Rev. A* **2006**, *74*, 033814.
(434) Spangle, C. W. *J. Mater. Chem*. **1999**, *9*, 2013.
(435) Swalen, J. D.; Kajzar, F. *MCLC S&T, Section B: Nonlinear Optics*, **2001**, *27*, 13.
(436) Lemercier, G.; Mulatier, J.-C.; Martineau, C.; Anemian, R.; Andraud, C.; Wang, I.; Stephan, O.; Amari, N.; Baldeck, P. *C. R. Chim.* **2005**, *8*, 1308.
(437) Van Stryland, E. W.; Vanherzeele, H.; Woodall, M. A.; Soileau, M. J.; Smirl, A. L.; Guha, S.; Boggess, T. F. *Optical Engineering* **1985**, *24*, 613.
(438) Boggess, T. F.; Smirl, A. L.; Moss, S. C.; Boyd, I. W.; Van Stryland, E. W. *IEEE J. Quantum Electron*. **1985**, *QE-21*, 488.
(439) Walker, A. C.; Kar, A. K.; Ji, W.; Keller, U.; Smith, S. D. *Appl. Phys. Lett*. **1986**, *48*, 683.
(440) Hagan, D. J.; Van, Stryland, E. W.; Soileau, M. J.; Wu, Y. Y.; Guha, S. *Opt. Lett*. **1988**, *13*, 315.

(441) Van Stryland, E. W.; Wu, Y. Y.; Hagan, D. J.; Soileau, M. J.; Mansour, K. *J. Opt. Soc. Am. B* **1988**, *5*, 1980.
(442) Jaroszynski, D. A.; Ortega, J. M.; Prazeres, R.; Glotin, F.; Murdin, B. N.; Merveille, C.; Kar, A. K.; Kimmitt, M. F.; Pidgeon, C. R. *Nucl. Instr. Methods Phys. Res., Sect. A* **1993**, *A331*, 640.
(443) He, G. S.; Xu, G. C.; Prasad, P. N.; Reinhardt, B. A.; Bhatt, J. C.; McKellar, R.; Dillard, A. G. *Opt. Lett.* **1995**, *20*, 435.
(444) Casstevens, M. K.; Kumar, D.; Ghosal, S.; Burzynski, R.; Spangler, C. W.; Elandaloussi, El, Hadj. *MCLC S&T, Section B: Nonlinear Optics* **1999**, *21*, 263.
(445) Nguefack, C.; Zabulon, T.; Anemian, R.; Andraud, C.; Collet, A.; Topcu, S.; Baldeck, P. L. *MCLC S&T, Section B: Nonlinear Optics* **1999**, *21*, 309.
(446) Sengupta, P.; Balaji, J.; Banerjee, S.; Philip, R.; Kumar, G. Ravindra; Maiti, S. *J. Chem. Phys.* **2000**, *112*, 9201.
(447) Zhou, G.; Wang, X.; Wang, D.; Wang, C.; Shao, Z.; Fang, Q.; Jiang, M. *Opt. Commun.* **2001**, *190*, 345.
(448) Lee, K.-S.; Lee, J.-H.; Kim, K.-S; Woo, H.-Y.; Kim, O.-K.; Choi, H.; Cha, M.; He, G. S.; Swiatkiewcz, J.; Prasad, P. N.; Chung, M.-A.; Jung, S.-D. *MCLC S&T, Section B: Nonlinear Optics* **2001**, *27*, 87.
(449) Morel, Y.; Irimia, A.; Najechalski, P.; Kervella, Y.; Stephan, O.; Baldeck, P. L.; Andraud, C. *J. Chem. Phys.* **2001**, *114*, 5391.
(450) Ventelon, L.; Morel, Y.; Baldeck, P.; Moreaux, L.; Mertz, J.; Blanchard-Desce, M. *MCLC S&T, Section B: Nonlinear Optics* **2001**, *27*, 249.
(451) Anemian, R.; Morel, Y.; Baldeck, P. L.; Paci, B.; Kretsch, K.; Nunzi, J.-M.; Andraud, C. *J. Mater. Chem.* **2003**, *13*, 2157.
(452) Silly, M. G.; Porres, L.; Mongin, O.; Chollet, P.-A.; Blanchard-Desce, M. *Chem. Phys. Lett.* **2003**, *379*, 74.
(453) Feneyrou, P.; Doclot, O.; Block, D.; Baldeck, P. L.; Zyss, J. *Journal of Nonlinear Optical Physics & Materials* **1996**, *5*, 767.
(454) Morel, Y.; Ibanez, A.; Nguefack, C.; Andraud, C.; Collet, A.; Nicoud, J.-F.; Baldeck, P. L. *Synth. Met.* **2000**, *115*, 265.
(455) Ganeev, R. A.; Ryasnyansky, A. I.; Tugushev, R. I.; Kodirov, M. K.; Akhmedjanov, F. R.; Usmanov, T. *Optical and Quantum Electronics* **2004**, *36*, 807.
(456) Morel, Y.; Zaccaro, J.; Ibanez, A.; Baldeck, P. L. *Opt. Commun.* **2002**, *201*, 457.
(457) Khoo, I. C.; Wood, M. V.; Guenther, B. D.; Shih, Min-Yi.; Chen, P. H. *J. Opt. Soc. Am. B* **1998**, *15*, 1533.
(458) Khoo, I. C.; Chen, P. H.; Wood, M. V.; Shih, M.-Y. *Chem. Phys.* **1999**, *245*, 517.
(459) Khoo, I. C.; Diaz, A.; Ding, J. *J. Opt. Soc. Am. B* **2004**, *21*, 1234.
(460) Nakazawa, M.; Watanabe, Y.; Tsuchiya, T.; Fujitsu, S. *J. Ceram. Soc. Jpn.* **1996**, *104*, 918.
(461) He, G. S.; Zheng, Q.; Prasad, P. N.; Helgeson, R.; Wudl, F. *Appl. Opt.* **2005**, *44*, 3560.
(462) He, G. S.; Zheng, Q.; Lu, C.; Prasad, P. N. *IEEE J. Quantum Electron.* **2005**, *41*, 1037.
(463) Maciel, G. S.; Rakov, N.; de Araujo, C. B.; Lipovskii, A. A.; Tagantsev, D. K. *Appl. Phys. Lett.* **2001**, *79*, 584.
(464) Sanz, N.; Ibanez, A.; Morel, Y.; Baldeck, P. L. *Appl. Phys. Lett.* **2001**, *78*, 2569−2571.
(465) Venkatram, N.; Rao, D. N.; Akundi, M. A. *Opt. Express.* **2005**, *13*, 867.
(466) He, G. S.; Bhawalkar, Jayant D.; Prasad, Paras N.; Reinhardt, Bruce A. *Opt. Lett.* **1995**, *20*, 1524.
(467) Ma, W.; Wu, Y.; Han, J.; Gu, D.; Gan, F. *Chem. Phys. Lett.* **2005**, *410*, 282.
(468) Zhang, J.; Cui, Y.; Xu, C.; Wang, M; Liu, J. *Jpn. J. Appl. Phys.* **2002**, *41*, L462.
(469) Zhou, G.; Wang, X.; Wang, D.; Shao, Z.; Jiang, M. *Appl. Opt.* **2002**, *30*, 1120.
(470) Zhan, C.; Li, D.; Zhang, D.; Li, Y.; Wang, D.; Wang, T.; Lu, Z.; Zhao, L.; Nie, Y.; Zhu, D. *Chem. Phys. Lett.* **2002**, *353*, 138.
(471) Giorgetti, E.; Toci, G.; Vannini, M.; Giammanco, F. *Opt. Commun.* **2003**, *217*, 431−439.
(472) Wang, D.-Y.; Zhan, C.-L.; Chen, Y.; Li, Y.-J.; Lu, Z.-Z.; Nie, Y.-X. *Chem. Phys. Lett.* **2003**, *369*, 621.
(473) He, G. S.; Yuan, L.; Cheng, N.; Bhawalkar, J. D.; Prasad, P. N.; Brott, L. L.; Clarson, S. J.; Reinhardt, B. A. *J. Opt. Soc. Am. B* **1997**, *14*, 1079.
(474) He, G. S.; Weder, C.; Smith, P.; Prasad, P. N. *IEEE J. Quantum Electron.* **1998**, *34*, 2279.
(475) He, G. S.; Yuan, L.; Bhawalkar, J. D.; Prasad, P. N. *Appl. Opt.* **1997**, *36*, 3387.
(476) He, G. S. *Progress in Quantum Electronics* **2002**, *26*, 131.
(477) Denk, W.; Strickler, J. H.; Webb, W. W. *Science* **1990**, *248*, 73.
(478) (a) Hell, S. W.; Bahlmann, K.; Schrader, M.; Soini, A.; Malak, H. M.; Gryczynski, I.; Lakowicz, J. R. *J. Biomedical Opt.* **1996**, *1*, 71. (b) Xu. C.; Zipfel, W.; Shear, J. B.; Williams, R. M.; Webb, W. W. *Proc. Natl. Acad. Sci. U.S.A.* **1996**, *93*, 10763.
(479) Bhawalkar, J. D.; Swiathiewicz, J.; Prasad, P. N.; Pan, S. J.; Shih, A.; Kamarabandu, J. K.; Cheng, P. C.; Reinhardt, B. A. *Polymer* **1997**, *38*, 4551.
(480) Minsky, M. Microscoy Apparatus. *U.S. Patent* 3013467, **1961**.
(481) Pawley, J. B. *Scanning* **2002**, *24*, 241.
(482) Pawley, J. B. *Fundamental and Practical Limits in Confocal Light-Microscopy. Scanning* **1991**, *13*, 184.
(483) Dong, C. Y.; Koenig, K.; So, P. *J. Biomed. Opt.* **2003**, *8*, 450.
(484) Dong, C. Y.; Bevin, E.; Koenig, K.; So, P. T. C. *Biophys. J.* **2001**, *80*, 159a.
(485) So, P. T. C.; Dong, C.; Bevin, E.; Koenig, K. *Biophys. J.* **2000**, *78*, 444a.
(486) Girkin, J. M.; Wokosin, D. L. In *Confocal and multiphoton microscopy*, Diaspro A, Ed. John Willey: New York 2001.
(487) Bewersdorf, J.; Hell, S. W. *Journal of Microscopy-Oxford* **1998**, *191*, 28.
(488) Koester, H. J.; Baur, D.; Uhl, R.; Hell, S. W. *Biophys. J.* **1999**, *77*, 2226.
(489) Xu, C.; Guild, J.; Webb, W. W.; Denk, W. *Opt. Lett.***1995**, *20*, 2372.
(490) Koenig, K.; So, P.; Mantulin, W. W.; Gratton, E.; Krasieva, T.; Berns, M. W.; Tromberg, B. J. *Proceedings of SPIE-The International Society for Optical Engineering* **1996**, *2628*, 12.
(491) Hell, S. W.; Booth, M.; Wilms, S.; Schnetter, C. M.; Kirsch, A. K.; Arndt-Jovin, D. J.; Jovin, T. M. *Opt. Lett.* **1998**, *23*, 1238.
(492) Uzunbajakava, N.; Otto, C. *Opt. Lett.* **2003**, *28*, 2073.
(493) Agate, B.; Brown, C. T. A.; Sibbett, W.; Dholakia, K. *Opt. Express.* **2004**, *12*, 3011.
(494) Xu, C.; Mertz, J.; Shear, J. B.; Webb, W. W. *Proceedings of SPIE-The International Society for Optical Engineering* **1996**, *2819*, 274.
(495) Shear, J. B.; Xu, C.; Webb, W. W. *Photochemistry & Photobiology* **1997**, *65*, 931−936.
(496) Xu, C.; Webb, W. W. *Topics in Fluorescence Spectroscopy* **1997**, *5*, 471.
(497) Albota, M. A.; Xu, C.; Webb, W. W. *Appl. Opt.* **1998**, *37*, 7352.
(498) Brown, E. B.; Shear, J. B.; Adams, S. R.; Tsien, R. Y.; Webb, W. W. *Biophys. J.* **1999**, *76*, (1 Part 1), 489.
(499) Furuta, T.; Wang, S. S. H.; Dantzker, J. L.; Dore, T. M.; Bybee, W. J.; Callaway, E. M.; Denk, W.; Tsien, R. Y. *Proc. Nat. Acad. Sci. U.S.A.* **1999**, *96*, 1193.
(500) Heikal, A. A.; Hess, S. T.; Baird, G. S.; Tsien, R. Y.; Webb, W. W. *Proc. Nat. Acad. Sci. U.S.A.* **2000**, *97*, 11996.
(501) Huang, S. H.; Heikal, A. A.; Webb, W. W. *Biophys. J.* **2002**, *82*, 2811.
(502) Bharali, D. J.; Lucey, D. W.; Jayakumar, H.; Pudavar, H. E.; Prasad, P. N. *J. Am. Chem. Soc.* **2005**, *127*, 11364.
(503) Jobsis, P. D.; Combs, C. A.; Balaban, R. S. *Journal of Microscopy-Oxford* **2005**, *217*, 260.
(504) Hebert, B.; Hulme, S. E.; Wiseman, P. W. *Proc. SPIE- Inter. Soc. Opt. Eng.* **2005**, *5700*, 109.
(505) Strickler, J. H.; Denk, W.; Webb, W. W. *Biophys. J.* **1990**, *57*, A374.
(506) Yuste, R.; Majewska, A.; Cash, S. S.; Denk, W. *J. Neuroscience* **1999**, *19*, 1976.
(507) Yuste, R.; Denk, W. *Nature* **1995**, *375*, 682.
(508) Konnerth, A. *Eur. J. Neuroscience* **1998**, *10*, 268.
(509) Dunn, K. W.; Sandoval, R. M.; Molitoris, B. A. *Nephron Experimental Nephrology* **2003**, *94*, E7.
(510) Kalb, J.; Nielsen, T.; Fricke, M.; Egelhaaf, M.; Kurtz, R. *Biochem. Biophys. Res. Commun.* **2004**, *316*, 341.
(511) Mueller, M.; Mironov, S. L.; Ivannikov, M. V.; Schmidt, J.; Richter, D. W. Experimental *Cell Research* **2005**, *303*, 114.
(512) Mironov, S. L. *Synapse* (New York, N.Y.) **2006**, *59*, 403.
(513) Kurtz, R.; Fricke, M.; Kalb, J.; Tinnefeld, P.; Sauer, M. *J. Neuroscience Methods* **2006**, *151*, 276.
(514) Masters, B. R.; So, P. T. C.; Gratton, E. *Lasers in Medical Science* **1998**, *13*, 196.
(515) Helmchen, F.; Svoboda, K.; Denk, W.; Tank, D. W. *Nat. Neurosci.* **1999**, *2*, 989.
(516) Kohler, R. H.; Schwille, P.; Webb, W. W.; Hanson, M. R. *J. Cell Sci.* **2000**, *113*, 3921.
(517) Oheim, M.; Beaurepaire, E.; Chaigneau, E.; Mertz, J.; Charpak, S. *J. Neuroscience Methods* **2001**, *111*, 29.
(518) Dunn, K. W.; Sandoval, R. M.; Kelly, K. J.; Dagher, P. C.; Tanner, G. A.; Atkinson, S. J.; Bacallao, R. L.; Molitoris, B. A. *Am. J. Physiology-Cell Physiology* **2002**, *283*, C905.
(519) Helmchen, F.; Waters, J. *Eur. J. Pharmacol.* **2002**, *447*, 119.
(520) Lin, S. X.; Maxfield, F. R. *Am. J. Physiology-Cell Physiology* **2004**, *287*, C257.
(521) Van Zandvoort, M.; Engels, W.; Douma, K.; Beckers, L.; Egbrink, M. O.; Daemen, M.; Slaaf, D. W. *J. Vascular Research* **2004**, *41*, 54.
(522) Berchner-Pfannschmidt, U.; Wotzlaw, C.; Merten, E.; Acker, H.; Fandrey, J. *Biol. Chem.* **2004**, *385*, 231.

(523) Van Zandvoort, M. A. M. J.; Buehler, A.; Hackeng, T.; Engels, W.; Slaaf, D.; Post, M.; Shapiro, L.; DeMuinck, E. *FASEB J.* **2004**, *18*, A256.
(524) Wei, S. H.; Miller, M. J.; Cahalan, M. D.; Parker, I. *Lymphocyte Activation and Immune Regulation Ix* **2002**, *512*, 203.
(525) Miller, M. J.; Wei, S. H.; Parker, I.; Cahalan, M. D. *Science* **2002**, *296*, 1869.
(526) Cahalan, M. D.; Parker, I. *Curr. Opin. Immunol.* **2006**, *18*, 476.
(527) Phillips, C. L.; Kojetin, D.; Arend, L. J.; Tuceryan, M.; Fang, S.; Dunn, K. W. *Mol. Biol. of the Cell* **1999**, *10*, 362a.
(528) Phillips, C. L.; Arend, L. J.; Filson, A. J.; Kojetin, D. J.; Clendenon, J. L.; Fang, S.; Dunn, K. W. *Am. J. Pathology* **2001**, *158*, 49.
(529) Bhawalkar, J. D.; Shih, A.; Pan, S. J.; Liou, W. S.; Swiatkiewicz, J.; Reinhardt, B. A.; Prasad, P. N.; Cheng, P. C. *Bioimaging* **1996**, *4*, 168.
(530) Bhawalkar, J. D.; Swiatkiewicz, J.; Pan, S. J.; Samarabandu, J. K.; Liou, W. S.; He, G. S.; Berezney, R.; Cheng, P. C.; Prasad, P. N. *Scanning* **1996**, *18*, 562.
(531) So, P. T. C. *J. Histotechnology* **2000**, *23*, 221.
(532) Konig, K. *J. Microscopy* (Oxford) **2000**, *200*, 83.
(533) Rubart, M. *Circ. Res.* **2004**, *95*, 1154.
(534) Helmchen, F.; Denk, W. *Nature Methods* **2005**, *2*, 932.
(535) Cruz, H. G.; Luscher, C. *Frontiers in Bioscience* **2005**, *10*, 2263.
(536) Yuste, R. *Nature Methods* **2005**, *2*, 902.
(537) Krebs, L. J.; Wang, X. P.; Pudavar, H. E.; Bergey, E. J.; Schally, A. V.; Nagy, A.; Prasad, P. N.; Liebow, C. *Cancer Res.* **2000**, *60*, 4194.
(538) Wang, X.; Pudavar, H. E.; Kapoor, R.; Krebs, L. J.; Bergey, E. J.; Liebow, C.; Prasad, P. N.; Nagy, A.; Schally, A. V. *J. Biomed. Opt.* **2001**, *6*, 319.
(539) Nagy, A.; Schally, A. V.; Armatis, P.; Szepeshazi, K.; Halmos, G.; Kovacs, M.; Zarandi, M.; Groot, K.; Miyazaki, M.; Jungwirth, A.; Horvath, J. *Proc. Nat. Acad. Sci. U.S.A.* **1996**, *93*, 7269.
(540) Miyazaki, M.; Nagy, A.; Schally, A. V.; Lamharzi, N.; Halmos, G.; Szepeshazi, K.; Groot, K.; Armatis, P. *Journal of the National Cancer Institute* **1997**, *89*, 1803.
(541) Synge, E. H. *Philos. Mag.* **1928**, *6*, 356.
(542) Phol, D. W.; Denk, W.; Lanz, M. *Apply. Phys. Lett.* **1984**, *44*, 7.
(543) Harootunian, A.; Betzig, E.; Isaacson, M.; Lewis, A. *Appl. Phys. Lett.* **1986**, *49*, 674.
(544) Liberman, K.; Harush, S.; Lewis, A.; Kopelman, R. *Science* **1990**, *247*, 59.
(545) Betzig, E.; Trautman, J. K.; Harris, T. D.; Weiner, J. S.; Kostalek, P. L. *Science* **1991**, *251*, 1468.
(546) Reddick, R. C.; Warmack, R. J.; Ferrell, T. L. *Phys. Rev. B* **1989**, *39*, 767.
(547) Courjoin, D.; Sarayeddine, K.; Spajer, M. *Opt. Commun.* **1989**, *71*, 23.
(548) Betzig, E.; Finn, P. L.; Weiner, J. S. *Appl. Phys. Lett.* **1992**, *60*, 18.
(549) Atia, W. A.; Davis, C. C. *Apply. Phys. Lett.* **1997**, *70*, 405.
(550) Lewis, M. K.; Wolanin, P.; Gafni, A.; Steel, D. G. *Opt. Lett.* **1998**, *23*, 1111.
(551) Jenei, A.; Kirsch, A. K.; Subramaniam, V.; Arndt-Jovin, D. J.; Jovin, T. M. *Biophys. J.* **1999**, *76*, 1092.
(552) Kirsch, A. K.; Subramaniam, V.; Striker, G.; Schnetter, C.; Arndt-Jovin, D. J.; Jovin, T. M. *Biophys. J.* **1998**, *75*, 1513.
(553) Jakubczyk, D.; Shen, Y.; Lal, M.; Friend, C.; Kim, K. S.; Swiatkiewicz, J.; Prasad, P. N. *Opt. Lett.* **1999**, *24*, 1151.
(554) Osborn, D. L.; Leone, S. R. *J. Appl. Phys.* **2001**, *89*, 626.
(555) Imura, K.; Nagahara, T.; Okamoto, H. *J. Am. Chem. Soc.* **2004**, *126*, 12730.
(556) Wang, H.; Huff, T. B.; Zweifel, D. A.; He, W.; Low, P. S.; Wei, A.; Cheng, J. X. *Proc. Nat. Acad. Sci. U.S.A.* **2005**, *102*, 15752.
(557) Imura, K.; Nagahara, T.; Okamoto, H. *Appl. Phys. Lett.* **2006**, *88*, 2.
(558) Yoshimasa, K.; Chris, X.; Winfried, D. *J. Appl. Phys.* **1999**, *85*, 1294.
(559) Sanchez, E. J.; Novotny, L.; Xie, X. S. *Phy. Rev. Lett.* **1999**, *82*, 4014.
(560) Shen, Y.; Swiatkiewicz, J.; Markowicz, P.; Prasad, P. N. *Appl. Phys. Lett.* **2001**, *79*, 2681.
(561) Chon, J. W. M.; Gu, M.; Bullen, C.; Mulvaney, P. *Opt. Lett.* **2003**, *28*, 1930.
(562) Shen, Y.; Jakubczyk, D.; Xu, F.; Swiatkiewicz, J.; Prasad, P. N. *Appl. Phys. Lett.* **2000**, *76*, 1.
(563) Shen, Y.; Swiatkiewicz, J.; Lin, T. C.; Markowicz, P.; Prasad, P. N. *J. Phys. Chem. B* **2002**, *106*, 4040.
(564) Shen, Y.; Swiatkiewicz, J.; Prasad, P. N.; Vaia, R. A. *Opt. Comm.* **2001**, *200*, 9.
(565) Shen, Y.; Swiatkiewicz, J.; Jakubczyk, D.; Xu, F.; Prasad, P. N.; Vaia, R. A.; Reinhardt, B. A. *Appl. Opt.* **2001**, *40*, 938.
(566) Yin, X. B.; Fang, N.; Zhang, X.; Martini, I. B.; Schwartz, B. J. *Appl. Phys. Lett.* **2002**, *81*, 3663.
(567) Kawata, S; Kawata, Y. *Chem. Rev.* **2000**, *100*, 1777.
(568) Belfield, K. D.; Schafer, Katherine J.; Liu, Yong; Liu, Jun; Ren, Xiaobin; Van Stryland, Eric W. *J. Phys. Org. Chem.* **2000**, *13*, 837.
(569) Parthenopoulos, D. A.; Rentzepis, P. E. *Science* **1989**, *245*, 843.
(570) Parthenopoulos, D. A.; Rentzepis, P. E. *J. Appl. Phys.* **1990**, *68*, 5814.
(571) Strickler, J. H.; Webb, W. W. *Opt. Lett.* **1991**, *16*, 1780.
(572) Kawata, Y.; Ishitobi, H.; Kawata, S. *Opt. Lett.* **1998**, *23*, 756.
(573) Toriumi, A.; Kawata, S.; Gu, M. *Opt. Lett.* **1998**, *23*, 1924.
(574) Kawata, S. *Proceedings of the IEEE* **1999**, *87*, 2009.
(575) Fukushima, M.; Yanagi, H.; Hayashi, S.; Sun, H.-B.; Kawata, S. *Physica E: Low-Dimensional Systems & Nanostructures* **2004**, *21*, 456.
(576) Gu, M.; Day, D. *Opt. Lett.* **1999**, *24*, 288.
(577) Day, D.; Gu, M.; Smallridge, A. *Opt. Lett.* **1999**, *24*, 948.
(578) Gu, M.; Amistoso, J. O.; Toriumi, A.; Irie, M.; Kawata, S. *Appl. Phys. Lett.* **2001**, *79*, 148.
(579) McPhail, D.; Gu, M. *Appl. Phys. Lett.* **2002**, *81*, 1160.
(580) Chon, J. W. M.; Zijlstra, P.; Gu, M.; van Embden, J.; Mulvaney, P. *Appl. Phys. Lett.* **2004**, *85*, 5514.
(581) Bhawalkar, J. D.; Kumar, N. D.; Swiatkiewicz, J.; Prasad, P. N. *MCLC S&T, Section B: Nonlinear Optics* **1998**, *19*, 249.
(582) Dagani, R. *Chem. Eng. News*, **1996**, September, 68.
(583) Pudavar, H. E.; Joshi, M. P.; Prasad, P. N.; Reinhardt, B. A. *Appl. Phys. Lett.* **1999**, *74*, 1338.
(584) Dvornikov, A. S.; Rentzepis. P. M. *Opt. Commun.* **1997**, *136*, 1.
(585) Liang, Y. C.; Oulianov, D. A.; Dvornikov, A. S.; Tomov, I. V.; Rentzepis, D. P. M. *NATO Science Series, 3: High Technology* **2000**, *79*, 1.
(586) Belfield, K. D.; Schafer, K. *J. Chem. Mater.* **2002**, *14*, 3656.
(587) Kubitscheck, U.; Tschodrich-Rotter, M.; Wedekind, P; Peters, R. *J. Microscopy* **1996**, *182*, 225.
(588) Akimov, D. A.; Zheltikov, A. M.; Koroteev, N. I.; Magnitskii, S. A.; Naumov, A. N.; Sidorov, -Biryukov, D. A.; Sokolyuk, N. T.; Fedotov, A. B. *Kvantovaya Elektronika* (Moscow) **1998**, *25*, 563.
(589) Kirkpatrick, S. M.; Baur, J. W.; Clark, C. M.; Denny, L. R.; Tomlin, D. W.; Reinhardt, B. R.; Kannan, R.; Stone, M. O. *Appl. Phys. A* **1999**, *69*, 461.
(590) Fischer, T.; Neebe, M.; Juchem, T.; Hampp, N. A. *IEEE transactions on nanobioscience* **2003**, *2*, 1.
(591) Konorov, S. O.; Sidorov-Biryukov, D. A.; Bugar, I.; Chorvat, D.; Chorvat, D.; Zheltikov, A. M. *Chem. Phys. Lett.* **2003**, *381*, 572.
(592) Polyzos, I.; Tsigaridas, G.; Fakis, M.; Giannetas, V.; Persephonis, P.; Mikroyannidis, J. *Chem. Phys. Lett.* **2003**, *369*, 264.
(593) Yao, B.; Lei, M.; Ren, L.; Menke, N.; Wang, Y.; Fischer, T.; Hampp, N. *Opt. Lett.* **2005**, *30*, 3060.
(594) Zhou, Y.; Tang, H.; Huang, W.; Xia, A.; Sun, F.; Zhang, F. *Optical Engineering* **2005**, *44*, 035202/1.
(595) Sun, H. B.; Kawata, S. *Adv. Polym. Sci.* **2004**, *170*(NMR, 3D Analysis, Photopolymerization), 169.
(596) Maruo, S.; Nakamura, O.; Kawata, S. *Opt. Lett.* **1997**, *22*, 132.
(597) Kawata, S.; Sun, H.-B, Tanaka, T.; Takada, K. *Nature* **2001**, *412*, 697.
(598) Sun, H.-B.; Tanaka, T.; Kawata, S. *Appl. Phys. Lett.* **2002**, *80*, 3673.
(599) Sun, H.-B.; Kawata, S. *J. Lightwave Tech.* **2003**, *21*, 624.
(600) Cumpston, B. H.; Ananthavel, S. P.; Barlow, S.; Dyer, D. L.; Ehrlich, J. E.; Erskine, L. L.; Heikal, A. A.; Kuebler, S. M.; Lee, I.-Y. S.; McCord-Maughon, D.; Qin, J.; Rockel, H.; Rumi, M.; Wu, X.-L.; Marder, S. R.; Perry, J. W. *Nature* **1999**, *398*, 51.
(601) Kuebler, S. M.; Rumi, M.; Watanabe, T.; Braun, K.; Cumpston, B. H.; Heikal, A. A.; Erskine, L. L.; Thayumanavan, S.; Barlow, S.; Marder, S. R.; Perry, J. W. *J. Photopolym. Sci. Technol.* **2001**, *14*, 657.
(602) Zhou, W.; Kuebler, S. M.; Braun, K. L.; Yu, T.; Cammack, J. K.; Ober, C. K.; Perry, J. W.; Marder, S. R. *Science* **2002**, *296*, 1106.
(603) Kuebler, Stephen M.; Braun, Kevin L.; Zhou, Wenhui; Cammack, J. Kevin; Yu, Tianyue; Ober, Christopher K.; Marder, Seth R.; Perry, Joseph W. J. *Photochem. Photobiol. A* **2003**, *158*, 163.
(604) Sun, H.-B.; Matsuo, S.; Misawa, H. *Appl. Phys. Lett.* **1999**, *74*, 786.
(605) Sun, H.-B.; Kawakami, T.; Xu, Y.; Ye, J.-Y.; Matuso, S.; Misawa, H.; Miwa, M.; Kaneko, R. *Opt. Lett.* **2000**, *25*, 1110.
(606) Schafer, K. J.; Hales, J. M.; Balu, M.; Belfield, K. D.; Van Stryland, E. W.; Hagan, D. J. *J. Photochem. Photobiol. A* **2004**, *162*, 497.
(607) Wang, I.; Bouriau, M.; Baldeck, P. L.; Martineau, C.; Andraud, C. *Opt. Lett.* **2002**, *27*, 1348.
(608) Martineau, C.; Lemercier, G.; Andraud, C.; Wang, I.; Bouriau, M.; Baldeck, P. L. *Synth. Met.* **2003**, *138*, 353.
(609) Lee, K.-S.; Kim, M.-S.; Yang, H.-K.; Soo, B.-K.; Sun, H.-B; Kawata, S.; Fleitz, P. *Mol. Cryst. Liq. Cryst.* **2004**, *424*, 35.
(610) Yang, H.-K.; Kim, M.-S.; Kang, S.-W.; Kim, K.-S.; Lee, K.-S.; Park, S. H.; Yang, D.-Y.; Kong, H. J.; Sun, H.-B.; Kawata, S.; Fleitz, P. *J. Photopolym. Sci. Technol.* **2004**, *17*, 385.
(611) Joshi, M. P.; Pudavar, H. E.; Swiatkiewicz, J.; Prasad, P. N.; Reinhardt, B. A. *Appl. Phys. Lett.* **1999**, *74*, 170.
(612) Dvornikov, A. S.; Bouas-Laurent, H.; Desvergne, J.-P.; Rentzepis, P. M. *J. Mater. Chem.* **1999**, *9*, 1081.

(613) Luo, L.; Li, C.; Wang, S.; Huang, W.; Wu, C.; Yang, H.; Jiang, H.; Gong, Q.; Yang, Y.; Feng, S. *J. Opt. A* **2001**, *3*, 489.
(614) Postnikova, B. J.; Currie, J.; Doyle, T.; Hanes, R. E.; Anslyn, E. V.; Shear, J. B.; Vanden, Bout, D. E. *Microelectron. Eng.* **2003**, *69*, 459.
(615) Teh, W. H.; Durig, U.; Salis, G.; Harbers, R.; Drechsler, U.; Mahrt, R. F.; Smith, C. G.; Guntherodt, H.-J. *Appl. Phys. Lett*. **2004**, *84*, 4095.
(616) Lu, Y.; Hasegawa, F.; Goto, T.; Ohkuma, S.; Fukuhara, S.; Kawazu, Y.; Totani, K.; Yamashita, T.; Watanabe, T. *J. Mater. Chem*. **2004**, *14*, 75.
(617) Stute, U.; Serbin, J.; Kulik, C.; Chichkov, B. N. *Int. J. Mater. Prod. Technol.* **2004**, *21*, 273−284.
(618) Teh, W. H.; Duerig, U.; Drechsler, U.; Smith, C. G.; Guentherodt, H.-J. *J. Appl. Phys*. **2005**, *97*, 054907/1.
(619) Nguyen, L. H.; Straub, M.; Gu, Min. *Adv. Func. Mater*. **2005**, *15*, 209.
(620) Fischer, T.; Hampp, N. A. *Biophy. J.* **2005**, *89*, 1175.
(621) Yan, Y.-X.; Tao, X.-T.; Sun, Y.-H.; Xu, G.-B.; Wang, C.-K.; Yang, J.-X.; Zhao, X.; Wu, Y.-Z.; Ren, Y.; Jiang, M.-H. *Opt. Mater*. **2005**, *27*, 1787.
(622) Zhou, H.-P.; Li, D.-M.; Zhang, J.-Z.; Zhu, Y.-M.; Wu, J.-Y.; Hu, Z.-J.; Yang, J.-X.; Xu, G.-B.; Tian, Y.-P.; Xie, Y.; Tao, X.-T.; Jiang, M.-H.; Tao, L.-M.; Guo, Y.-H.; Wang, C.-K. *Chem. Phys*. **2006**, *322*, 459.
(623) Wang, I.; Baldeck, P. L.; Martineau, C.; Lemercier, G.; Mulatier, J.-C.; Andraud, C. *Nonlinear Optics, Quantum Optics* **2004**, *32*, 161.

CR050054X